AFAPL-TR-79-2018
CEEDO-TR-79-07

EVALUATION OF FUEL CHARACTER EFFECTS ON F101 ENGINE COMBUSTION SYSTEM

General Electric Company
Advanced Engineering & Technology Programs
1 Neumann Way
Cincinnati, Ohio 45215

JUNE 1979

FINAL REPORT August 1977 - September 1978

Approved for public release; distribution unlimited

Air Force Aero-Propulsion Laboratory
Air Force Wright Aeronautical Laboratories
Air Force Systems Command
Wright-Patterson Air Force Base, Ohio 45433

NOTICE

When Government drawings, specifications, or other data are used for any purpose other than in connection with a definitely related Government procurement operation, the United States Government thereby incurs no responsibility nor any obligation whatsoever; and the fact that the government may have formulated, furnished, or in any way supplied the said drawings, specifications, or other data, is not to be regarded by implication or otherwise as in any manner licensing the holder or any other person or corporation, or conveying any rights or permission to manufacture, use, or sell any patented invention that may in any way be related thereto.

This report has been reviewed by the Information Office (OI) and is releasable to the National Technical Information Service (NTIS). At NTIS, it will be available to the general public, including foreign nations.

This technical report has been reviewed and is approved for publication.

Thomas A. Jackson

THOMAS A. JACKSON
Fuels Branch
Fuels and Lubrication Division

Arthur V. Churchill

ARTHUR V. CHURCHILL
Chief, Fuels Branch
Fuels and Lubrication Division

FOR THE COMMANDER

Blackwell C. Dunnam

BLACKWELL C. DUNNAM, Chief
Fuels and Lubrication Division

"If your address has changed, if you wish to be removed from our mailing list, or if the addressee is no longer employed by your organization please notify AFAPL/SFF ,W-PAFB, OH 45433 to help us maintain a current mailing list".

Copies of this report should not be returned unless return is required by security considerations, contractual obligations, or notice on a specific document.

Unclassified

SECURITY CLASSIFICATION OF THIS PAGE (When Data Entered)

REPORT DOCUMENTATION PAGE

READ INSTRUCTIONS BEFORE COMPLETING FORM

1. REPORT NUMBER: AFAPL-TR-79-2018
CEEDO-TR-79-07

2. GOVT ACCESSION NO.

3. RECIPIENT'S CATALOG NUMBER

4. TITLE (and Subtitle)
Evaluation of Fuel Character Effects on the F101 Engine Combustion System

5. TYPE OF REPORT & PERIOD COVERED
Final Technical Report, 1 Aug 77 - 30 Sep 78, 8/1/77 thru 9/30/78

6. PERFORMING ORG. REPORT NUMBER
R79AEG405

7. AUTHOR(s)
C.C. Gleason, T.L. Oller, M.W. Shayeson, D.W. Bahr

8. CONTRACT OR GRANT NUMBER(s)
F33615-77-C-2043

9. PERFORMING ORGANIZATION NAME AND ADDRESS
General Electric Company
Aircraft Engine Group
Cincinnati, Ohio - 45215

10. PROGRAM ELEMENT, PROJECT, TASK AREA & WORK UNIT NUMBERS
62203F
3048-05-84
19 05

11. CONTROLLING OFFICE NAME AND ADDRESS
Air Force Aero Propulsion Laboratory (SFF)
Air Force Wright Aeronautical Laboratories
Wright-Patterson AFB, Ohio - 45433

12. REPORT DATE
June 1979

13. NUMBER OF PAGES
199

14. MONITORING AGENCY NAME & ADDRESS (if different from Controlling Office)

15. SECURITY CLASS. (of this report)
Unclassified

15a. DECLASSIFICATION/DOWNGRADING SCHEDULE

16. DISTRIBUTION STATEMENT (of this Report)
Approved for public release; distribution unlimited.

17. DISTRIBUTION STATEMENT (of the abstract entered in Block 20, if different from Report)

18. SUPPLEMENTARY NOTES
Partial funding and technical support in the area of the measurement and analysis of gaseous emissions and smoke data was provided by the Environmental Sciences Branch of the Environics Division in the Research and Development Directorate of HQ Air Force Engineering and Services Center. (HQ AFESC/RDVC)

19. KEY WORDS (Continue on reverse side if necessary and identify by block number)
Fuels
Alternate Fuels
Gas Turbine Combustion
Exhaust Emissions
F101 Engine Combustor

20. ABSTRACT (Continue on reverse side if necessary and identify by block number)
Results of a program to determine the effects of broad variations in fuel properties on the performance, emissions and durability of the General Electric F101 augmented turbofan engine main combustion system are presented. Combustor rig tests conducted at engine idle, takeoff, cruise, dash, cold

DD FORM 1 JAN 73 1473 EDITION OF 1 NOV 65 IS OBSOLETE

Unclassified

SECURITY CLASSIFICATION OF THIS PAGE (When Data Entered)

BLOCK 20 (Cont'd)

day ground start and altitude relight operating conditions with 13 different fuels are described. Fuel nozzle fouling tests conducted with the same fuels are also described. The test fuels covered a range of hydrogen contents (12.0 to 14.5%), aromatic type (monocyclic and bicyclic), initial boiling point (285 to 393 K), final boiling point (552 to 679 K) and viscosity (0.83 to 3.25 mm^2/s at 300 K).

At high power conditions, fuel hydrogen content was found to have a very significant effect on liner temperature, smoke, and NO_x levels. While smoke levels decreased with increasing hydrogen content, the levels were very low with all the fuels.

At idle conditions, CO and HC levels correlated with fuel atomization/volatility parameters, but showed no relationship to hydrogen content.

Cold day ground start and altitude relight also correlated with fuel atomization/volatility parameters, but showed no dependence on hydrogen content.

Combustor liner life analyses yielded relative life predictions of 1.00, 0.72, 0.52, and 0.47 for fuel hydrogen contents of 14.5, 14.0, 13.0, and 12.0 percent, respectively. At the present state of turbine stator development, no fuel effect on life is predicted.

Extended cyclic fuel nozzle valve gumming tests revealed significant effects of fuel type and temperature on nozzle life. The results correlated with laboratory thermal stability ratings of the fuels based on tube deposits alone.

PREFACE

This final report is submitted by the General Electric Company, Aircraft Engine Group located at Evendale, Ohio. The work was conducted under Contract No. F33615-77-C-2043. Program sponsorship and guidance was provided by the Air Force Aero Propulsion Laboratory (AFAPL), Air Force Wright Aeronautical Laboratories, Air Force Systems Command, Wright-Patterson Air Force Base, Ohio under Project 3048, Task 05, and Work Unit 84. Thomas A. Jackson was the government project engineer.

Supplemental funding and technical guidance were provided in the area of gaseous emissions and smoke, measurement and analysis by the Environmental Sciences Branch of the Environics Division in the Research and Development Directorate of HQ Air Force Engineering and Services Center located at Tyndall Air Force Base, Florida. This organization has been formerly referred to as CEEDO or the Civil Engineering Center.

Test fuel analysis was provided by AFAPL, the Monsanto Research Laboratory (under contract to AFAPL), and the Air Force Logistics Command Aerospace Fuels Laboratory (SFQLA). The cooperation of these organizations is appreciated.

An addendum to the text of this report is presented after the List of Tables on pages xv to xvii . It contains information pertinent to the thermal stability evaluations discussed in section III.C.2. It has been prepared by T. A. Jackson from Monsanto Research Company data.

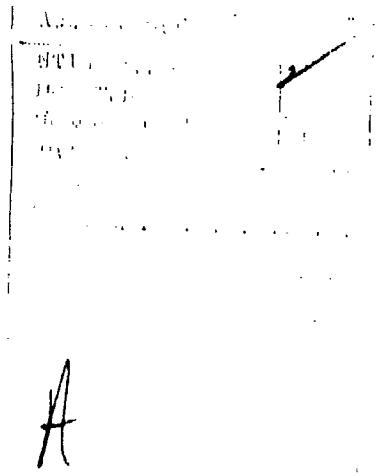

TABLE OF CONTENTS

TABLE OF CONTENTS (Concluded)

LIST OF ILLUSTRATIONS

LIST OF ILLUSTRATIONS (Continued)

LIST OF ILLUSTRATIONS (Continued)

LIST OF ILLUSTRATIONS (Continued)

LIST OF ILLUSTRATIONS (Concluded)

LIST OF TABLES

LIST OF TABLES (Continued)

LIST OF TABLES (Concluded)

ADDENDUM - FUEL THERMAL STABILITY

In an effort to resolve the differences of opinion as to the breakpoint of JP8 (Reference, section III.C.2.), the fuel sampling procedures of General Electric and AFAPL were reviewed. The only apparent difference in the techniques is the nature of the container used to obtain the fuel sample. General Electric uses an unlined fuel can, properly rinsed with a small quantity of the fuel to be sampled. The AFAPL uses epoxy-lined fuel cans, also properly rinsed.

Three test fuels (two blends and the baseline JP8) were identified as exhibiting peculiar behavior in the Jet Fuel Thermal Oxidation Tester (JFTOT) when samples of these fuels from each of the two types of containers were evaluated. Typically, the fuel samples contained in the GE vessels exhibited unusually high pressure drop and failed the test at relatively low fuel temperatures due to the pressure drop criteria. On the other hand, fuels from the epoxy-lined containers passed at higher temperatures and pressure drop was not their failure mode. Results of the JFTOT runs on these six fuels are presented in Table A.

Residue fuel from each of the six fuel containers (three unlined, three lined) was evaluated by Monsanto Research Company for any differences that may exist between the same fuels from different containers. The fuels were analyzed as follows (extracted from the Monsanto test report):

> Emission spectrographic analyses of the fuels were conducted to determine any difference in metals content. For semi-quantitative results, the fuels were extracted with dilute Ultrar metals-free hydrochloric acid (Hopkin and Williams Co., Essex, England). This approach allows metals to be concentrated in the acid layer, a portion of which is then evaporated in the cup of a spectrographic electrode. Most metals are efficiently extracted in this manner. However, a few, such as silicon and aluminum, are not. Any significant amount of these metals tend to form a scum at the fuel/acid interface. In conducting the analyses, therefore, a specimen taken from the fuel/acid boundary was also analyzed.

The results of this analysis are presented in Table B.

From Table B it can be seen that fuel samples from the unlined vessels contained higher trace quantities of several elements, most notably lead, tin, and zinc. These elements would be expected in unlined vessels with soldered joints, similar to the GE containers. Since these trace contaminants are in very small quantities this evaluation is not conclusive in explaining the differences in JFTOT readings between AFAPL and GE samples of the same fuels. The influence of the containment vessel on a fuel's thermal stability is, however, offered as a possible explanation based on this information.

TABLE A: JFTOT Breakpoints -

Evaluation of the Influence of Fuel Sample Cans

TYPE SAMPLE: TYPE CONTAINER: FUEL NUMBER:	Control Lined Can 4	Test Unlined Can 4	Control Lined Can 5	Test Unlined Can 5	Control Lined Can 2	Test Unlined Can 2
ESTIMATED BREAKPOINT (K)*:	563-568	<573	>583	<533	559	<553
FAILURE MODE:	ΔTDR	Unknown	--	--	ΔTDR	Δp
COMMENT:	Minimal Δp	Fuel could not be properly pumped	zero Δp	Insufficient data to isolate breakpoint	Minimal Δp	Very high Δp

* A definitive breakpoint was often not reached due to insufficient fuel or test difficulties (such as inability to pump the test fuel). The qualitative information is, however, sufficient for this evaluation of containment vessels.

TABLE B: SPECTROGRAPHIC ANALYSIS OF FUEL EXTRACTS AND EXTRACTION INTERFACES

ppb and Qualitative Amounts of Metals* Found in Following Fuels:

Type Sample:	Control		Test		Control		Test		Control		Test	
Type Container:	Lined Can		Unlined Can		Lined Can		Unlined Can		Lined Can		Unlined Can	
Fuel Number:	4		4		5		5		2		2	
	Fuel	Surface	Fuel	Surface	Fuel	Surface	Fuel	Surface	Fuel	Surface	Fuel	Surface
Metal												
Fe		trace	110	trace	4	trace	9	trace		trace		trace
Cu	5	trace	8	trace	4	trace	4	trace	4	trace	8	trace
Mn			3	trace	0.1-1.0	trace	0.1-1.0	trace		trace	0.1-1.0	trace
Pb	5		15		4		13		12		25	
Sn	0.1-1.0		38	trace			44	trace			3	
Ca			4	minor		major		major				minor
Si		major		major		major		major		trace		major
Al		trace		major		trace		major		trace		trace
Na		minor		minor		minor		trace		major		trace
Mg		trace				trace		trace		trace		trace
Cr			0.1-1.0			trace		trace				
V						trace				trace		
Zn											170	
Ag			0.1-1.0									
Ni						trace						
Ti						trace						

*Most metals could be detected at levels as low as 0.2-1.0 ppb, except for zinc which can be detected only as low as 50 ppb. For the qualitative analyses of the fuel/extract interface surface, a "major" designation indicates that this metal consisted of 10-100% of the total metals detected, a "minor" designation means 1-10% of the total metals, and "trace" means less than 1%.

SECTION I

SUMMARY

The purpose of this program was to determine by combustor rig test and data analyses, the effects of fuel property variations on the performance, exhaust emission and durability characteristics of the General Electric F101 augmented turbofan engine combustion/turbine system. Thirteen refined and blended fuels which incorporated systematic variations in hydrogen content (12.0 to 14.5 weight percent), aromatic type (monocyclic or bicyclic), initial boiling point (285 to 393 K by gas chromatograph), final boiling point (532 to 679 K also by gas chromatograph), and viscosity (0.83 to 3.25 mm^2/s at 300 K) were evaluated in (a) 13 high pressure/temperature full annular combustor performance/emmissions/durability tests; (b) 13 atmospheric pressure/high temperature full-annular combustor pattern factor performance tests; (c) 13 high pressure/temperature single fuel nozzle/swirl cup carbon deposition tests; (d) 14 low pressure/temperature 54-degree sector combustor cold day ground start/altitude relight tests; (e) 15 high temperature short duration fuel nozzle fouling tests; and, (f) 8 high temperature longer cyclic fuel nozzle valve gumming tests.

At high engine power operating conditions (takeoff, high altitude cruise, and low altitude penetration), fuel hydrogen content was found to be a very significant fuel property with respect to liner temperature, smoke, and oxides of nitrogen (NO_x) levels. Each of these parameters decreased with increasing fuel hydrogen content, but no discernible effect of any of the other fuel properties was found. Carbon monoxide (CO) and unburned hydrocarbon (HC) emission levels were so low at these operating conditions that no trend with fuel properties could be detected. While smoke levels were found to decrease with increasing fuel hydrogen content, the levels were still very low with all fuels.

At engine idle operating conditions, the same strong effect of fuel hydrogen content on smoke level was evident. However, CO and HC emission levels were found to correlate with fuel atomization/volatility parameters with no hydrogen content dependency.

Cold day ground start and altitude relight capabilities were also found to correlate with the fuel atomization/volatility parameters and exhibit no hydrogen content dependency. Capabilities with JP-8 fuel blends were generally reduced relative to those with JP-4 fuel blends.

Pattern factor (in atmospheric pressure tests) was found to be fuel dependent and to correlate with the fuel atomization parameter. This finding was a surprise and had not been observed in any other combustion systems. Verification data are therefore needed, but there is considerable evidence to indicate that (1) this is not a general effect and (2) at true engine operating pressure levels in the F101 engine, pattern factors are not fuel-type dependent. TF39, CF6, J79, T700, and TF34 combustor rig

pattern factor tests have been run in which no fuel effects were detected. Further, all of these engines, including the F101, have been run with JP-4 and JP-5 (or Jet A) fuels and no fuel effects on turbine condition have been detected.

Combustor liner life analyses based on these test data were conducted. These analyses resulted in relative life predictions of 1.00, 0.72, 0.52, and 0.47 for fuel hydrogen contents of 14.5, 14.0, 13.0, and 12.0 percent, respectively, due to increased liner temperatures. Turbine stator leading edge temperatures are also predicted to increase with decreasing fuel hydrogen content, but stator life is currently limited by trailing edge cracking, so no fuel effect on life is predicted.

A series of short but severe fuel nozzle fouling tests did not reveal any major problems with the fuels in this matrix. However, a series of longer cyclic JP-4 and JP-8 fuel nozzle valve gumming tests did reveal significant effects of fuel type and temperature on useful fuel nozzle life. These results were correlated by the temperature difference between the breakpoint by visual tube rating (JFTOT) and the test fuel operating temperatures.

SECTION II

INTRODUCTION

For more than 25 years, the primary fuel for USAF gas turbine powered aircraft has been JP-4, a wide-cut distillate with excellent combustion characteristics and low-temperature capability. Typically, its heating value has been over 43.5 MJ/kg (18,700 Btu/lb), its freezing point below 219 K (-65° F), and its aromatic content quite low, around 11 percent by volume. A prime consideration in the definition of JP-4 was that during wartime, a large percentage of domestic crude oil could be converted into this product with minimum delay and minimum impact on other major users of petroleum products.

Conversion from high volatility JP-4 to lower volatility JP-8, which is similar to commercial Jet A-1, as the primary USAF aircraft turbine fuel has been under consideration since 1968. The strong reasons for the change are NATO standardization and reduced combat vulnerability.

Domestic crude oil production peaked in 1971 and has been steadily declining since that time, while demand has continued to increase. Thus, particularly since 1973, the cost and availability of high-grade aircraft turbine fuels has drastically changed. These considerations have spurred efforts to determine the extent to which current USAF fuel specifications can be broadened to increase the yield from available petroleum crudes and, ultimately, permit production from other sources such as coal, oil shale and tar sands.

As a result of the current and projected fuel situation, the USAF has established an aviation turbine fuel technology program to identify JP-4 and/or JP-8 fuel specifications which:

1) Allow usage of key worldwide resources to assure availability.

2) Minimize the total cost of aircraft system operation.

3) Avoid sacrifices of engine performance, flight safety, or environmental impact.

Engine, airframe, logistic, and fuel processing data are being acquired to establish these specifications. This report contributes to the needed data base by describing the effects of fuel property variations on the General Electric F101 engine main combustion system with respect to performance, exhaust emissions, and durability. Similar programs based on the General Electric J79 engine (Reference 1) and the Detroit Diesel Allison TF41 and High Mach engines are also being conducted. Collectively, these programs will provide representative data for the engine classes which are expected to be in substantial use by the USAF in the 1980's.

This report summarizes the results of a 13-month, three-task program which was conducted to clearly identify which fuel properties are important to F101 engine combustor operation, and quantitatively relate fuel property variations to combustor performance, emission, and durability characteristics. Thirteen test fuels provided by the USAF were utilized. Descriptions and properties of these fuels are presented in Section III. In Task I of the program, test planning and preparations were made, based on use of the F101 engine combustion system components and operating characteristics described in Section IV and the three test rigs and procedures described in Section V. In Task II of the program, full-annular combustor performance/emissions/durability tests, low pressure/temperature sector combustor cold day ground tests, and high temperature fuel nozzle fouling/gumming tests were conducted and are summarized in Section VI.A. In Task III of the program, these tests were analyzed to establish the fuel property correlations also presented in Section VI.A and to establish the engine system life predictions presented in Section VI.B.

SECTION III

TEST FUEL DESCRIPTION

A. General Description

Thirteen test fuels were supplied by the USAF for combustion system evaluation in this program. These fuels included a current JP-4, a current JP-8 (which was out of specification on freeze point), five blends of the JP-4, five blends of the JP-8, and a No. 2 diesel. The blends were made up by the USAF to achieve three different levels of hydrogen content: 12, 13, and about 14 percent by weight. Two different types of aromatics were used to reduce the hydrogen content of the base fuels: a monocyclic aromatic (xylene bottoms), and a bicyclic aromatic described by the supplier as a "2040 solvent" (a naphthalene concentrate). A third blend component, used to increase the final boiling point and the viscosity of two blends is described as a Mineral Seal Oil, a predominately (90 percent) paraffinic white oil.

The rationale for the selection of this test fuel matrix was to span systematically the possible future variations in key properties that might be dictated by availability, cost, and the change from JP-4 to JP-8 as the prime USAF aviation turbine fuel, and the use of nonpetroleum sources for jet fuel production. The No. 2 diesel was selected to approximate the Experimental Referee Broad Specification (ERBS) aviation turbine fuel that evolved in the NASA-Lewis workshop on Jet Aircraft Hydrocarbon Fuel Technology (Reference 2).

B. Physical and Chemical Properties

Fuel properties shown in Tables 1, 2, and 3 were determined for the most part by Monsanto Research Corporation under contract to the USAF. Table 4 presents conventional fuel inspection data determined by the Aerospace Fuels Laboratory, WPAFB. These data may be useful for assessing the accuracy of test methods and comparing these fuels to those used in other investigations.

In Table 1, density, viscosity, surface tension, and vapor pressure are presented at a common temperature together with temperature coefficients which were calculated by GE from Monsanto 3-point data. Also shown in Table 1 are the fuel components, hydrogen content determined by the USAF using ASTM Method D3701 (Nuclear Magnetic Resonance), and heating value determined by Monsanto using ASTM Method D240-64. Heating value of these fuels (Q_{net}, MJ/kg) is very nearly a unique function of hydrogen content (H, percent) which can be closely approximated by:

$$Q_{net} = 35.08 + 0.5849\ H \qquad (1)$$

Surface tension is virtually the same for all of the fuels. The other properties are, in general, quite dependent upon fuel components as well as

Table 1. Test Fuel Chemical and Physical Properties.

Fuel No.	Fuel Components		Hydrogen Content % Weight	Heating Value	Density		Viscosity		Surface Tension		Vapor Pressure	
	Base Fuel	Blending Agents		(net) MJ/kg	$\rho_{300\ K}$ kg/m^3	$\frac{\partial\rho}{\partial T} \times 10^4$	$\nu_{300\ K}$ mm^2/S	$\frac{\partial[\ln(\ln(\nu+0.7))]}{\partial[\ln T]}$	$\sigma_{300\ K}$ mN/m	$\frac{\partial\sigma}{\partial T} \times 10^4$	$P_{300\ K}$ kPa	$\frac{\partial[\ln P]}{\partial[\ln T]}$
1	JP-4	-	14.5	43.603	752.7	7.935	0.924	4.112	23.27	10.01	12.04	9.80
2	JP-8	-	14.0	43.210	799.5	7.363	1.849	4.009	25.85	9.53	2.15	6.19
3	JP-8	Gulf Mineral Seal Oil	13.9	43.189	801.2	7.330	2.071	3.985	25.92	9.78	1.97	5.84
4	JP-8	2040 Solvent	12.0	41.947	852.3	7.455	1.809	4.170	27.62	8.24	1.16	7.78
5	JP-8	Xylene Bottoms	13.0	42.724	813.4	7.525	1.428	4.051	26.38	9.50	1.48	10.86
6	JP-8	Xylene Bottoms	12.0	42.129	827.6	7.775	1.160	4.111	26.66	9.47	1.33	10.77
7	JP-8	2040	13.0	42.556	825.2	7.437	1.804	4.103	26.42	6.29	1.38	7.48
8	JP-4	2040	12.0	42.203	829.7	7.832	1.141	4.179	25.22	7.31	7.38	11.60
9	JP-4	2040	13.0	42.629	790.3	7.758	1.028	4.144	23.75	6.94	8.61	11.41
10	JP-4	Xylene	12.0	42.196	808.0	8.150	0.830	4.237	25.21	7.97	6.17	11.31
11	JP-4	Xylene	13.0	42.682	786.5	8.072	0.835	4.328	24.20	5.40	9.08	10.47
12	JP-4	Xylene & GMSO	14.0	43.366	769.6	7.813	1.057	4.027	23.45	7.20	10.25	10.57
13	2-D	-	13.1	42.691	837.2	7.041	3.245	4.315	27.35	6.35	1.58	6.43
Test Method			D3701 (NMR)	D240 (Bomb)	Dilatometer		D445		Capillary Rise		Micro-vapor Pressure Apparatus	

Table 2. Test Fuel Hydrocarbon Type Analyses (Mass Spectroscopy, ASTM Method D2789-71).

Compound Type	Volume Percent in Fuel Number												
	1	2	3	4	5	6	7	8	9	10	11	12	13
Paraffins	62.4	48.4	49.0	29.9	35.6	25.7	39.1	38.4	47.2	33.0	45.8	58.4	44.9
Cycloparaffins	21.4	32.8	31.9	26.4	30.6	21.5	34.1	20.4	25.4	11.2	15.1	20.1	32.7
Dicycloparaffins	5.3	5.4	5.5	1.7	2.3	1.9	1.5	--	--	2.4	3.4	5.0	2.5
Tricycloparaffins	--	0.9	0.8	--	--	--	--	--	--	--	--	--	--
Alkylbenzenes	8.6	7.8	7.4	11.7	28.9	49.9	9.5	12.4	10.7	53.1	34.7	14.8	8.6
Indans and Tetralins	1.5	2.7	3.0	5.7	1.0	--	3.8	4.4	3.0	--	0.6	1.1	6.1
Indenes	--[a]	0.8	0.9	--	--	--	--	--	--	--	--	--	--
Naphthalene	--[b]	0.1	0	--	--	--	--	--	--	--	--	--	--
Naphthalenes	0.8	0.9	1.0	24.6	1.6	1.0	12.0	24.4	13.7	0.3	0.4	0.6	5.2
Acenaphthenes	--	0.04	0.1	--	--	--	--	--	--	--	--	--	--
Acenaphthylenes	--	--	0.01	--	--	--	--	--	--	--	--	--	--
Tricyclicaromatics	--	0.02	0.06	--	--	--	--	--	--	--	--	--	--
Total Aromatics	10.9	12.4	12.5	42.0	31.5	50.9	25.3	41.2	27.4	53.4	35.7	16.5	19.9

[a] If present, included with indans.

[b] If present, included with general naphthalene group.

Table 3. Test Fuel Gas Chromatographic Simulated Distillation (ASTM Method D2887).

Fuel No.	Temperature (K) at Percent Recovered														
	0.5	1.0	5.0	10	20	30	40	50	60	70	80	90	95	99	99.5
1	299	-	342	362	381	392	407	426	451	472	491	510	525	-	552
2	383	-	432	446	459	472	481	494	504	515	530	547	561	-	589
3	383	-	431	443	455	472	489	498	510	526	543	566	579	-	609
4	391	-	434	446	463	475	486	499	503	512	524	542	557	-	590
5	393	-	412	418	434	443	456	469	485	501	514	534	549	-	582
6	377	-	411	413	423	433	439	444	461	480	501	526	543	-	601
7	391	403	430	442	458	470	481	493	504	515	526	539	556	579	592
8	297	306	353	368	392	422	452	471	487	503	515	530	545	569	574
9	293	303	341	360	387	406	434	456	476	492	506	526	541	570	578
10	292	300	335	356	384	406	415	430	438	452	475	502	519	545	559
11	285	292	332	353	377	399	414	431	445	465	487	509	523	548	560
12	285	292	332	354	381	404	423	447	471	495	521	565	583	611	623
13	371	393	441	460	482	500	516	531	546	563	580	601	623	658	679

Table 4. Test Fuel Conventional Inspection Data.

Fuel Number	1	2	3	4	5	6	7	8	9	10	11	12	13
Gravity, ^{o}API	54.1	43.7	43.3	32.8	40.5	37.5	38.3	37.3	44.3	41.6	46.4	50.3	35.6
Freezing Point, K	209	228	241	224	225	220	228	229	219	<215	<215	238	247 (1)
Existent Gum, mg/100 ml	1.4	0.2	2.6	1.2	0.8	1.6	0.0	0.8	1.0	1.8	1.2	1.0	-
Luminometer Number	73	53	55	17	38	18	34	24	37	24	37	65	-
Viscosity, mm^2/s at 239 K	2.68	9.54	(solid)	10.18	5.90	4.09	9.62	4.39	3.59	-	-	-	-
Total Sulphur, wt %	0.04	0.06	0.07	0.05	0.06	0.05	0.07	0.02	0.04	0.03	0.04	0.04	0.18
Smoke Point, mm	32.5	26.5	-	12.5	20.5	13.5	17.0	12.0	15.0	13.0	18.0	25.0	18.0
Aromatics, volume % (D1319)	12.2	15.1	15.4	44.7	41.6	63.4	31.8	45.3	30.6	57.5	40.1	20.3	21.4
Olefins, volume %	1.1	1.6	1.2	1.8	2.7	2.2	2.1	0.5	0.7	1.1	0.8	1.1	1.2
Flashpoint, K	-	324	327	333	319	314	329	-	-	-	-	-	335
Distillation (D86)													
Initial Boiling Point, K	338	444	436	449	423	423	445	340	339	346	339	341	444
10%	375	462	460	465	441	431	462	385	379	399	389	380	488
20%	388	469	469	473	447	435	470	406	394	409	402	395	-
50%	425	487	494	494	471	450	492	472	448	425	426	435	531
90%	499	526	549	526	522	514	528	516	506	471	492	541	585
Endpoint	524	552	572	547	544	541	546	544	539	512	520	573	615

(1) Pour Point

hydrogen content.

Table 2 shows hydrocarbon type analyses by mass spectroscopy (ASTM Method D2789) and Figure 1 shows a comparison of total aromatics determined by mass spectroscopy (from Table 2) and by fluorescent indicator adsorption (ASTM Method D1319 from Table 4). It is apparent that there is a consistent bias between the results of the two methods, with the mass spectrometer yielding the more favorable (lower aromatic) results, particularly with the JP-8 based fuels. Aromatic type (monocyclic or bicyclic) does not appear to affect this bias.

Figure 2 shows the variation in fuel aromatic content (by mass spectroscopy) with hydrogen content for these fuels. There is, of course, strong negative correlation, but both base fuel type and aromatic component structure affect this relationship.

Table 3 lists the Gas Chromatographic Simulated Distillation (ASTM Method D2887) data for each of the test fuels. Among the blended fuels, those containing the Mineral Seal Oil (Fuels 3 and 12) had the highest final boiling points. Figure 3 shows the complete simulated distillation curves for the three basic fuels and the variation in initial and end points for all of the blends. Points worthy of note are:

1) All of the JP-4 blends had initial boiling points (IBP's) essentially identical to that of the base JP-4 fuel (about 300 K).

2) All of the JP-8 blends and the diesel fuel had IBP's essentially identical to that of the base JP-8 fuel (about 385 K).

3) All of the JP-8 blends had final boiling points (FBP's) not greatly different from that of the base JP-8 fuel (about 590 K).

4) The JP-4 blends had a broad range of FBP's, spanning those of the JP-8 blends (about 585 $\pm$ 35 K).

5) The diesel fuel had a significantly higher FBP (about 680 K).

Figure 4 compares fuel volatility characteristics as measured by gas chromatography and conventional distillation (ASTM Method D86). It is apparent that gas chromatography significantly extends the apparent boiling range in both directions; the IBP and 10 percent recovery temperatures are lowered while the 90 percent recovery and FBP temperatures are raised. Temperature differences of up to about 70 K are obtained by the two procedures.

C. Thermal Stability Characteristics

The thermal stability of test fuels was determined by the Jet Fuel Thermal Oxidation Tester (JFTOT) described in ASTM Method D3241. The actual thermal stability is given in terms of the breakpoint which is

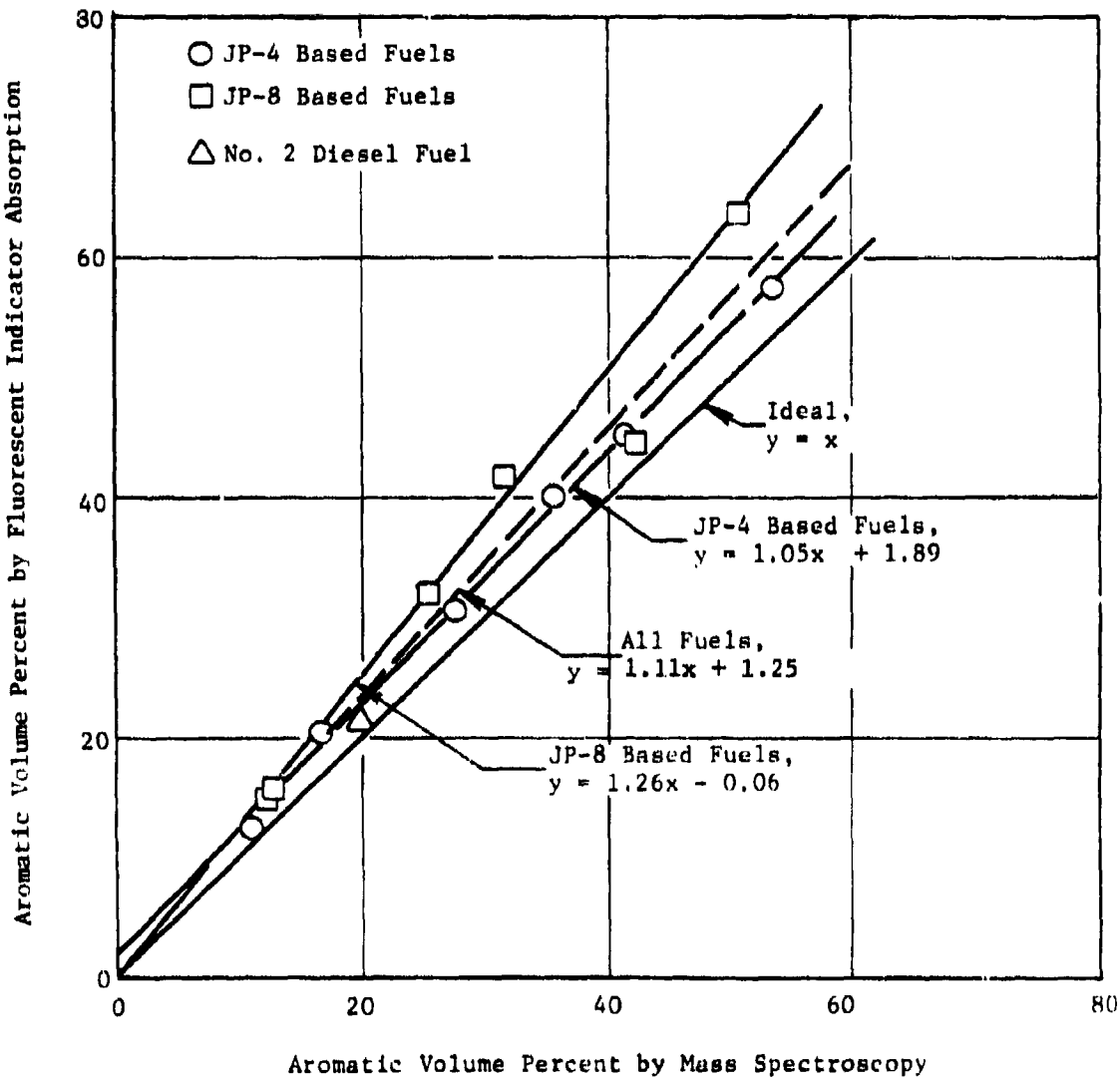

Figure 1. Comparison of Fuel Aromatic Content by Two Test Methods.

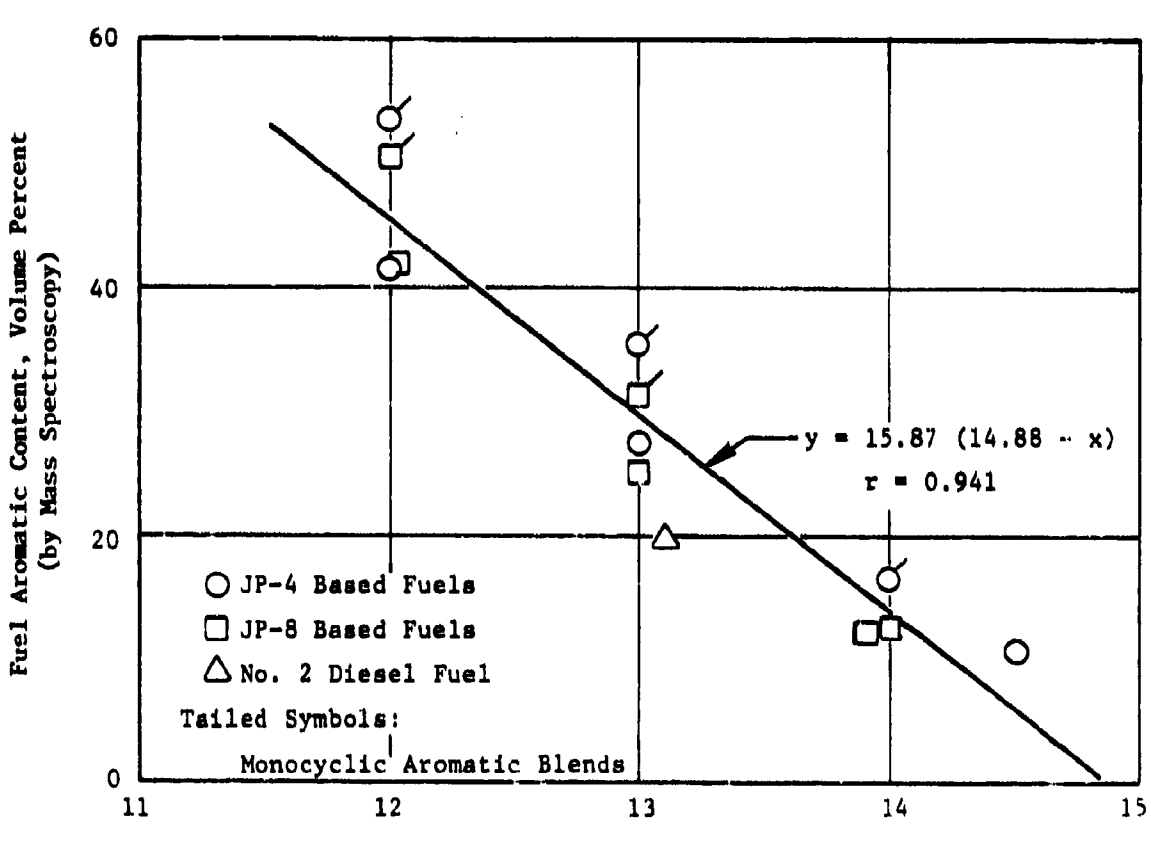

Figure 2. Variation of Fuel Aromatic Content with Hydrogen Content.

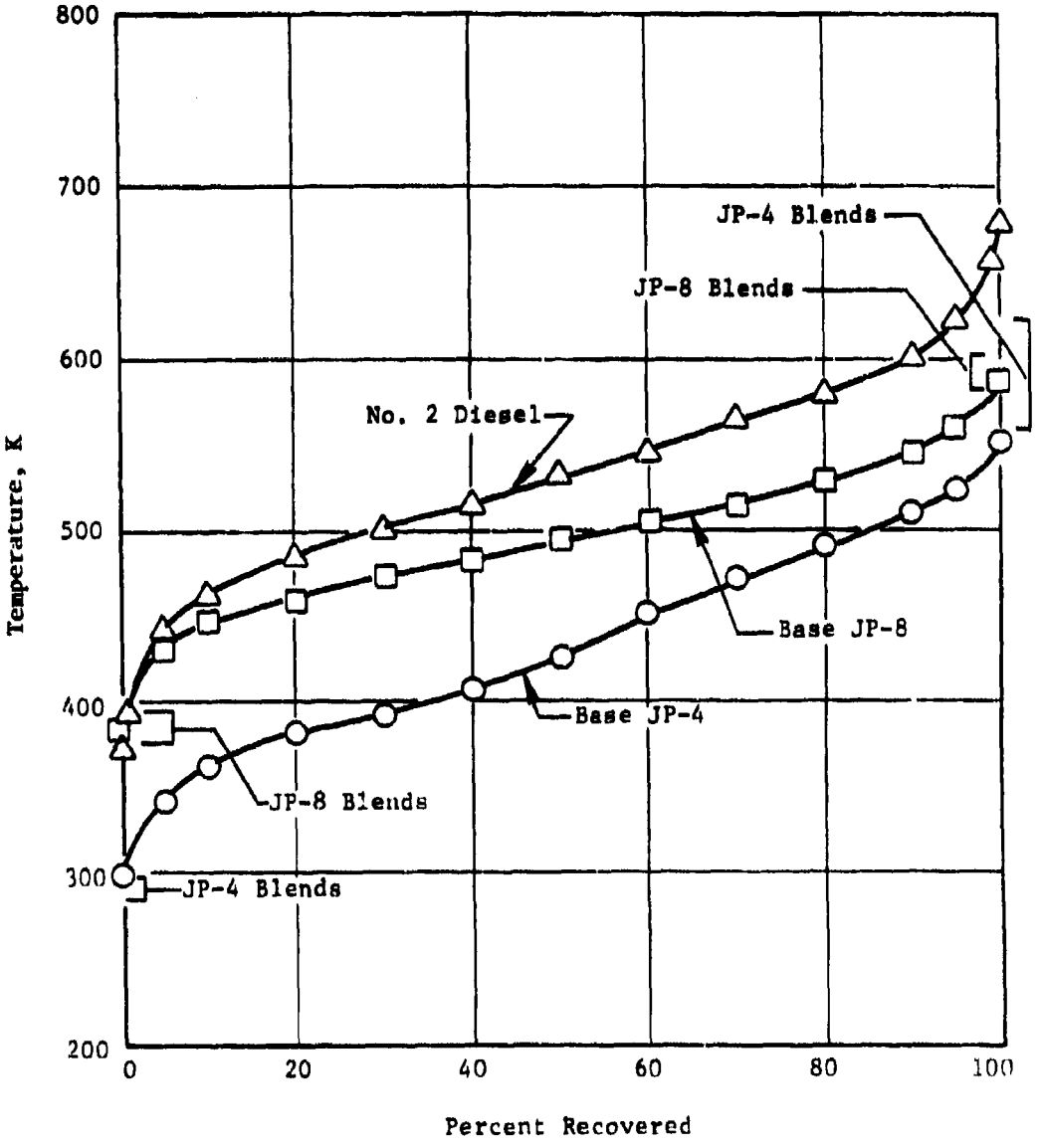

Figure 3. Comparison of Gas Chromatographic Simulated Distillation Characteristics of the Test Fuels.

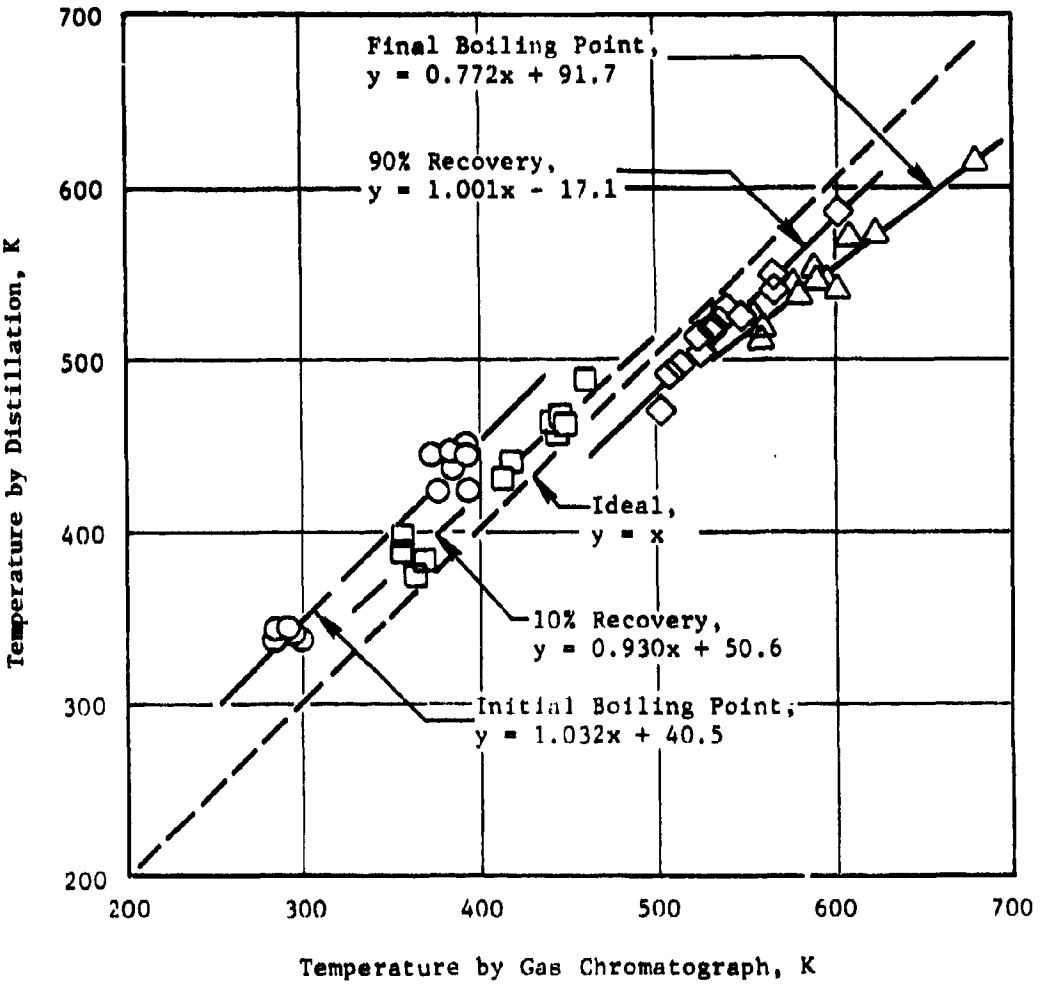

Figure 4. Comparison of Fuel Recovery Points by Distillation and Gas Chromatography.

defined as the highest (metal) temperature at which the fuel "passes" by both filter pressure drop and tube rating. A fail on pressure drop is 25 mm Hg pressure drop or more in less than 150 minutes. A "fail" on the tube is a color code of 3 or darker as described in the ASTM procedure. In practice, the fuel is tested first at the estimated breakpoint, then depending upon whether it fails or passes, it is rerun at a temperature 10 K lower or higher until the breakpoint is established.

1. Original Test Fuels

Table 5 shows the JFTOT data that were provided by the USAF for the original fuels. Occasionally, anomalous or indeterminate results were obtained, and sometimes the fuel sample (one gallon) was expended before the breakpoint was determined. For these reasons, breakpoints are not shown for all of the test fuels. Anomalous results are those in which two or more tests of the same fuel at the same temperature showed both a "pass" and a "fail". Indeterminate results are those in which a fuel passes or fails by both tube color and pressure drop, but no additional tests were run at higher or lower temperature to determine by which criterion it would fail first. Generally, it appears that the repeatability and reproducibility of the breakpoint is greater than the difference in thermal stability of the base fuels and their blends.

Table 6 is an attempt to assign ratings to the fuels, despite some apparent lack of precision in the test results. The JP-8 base fuel appears to be significantly more stable than the JP-4 base fuel in these tests. However, later cooperative tests described in the following section indicated less difference. The addition of Mineral Seal Oil has no apparent effect on the thermal stability. This would be expected, since it is a high purity white oil, suitable for medicinal and food applications. The addition of both types of aromatics appears to have little or no adverse effect on thermal stability.

2. Long Time Cyclic Test Fuels

Because the originally planned fuel nozzle fouling tests did not yield definitive results, the scope of the program was increased to include a series of long-time cyclic tests using current JP-4 and JP-8 fuels. In order to establish more precisely the thermal stability breakpoint ratings of the two test fuels used in these long-time tests, a cooperative program was established to test the fuels in other laboratories. The following organizations participated in this work:

Texaco, Inc.
Port Arthur, Texas

Exxon Research and Engineering Co.
Linden, New Jersey

Table 5. Fuel Sample Thermal Stability Test Results (ASTM Method D3241).

Fuel No.	Breakpoint, K	Mode of Failure
1	<518, 518	Tube
1	533	Tube
1	528	Tube
1	538, 543	Tube
2	<563	ΔP
2	548, 553	Tube
2	558	Tube
2	563	Tube
2	593, 603	Tube
2	603	Tube
2	553	Tube
2	573	Tube
3	568	Tube and ΔP
3	583	Tube
3	573	Tube
4	<573	Indeterminate
4	>533, <573	Indeterminate
4	573	Tube
5	<533	Indeterminate
5	<533	Tube
5	>583	Indeterminate
6	513	ΔP
6	>583	Indeterminate
6	>553, <583	Tube
7	>573	Indeterminate
8	<523	ΔP
8	553	Tube
9	>513, <533	Tube
9	533	Tube
10	553	Tube
11	543, 553	Tube and ΔP
12	543	Tube

Table 6. Estimated Thermal Stability Ratings of Test Fuels (ASTM Method D3241).

Fuel No.	Breakpoint Range, K	Estimated Rating, K
1	<518-548	533 ± 15
2	548-603	576 ± 28
3	568-583	576 ± 8
4	>533-<573	553 ± 20
5	<533->583	558 ± 25
6	513-583	548 ± 35
7	>573	573
8	<523-553	538 ± 5
9	>513-533	523 ± 10
10	553	553
11	543-553	548 ± 5
12	543	543

Alcor, Inc.
San Antonio, Texas

The Dupont Co.
Tulsa, Oklahoma

Naval Research Laboratory
Washington, D.C.

Ashland Petroleum Co.
Catlettsburg, Kentucky

Aero Propulsion Laboratory
Wright-Patterson Air Force Base, Ohio

Representative samples of the fuels were taken from the line supplying the rig, while testing was in progress, using well-rinsed metal sample cans. At about the same time, Air Force personnel took samples of their retain fuels, for testing by the same laboratories.

The data secured from the cooperative program on thermal stability testing of the JP-4 and JP-8 base fuels are shown in Table 7. The data are surprising in that they indicate the JP-8 samples from GE are much lower quality than the JP-8 samples from the Air Force, although they all represent the same fuel. This might imply that the JP-8 degraded in storage at GE, or the samples were contaminated. However, both theories appear invalid since the JP-4 samples from both sources showed excellent agreement, and the JP-4 at GE was stored and sampled in the same manner as the JP-8.

Based on the above program, the JP-8 would be rated lower than the JP-4, and the fuel nozzle valve tests would show a reverse correlation with the laboratory results. However, the D3241 data appear abnormal in that they all showed failure by pressure drop on the samples from GE. A review of all of the original data submitted by the cooperative laboratories showed that if pressure drop failures were ignored, all of the JP-8 samples from GE would show breakpoints in the range of 553 to 593 K based on the visual tube ratings only (Table 8), and the JP-8 would rate better than the JP-4. This would then correlate quite well with the fuel nozzle valve test results which are described in Section VI.A.10.

In view of these findings, it appears that the development of pressure drop in the JFTOT has no relationship to the performance of hot fuels in close-fitting valves, and it is suggested that thermal stability ratings based on JFTOT tube deposits alone may correlate better with the performance of engine hardware with hot fuels.

D. Computed Combustion Parameters

Table 9 shows several fuel parameters which were computed from the physical and chemical properties for use in conducting the combustion

Table 7. Results of All Cooperative D3241 Thermal Stability Tests

Test Laboratory	Samples from GE Supply				Samples from WPAFB Supply			
	JP-4		JP-8		JP-4		JP-8	
	Break-point, K	Failure Mode	Break-point, K	Failure Mode	Break-point, K	Failure Mode	Break-point, K	Failure Mode
Texaco	<538	Tube	<533	ΔP	538	Tube	<583	Tube
Exxon	523	Tube & ΔP	<533	ΔP	-	-	-	-
Alcor	513	ΔP	493	ΔP	533	ΔP	563	Tube
du Pont	<533, 533	ΔP, ΔP	<533	ΔP	538	Tube & ΔP	573	ΔP
NRL	533	Tube & ΔP	503	ΔP	<533, 538	Tube & ΔP	>543, <558	Tube
Ashland	538	Tube & ΔP	523	ΔP	533	ΔP	568	Tube
WPAFB	533	Tube	<553	ΔP	-	-	-	-
Averages*	(5)533 (5)528	Tube ΔP	(3)506	ΔP	(2)538 (4)536	Tube ΔP	(3)561 (1)573	Tube ΔP

*( ) = Number of Definitive Ratings used in averaging.

Table 8. Results of Cooperative D3241 Thermal Stability Tests of JP-8 Fuel.

Laboratory	Breakpoint by Visual Tube Rating Only, K	
	Samples From GE	Samples From WPAFB
Texaco	>573	<583
Exxon	>533, <568	-
Alcor	>563, <583	563
du Pont	>593	583
NRL	>513, <563	>543, <558
Ashland	>553, <573	568
WPAFB	573	-

Table 9. Test Fuel Combustion Parameters

Fuel Number	n, Hydrogen-to-Carbon Atom. Ratio	f_{st}, Stoichiometric Fuel-Air Ratio g/kg	T_{st}, Stoichiometric Flame Temperature at Takeoff, K	$(W_f)/(W_f)_{JP-4}$ Relative Required Fuel Flow Rate	$(SMD)/(SMD)_{JP-4}$ Relative Fuel Spray Droplet Size
1	2.021	67.50	2592	1.000	1.00
2	1.940	68.02	2596	1.0091	1.19
3	1.924	68.12	2597	1.0096	1.21
4	1.625	70.19	2613	1.0395	1.29
5	1.780	69.09	2605	1.0206	1.18
6	1.625	70.19	2613	1.0350	1.18
7	1.780	69.09	2605	1.0246	1.23
8	1.625	70.19	2613	1.0332	1.14
9	1.780	69.09	2605	1.0228	1.06
10	1.625	70.19	2613	1.0333	1.09
11	1.780	69.09	2605	1.0216	1.05
12	1.940	68.02	2596	1.0055	1.03
13	1.796	68.98	2604	1.0214	1.40

tests and analyses of the results.

Fuel hydrogen-to-carbon atom ratio (n) was used in the exhaust gas sample calculation. It was calculated directly from the hydrogen weight percent (H) by the relationship:

$$n = \frac{11.915\ H}{100 - H} \tag{2}$$

and ranged from 1.625 to 2.021 as hydrogen content increased.

Stoichiometric fuel-air ratio (f_{st}) was used to calculate comparative adiabatic flame temperatures. It was calculated from the fuel hydrogen-to-carbon ratio (n) by the relationship:

$$f_{st} = \frac{0.0072324\ (1.008\ n + 12.01)}{(1 + 0.25\ n)} \tag{3}$$

which assumes that the fuel is CH_n, the air is 20.9495 volume percent oxygen, and the air has a molecular weight of 28.9666. For the test fuels the stoichiometric fuel-air ratio ranged from 67.50 to 70.19 g fuel/kg air as hydrogen content decreased.

Stoichiometric flame temperature was used in analyses of NO_x emissions. It was calculated at takeoff operating conditions (T_3 = 829 K, P_3 = 2.718 MPa) using a standard equilibrium-thermodynamics computer program (Reference 3) and ranged from 2592 to 2613 K as hydrogen content decreased.

Relative required fuel flow rate was used in all combustion tests to adjust the JP-4 fueled engine cycle operating fuel flow rates for the reduced heating values of the other fuels. The factor is merely the ratio (Q_{JP-4}/Q) and ranged from 1.000 to 1.0395.

Relative fuel spray droplet size was used in analyses of the low power emissions and relight performance. The F101 combustion system employs airblast atomizing fuel nozzles, so Rizkalla and Lefebvre's correlation parameter for this type atomizer (Reference 4) was used to estimate the relative fuel spray droplet Sauter Mean Diameter (SMD) at idle conditions from the test fuel density (ρ), surface tension (σ) and viscosity (ν) by the empirical relationship:

$$SMD = \left\{ 521\ \sigma^{0.5}\ \rho^{0.75} \left\{ \frac{1+W_\ell/W_a}{V_a} \right\} + \left\{ 0.037 \left[\nu/\rho \right]^{0.85} \left[\sigma\rho \right]^{1.2} \right\} \left\{ 1+W_\ell/W_a \right\}^2 \right. \tag{4}$$

In this relationship, W_ℓ/W_a is the ratio of fuel flow to airflow in the atomizer and V_a is the air velocity in the atomizer. For the F101 combustor at idle operation conditions, these two values were approximately

0.5 and 100 m/s, respectively, for all fuels. As shown in Table 9, none of the blending agents appreciably changed the predicted relative droplet size of the base fuel. However, the JP-8 based fuels are predicted to produce mean droplet sizes about 20-30 percent larger than those of the JP-4 fuel. Further, the diesel fuel is expected to produce mean droplet sizes about 40 percent larger than those of the JP-4 fuel.

SECTION IV

F101 ENGINE COMBUSTION SYSTEM DESCRIPTION

A. Overall Engine Description

The F101 engine is an advanced, light-weight, fully-augmented turbofan engine. A cross-sectional view is shown in Figure 5. This engine completed product verification (PV) testing in 1976. The F101 has a two-stage fan and a nine-stage compressor. The fan/compressor pressure ratio is approximately 26.8:1 at standard day sea level takeoff conditions. The combustion system employs a very short annular liner. The turbine has a single stage air cooled high pressure turbine, coupled directly to the compressor and a two-stage low pressure turbine which drives the fan. The engine has a fully modulating mixed flow augmentor.

Mixing of the core and fan air streams is accomplished with a 26 lobed daisy mixer. The augmentor has 2 circumferential V gutters at the hub and tip connected by 28 radial (sloped) V gutters. The radial V gutters are located in the mixer chutes which define the hot core stream flowpath. At lightoff conditions, only the inner ring gutter is fueled. At higher power conditions, the entire core stream (entire flameholder) is fueled. At maximum augmentation, the fan stream is also fueled. The tailpipe has a convectively cooled liner and the engine has a variable area converging-diverging exhaust nozzle.

B. Combustion System Description

The F101 main combustor is a short length annular design which features machined ring liners, a step diffuser and two-stage counter rotating swirlers which permit the use of a low pressure fuel injection system. A photograph of the combustor assembly is shown in Figure 6 and the flowpath showing the major components of the combustion system is illustrated in Figure 7. Compressor discharge air is delivered to the combustor through the compressor outlet guide vanes (OGV's) which are part of the one-piece diffuser - OGV casting. The OGV's provide structural support, so that there are no compressor rear frame struts in the flowpath. After passing through the vanes, the velocity of the flow is reduced in the diffuser. At the end of the diffuser, the flow is essentially dumped and divides into three streams, to supply the dome and the two combustor passages.

A portion of the flow enters the combustion zone through two-stage counter rotating swirlers (twenty total) which provide fuel atomization as well as flow recirculation and flame stabilization in the primary zone. Additional dome air enters through perforations in the structure to provide impingement cooling of the splash plates. The splash plates serve as transitions from the circular swirler exits to the annular dome. The splash plate impingement cooling air also provides for hot side film cooling for the dome structure. Figure 8 is a view looking forward into a dome.

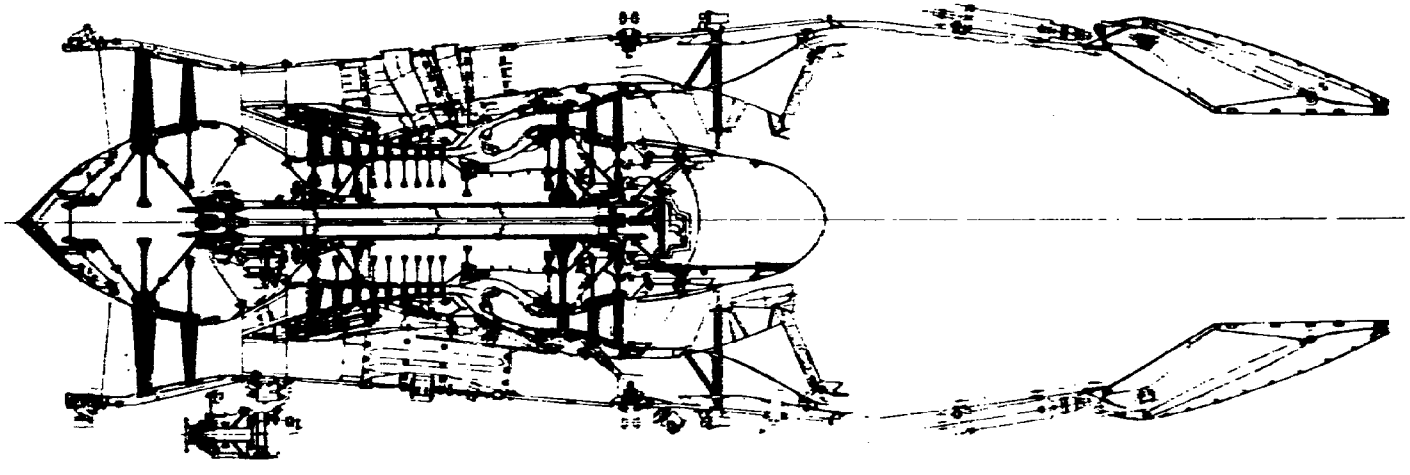

Figure 5. General Electric f101 Augmented Turbofan Engine.

Figure 6. F101 Engine Combustor Assembly.

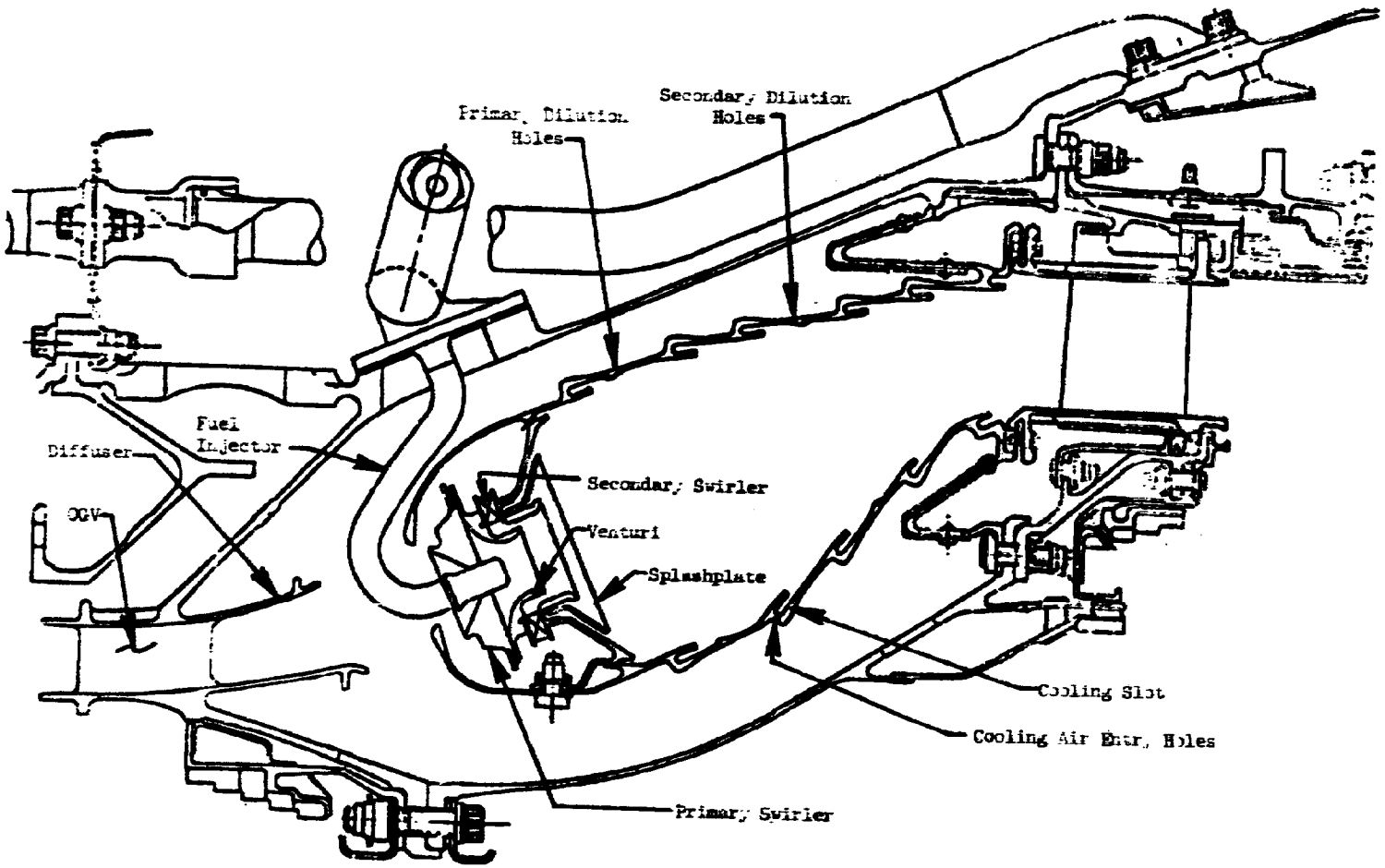

Figure 7. F101 Engine Combustor Flowpath.

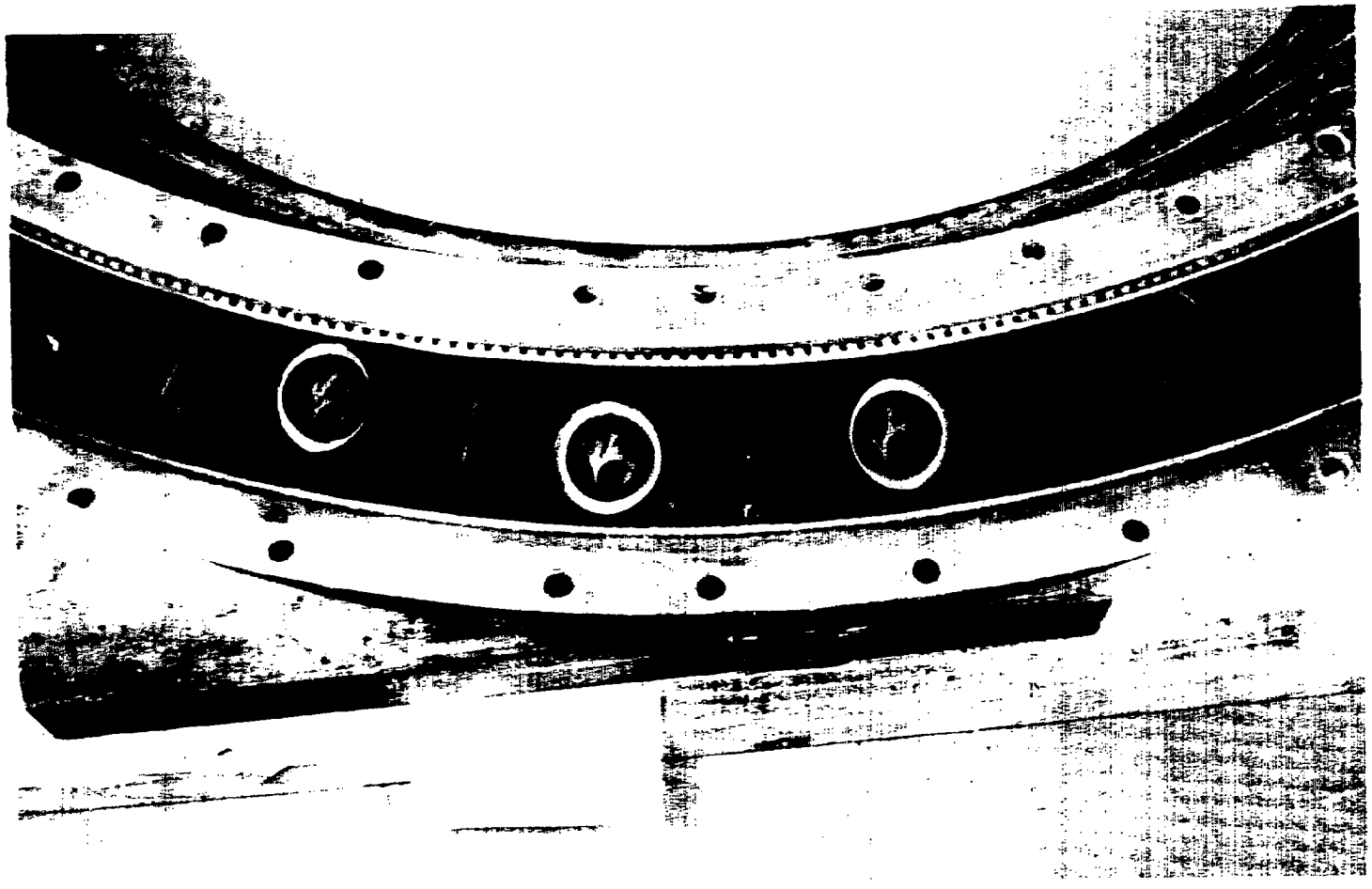

Figure 8. F101 Combustor Dome Details, Aft Looking Forward.

Approximately half of the airflow delivered to the liners is used for film cooling. The remainder is introduced through primary and secondary dilution holes. The primary flow enters the reaction zone and serves to stabilize and complete the combustion process. The secondary air mixes with the hot gases from the primary zone to provide the desired turbine temperature profile.

The combustor liners are each machined from individual forgings of Hastelloy X. A series of slots are machined into the walls to provide film cooling. The slots are fed with cooling air through a series of perforations in the upstream side of the slots. Figure 9 illustrates the cooling scheme. The combustor contains a bolted joint which secures the dome to the inner cowl and the inner liner. The dome, outer liner, and outer cowl are a single welded assembly. Provisions for differential expansion between the fuel injectors and the combustor are provided by allowing the primary swirler to move in both the radial and circumferential directions with respect to the secondary swirler.

The combustor is mounted at the downstream end of each liner. The liner is bolted to the inner combustion casing through a structure which also provides support for turbine nozzle cooling air filtering screens. The outer liner is mounted through a similar screen structure which is trapped in the casing assembly by a bolted flange. Leaf seals prevent leakage of air between the combustor and high pressure turbine nozzle. The combustor casing has provisions for two externally removable igniters, borescope inspection ports and bosses for the 20 fuel injectors.

The fuel system consists of 20 individual injectors and a fuel manifold. Each fuel injector has a valve mounted externally to the combustor casing, a dual wall stem and tip with four ports which spray fuel radially outward from the swirl cup centerline. A photograph of the nozzle and a cross-sectional drawing are shown in Figure 10. The double wall minimizes heat transfer to prevent fuel coking and to reduce thermal gradients in the outer structural elements. The smallest fluid passages in the injector tip are the four ports which are 0.140 cm diameter each. A fuel flow schedule versus pressure drop for a single injector is shown in Figure 11.

C. Combustor Operating Conditions

The combustor must operate over a wide range of fuel flow, inlet airflow, temperature and pressure. Table 10 presents the combustor operating parameters at several important steady state operating conditions as well as for the ground starting conditions. At these conditions, fuel effects on combustor performance, emissions and combustor and turbine life are of particular interest.

The combustion system must also provide for starting over a wide range of altitude conditions. Figures 12 and 13 present altitude relight windmilling flow conditions (W_c and P_3) for both an open exhaust nozzle and a closed nozzle. For the purposes of this program, the open nozzle condi-

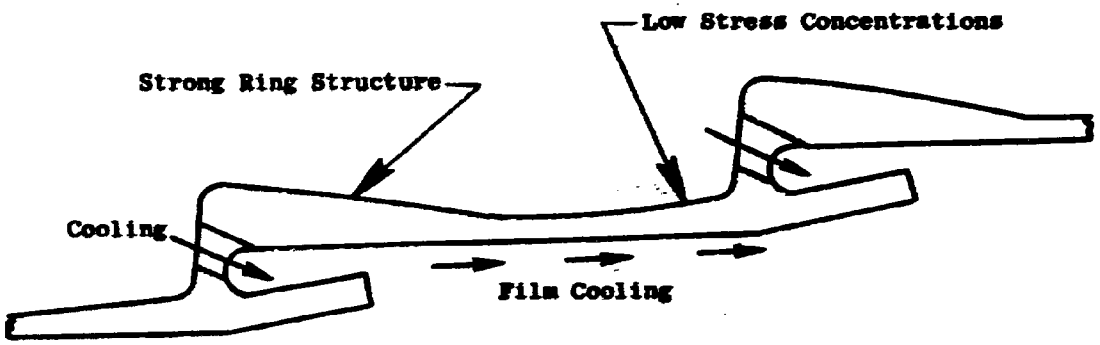

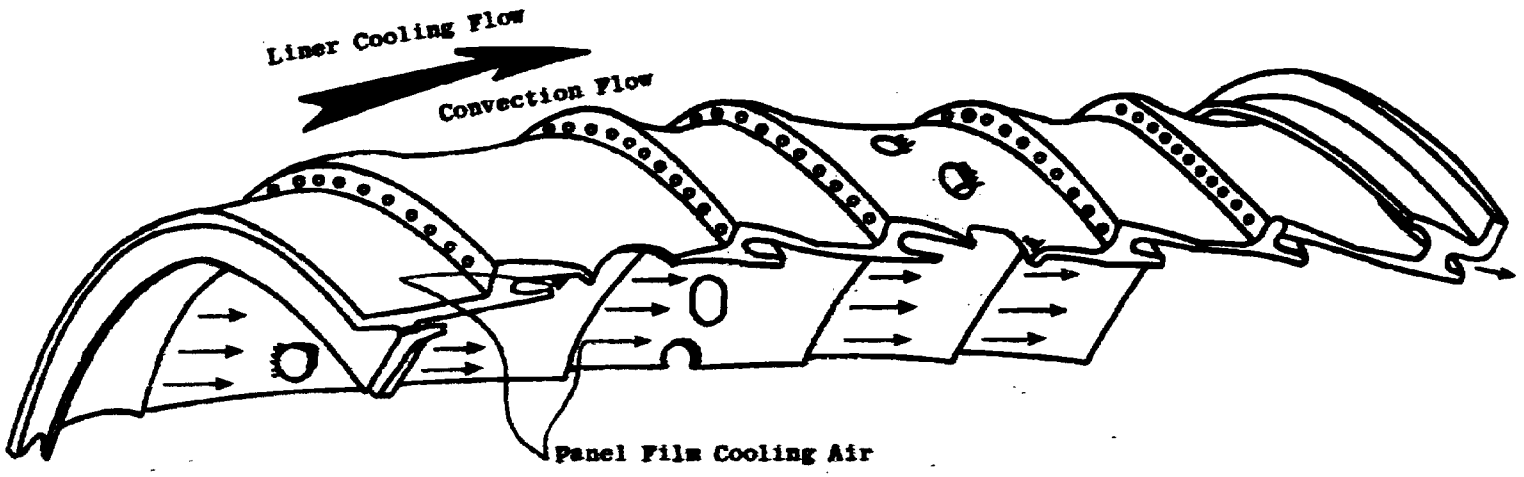

Figure 9. F101 Combustor Liner Cooling Scheme.

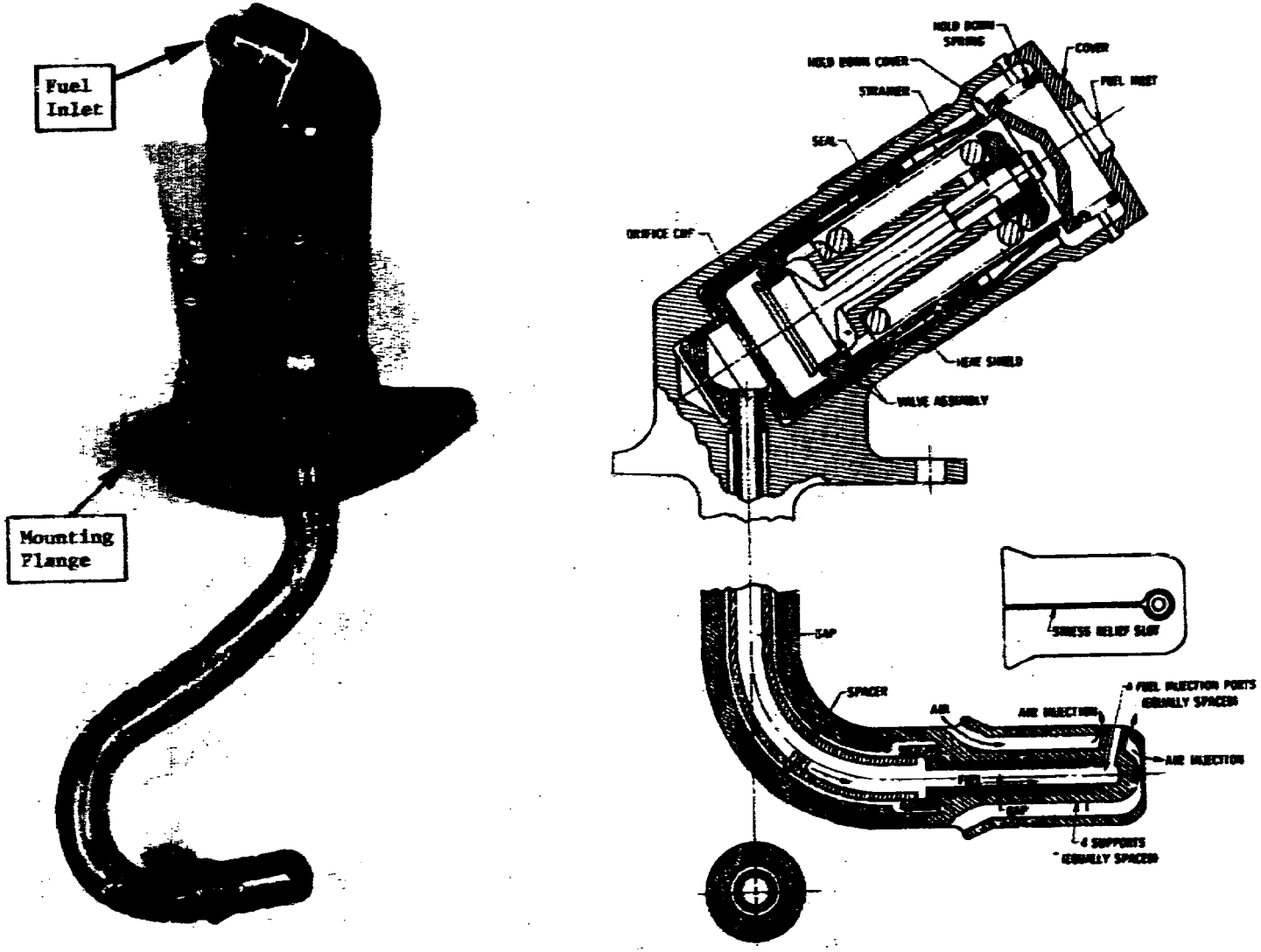

Figure 10. F101 Engine Fuel Nozzle.

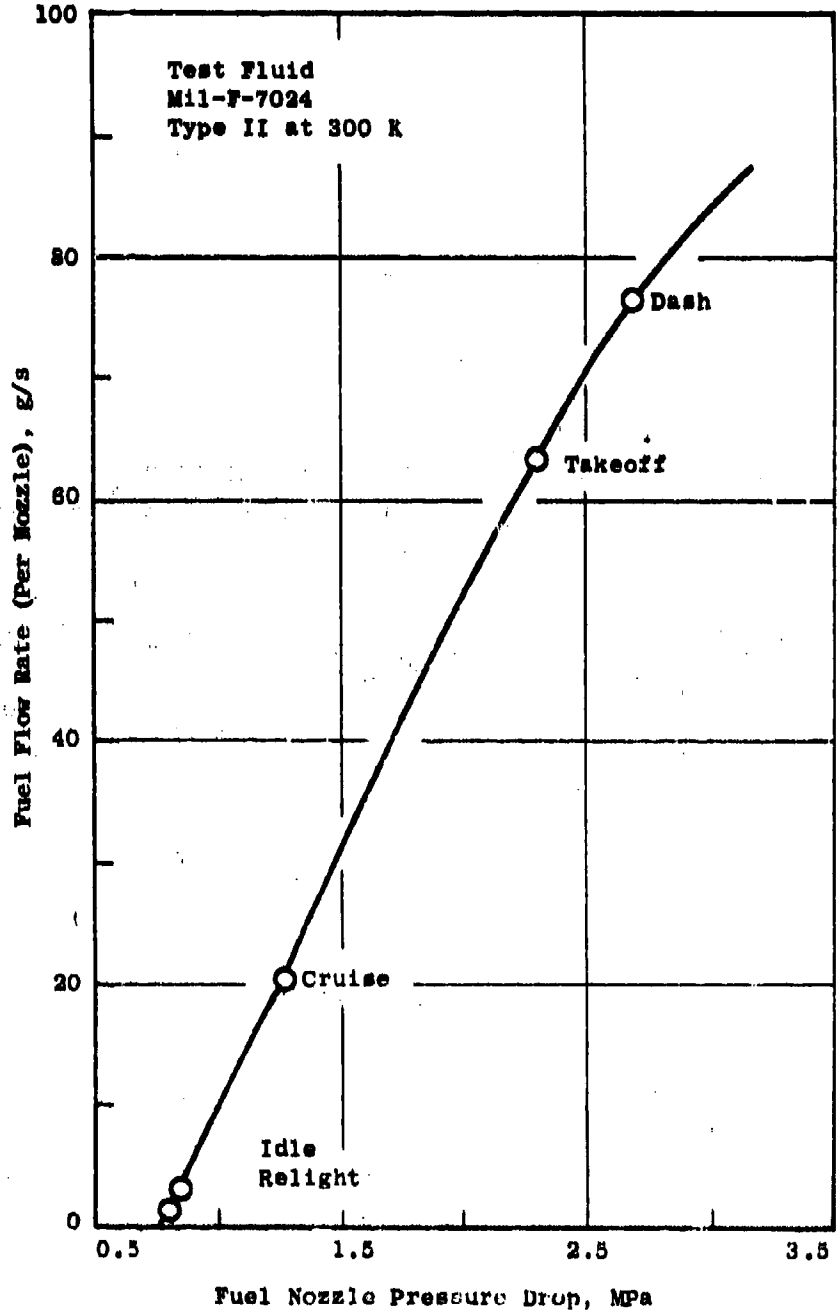

Figure 11. F101 Engine Fuel Nozzle Flow Characteristic.

Table 10. F101 Engine Combustor Operating Conditions.

	Flight Altitude km	Flight Mach No.	W_3 Total Airflow kg/s	W_c Combustor Airflow kg/s	W_f (JP-4) Fuel Flow kg/s	T_3 Inlet Total Temperature, K	P_3 Inlet Total Pressure, MPa	f_4 (JP-4) Fuel-Air Ratio, g/kg	T_4 Exit Total Temperature, (Ideal) K	V_r (1) Reference Velocity m/s
Ground Idle	0	0	10.43	8.62	0.121	468.2	0.390	14.0	998.8	18.3
Takeoff	0	0	52.57	43.27	1.265	828.7	2.718	29.2	1772.0	23.5
Subsonic Cruise	8.53	0.74	20.64	16.96	0.408	677.6	0.977	24.0	1495.9	21.0
Dash	0.06	0.95	66.45	54.84	1.530	849.3	3.425	27.9	1747.1	24.1
Ground Start(2)	0	0	~1.15	~1.15	0.038(3)	$\geq$239	~0.101	~43.8(3)	-	$\geq$4.8

(1) Based on W_3 and A_r = 1618 cm^2

(2) 2500 rpm, typical starting speed

(3) Minimum engine fuel flow schedule (normal)

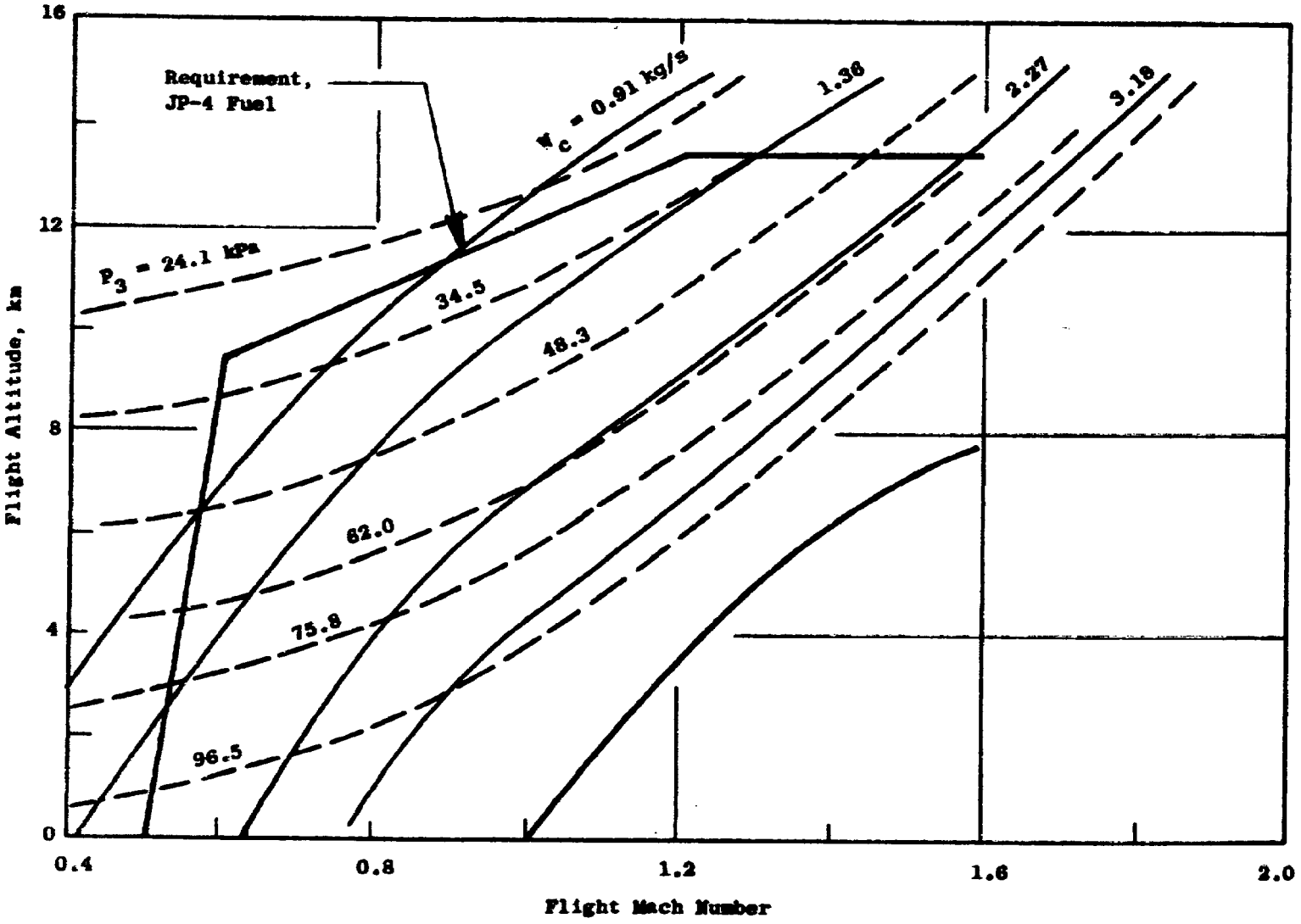

Figure 12. F101 Engine Open Exhaust Nozzle Altitude Windmilling/Relight Requirement Map.

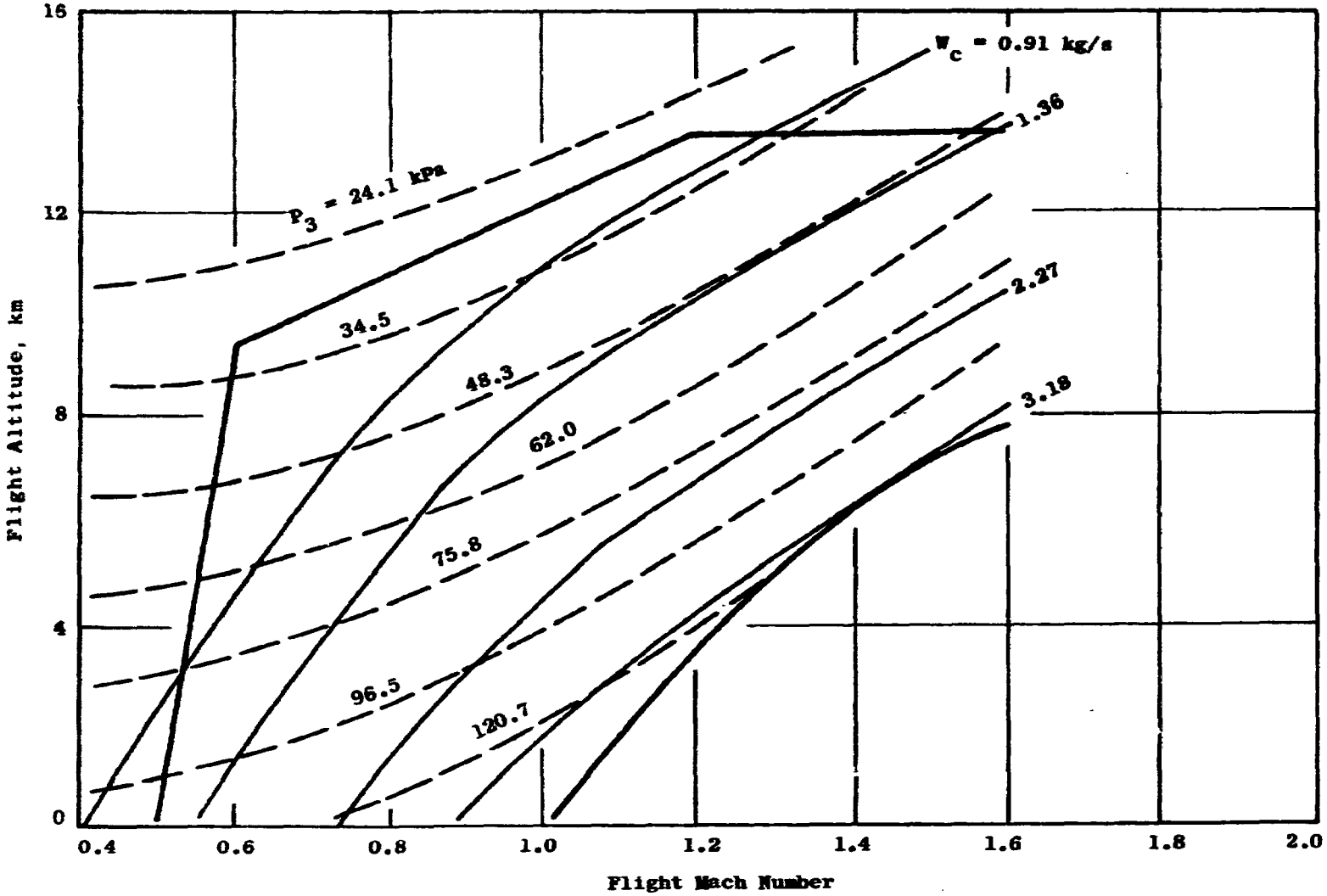

Figure 13. F101 Engine Closed Exhaust Nozzle Altitude Windmilling/Relight Requirement Map.

tions which are more severe relative to combustor relight were used. During actual altitude starting, the control commands the nozzle to the closed stop position.

D. Combustor Life Experience

The mechanical durability of the combustor (using current JP-4 fuel) has been determined during an extensive factory engine test program. Following are brief descriptions of several types of engine tests that are conducted with the test hours and cycles that have been accumulated on individual combustors.

PV Endurance Testing

Each standard endurance test consists of 1.7 operating hours, including operation at the low altitude-high Mach penetration condition. One PV combustor accumulated the following operating time and cycles during 2 such back-to-back endurance tests:

Total Time	373 hours
Time at Max T_4 (Over Approx. 1672 K)	145 hours
Thermal Cycles	2155
Starts	292

PV Low Cycle Fatigue (LCF)

The LCF test consists of a 13-minute sea level cyclic test. Each cycle has 2 rapid throttle movements (bursts) to maximum temperature conditions from idle and 5 minutes at maximum power. A shutdown and motoring is included between each cycle. An example of the time accumulated on a single PV combustor is:

Total Time	350 hours
Time at Max T_4	72 hours
Thermal Cycles	3330
Starts	1685
LCF Cycles	1634

PV Life Cycle Testing

The life cycle test consists of a 30-minute sea level cyclic test which

includes 2 idle-to-maximum power bursts. Twenty-two minutes of each cycle is spent at maximum T_4 conditions to evaluate the effects of long hold time on the hot section. One PV combustor accumulated the following experience in this type of testing:

Total Time	643 hours
Time at Max T_4	375 hours
Thermal Cycles	2155
Starts	1021
Life Cycles	929

Status

The various PV combustors evaluated to date exhibited distress in the same general regions regardless of which of the above tests were conducted. Figure 14 indicates the location and type of distress typically observed. In the dome region, erosion was experienced on the edges of the splash plate and in the dome structure between cups. The cooling slots adjacent to the liners between cups also were eroded.

The last panel of the inner liner suffered from local hot spots which eventually become holes typically 0.13 to 0.25 cm in diameter. These holes are located axially downstream of the corners of the splash plate.

The outer liner distress is also experienced at the downstream end of the last two panels. Axial cracks of approximately 2.5 cm in length were observed locally after endurance testing.

At the completion of 2 back-to-back engine PV endurance tests (approximately 370 hours), the 20 fuel injectors typically meet the new flow calibration characteristics and there is no plugging or blocking of the flow passages or exit ports.

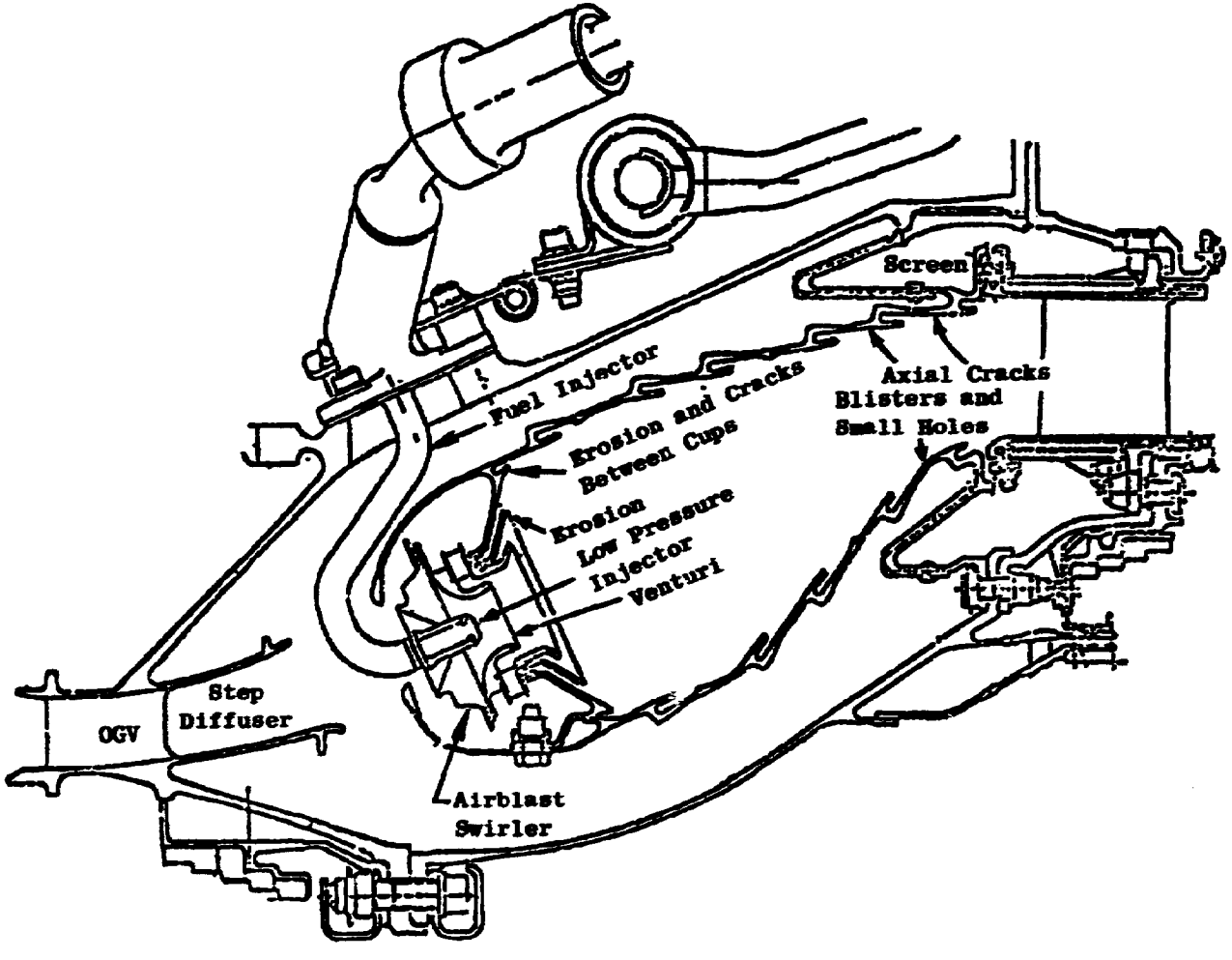

Figure 14. Typical Engine Combustor Distress.

SECTION V

APPARATUS AND PROCEDURES

All combustor and fuel nozzle testing in this program was conducted in specialized facilities at the General Electric, Evendale, Ohio, Plant, using apparatus and procedures which are described in the following sections. Combustor performance/emissions/durability tests were conducted in a high pressure/temperature full-annular combustor rig which is described in Section V.A. Atmospheric pressure tests were also conducted in this facility, chiefly to determine combustor discharge temperature distribution. In parallel, carbon deposition tests were conducted in a single-cup facility described in Section V.B, and combustor cold day ground start/altitude relight tests were conducted in a low pressure/temperature 54-degree sector rig which is described in Section V.C. Also in parallel, high temperature fuel nozzle fouling tests were conducted in a small specialized test rig described in Section V.D. Special fuel handling procedures used in all of these tests are described in Section V.E. Finally, procedures employed in analyses of these data are described in Section V.F.

A. Performance/Emissions/Durability Tests

High pressure/temperature combustor rig tests were conducted at simulated F101 engine idle, cruise, takeoff, and dash operating conditions with each of the fuels to determine the following characteristics:

1) Gaseous emissions (CO, HC, and NO_x).

2) Smoke emissions.

3) Liner temperatures.

Combustion exit temperature profile and pattern factor were also determined in this rig, but with atmospheric discharge pressure. Thus, a large part of the total data was obtained in these tests using apparatus and procedures described in the following sections.

1. Full Annular Combustor Test Rig Description

These tests were conducted in Cell A3, located in Building 303 of the Evendale Plant. This test cell is equipped with all of the ducting, fuel and air supplies, controls, and instrumentation required for conducting combustor high pressure/temperature tests. High pressure air is obtained from a central air supply system, and a gas-fired indirect air heater is located adjacent to the test cell. For the full-annular combustor rig, F101 engine idle and cruise operating conditions were exactly duplicated. Takeoff and dash operating conditions were exactly duplicated with respect to temperature, velocity, and fuel-air ratio, but pressure and flow rates

were reduced to 46 percent and 36 percent, respectively, of the true engine conditions to be within the facility airflow capability.

The High Pressure Combustor Test Rig, shown in Figures 15 and 16, simulates the engine flow path from the compressor outlet guide vane (OGV) to the first-stage turbine stator vanes. Since turbine bleed air is not included in the rig simulation, its effect on liner airflow or backside cooling is not present in this rig. As shown in Figure 15, the test rig inlet flange bolts up to a plenum chamber in the test cell. Figure 16 shows the discharge instrumentation for the higher pressure tests. Figure 17 shows the exit instrumentation for atmospheric testing. In this testing, a rotating rake with four instrumentation stations is traversed around the annulus to obtain a detailed exit temperature profile.

2. High Pressure Test Instrumentation

A summary of the important combustor operating, performance and emission parameters which were measured or calculated in these tests is shown in Table 11. Airflow rates were measured with standard ASME orifices. Fuel flow rates were measured with calibrated turbine flowmeters corrected for the density and viscosity of each test fuel at the measured supply temperature. Combustor inlet temperature and pressure were measured with plenum chamber probes.

Combustor outlet gas samples were measured as shown in Figure 18 and 19. Each rake contained five impact pressure/gas sample probes located on radial centers of area. As shown in Figure 19, the impact probe elements were manifolded to three heated gas sample transfer lines leading out of the test cell to the gas composition measurement instruments. Rakes A and B were connected through selector valves to a smoke measurement console (Figure 20) and rakes D, E, I, and H were connected to a gas analysis console (Figure 21). Rakes B and G were connected to record exit pressure.

The General Electric smoke measurement console shown in Figure 20 contains standard test equipment which fully conforms to SAE ARP 1179 (Reference 5). Smoke spot samples are collected on standard filter paper at the prescribed gas flow rate and at four soiling rates spanning the specified quoted soiling rate. The spot samples are later delivered to the data processing area, where the reflectances are measured and the SAE Smoke Number is calculated.

The gaseous emissions measurement console shown in Figure 21 is one of several assembled to General Electric specifications for CAROL systems (Contaminants Analyzed and Recorded On-Line) that conform to SAE ARP 1256 (Reference 6). This system consists of four basic instruments: a flame ionization detector (Beckman Model 402) to measure total hydrocarbon (HC) concentrations, two nondispersive infrared analyzers (Beckman Models 865 and 864) for measuring carbon monoxide (CO) and carbon dioxide (CO_2) concentrations, and a heated chemiluminescent analyzer (Beckman Model 951) for measuring oxides of nitrogen (NO or NO_x = NO + NO_2) concentrations.

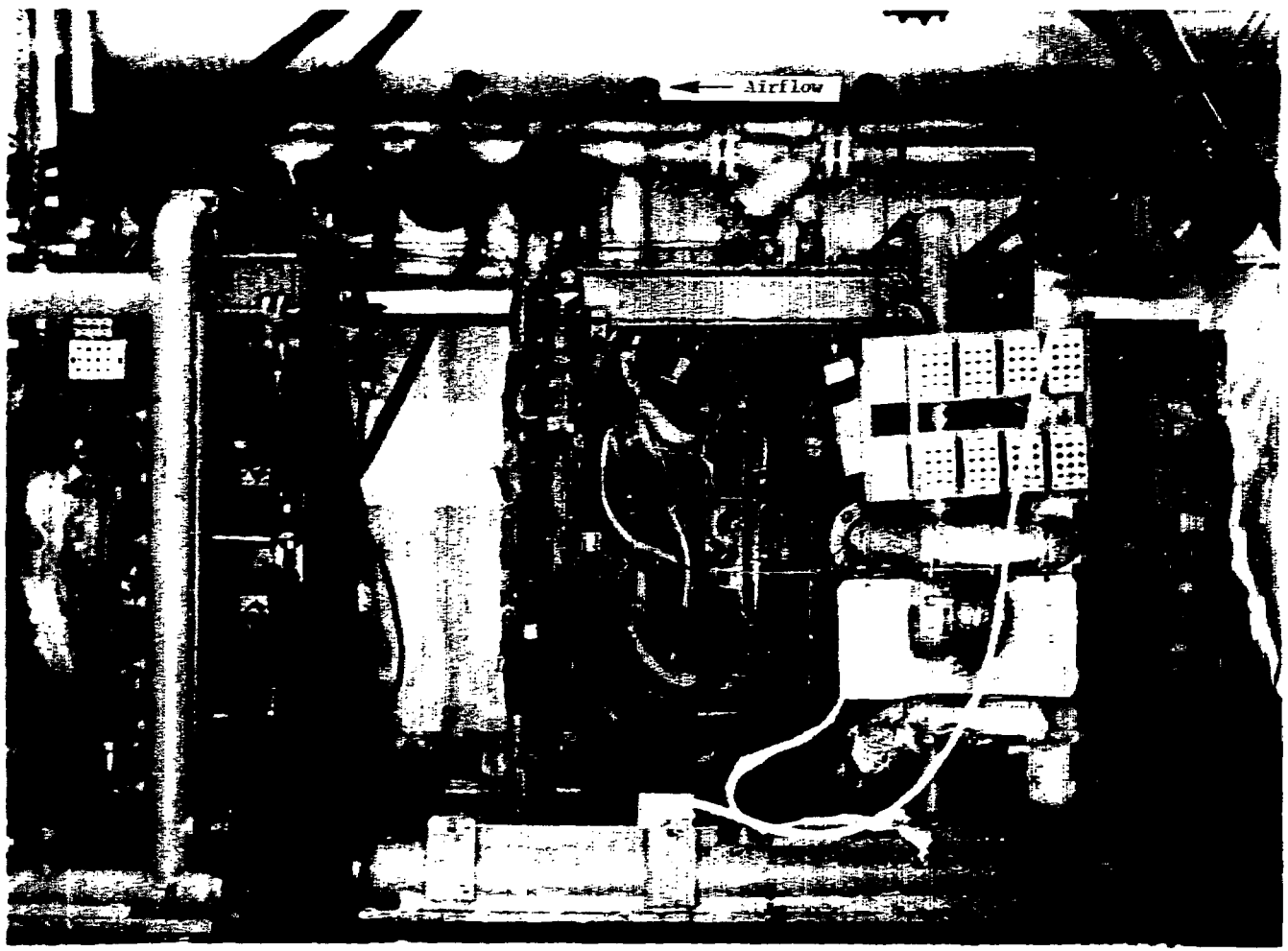

Figure 15. Full Annular F101 Combustor Test Rig.

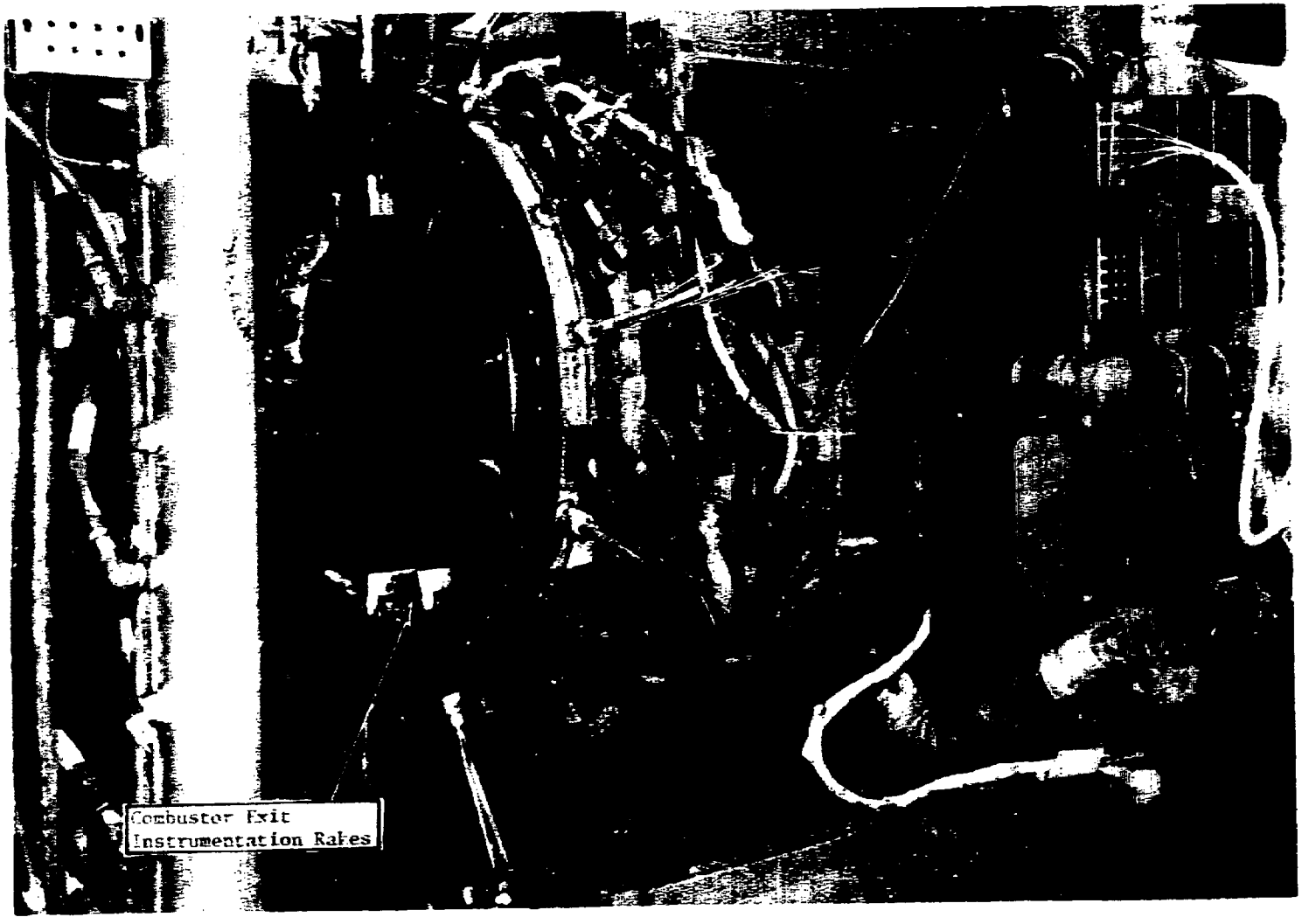

Figure 16. Rear Quarter View of Full Annular Combustor Test Rig.

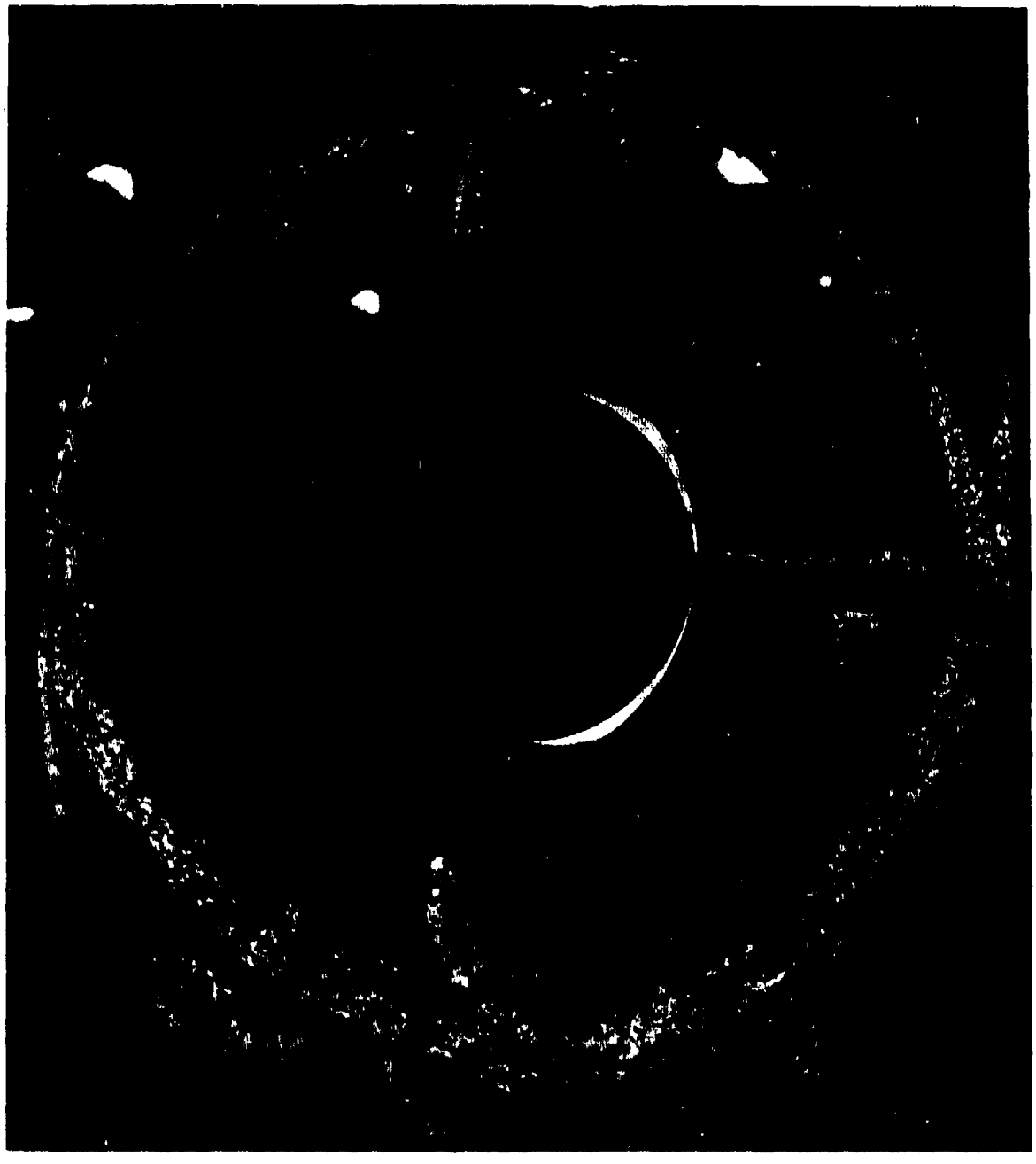

Figure 17. Full Annular Combustor Test Rig Undergoing Atmospheric Testing.

Table 11. Summary of Measured and Calculated Combustor Parameters in Full Annular Combustor Tests.

Parameter	Symbol	Units	Test		Measurement/Calculation Method
			High Pressure	Atmospheric	
Inlet Total Pressure	P_3	MPa	X	X	Average of Measurements from 3 Impact Probes
Exit Total Pressure	P_4	MPa	X	X	Average of Measurements from 2 Impact Probes
Total Pressure Loss	$\Delta P_T/P_3$	%	X	X	$100\ (P_3 - P_4)/P_3$
Combustor Airflow	W_c	kg/s	X	X	ASME Orifice
Fuel Flow	W_f	g/s	X	X	Turbine Flowmeter Corrected for Density and Viscosity
Metered Fuel-Air Ratio	f_m	g/kg	X	X	W_f/W_c
Inlet Air Humidity	h_3	g/kg	X		Dewpoint Hygrometer
Inlet Total Temperature	T_3	K	X	X	Average of Measurements from 3 Probes
Exit Total Temperature	T_4	K		X	Average of Measurements at 1200 Locations
Pattern Factor	PF	-		X	$(T_{4max} - T_{4avg})/(T_{4avg} - T_3)$
Profile Factor	PrF	-		X	$(T_{4Rm,max} - T_3)/(T_{4avg} - T_3)$
Reference Velocity	V_r	m/s	X	X	$V_r = W_3/P_3Ar = 0.001777\ (W_cT_3/P_3)$
Combustor Metal Temperature	T_L	K	X		33 Metal Thermocouples
Fuel/Temperature	T_f	K	X	X	Thermocouple in Fuel Nozzle Manifold
Fuel Nozzle Pressure Drop	ΔP_f	MPa	X	X	Pressure in Fuel Nozzle Manifold $(P_f - P_4)$
Fuel Nozzle Effective Area	A_{fc}	mm^2	X	X	$A_{fc} = W_f/20\sqrt{2g\rho_f\Delta P_f}$
Combustor Exit Smoke Number	SN_4	—	X		Manifolded 10-Point Gas Sample & ARP 1179 (Ref. 5)
Smoke Emission Index	EI_s	g/kg	X		GE Correlation at SN_4 and f_s (Appendix E)
Engine Exit Smoke Number	SN_B	—	X		GE Correlation at EI_s and f_g (Appendix E)
Gas Sample Fuel-Air Ratio	f_s	g/kg	X		Manifolded 20 Point Gas Sample & ARP 1256 (Ref. 6)
CO Emission Index	EI_{CO}	g/kg	X		Manifolded 20 Point Gas Sample & ARP 1256 (Ref. 6)
HC Emission Index	EI_{HC}	g/kg	X		Manifolded 20 Point Gas Sample & ARP 1256 (Ref. 6)
NO_x Emission Index	EI_{NO_x}	g/kg	X		Manifolded 20 Point Gas Sample & ARP 1256 (Ref. 6)
Gas Sample Combustion Efficiency	η_{gs}	%	X		$\eta_{gs} = 100 - [(EI_{HC}/10.0) + (EI_{CO}/82.8)]$ (Ref. 7)
Thermocouple Combustion Efficiency	η_{tc}	%		X	$\eta_{tc} = 100\ [\text{Ideal Fuel-Air Ratio, @ } (T_{4avg} - T_3)]/f_r$ (Ref. 7)

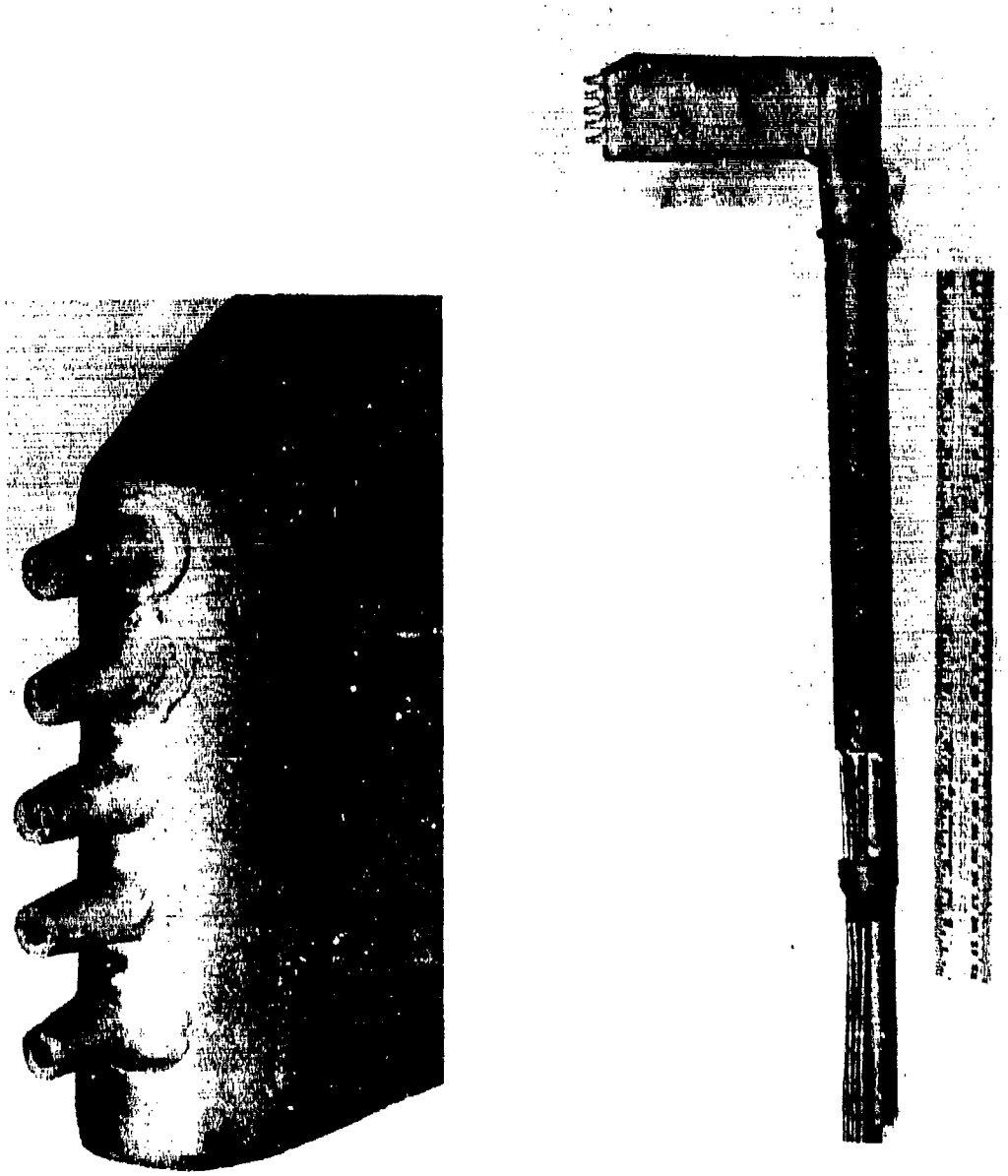

Figure 18. F101 Gas Sample Rake.

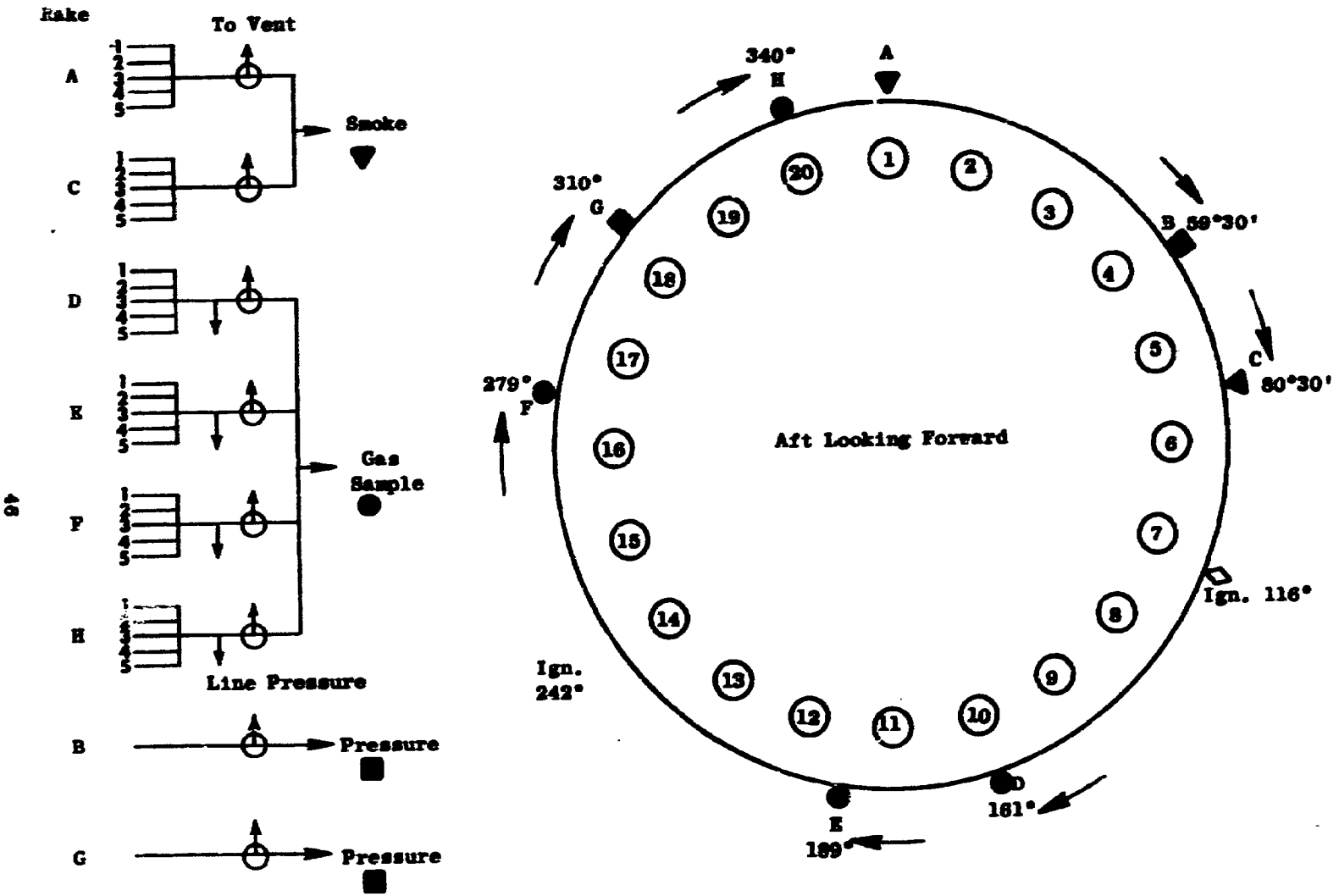

Figure 19. High Pressure Test Combustor Exit Instrumentation.

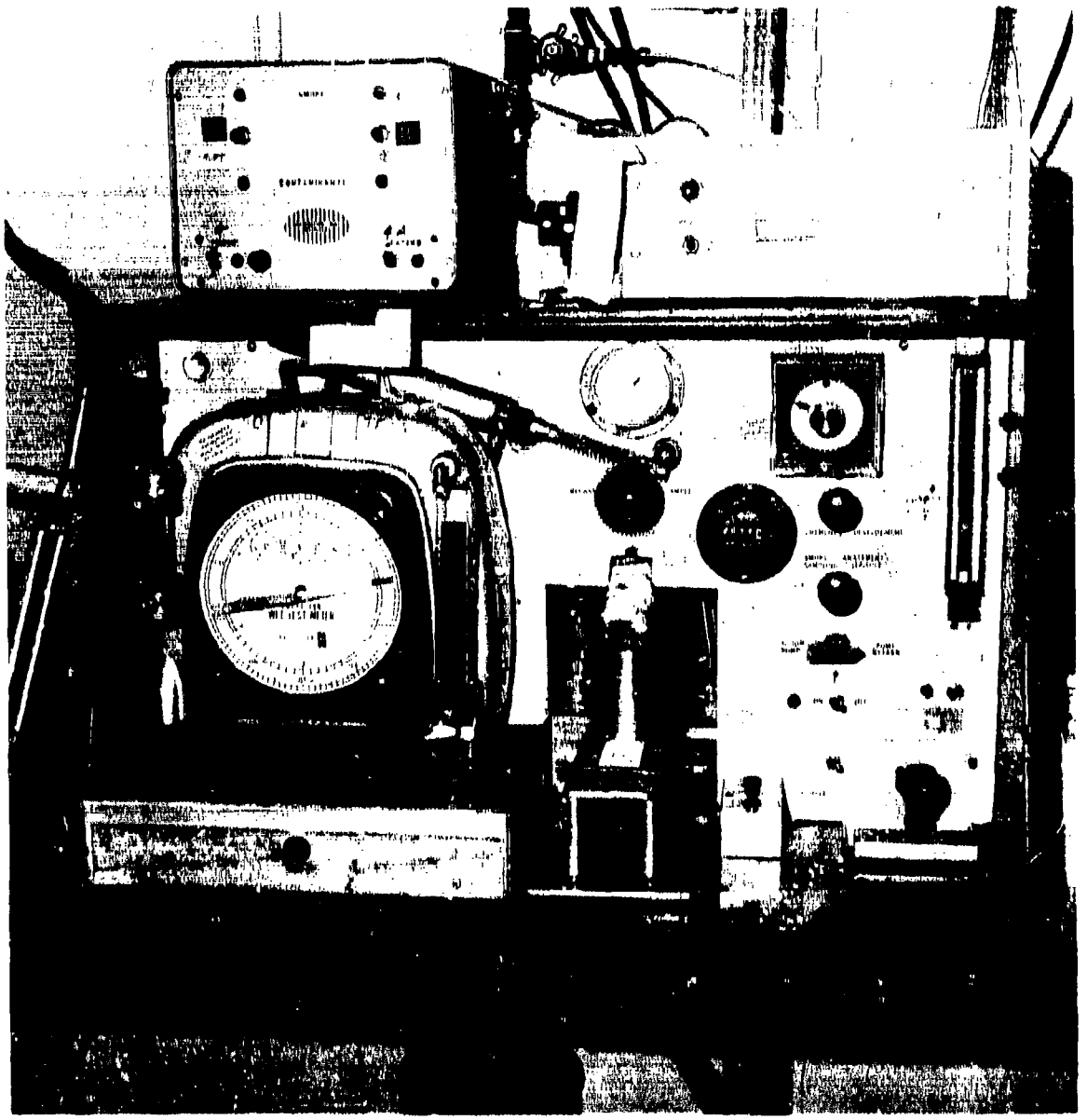

Figure 20. General Electric Smoke Measurement Console.

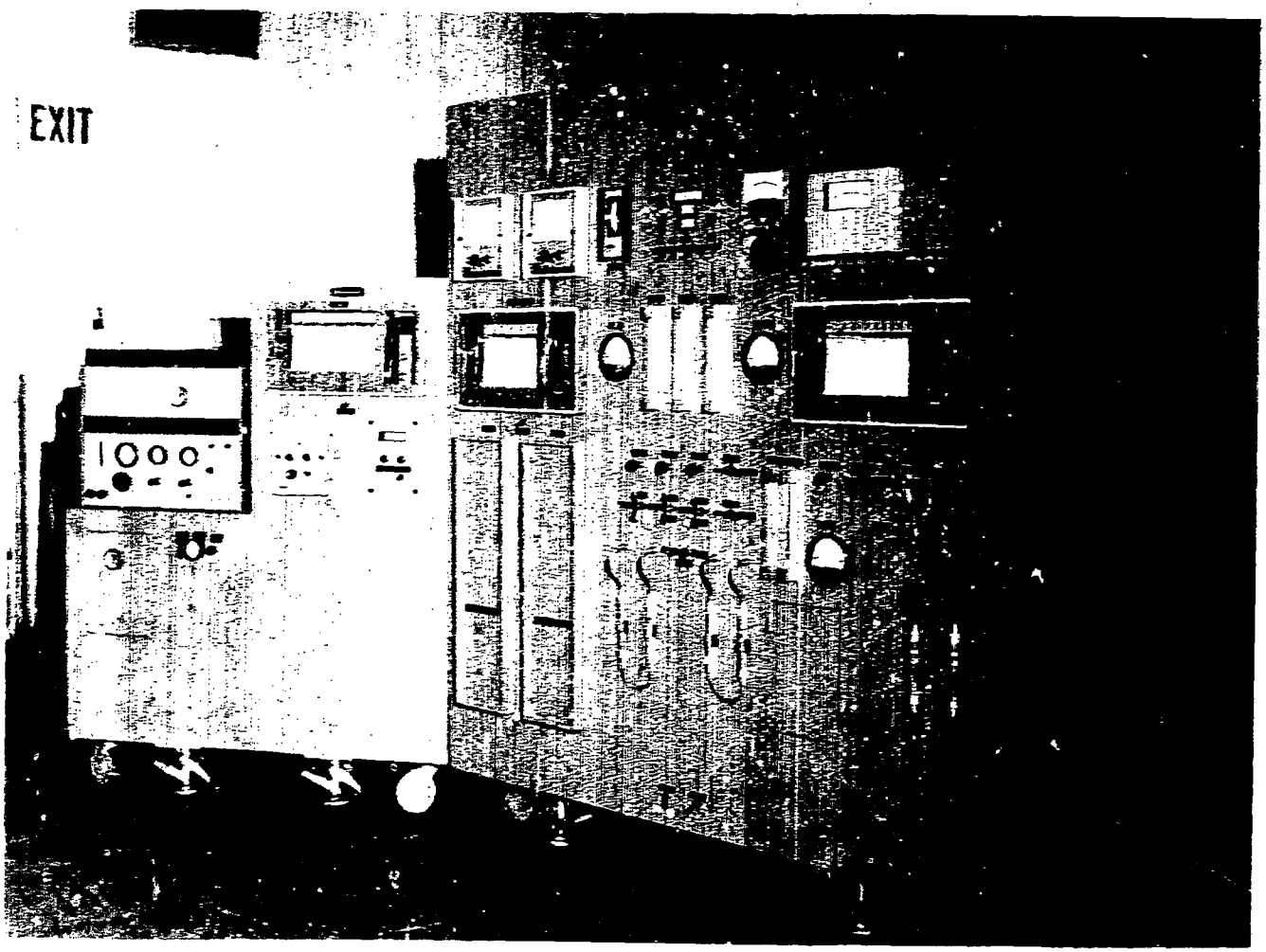

Figure 21. General Electric Emissions Measurement System, CAROL II.

Each of the instruments are fully calibrated with certified gases before and after each test run, and periodically during test, zero and span checks are made. Readings from the instruments are continuously recorded on strip charts and hand-logged on test and calibration points for later calculation of concentration, fuel-air ratio, and emission indices using a computer program which incorporates the equations contained in ARP 1256.

Combustor liner temperature was measured by an array of 33 thermocouples located on the inner and outer liner as shown in Figure 22. This instrumentation pattern was selected to provide detailed data in the vicinity of the known hottest regions of the combustor. Table 12 presents the specific thermocouple locations. Figures 23, 24, and 25 show the actual liner thermocouple installations on the liners.

3. High Pressure Test Procedures

A total of 13 high pressure rig tests were run, one for each test fuel. Each test was conducted to the eight-point test schedule shown in Table 13, steady-state operating, performance and emissions measurements were obtained at simulated engine idle, cruise, takeoff, and dash operating conditions. At each of these simulated engine operating conditions, data were recorded at two nominal fuel-air ratios; 80 and 100 percent of the engine cycle value corrected for the test fuel heating value.

4. Atmospheric Discharge Test Instrumentation

For atmospheric discharge tests, the test rig was installed in the west stand of Test Cell A3 and an external traverse ring was attached to the combustor housing exit flange. An array of five-element thermocouple rakes was attached to the ring, which was remotely actuated, to obtain a detailed survey of the combustor exit temperature distribution. Four rakes mounted 90 degrees apart were used, and a survey consisted of rotating the ring in a clockwise direction, aft looking forward, through an angle of 90 degrees. However, the ring was also rotated in the counterclockwise direction on one test point in a run, so in each quadrant readings from two different rakes were available. These readings could then be compared to insure that each rake was reading correctly.

5. Atmospheric Discharge Test Procedure

Thirteen atmospheric pressure rig tests were run, one for each fuel. Each fuel was tested according to the six point test schedule as shown in Table 14, except in order to avoid exceeding the temperature capability of the exit thermocouple rakes, it was necessary to limit fuel-air ratio at takeoff and dash. Point 6, which is the same as point 5, except for the direction of rotation of the traverse, was taken only on selected fuels since no significant differences were noticed.

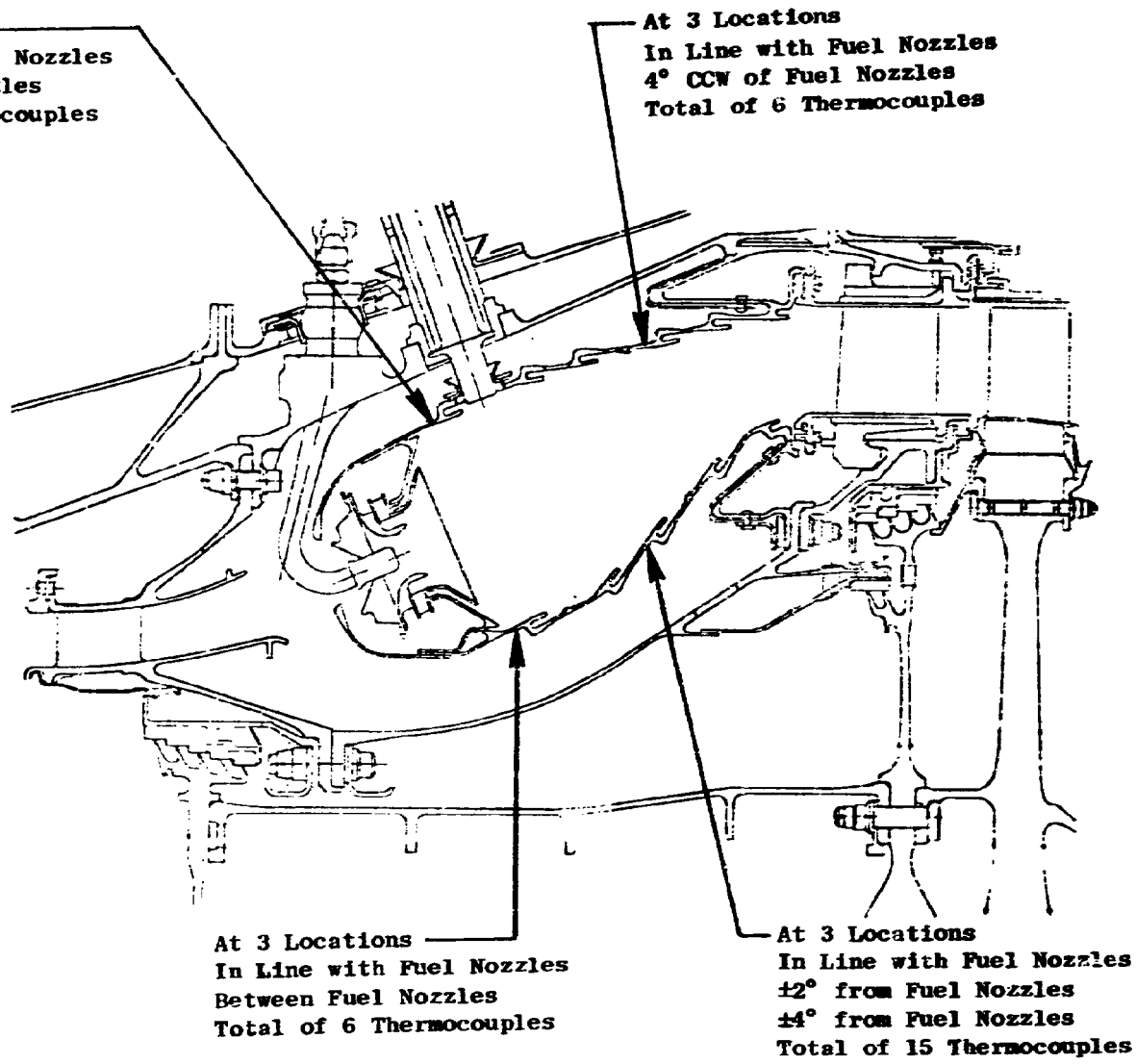

Figure 22. Combustor Liner Temperature Measurement Locations.

Table 12. Combustor Liner Temperature Instrumentation.

OUTER LINER							
Panel	Fuel Nozzle	Angle	T/C Number	Panel	Fuel Nozzle	Angle	T/C Number
Forward of First	2	18	1	3rd	2	18	7
		27	2		–	14	8
↓	3	36	3	↓	3	36	9
		45	4		–	32	10
	7	108	5		7	108	11
		117	6		–	109	12

INNER LINER							
Panel	Fuel Nozzle	Angle	T/C Number	Panel	Fuel Nozzle	Angle	T/C Number
Forward of First	18	306	13	2nd	–	302	19
		315	14		–	304	20
↓	19	324	15	↓	18	306	21
		333	16		–	308	22
	20	342	17		–	310	23
		351	18		–	320	24
					–	322	25
					19	324	26
					–	326	27
					–	328	28
					–	336	29
					–	340	30
					–	342	31
					20	344	32
					–	346	33

All Angle Callouts Are CWALF

Location Relative to Cooling Slot
(All Thermocouples)

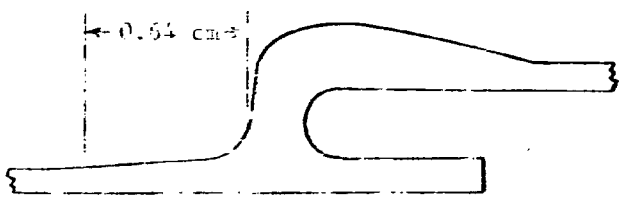

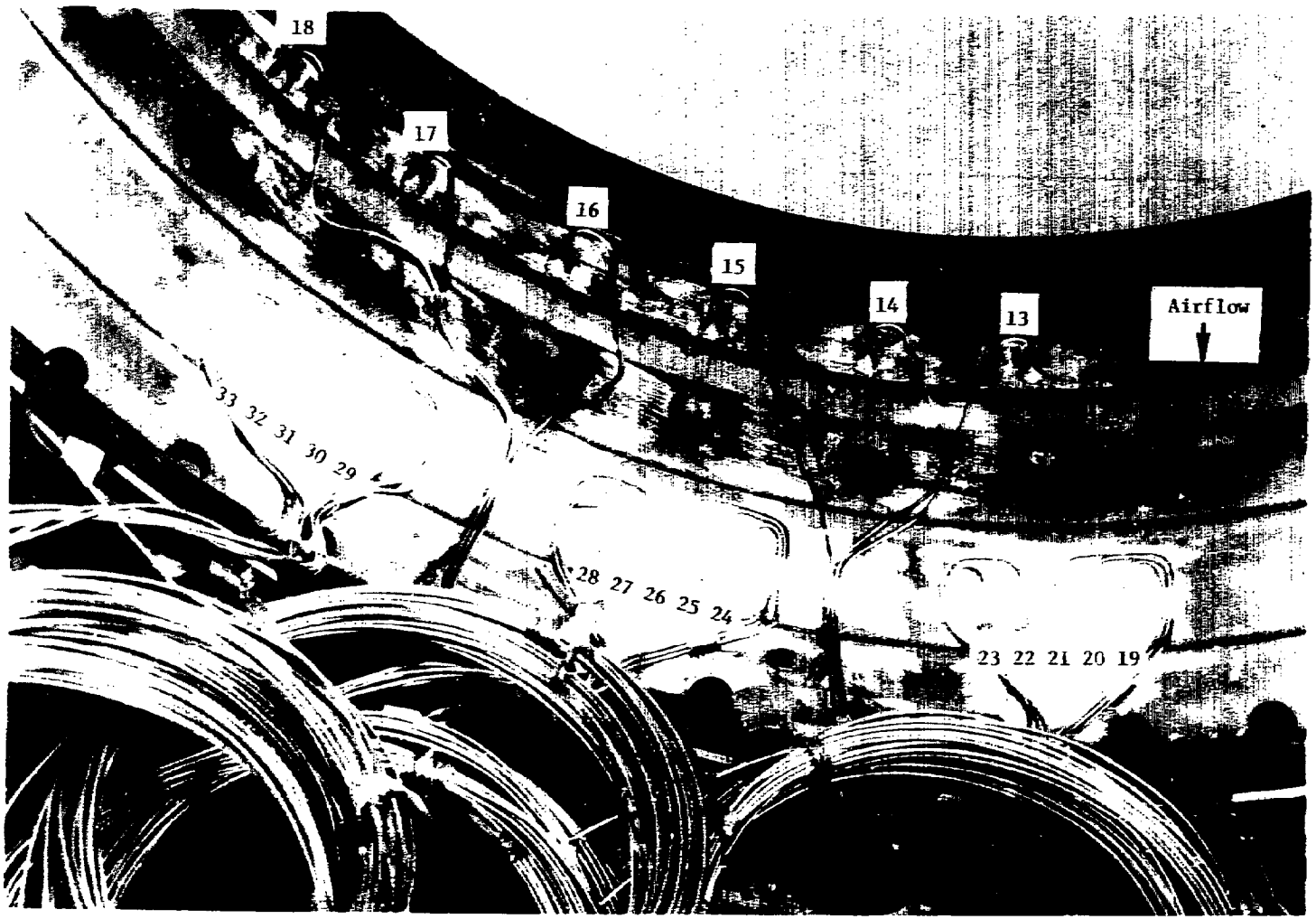

Figure 23. Inner Liner Temperature Instrumentation.

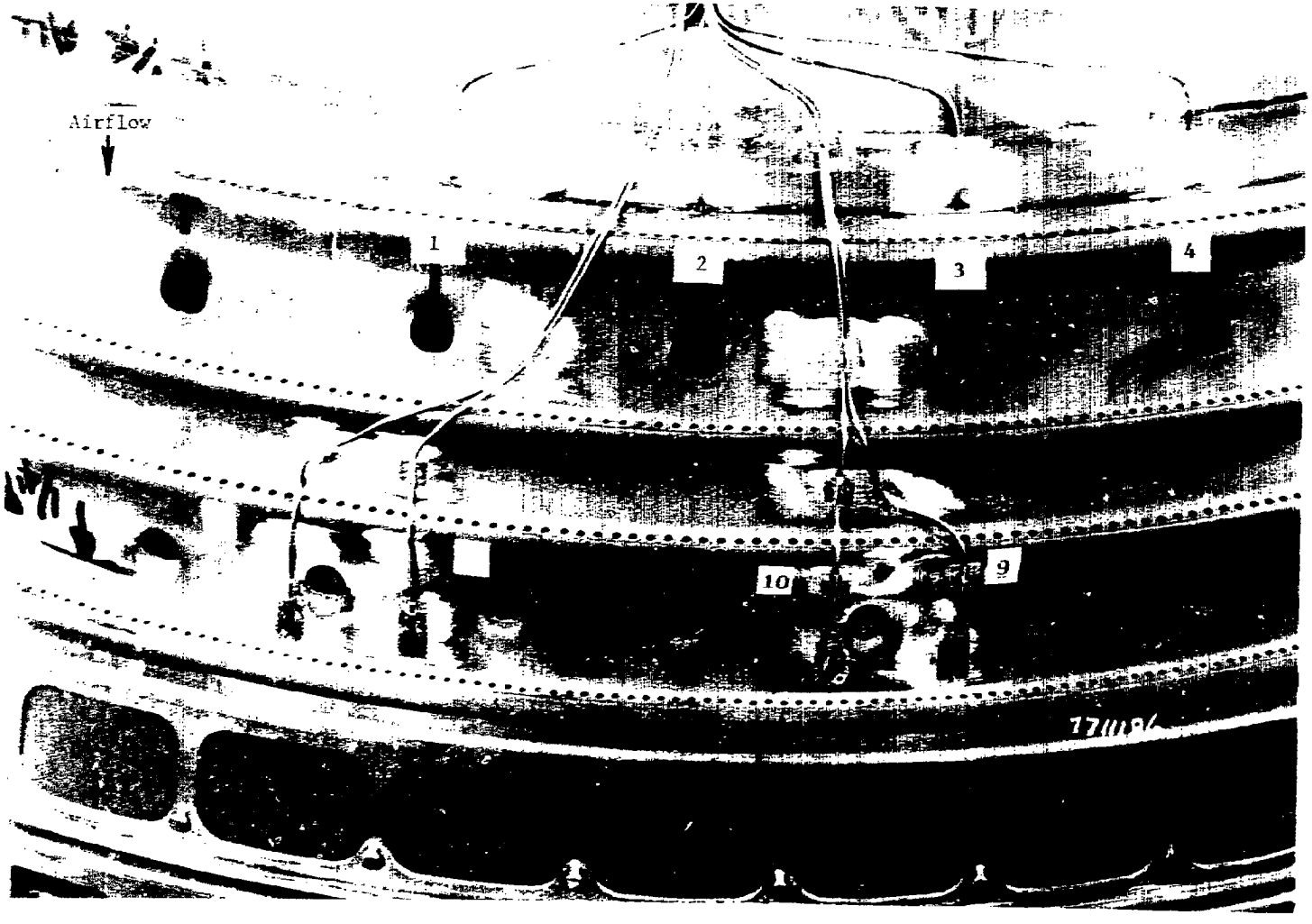

Figure 24. Outer Liner Temperature Instrumentation at Fuel Nozzle Numbers 1-3.

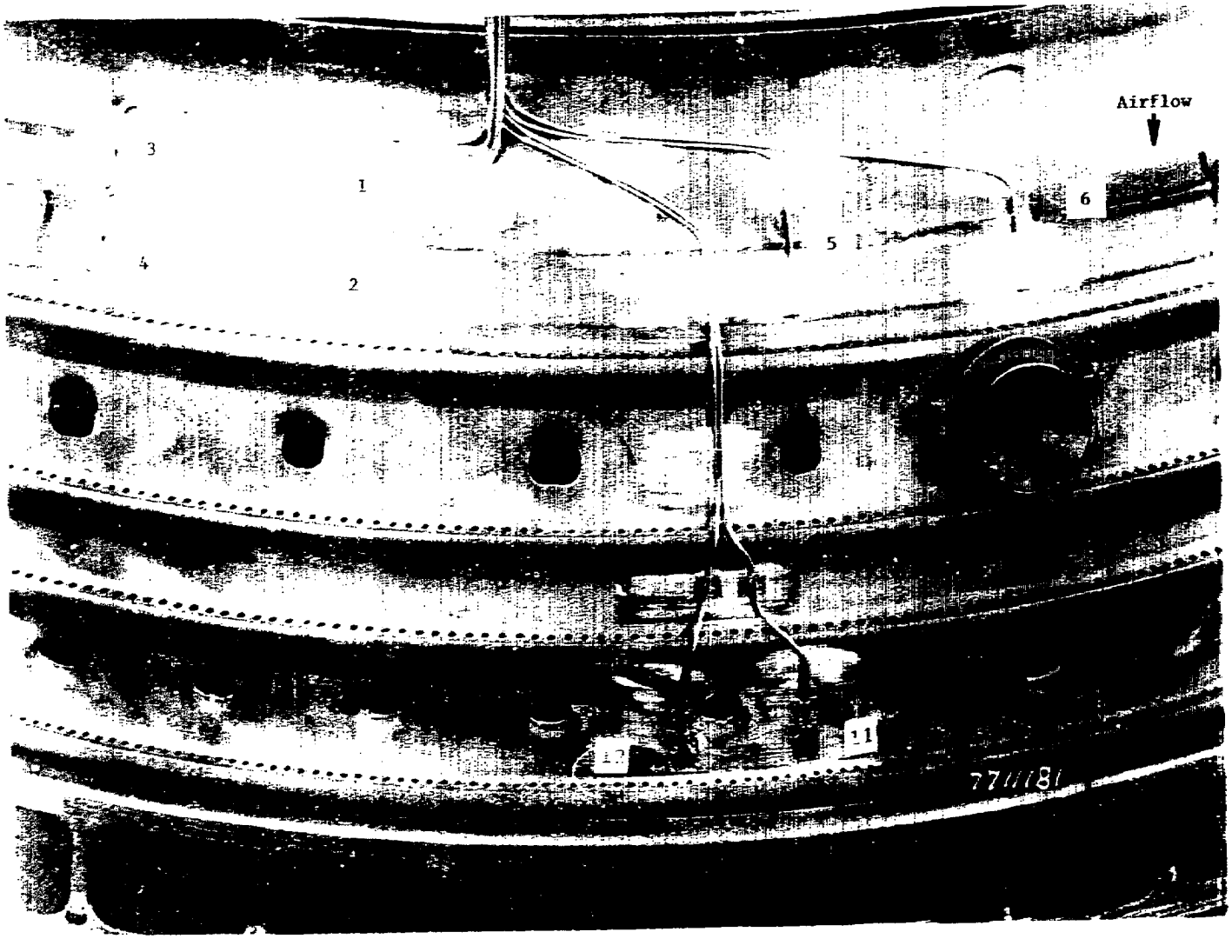

Figure 25. Outer Liner Temperature Instrumentation at Fuel Nozzle Numbers 6-8.

Table 13. Full-Annular High Pressure Test Point Schedule.

Test Point Number	W_3 Total Airflow, kg/s	W_c Combustor Airflow, kg/s	P_3 Inlet Total Pressure MPa	T_3, Inlet Total Temperature K	V_r (1) Reference Velocity m/s	W_f (2) Fuel Flow Rate g/s	f (2) Fuel-Air Ratio, g/kg	Comments
1	8.62	8.62	0.390	468.2	18.3	95.1	11.0	
2	8.62	8.62	0.390	468.2	18.3	118.8	13.8	True Idle Condition
3	16.96	16.96	0.977	677.6	21.0	320.5	18.9	
4	16.96	16.96	0.977	677.6	21.0	400.7	23.6	True Subsonic Cruise
5	19.96	19.96	1.253	828.7	23.5	458.3	23.0	
6	19.96	19.96	1.253	828.7	23.5	572.9	28.7	Simulated Takeoff
7	19.96	19.96	1.245	849.3	24.1	437.5	21.9	
8	19.96	19.96	1.245	849.3	24.1	547.3	27.4	Simulated Dash

(1) Based on W_c and A_r = 1618 cm^2 (Simulated W_3/W_c = 1.212).

(2) Based on JP-4 fuel. For other fuels, adjust for heating value.

Table 14. Full-Annular Atmospheric Discharge Test Point Schedule.

Test Point Number	W_c Combustor Airflow kg/s	T_3 Combustor Inlet Temperature K	V_r Simulated Combustor Reference Velocity, m/s	W_F (1) Fuel Flow Rate g/s	f (1) Fuel-Air Ratio g/kg	Comments
1	2.22	468	18.3	31.0	14.0	Simulated idle, 4.5°/0-90° traverse
2	2.22	468	18.3	—	—	Determine idle lean blowout and lightoff fuel flow rate
3	1.74	678	18.3	41.8	24.0	Simulated cruise, 4.5°/0-90° traverse
4	1.60	829	23.5	38.3	24.0	Simulated takeoff, 80% f - 1.5°/0-90° traverse
5	1.60	829	23.5	46.6	29.2	Simulated takeoff, 1.5°/0-90° traverse
6	1.60	829	23.5	46.6	29.2	Simulated takeoff, 1.5°/270-0° traverse
7	1.61	849	24.1	44.7	27.9	Simulated dash, 1.5°/270-0°

(1) Based on JP-4 fuel. For other fuels, adjust for heating value. For all fuels, adjust (reduce) if necessary to exit rake peak temperature limit.

B. Carbon Deposition Tests

1. High Pressure, Single-Cup Test Rig Description

The tests were performed in Test Cell A5, located in Building 304 at the Evendale Plant. This cell has all the necessary ducting, controls, instrumentation, fuel supplies, and high pressure and temperature air supplies required for the testing. The rig shown in Figure 26 is a single 8-inch diameter pipe in which is mounted a J79 low-smoke combustor inner liner. All dilution holes of this liner were closed, leaving only cooling slots open. The F101 swirler and splash plate assembly was mounted on the dome of this liner.

The test rig was instrumented with static pressure taps located in the air passage both upstream and downstream of the J79 dome, and in the fuel line near the fuel nozzle inlet.

Approximately six skin thermocouples were attached to the liner, splash plate, and swirler, in locations selected from previous test experience. Combustor inlet airflow was measured by a thin plate orifice flowmeter constructed according to ASME standards. Fuel flow was measured by turbine-type flowmeters.

2. Carbon Deposition Test Procedure

All 13 fuels were tested in the carbon deposition test rig. The schedule of test conditions shown in Table 15 was derived from actual F101 engine operating conditions, except that it was made intentionally severe with respect to both dome pressure drop (25 percent low) and fuel temperature (at least 14 K higher than the usual 436 K) in order to accentuate carbon deposition tendencies in the short test (5-1/4 hr).

The test point schedule shown in Table 15 consists of seven test conditions with a hold time of 45 minutes at each condition. At each point, the airflow was set to obtain the prescribed dome pressure drop. Data readings were taken upon establishing each point, and at 15-minute intervals thereafter.

Prior to each test, the swirler assembly and fuel nozzle was cleaned and flow-calibrated. Instrumentation was refurbished as required.

After the test, the swirler-dome assembly and the fuel nozzle were removed from the rig, inspected visually, photographed, and recalibrated in the appropriate flow laboratories.

C. Cold Day Ground Start/Altitude Relight Tests

Low pressure/temperature 54-degree sector combustor rig tests were conducted at simulated F101 engine ground cranking and altitude windmilling operating conditions to determine the cold-day ground start and altitude

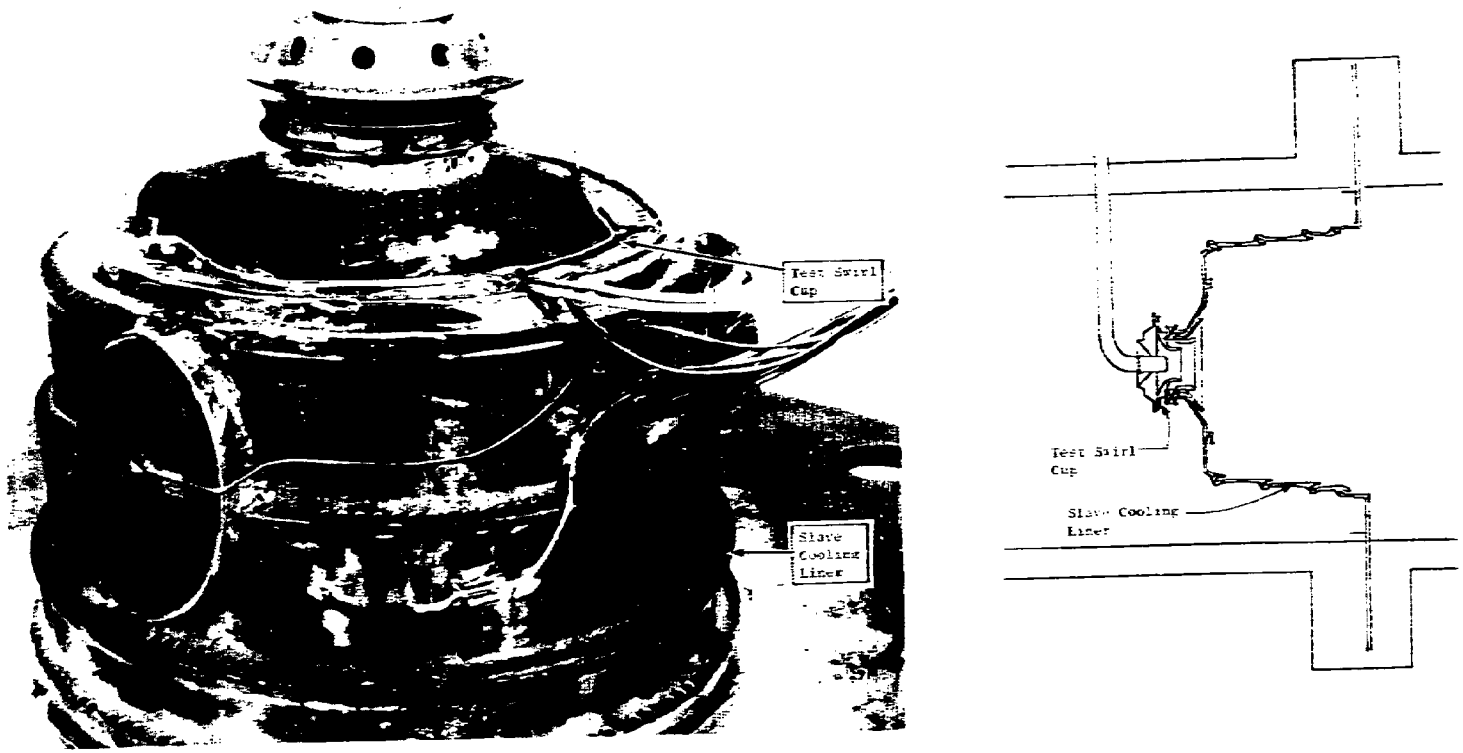

Figure 26. Carbon Deposition Test Rig.

Table 15. Single-Cup Carbon Deposition Rig Test Point Schedule.

Fuel Temperature: 436 K							
Test Point Number	P_3 Combustor Inlet Total Pressure, MPa	T_3 Combustor Inlet Total Temperature, K	W_f Fuel Flow Rate, pph g/s	$\Delta P/P_3$ (1, 2) Dome Pressure Drop Z	V_r Simulated Combustor Reference Velocity m/s	Hold Time Minutes	Simulated Condition
1.5	0.390	468	6.05	4.00	15.8	45	Idle
2.4	0.977	678	20.4	3.62	18.2	45	Cruise
3.6	1.897	829	37.9	3.72	20.3	45	Takeoff
4.4	1.897	849	42.3	3.86	20.9	45	Dash
3.6	1.897	829	37.9	3.72	20.3	45	Takeoff
2.4	0.977	678	20.4	3.62	18.2	45	Cruise
1.5	0.390	468	6.05	4.00	15.8	45	Idle

(1) Airflow adjusted to give this pressure drop.

(2) Percent pressure drop is 75% of true engine Z pressure drop to increase test severity.

relight characteristics of each of the test fuels. Apparatus and procedures which were utilized are described in the following sections.

1. 54-Degree Sector Test Rig Description

These tests were conducted in the Building 301 Combustion Laboratory at the Evendale Plant. This facility has capabilities for testing small combustor rigs over a wide range of simulated ground start and altitude relight conditions. Liquid nitrogen heat exchangers are used to obtain low fuel and air temperatures, and steam ejectors in the exhaust ducting are used to obtain low combustor inlet pressures.

The low pressure F101 54-degree sector combustor rig used in these tests is shown in Figures 27 and 28. The combustor housing simulates a 54-degree segment of the engine combustion system flowpath. Combustor inlet temperature and pressure are measured with probes in the plenum chamber. The combustor assembly is installed from the rear of the combustor housing which bolts up to a flange simulating the turbine inlet. An array of thermocouples is located in the primary zone to sense ignition and blowout. This rig has no provisions for turbine cooling air extraction.

Air obtained from the central supply system was dried at the facility to a dew point of about 240 K and metered with a standard ASME orifice. Fuel flow rates were measured with calibrated turbine meters corrected for the density and viscosity of each test fuel at the measured supply temperature. All temperature, pressure, and flow data were read on direct indicating instruments (manometers, potentiometers, etc.) and hand logged by the test operator.

2. 54-Degree Sector Test Procedure

The first part of the test with each fuel was structured to evaluate cold-day ground starting characteristics. The test point schedule is shown in Table 16. The airflow rate (1.15 kg/s) and combustor inlet pressure (101 kPa) were set to simulate typical engine ground starting conditions (2500 rpm). Fuel and air temperature were lowered from ambient to 239 K minimum (JP-8 freeze point) in steps to simulate progressively colder days. At each temperature step, minimum ignition and lean blowout fuel flow rates were determined. The test sequence was as follows:

1) With inlet conditions set, energize the ignitor and slowly open the fuel control valve until lightoff is obtained. Record lightoff fuel flow rate. Deenergize ignitor.

2) Slowly decrease fuel flow rate to blowout. Record lean blowout fuel flow rate.

3) Decrease fuel and air inlet temperatures in 5 to 8 K increments and repeat Steps 1 and 2.

When the minimum temperature limit was established, the second portion of the test, altitude relight, was begun.

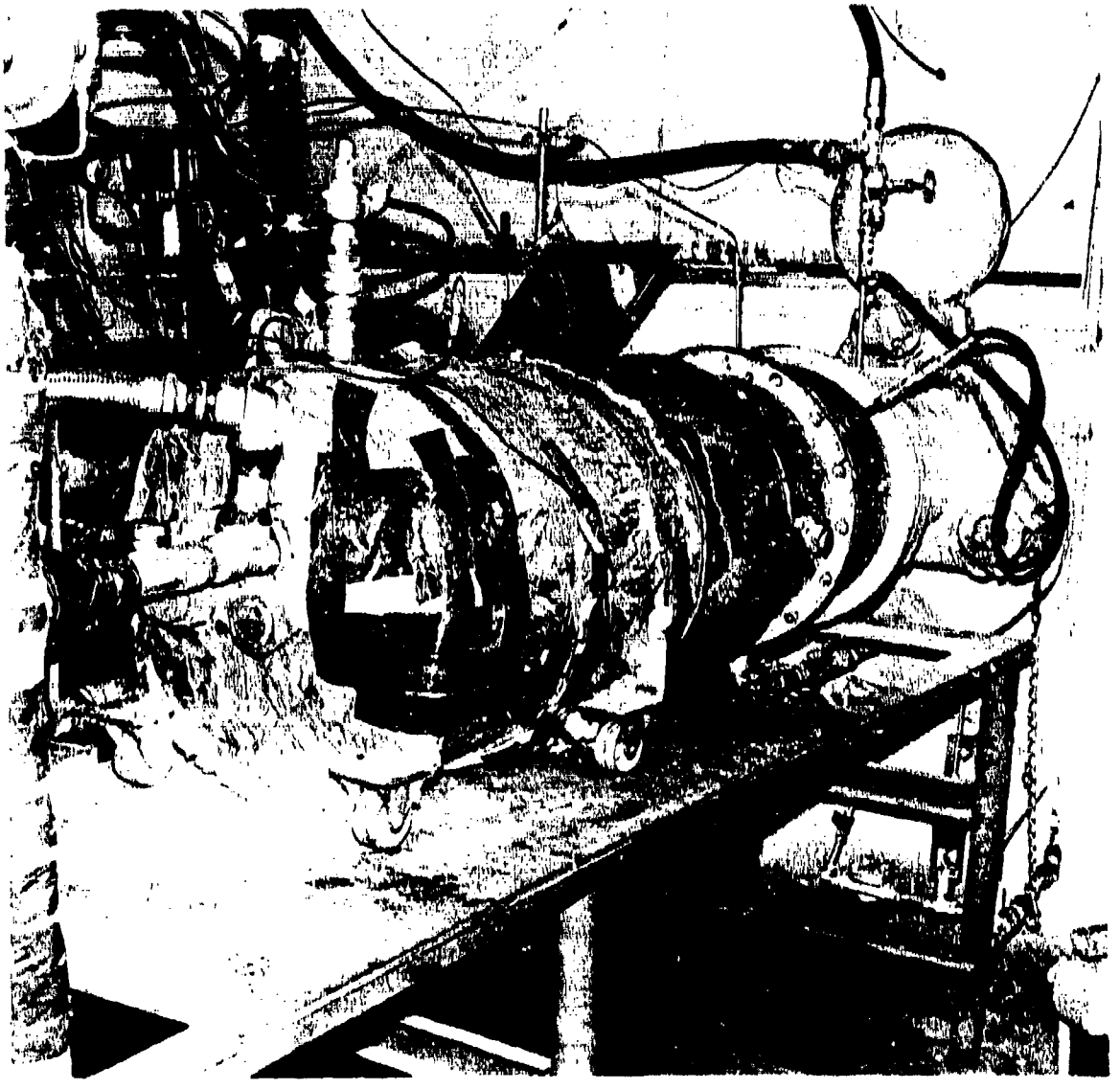

Figure 27. 54-Degree Sector Combustor Test Rig.

Figure 28. 54-Degree Sector Combustor Test Rig, Rear View.

Table 16. 54-Degree Sector Test Point Schedule.

Test Point Number	Simulated Flight Altitude km	Simulated Flight Mach Number	W_c Combustor Airflow kg/s	P_3 Air Inlet Pressure kPa	T_3 Air Inlet Temperature K	T_f Fuel Temperature K	W_f Fuel Flow g/s	Comments[1]
5.1.1	0	0	0.172	101	278	278	0-7.56	Determine W_f @ LO
5.1.2	0	0	0.172	101	278	278	0-7.56	Determine W_f @ LBO
5.2.1	0	0	0.172	101	272	272	0-7.56	Determine W_f @ LO
5.2.2	0	0	0.172	101	272	272	0-7.56	Determine W_f @ LBO
5.3.1	0	0	0.172	101	267	267	0-7.56	Determine W_f @ LO
5.3.2	0	0	0.172	101	267	267	0-7.56	Determine W_f @ LBO
	Continue 5.X.X. Sequence Until Ground Start T_3 is Determined							
6.1.0	15.2	1.25	0.136	24	251	251	5.67	Starting Point for Series
6.1.1	-	-	0.136	-	251	251	5.67	Determine $P_{3min.}$ @ LO
6.1.2	-	-	0.136	-	251	251	5.67	Determine $P_{3min.}$ @ PBO
6.1.3	-	-	0.136	-	251	251	0-7.56	Determine $W_{fmin.}$ @ LO
6.1.4	-	-	0.136	-	251	251	0-7.56	Determine $W_{fmin.}$ @ LBO
6.2.0	15.2	1.47	0.204	34	268	268	5.67	Same Sequence at 6.1.X to Determine Altitude LO, LBO, and PBO Limits
6.3.0	15.2	1.70	0.340	59	amb	amb	5.67	
6.4.0	15.2	1.85	0.476	83	amb	amb	5.67	

(1) LO = Lightoff (Increasing W_f or P_3)

LBO = Lean Blowout (Decreasing W_f)

PBO = Pressure Blowout (Decreasing P_3)

The second portion of the test with each fuel was structured to evaluate altitude relight and stability characteristics. The test schedule is also shown in Table 16. Investigations were carried out at four airflow rates (0.91, 1.36, 2.27 and 3.18 kg/s) selected to span the F101 engine altitude relight requirement map (Figures 13 and 14). Air temperature was selected from the windmilling data and ranged from 250 K to ambient. Fuel temperature was matched to the air temperature. The test sequence was structured to determine:

1) The maximum relight and blowout pressure altitudes with current engine minimum fuel flow rates (37.8 g/s - engine = 5.67 g/s - sector).

2) The minimum relight and lean blowout fuel flow rates at the relight altitudes determined in (1).

The test sequence was as follows:

1) With altitude conditions set, energize the ignitor, set fuel flow rate at 5.67 g/s, then increase combustor inlet pressure (decreasing altitude and flight Mach number) until ignition occurs. Deenergize the ignitor and record maximum relight altitude conditions.

2) With fuel flow rate at 5.67 g/s, slowly reduce combustor inlet pressure until blowout occurs. Record maximum pressure altitude blowout conditions.

3) Reestablish conditions of sequence #1. Energize ignitor and increase fuel flow until lightoff. Deenergize ignitor and record minimum lightoff fuel flow rate at maximum relight altitude.

4) Slowly decrease fuel flow rate until blowout, record lean blowout fuel flow rate at maximum relight altitude conditions.

5) Repeat Steps 1 through 4 at each airflow setting.

D. Fuel Nozzle Fouling Tests

1. Short-Time Fuel Nozzle Fouling Tests

Tests with each of the fuels were conducted to determine the relative tendency to cause fuel nozzle malfunction. Previous experience with the F101 fuel nozzle operating with hot fuel has shown that the part most affected by fuel deposits is the flow metering valve, which has extremely small clearances. Deposits that form in these clearances can increase the hysteresis of the valve action after some period of operation with hot fuel. Since operation of the nozzle in actual service has not revealed significant problems, it was anticipated that fuel temperatures would need to be higher than those encountered in actual service to produce significant fouling in the short test times planned.

The tests were conducted in the Building 304-1/2 Combustion Laboratory using the test rig shown in Figure 29. In this setup, hot fuel is pumped through the fuel nozzle which is immersed in a high velocity hot gas stream. Initially selected test conditions were:

Gas Temperature	811 K
Gas Velocity at Fuel Nozzle Stem	304 m/s
Gas Pressure Drop Across Fuel Nozzle Air Shroud	13.8 - 20.7 kPa
Fuel Flow Rate	5.04 g/s
Fuel Temperature	436 K
Run Time	
Between Calibrations	100 minutes
Total	300 minutes

After each 100 minutes of operation, the rig was shut down, allowed to cool, and the nozzle removed for recalibration in the Nozzle Lab.

The fuel temperature was increased to 478 K after the second test because no significant fouling had been observed after the runs with fuel temperature of 436 K.

2. Long-Time Fuel Valve Gumming Tests

Since the short term fouling tests did not show significant nozzle malfunction even at the abnormal high fuel temperature of 478 K, it was suggested that meaningful results might require up to 100 hours of test time. This was based on the results of many General Electric tests with F101 fuel injectors wherein partial seizure of the valves usually occurred somewhere between 60 and 120 hours, using fuel at around 419 to 436 K.

The scope of the program was, therefore, increased to include a series of long-time cyclic tests of F101 fuel metering valves. Since these valves are the most susceptible part of the nozzles to fuel gumming, this was considered more economical, and just as meaningful, as tests of complete nozzles.

Each test was scheduled to run 100 hours unless complete seizure occurred earlier. The test cycle consisted of

20 minutes at 63 g/s
90 minutes at 18.9 g/s
10 minutes at 10.7 g/s

This cycle is in accordance with most recent practice. The test schematic is shown in Figure 30. One significant change to the test setup was that two F101 fuel nozzle metering valves were installed in series, and tested simultaneously. This had never been done before, and might yield duplicate data at virtually no extra cost. If the concept did not prove valid, no loss in validity of the single nozzle data would result.

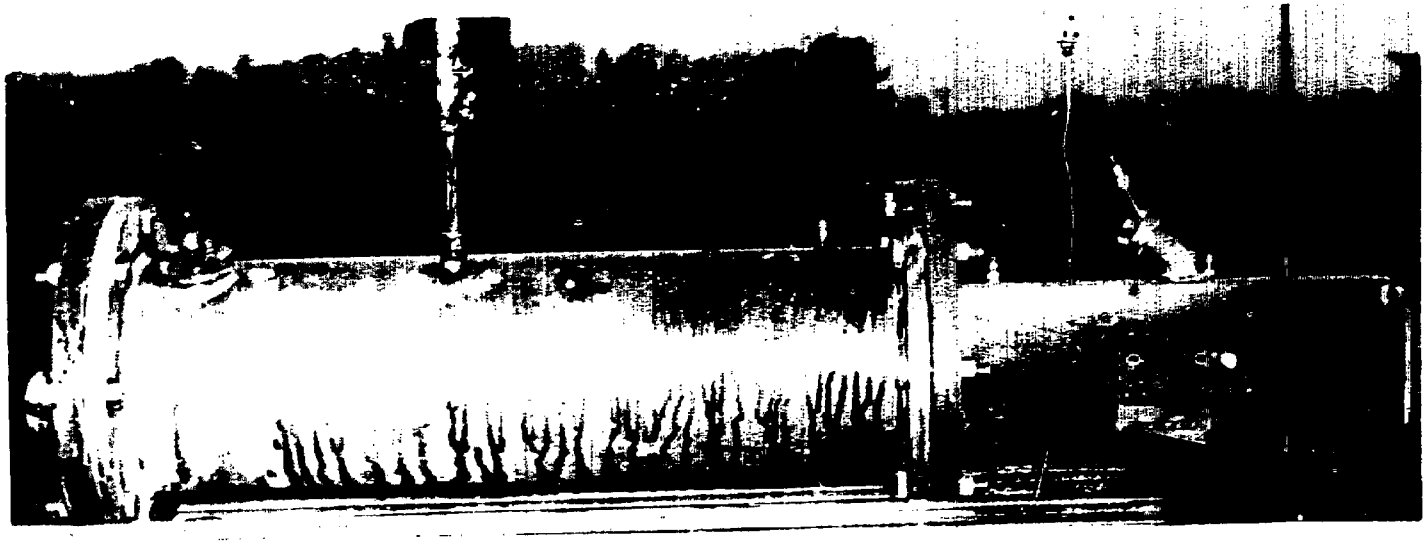

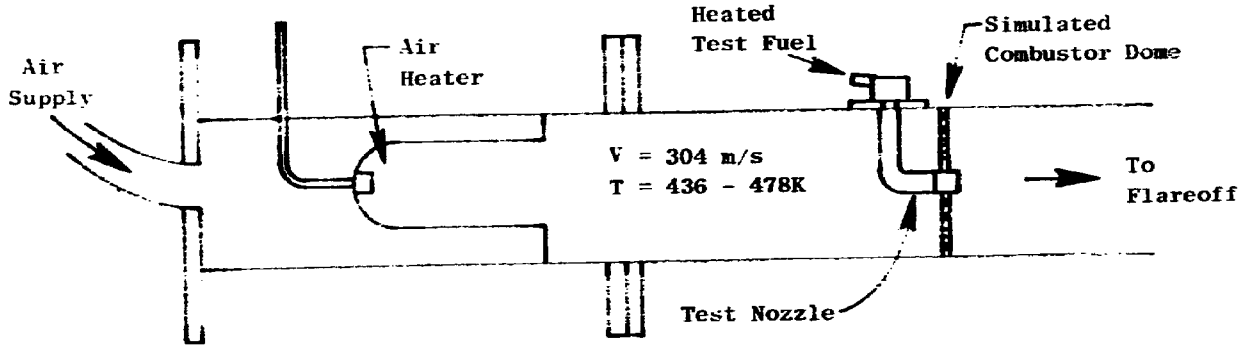

Figure 29. Fuel Nozzle Fouling Test Setup.

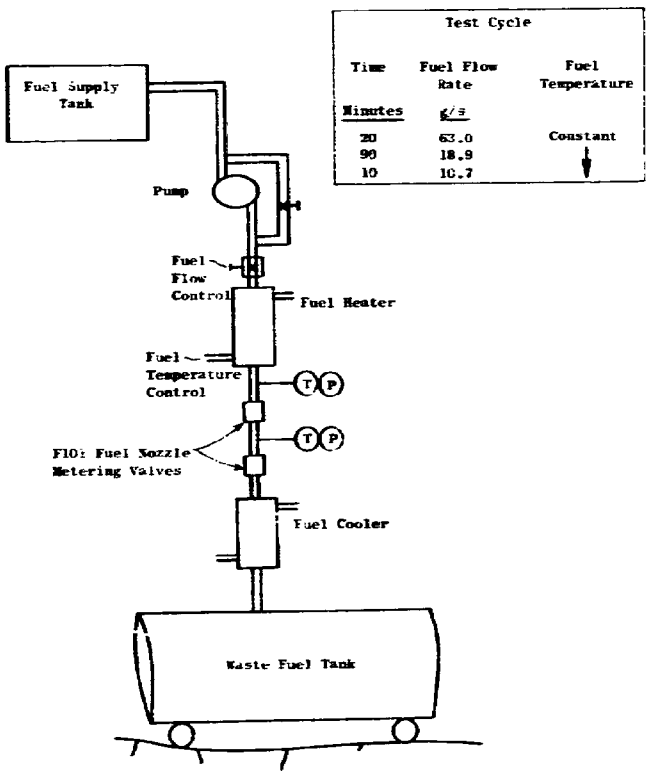

Figure 30. Fuel Nozzle Valve Gumming Test Setup.

The three tests were scheduled at the following conditions:

Test Number	Fuel Type	Fuel Temperature, K
1	JP-4	436
2	JP-8	436
3	JP-8	494

The first two tests were intended to provide a direct comparison of the JP-4 with the JP-8 fuel. The third test was intended to provide a direct comparison of the performance of JP-8 at two temperatures differing by 58 K. This temperature difference was selected to approximate the difference in breakpoint temperature between the JP-4 and the JP-8 by the laboratory fuel thermal stability tests.

In an attempt to achieve meaningful results, eight tests were actually run, since the three originally scheduled did not reach definitive end points, and since fuel was available. This series demonstrated the difficulty of attempting to estimate component performance at fuel temperatures beyond those normally encountered in engine use.

E. Test Fuel Handling Procedures

Special procedures were followed in all of the tests to insure that the test fuels were not contaminated or mistakenly identified. Hand valves were installed in the fuel lines near each of the test rigs for obtaining fuel samples while a test was in progress.

The fuels were delivered in tank trailers, as needed, and transferred into three isolated, underground storage tanks of 40 m^3 capacity each. These tanks had previously contained only clean, light distillates. Nevertheless, to assure their suitability for this program, they were first emptied as far as possible, using the permanently-installed unloading pumps. The manhole covers were then removed, and the few inches of remaining liquid were pumped out, using a portable pump. The tanks were then inspected and found to be in good condition, with only a light, adherent coating of rust on all interior surfaces. These surfaces were washed down with a small quantity of the next test fuel, and this was then removed with the portable pump. After replacing each manhole cover, the test fuel was transferred into the tank, and a sign identifying the test fuel was placed on the switch controlling the tank unloading pump. This procedure was repeated for each of the first 12 test fuels. The thirteenth test fuel, the diesel, was handled in a similar manner except that it was stored in a tank trailer parked near the underground storage tanks. For the full-annular combustor tests, fuels were pumped directly from these tanks to the test rig.

As fuel was needed for the other tests, it was transferred from the appropriate tank, using a 4 m^3 stainless steel tank trailer. This tank also was drained and flushed with the next test fuel before being loaded. After filling, it was marked with the proper fuel number, hauled to the test site, and parked adjacent to the test cell. The tank drain valve was connected

directly to the cell system by a flexible hose, after flushing the hose with a suitable volume of test fuel.

In each of the tests, the fuel sampling procedure consisted of drawing a sample just before the first data point was taken and again after the last data point was taken. In each case, the sample container was rinsed twice with a small portion of the fuel being sampled, before actually taking the sample.

Similar sampling procedures were followed in both the altitude relight and the fuel nozzle fouling tests. For both of these tests, fuel was transferred from the trailer to clean drums which were clearly marked and moved to the test sites. These drums were in good condition and had previously contained only clean materials, such as calibrating fluid. Before filling, they were drained, inspected, and rinsed with the next test fuel.

Pre-test samples taken at the test sites were returned to Wright-Patterson Air Force Base for verification of significant characteristics, to determine whether fuel quality had been compromised during storage or handling at the several test sites. Analyses included density, viscosity, surface tension, and vapor pressure. These analyses were performed by Monsanto Research Corporation.

A compilation of these data is shown on Table 17. From a comparison of the properties of the original samples with those of samples returned from the several test sites, it is apparent that no significant change in fuel properties occurred. Therefore, it was concluded that fuel handling procedures were satisfactory, and analysis of samples of the remaining test fuels was considered unwarranted.

F. Data Analysis Procedures

Generally standard data reduction and presentation techniques were employed. Key parameters and calculation procedures are indicated in Table 11 and Appendix A. Some additional special procedures are described in the following sections.

1. Fuel Property Correlation Procedures

Analyses of the experimental test results were conducted to: (1) correlate the performance and emission parameters with combustor operating conditions; (2) as appropriate, correct the measured rig data to true standard day engine conditions; and, (3) correlate the corrected data with the appropriate fuel properties from Section III. To illustrate the procedure, the NO_x emission data procedure is outlined below.

Inspection of the NO_x emission data for the first high pressure test (JP-4 fuel, Figure 39) showed that as in Reference 6 the data were of the form:

Table 17. Fuel Verification Analyses.
(All Properties at 311K)

Sample Source	Fuel No.	Density, kg/m^3	Viscosity, mm^2/s	Surface Tension, mN/m	Vapor Pressure kPa
Original	1	744.0	0.816	22.17	17.1
Relight Test	1	744.0	-	21.4	16.5
Relight Test	1	743.5	-	22.6	16.3
Fouling Test	1	744.0	-	22.3	15.9
Fouling Test	1	743.9	-	21.8	16.1
Perf./Emission Test	1	745.3	0.825	-	-
Perf./Emission Test	1	744.8	0.823	-	-
Original	2	791.4	1.555	24.80	2.7
Relight Test	2	791.6	-	25.1	2.5
Fouling Test	2	791.8	-	25.0	2.3
Fouling Test	2	791.2	-	25.5	2.5
Perf./Emission Test	2	791.1	1.530	-	-
Original	3	793.2	1.721	24.87	2.4
Fouling Test	3	793.7	-	25.0	1.5
Fouling Test	3	793.1	-	25.2	1.5
Relight Test	3	793.3	-	25.5	2.6
Perf./Emission Test	3	793.5	1.708	-	-

$$EI_{NO_x} = \left[k_o\right]\left(\frac{23.5}{V_r}\right)\left(\frac{P_3}{1.265}\right)^{k1}\left[\phi(f)\right]\quad \exp\left\{\left[\left(\frac{T_3 - 828.7}{k_2}\right) + \left(\frac{6.29 - h}{53.2}\right)\right]\right\} \quad (5)$$

$$= k_o\left[S_{NO_x}\right]$$

where the combustor operating parameters (V_r, P_3, T_3 and h) have been normalized to standard day operating conditions at takeoff. A very good correlation was obtained (Figure 39) using values for k_1, k_2 and $[\phi(f)]$ determined from previous F101 rig and engine tests to be:

$$k_1 = 0.37 \quad (6)$$

$$k_2 = 191.7\ K \quad (7)$$

$$\phi(f) = 0.325 + 0.945\ (f/14.0) \text{ when } f \leq 14.0\ g/kg \quad (8a)$$

$$= 1.648 - 0.648\ (f/14.0) \text{ when } 14.0 \leq f \leq 24.0\ g/kg \quad (8b)$$

$$= 1.00 \text{ when } f \geq 24.0 \quad (8c)$$

Additional analyses then showed that k_o was fuel dependent but k_1, k_2 and $\phi(f)$ were not fuel dependent. The NO_x severity operating parameter was then taken to be:

$$S_{NO_x} = \left(\frac{23.5}{V_r}\right)\left(\frac{P_3}{1.265}\right)^{0.37}\quad \left[\phi(f)\right]\left\{\exp\left[\left(\frac{T_3 - 828.7}{191.7}\right) + \left(\frac{6.19 - h}{53.2}\right)\right]\right\} \quad (9)$$

which is tabulated in Table A-2, and was used to calculate NO_x emission levels at true standard day engine operating conditions (Table A-5a), using multiple regression curve-fit techniques, as illustrated in Figure 39. Engine emission levels were then tabulated (Table 20, for example) and plotted against appropriate fuel properties (Figures 40 and 41, for example). Equations for the effect of fuel hydrogen content on NO_x emissions shown in Figure 40 are the result of regression analyses (Table A-5b), and show, for example, that

$$EI_{NO_x}\ \text{cruise} = 8.9\left(\frac{H}{14.5}\right)^{-0.86}\ g/kg \quad (10)$$

Smoke emission data were correlated in a similar manner. The data for fuel Number 2 (JP-8) correlates well with engine test data using very similar JP-5 fuel, see Figure 42, for example, when the appropriate severity parameter was used. This parameter has been derived from engine tests. In this case:

$$S_S = \left[\left(\frac{P_3}{2.718}\right)\left(\frac{f_4}{29.2}\right)\left(\frac{828.7}{T_3}\right)\right]^{1.5}\left(\frac{W_c/P_3}{15.92}\right),\ MPa,\ g/kg,\ K,\ kg/s \quad (11)$$

Use of this parameter thus enables the takeoff and dash rig data to be corrected to engine conditions (Table A-6).

2. Combustor Life Prediction Procedures

The F101 combustor liner is life-limited by low cycle fatigue from thermal gradients where the coolest regions are on the cold side of the film

cooling slots and the hottest region is just upstream of the cooling slot structure. The liner has been life optimized both in its cooling flow distribution and in the metal thickness distribution.

In its initial design and throughout its development, the liner temperatures, stresses, and life have been calculated with detailed computer analyses, with adjustments to the heat transfer inputs as test data identified the magnitude of specific contributors to the liner heating. Referring to Figure 31, the combustor is heated by convection and radiation from the hot combustion gases. These gases are hottest in the upstream end of the burner and drop toward the exit temperature as the air entering through the dilution holes mixes and cools the gas. The local gas velocities and temperatures are calculated by computer program based on the air distribution, and these values are then modified as indicated by subsequent combustor test data. The combustor liner is protected by the film air introduced through the film cooling slot. The rate at which the hot combustor gases mix through this protective film has been established from laboratory test data and combustor experience for the various specific film slots throughout the liner. Additional inputs to the heat transfer calculation include the flame radiation heating, metal radiation cooling, the convective cooling rates on the cold side of the liner, and the impingement cooling rate on the cooling slot overhang. The flame radiation being the least well-defined from other data can be determined by back calculation from measured metal temperatures. With the aid of a computer program to calculate the thermal conduction through the metal structure, the above heat transfer inputs or correlations are used to calculate the detailed temperature distribution within the combustor liner. These temperatures are then used as input to a stress analysis program together with inputs for mechanical and aerodynamic loads, which then calculates the elastic stresses throughout the structure. These stresses are then used together with low cycle fatigue material properties (Figure 32) to predict life to first cracking, with an appropriate multiplier from experience to determine total life.

3. Turbine Life Prediction Procedures

If alternate fuels created substantial changes in temperature pattern factor or temperature profile in the combustor exit gases, changes in turbine component life would be predicted. However, previous experience has not identified changes in these combustor exit temperature patterns at the full power conditions where combustor life is limited. As discussed in Section VI.A.3., the temperature pattern changes that were measured in the combustor exit gases at one-atmosphere pressure apparently do not exist at true engine pressure conditions.

However, in addition to the effects of combustor exit gas temperature, the same luminous flame radiation that affects the combustor liner can also radiate downstream into the turbine components. The leading edge of the stator vanes in the turbine diaphragm receives the most radiation. The turbine blades are shielded from direct radiation from the flame and are, therefore, not affected; the combustor exit gas radiation and gases passing through the turbine are not believed to have the luminous component in their

$$T_{Film} = T_{Gas} - \eta\,(T_{Gas} - T_{Coolant})$$

where

η = Film Effectiveness

T_{Gass} = Flame Temperature

$T_{Coolant}$ = Coolant Temperature

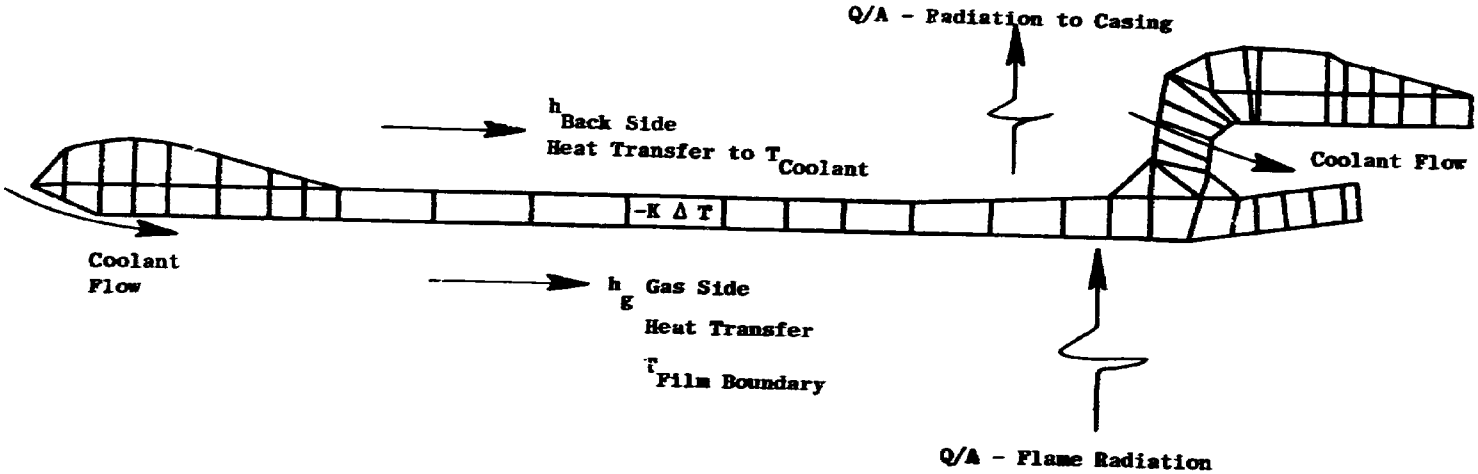

Figure 31. Node Model for F101 Combustor Showing Heat Transfer Quantities.

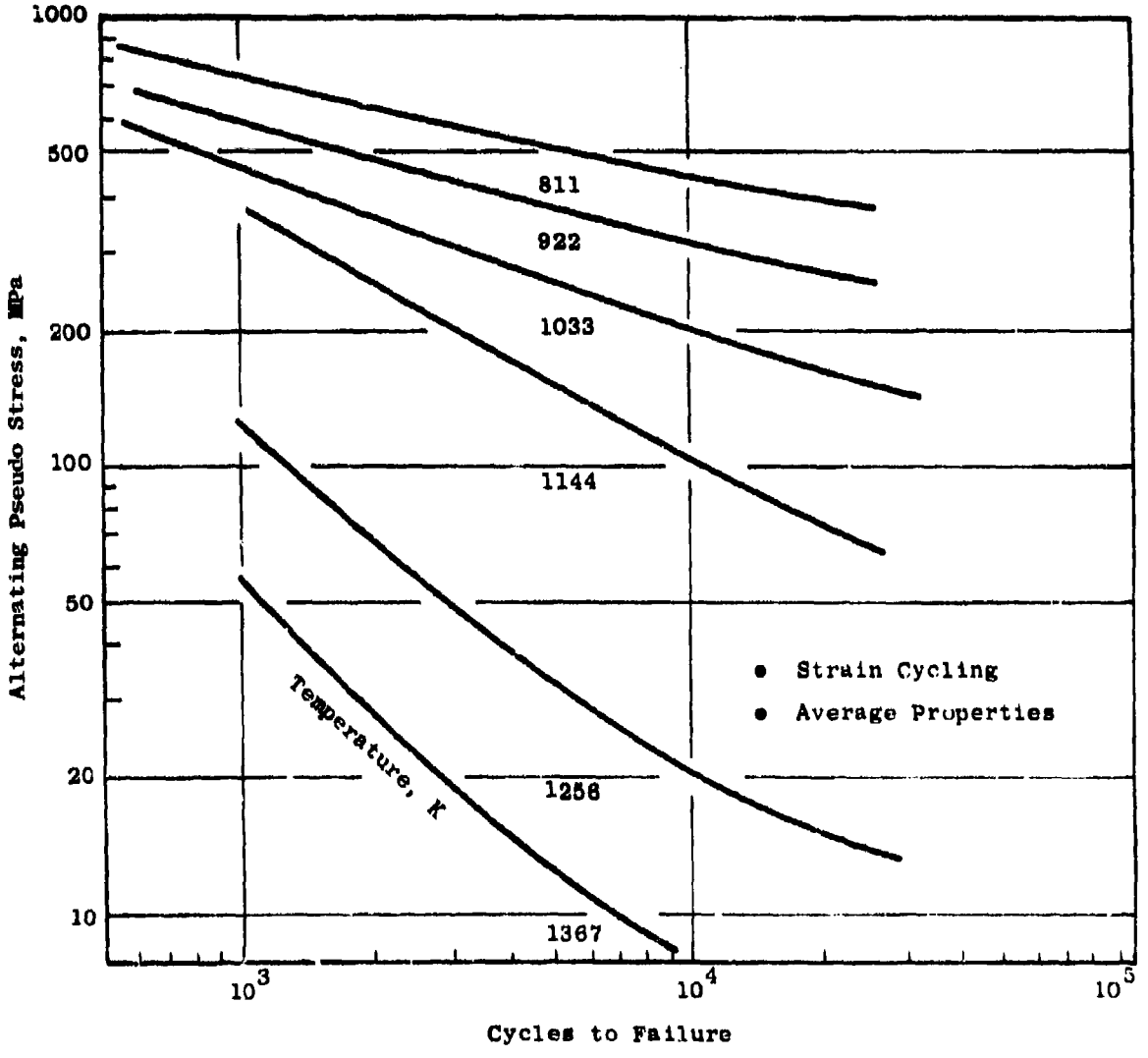

Figure 32. Fatigue Diagram for Hastelloy -X Sheet Stock.

radiation that exists in the dome region.

From previous data in combustors other than the F101 including the J79 and the CF6, it has been observed that fuel changes that create metal temperature changes from flame luminosity in the front end of the combustor do not also result in metal temperature changes at the aft end of the combustor. The intense luminosity exists in the regions where the combustion of the fuel is taking place, resulting in intermediate combustion products, but not in the downstream regions where the combustion is complete and only dilution and mixing are taking place.

Liner metal temperatures can respond to luminosity even in the portion of the liner downstream of the end of the luminous region because the metal still has a partial view upstream into the dome. The cooler intervening gases do not completely shield the liner from the upstream luminous radiation. These intervening gases absorb heavily in the nonluminous wavelength bands for water vapor and carbon dioxide and essentially shield the downstream parts from upstream radiation in these wavelength bands. The luminous components of the dome radiation, however, include radiation in wavelength regions that are not easily absorbed by the intervening gases. It is largely this latter component of the radiation that reaches the aft liner and vane leading edge.

However, far downstream on the liner the view factor to the luminous region (the fraction of the effective radiating space to the metal surface that is coming from the luminous region) gets quite small and the effects of the luminous region become negligible at the aft end of the J79 and CF6 combustors. The F101 combustor is, however, a very short combustor and the luminous region is close to the end of the combustor. Not only might the aft liner panels be affected but also the vane leading edge.

The view factor from the F101 vane leading edge to the luminous fire is higher than in, for example a J79 combustor, both because the combustor is shorter and because the combustor is annular. A much wider view around the circumference is present because it is not interrupted by the sides of can liners.

In addition to this direct radiation effect from the luminous region to the vane, a less direct effect of dome luminous flame radiation also exists. If the combustor liner metal temperatures at the end of the combustor are affected by this luminosity, they in turn will radiate at a different rate to the vane leading edge. This effect is, however, much smaller than the direct radiation effect, generally less than 10 percent of the direct radiation effect.

At the present state of development, the F101 stator vane is life-limited primarily by low cycle fatigue cracking of the trailing end of the vane. This region is not affected by combustor luminosity radiation. However, as this region is improved through further development, cracking at the leading edge could become life-limiting, and hence, affected by fuel type. The vane could then be reoptimized in development for the specific fuel type expected in operation with some increase in cooling flow or cooling complexity needed for the most difficult fuel type.

Even though the leading edge is not the primary life-limiting region of the stator vane, the effect of fuel type on low cycle fatigue of the leading edge was calculated. This was done to illustrate the potential life effects for future vanes with improved trailing edge designs where the leading edge life becomes a significant contributor to the overall vane life.

The same steps used in calculating combustor liner life are used in calculating vane life. First a detailed metal temperature distribution is calculated by computer program using appropriate heat transfer inputs. Then, stresses are calculated from this temperature distribution. Cycles to low cycle fatigue cracking are then calculated from these stresses.

Figure 33 shows the node model used for the latest design of the F101 turbine stator vanes.

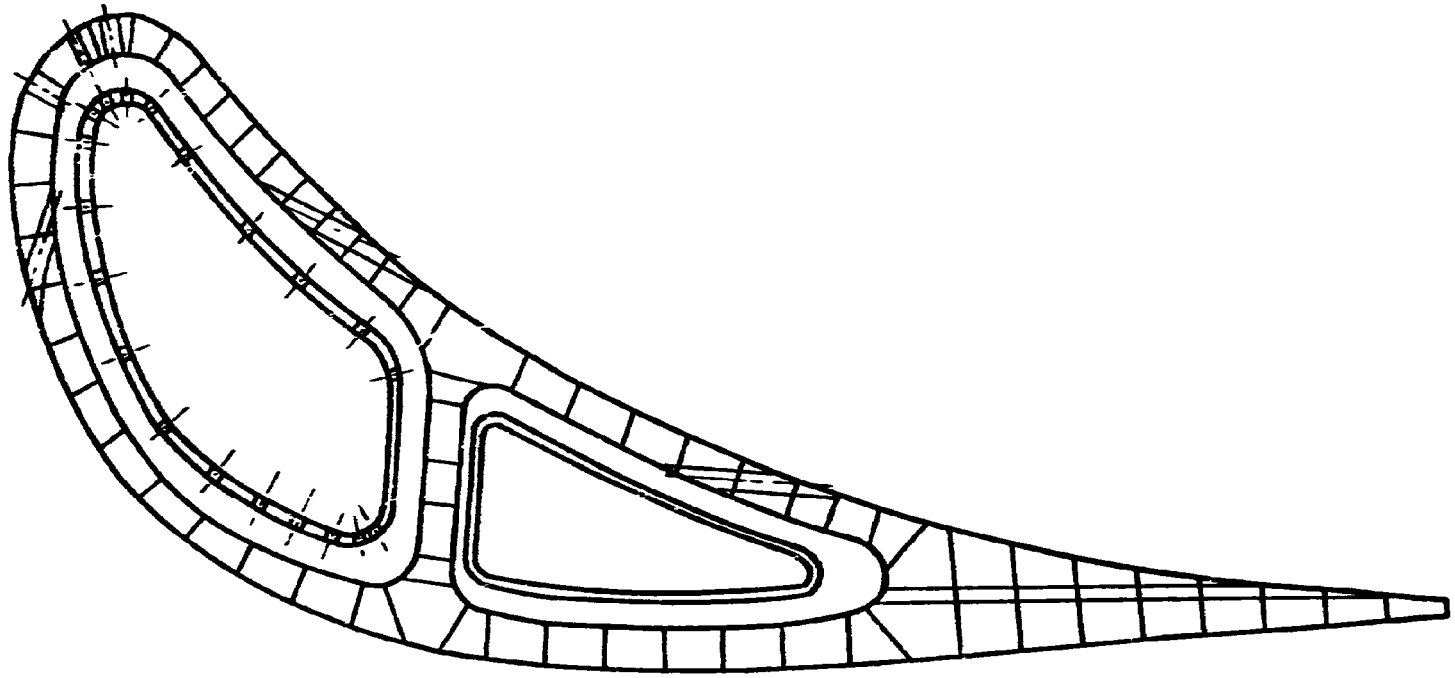

Figure 33. Node Model for F101 Turbine Stator Vane Analysis.

SECTION VI

RESULTS AND DISCUSSION

All planned test series (76 total) were completed and no major problems were encountered. In general, results were well ordered and consistent with prior data insofar as comparisons could be made. Detailed test results, which are listed in Appendices A through E, are summarized and discussed in Section VI.A. Engine system life prediction analyses based on these results are then presented in Section VI.B. Further, an overall assessment of these tests and analyses is presented in Section VI.C

A. Experimental Test Results

Twenty-six full-annular rig tests were conducted to obtain the performance emissions/durability data which are listed in Appendix A and summarized in Sections VI.A.1 through VI.A.5. Thirteen carbon deposition tests were also conducted and results are listed in Appendix B and discussed in Section VI.A.6. Fourteen low-pressure rig tests were conducted in parallel to obtain the ground start and altitude relight data which are listed in Appendix C and summarized in Sections VI.A.7 and VI.A.8. Also in parallel, 15 short-term fuel nozzle fouling tests and 8 long-term fuel nozzle valve gumming tests were conducted to obtain the data listed in Appendix D and summarized in Section VI.A.9 and VI.A.10.

1. CO and HC Emissions

Carbon monoxide (CO) and unburned hydrocarbons (HC) are both products of incomplete combustion, and are, therefore, generally highest at low power operating conditions (idle). Figure 34 shows the strong effect of combustor operating conditions (fuel-air ratio) on CO emission levels with three fuels at idle. At the true engine idle fuel-air ratio, the CO emission index is 28.7 g/kg with JP-4 fuel in these tests which is in good agreement with previous rig and engine measurements.

Idle CO emission results very similar to those shown in Figure 34 were obtained with each of the other fuels, and the results corrected to true idle fuel-air ratio are listed in Table 18 and A-3.

Table 18 also summarizes cruise, takeoff, and dash results. True engine takeoff and dash CO emissions have been corrected for pressure as shown in Table A-4 using an exponent (1.5) estimated from previous rig and engine test data comparisons. At cruise, takeoff and dash operating conditions, the CO emission levels are approximately 7, 2, and 1 percent, respectively, of the idle CO emission level, which indicates the strong effect of combustor inlet temperature and pressure on combustion reaction rates and, hence, combustion efficiency and CO emission levels. These CO levels are very low and virtually independent of any fuel property.

Figure 35 shows idle CO data plotted against relative spray droplet size (from Table 9) or fuel 10 percent recovery temperature (from Table 3), which is one of the more commonly used indicators of fuel volatility. It appears that either of

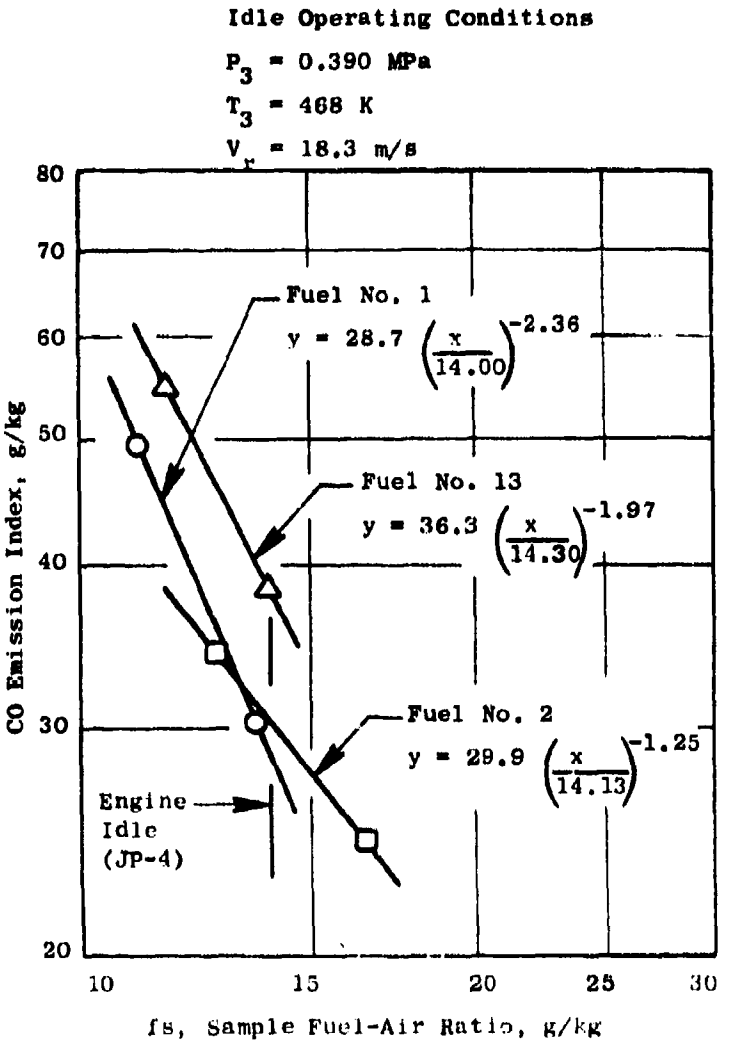

Figure 34. Effect of Fuel-Air Ratio on Idle CO Emission Levels.

Table 18. Summary of CO Emission Test Results.

Fuel Number	CO Emission Index, g/kg (1)			
	Idle	Cruise	Takeoff	Dash
1	28.7	2.0	0.5	0.3
2	29.9	2.3	0.7	0.4
3	30.6	2.2	0.5	0.4
4	34.6	2.4	0.5	0.3
5	31.8	2.6	0.5	0.4
6	32.9	2.3	0.5	0.3
7	34.1	2.3	0.7	0.4
8	29.1	2.5	0.6	0.4
9	25.2	2.4	0.6	0.4
10	30.1	2.3	0.6	0.3
11	28.9	2.2	0.5	0.3
12	26.5	2.1	0.4	0.3
13	36.3	2.2	0.5	0.3

(1) Corrected to true engine operating conditions.

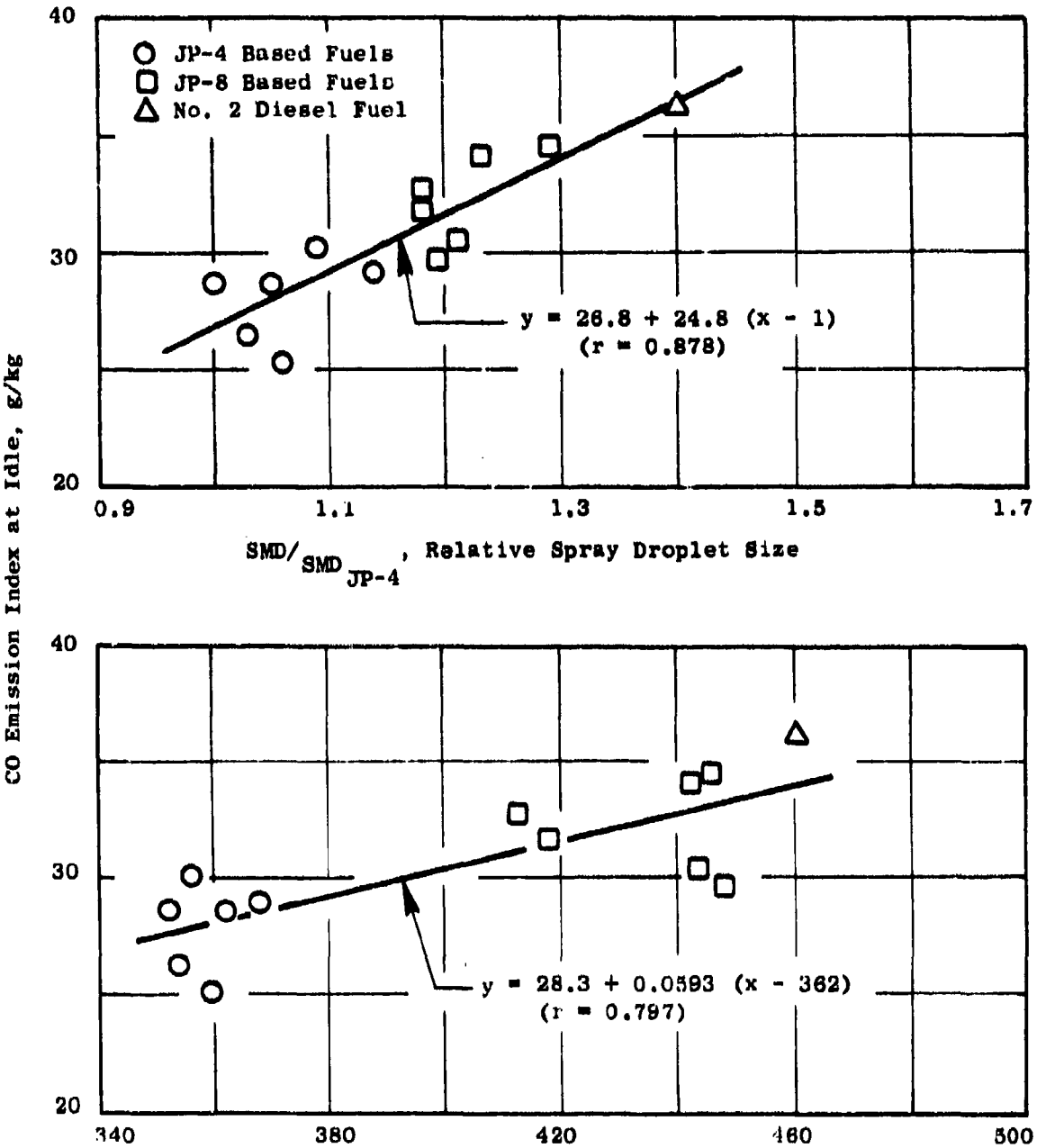

Figure 35. Effect of Fuel Atomization and Volatility on Idle CO Emission Levels.

these parameters correlates the idle CO data quite well. Both of these properties can be expected to affect idle emissions, but for these tests, it is difficult to judge which property is most important since, for these fuels at least, they turn out to be highly interrelated. There is some indication in Figure 35 that for the JP-8 based fuels, the drop size parameter better correlates the results than does the volatility parameter.

Hydrocarbon emission levels generally have been found to follow the same trends as do CO emissions, but to be more sensitive to combustor operating conditions and exhibit more variability. Both of these trends were observed in the present tests and are illustrated in Figure 36, where HC emission levels are plotted against CO emission levels for the two idle test points and all fuels.

Figure 37 presents the idle HC emission versus fuel-air ratio for the three base fuels. As with the CO emission, a strong fuel-air ratio effect is evident. Idle HC emission was therefore adjusted to the true engine fuel-air ratio as shown in Table A-3. These results are summarized in Table 19. For all fuels, HC emissions at cruise, takeoff and dash were essentially zero and too low to measure.

Figure 38 presents the idle HC emission plotted against the spray drop size and volatility parameters. As with the CO emissions, a good correlation is evident for both parameters. These plots show a 150 percent increase in HC emissions for the worst fuel (No. 2 diesel) compared to the JP-4 fuel.

2. NO_x Emissions

Oxides of nitrogen (NO_x) may form from oxidation of nitrogen which originated either in the air or in the fuel. Current jet engine fuels and all of the fuels used in this program contained negligible amounts of bound nitrogen, but in the future, alternate sources and/or processing economics may result in significant quantities of bound nitrogen in aircraft fuels. The following discussion is, therefore, applicable only to the "thermal" NO_x production characteristics of current and advanced fuels. Fuels containing significant quantities of bound nitrogen have been investigated in other programs, and typical results are contained in References 8, 9 and 10.

In contrast to CO and HC which are products of incomplete combustion and are, therefore, generally significant only at low power conditions, "thermal" NO_x is an equilibrium product of high temperature combustion and is therefore highest at high power operating conditions. Figure 39 shows the strong effect of combustor operating conditions on NO_x emission levels with JP-4 and JP-8 fuels. The data for both fuels correlates very well with a combustor operating parameter (S_{NOx}) developed for several General Electric "rich-dome" combustors, and shows the significant effects of inlet pressure, temperature, humidity, velocity and fuel-air ratio. At takeoff conditions, the NO_x emission index is about 26 g/kg which is in very good agreement with previous engine and rig test results. At dash, cruise and idle operating conditions, the NO_x levels are approximately 117, 35, and 12 percent, respectively, of the takeoff NO_x level.

NO_x results very similar to those shown in Figure 39 were obtained in each of the tests and results are summarized in Table 20. The effect of fuel properties are illustrated in Figure 40. At each of the operating conditions, NO_x levels correlate very well with fuel hydrogen content, and appear to be independent of

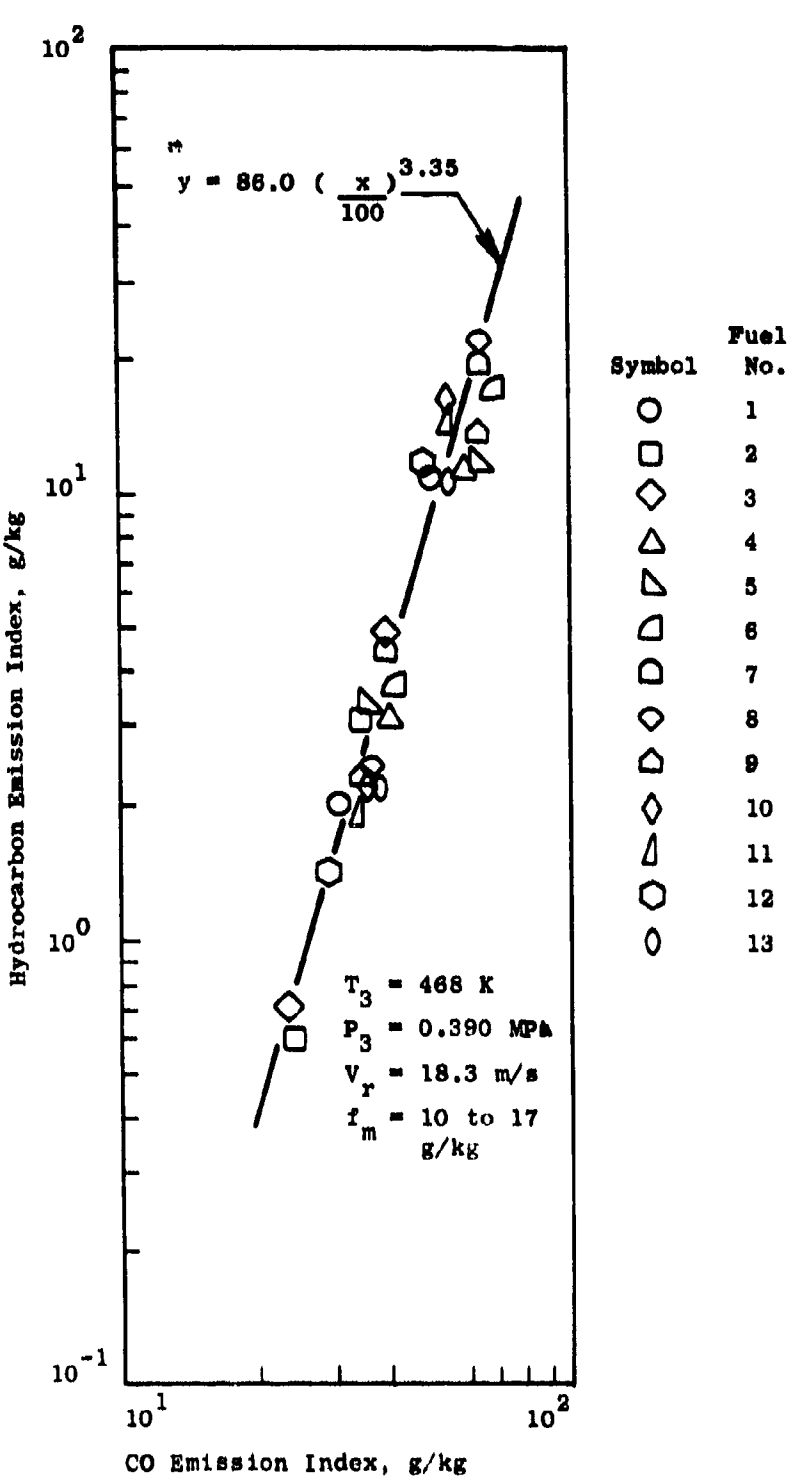

Figure 36. Variation of HC Emission Levels With CO Emission Levels at Idle Operating Conditions.

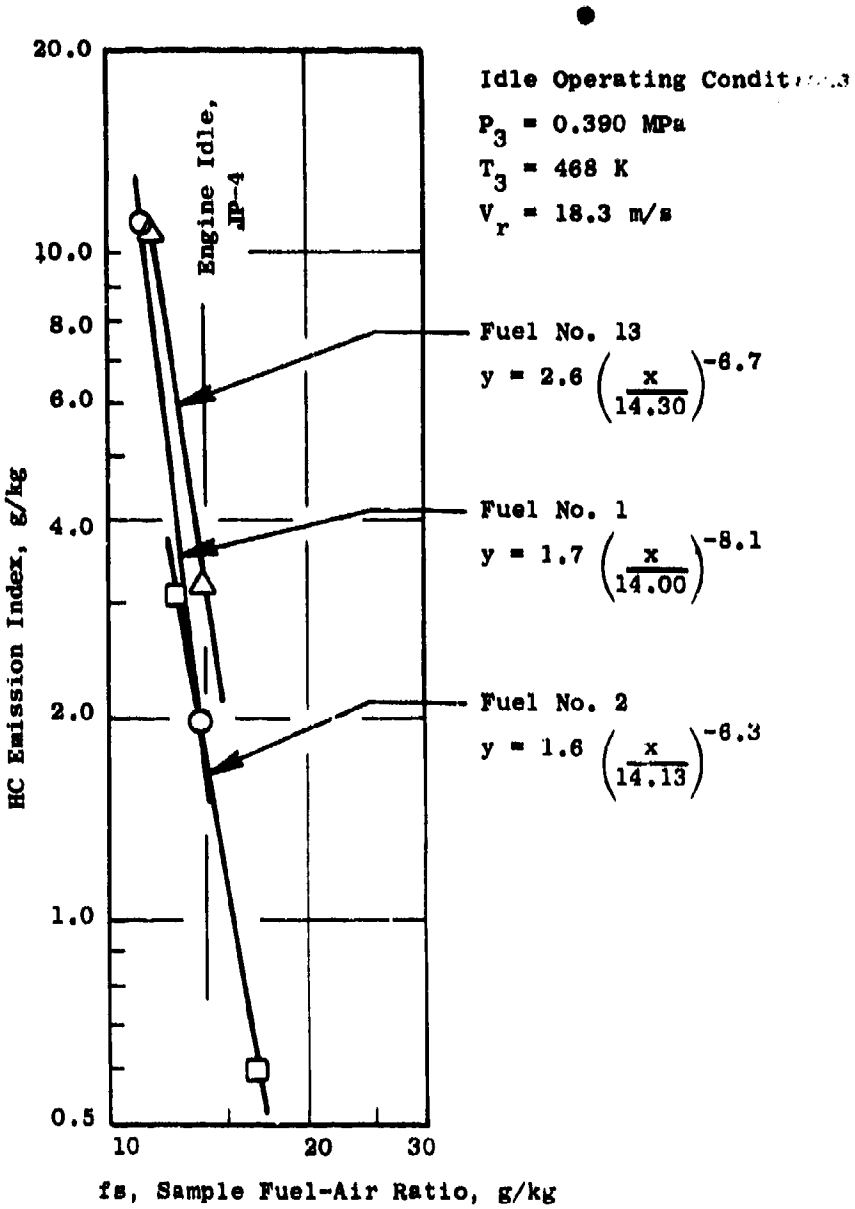

Figure 37. Effect of Fuel-Air Ratio on Idle HC Emission Levels.

Table 19. Summary of HC Emission Test Results.

Fuel Number	HC Emission Index, g/kg (1)			
	Idle	Cruise	Takeoff	Dash
1	1.68	0.1	0	0
2	1.59	0	0	0
3	1.83	0.1	0	0
4	1.85	0	0	0
5	2.23	0	0	0
6	1.82	0	0	0
7	2.73	0	0	0
8	1.03	0	0	0
9	0.88	0	0	0
10	1.11	0	0	0
11	0.96	0	0	0
12	0.90	0	0	0
13	2.65	0	0	0

(1) Corrected to true engine operating conditions.

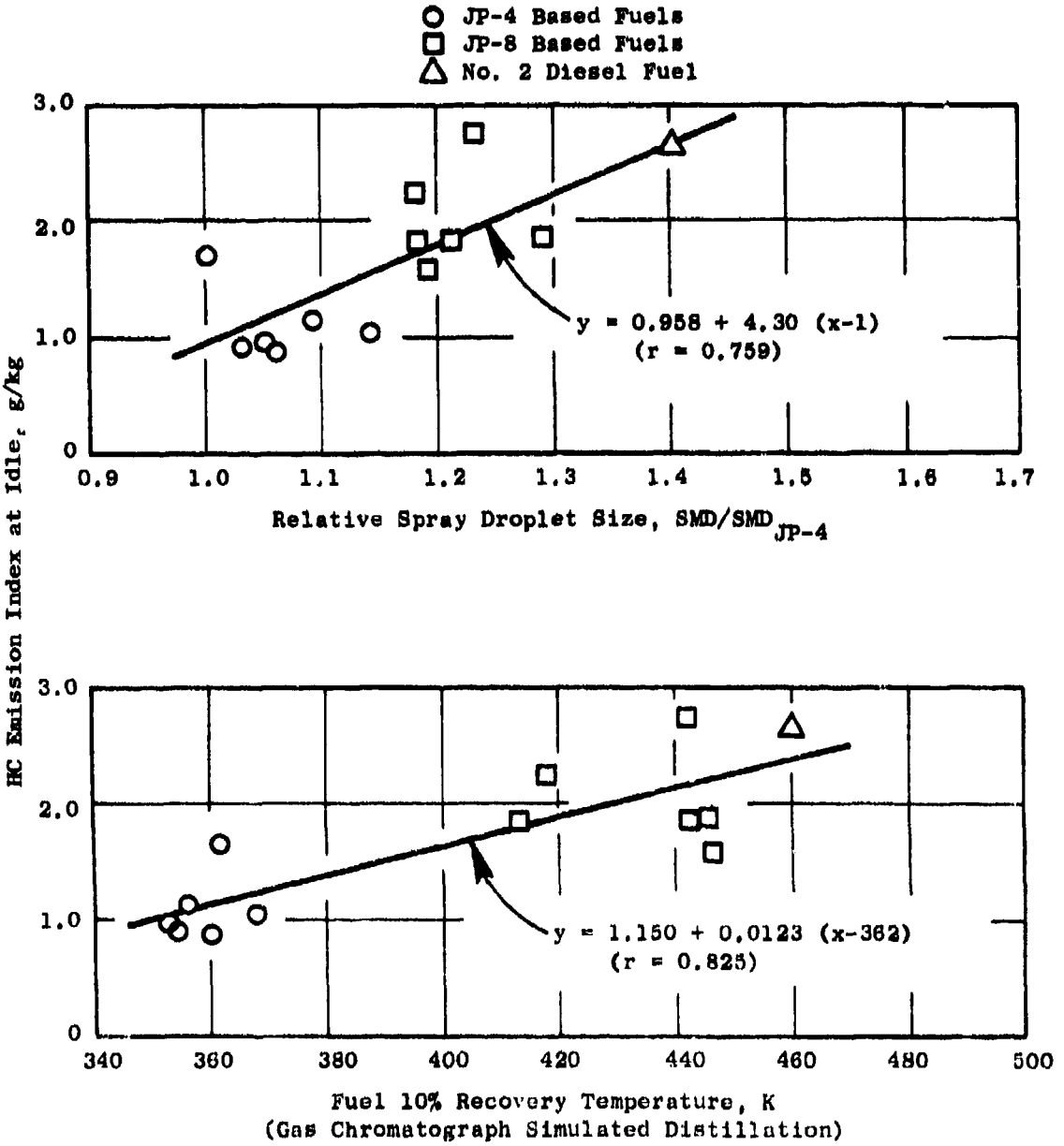

Figure 38. Effect of Fuel Atomization and Volatility on Idle HC Emission Levels.

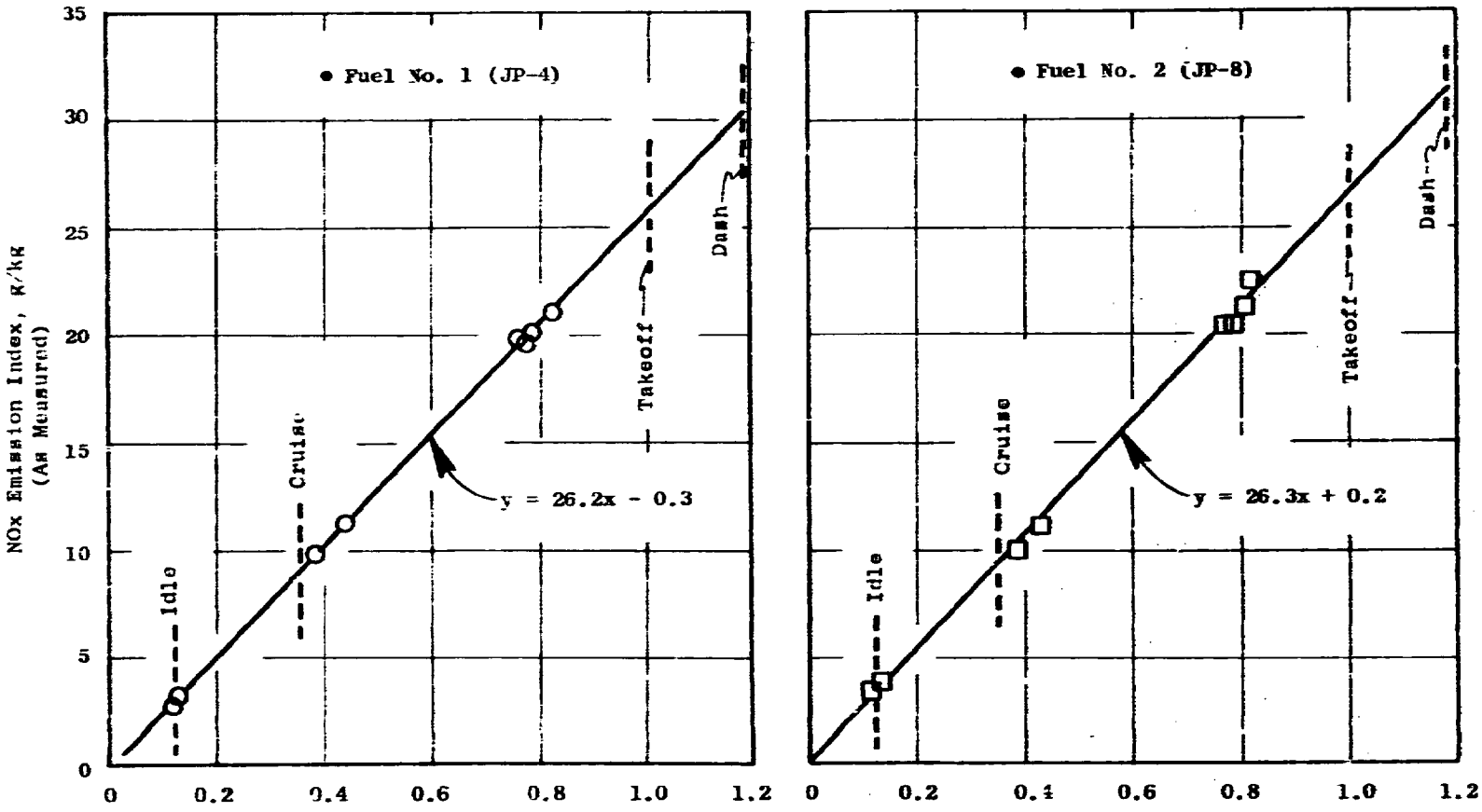

$$S_{NOx} = \left(\frac{23.5}{V_r}\right)\left(\frac{P_3}{2.718}\right)^{0.37}\left[\ddagger(f)\right]\left\{\exp\left[\left(\frac{T_3 - 828.7}{191.7}\right) + \left(\frac{6.29 - H}{53.2}\right)\right]\right\}, \quad \text{m/s, MPa, K, g/kg}$$

Figure 39. Effect of Operating Conditions on NOx Emission Levels.

Table 20. Summary of NO_x Emission Test Results.

Fuel Number	NOx Emission Index, g/kg (1)			
	Idle	Cruise	Takeoff	Dash
1	2.89	8.88	25.94	30.55
2	3.36	9.38	26.52	31.15
3	3.33	9.15	25.71	30.17
4	4.52	10.85	28.87	33.73
5	4.34	10.33	27.40	32.00
6	3.83	10.38	29.02	34.05
7	3.51	9.68	27.24	31.98
8	4.19	10.41	28.11	32.88
9	3.54	~9.4 (2)	~27.1 (2)	~31.9 (2)
10	3.65	10.26	29.09	34.17
11	3.51	9.54	26.73	31.37
12	3.50	9.07	24.93	29.21
13	3.62	9.50	26.25	30.77

(1) Corrected to ambient humidity of 6.3 g/kg and true standard day engine conditions.

(2) Estimated (Span calibration drifted approximately 10%).

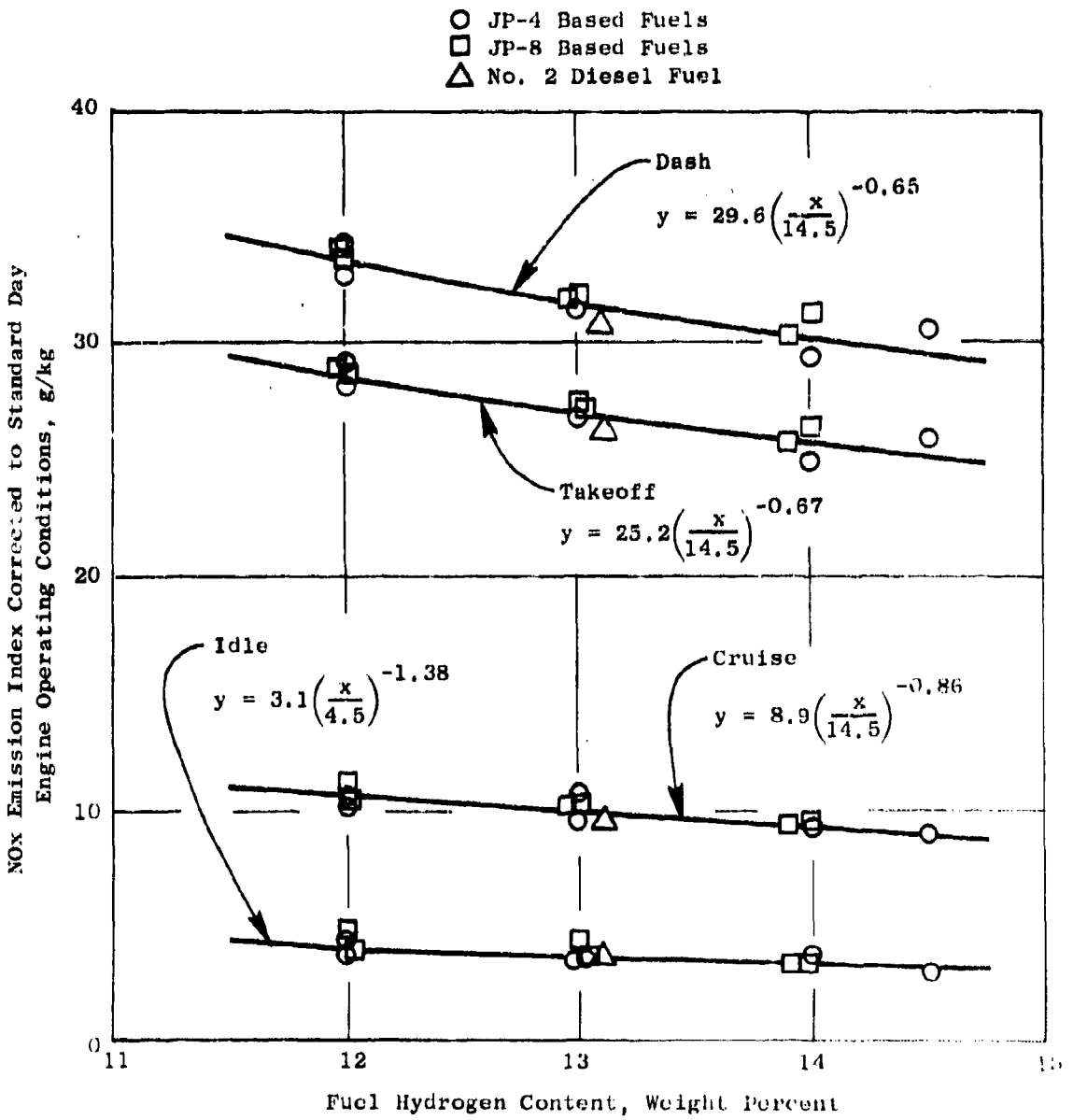

Figure 40. Effect of Fuel Hydrogen Content on NOx Emission Levels.

other fuel effects. This dependence on fuel hydrogen content can be predicted qualitatively at least, from the flame temperatures dependence on fuel hydrogen content and, in turn, the effect of flame temperature on NO_x formation rates in diffusion flame processes. Figure 41 shows the effect of flame temperature (from Table 9) on the NO_x emission levels at takeoff.

3. Smoke Emissions

Smoke, like CO and HC, is a product of incomplete combustion. Combustors with virtually 100 percent combustion efficiency can produce highly visible exhaust plumes, because the soot particle sizes are of the same order of magnitude as the visible light wavelengths. As described in Section IV, the F101 engine combustion system has been designed to produce very low smoke levels, and these tests provide further verification that the design intent has been achieved.

Combustor exit plane smoke measurements were obtained in each of the high pressure combustor rig tests with each of the fuels and operating conditions. These data were then processed as described in Section V.F.1 to correct the data from rig to full density/mixed-flow turbofan engine exhaust plane conditions. Figure 42 illustrates the effects of combustor operating conditions on smoke levels, and also the good correlation between test rig and engine smoke data for this combustion system. At true F101 engine mixed flow exhaust nozzle conditions, smoke levels with JP-5 or JP-8 fuel at idle, cruise, takeoff and dash conditions are approximately 0.4, 1.7, 2.9, and 3.2, respectively, which are on the threshold of smoke measurement system accuracy.

Rig smoke results very similar to that included in Figure 42 were obtained with each of the fuels in this program, and are listed in Appendix A. A summary of smoke levels corrected to true engine conditions are presented in Table 21. Also included in Table 21 are smoke emission indices (grams carbon/kilogram of fuel) computed from the smoke numbers according to the procedure described in Appendix E.

Effects of fuel properties are illustrated in Figure 43. At each engine combustor operating condition, smoke levels decrease with fuel hydrogen content, but no effect of fuel volatility or aromatic type (mono or bicyclic) is evident. The F101 engine exhaust smoke levels would be expected to be well below the visible threshold with any of these fuels.

4. Liner Temperature

Liner temperature measurements were obtained in the high pressure combustor tests at the locations described in Section V.A.2, and detailed data are listed in Appendix A. Figure 44 shows typical variations in measured liner temperature rise ($T_L - T_3$). Peak temperatures always occurred on the outer liner third panel and either at the 18-degree or 36-degree CWALF thermocouple location. Figure 45 shows typical test data for panel 3 outer along with a computer estimate of the temperature profile along the panel. Good correlation is evident. The effect of combustor fuel-air ratio on peak inner liner temperatures with fuels 1 to 4 is shown in Figure 46. Very good correlations were obtained with all 13 fuels (Table A-9), and results are summarized in Table 22.

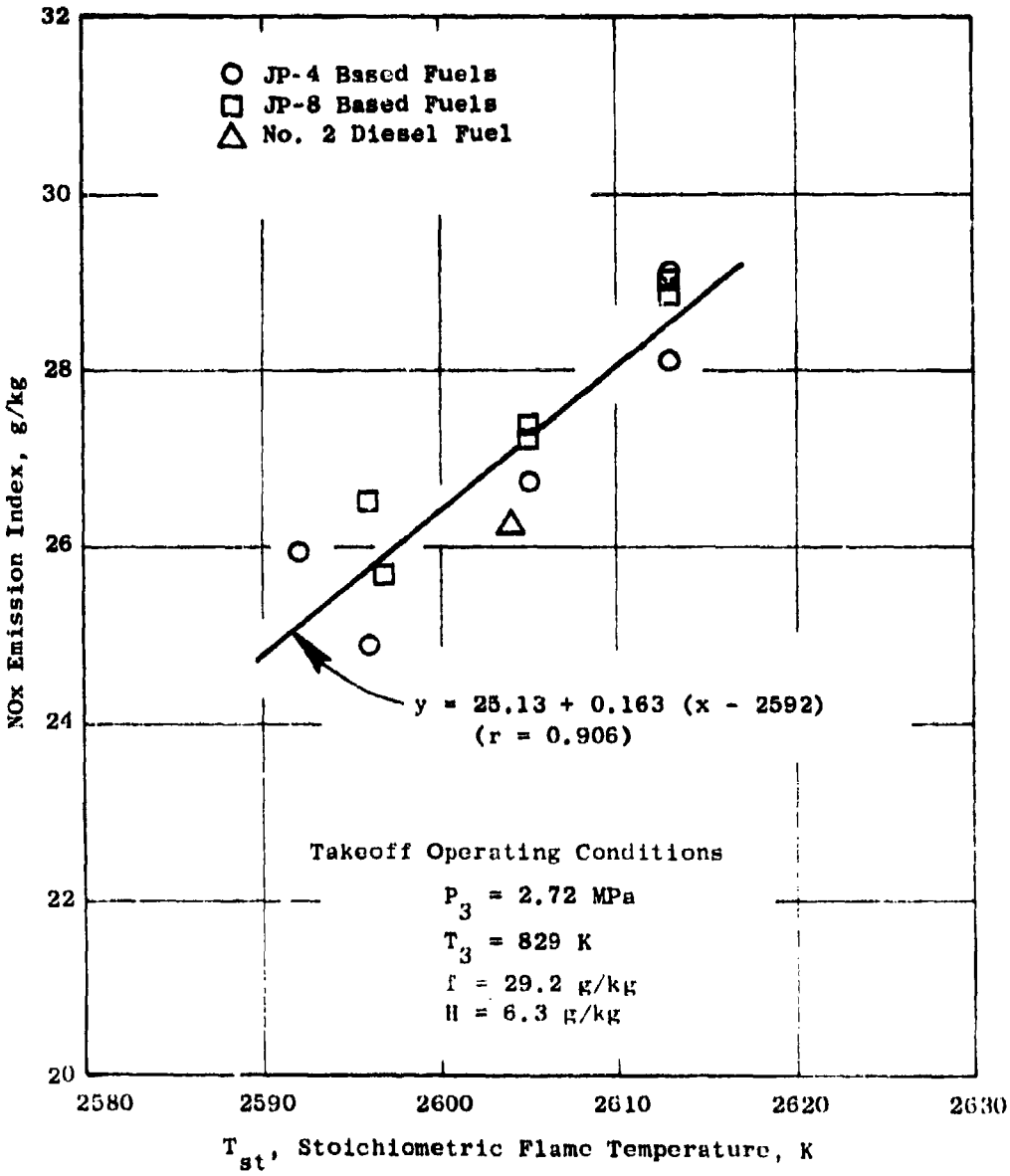

Figure 41. Effect of Flame Temperature on NOx Emission Levels.

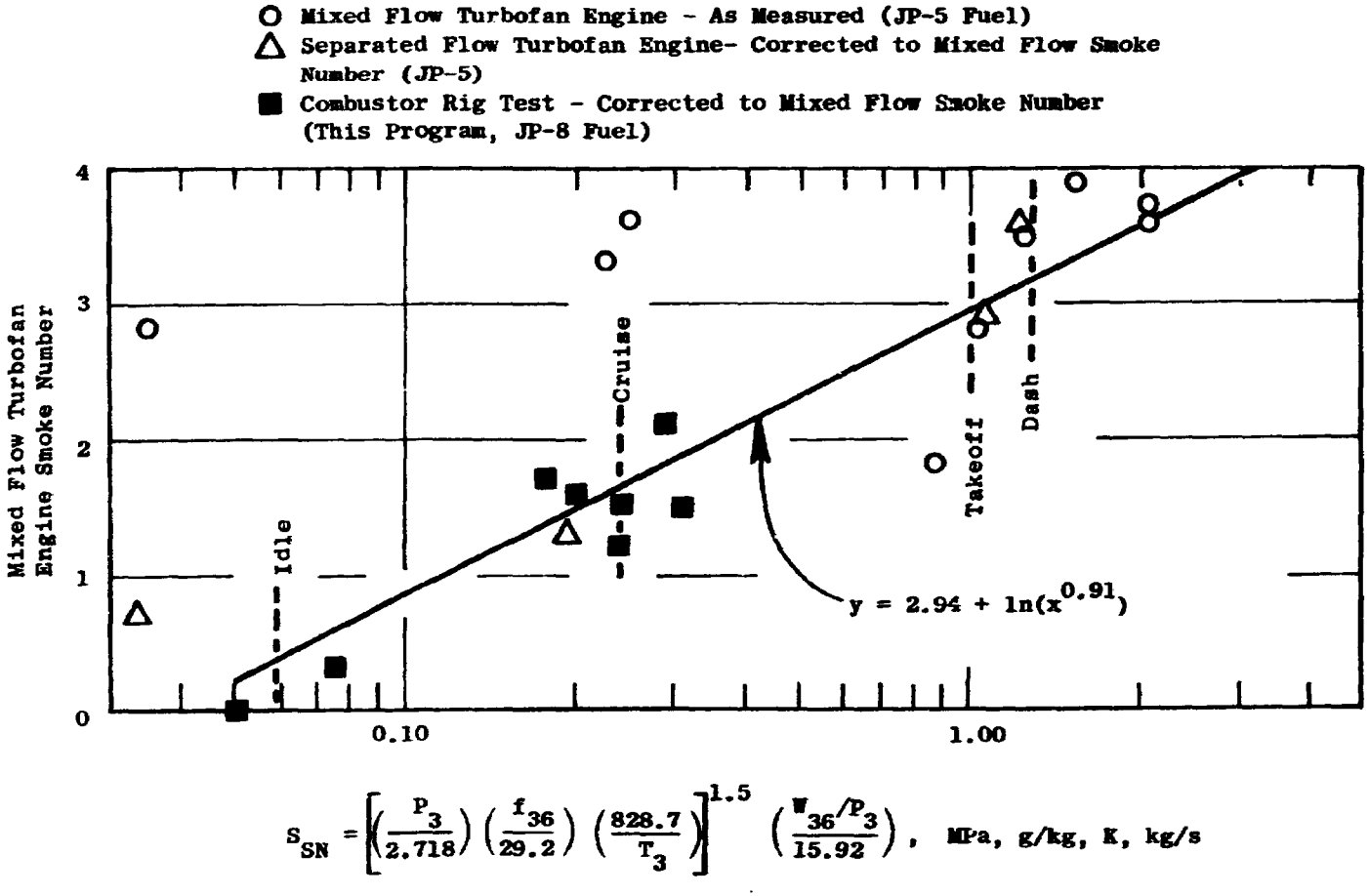

$$S_{SN} = \left[\left(\frac{P_3}{2.718}\right)\left(\frac{f_{36}}{29.2}\right)\left(\frac{828.7}{T_3}\right)\right]^{1.5}\left(\frac{W_{36}/P_3}{15.92}\right), \text{ MPa, g/kg, K, kg/s}$$

Figure 42. Correlation of Combustor Rig and Engine Smoke Data.

Table 21. Summary of Smoke Emission Test Results.

Fuel Number	SN_8 Smoke Number at Engine Exit (1)				EIs Smoke Emission Index, g/kg (1)			
	Idle	Cruise	Takeoff	Dash	Idle	Cruise	Takeoff	Dash
1	0.2	1.4	2.6	2.8	< 0.06	0.02	0.02	0.03
2	0.2	1.6	3.0	3.3	< 0.06	0.02	0.03	0.03
3	0.1	2.0	3.9	4.2	< 0.06	0.02	0.04	0.04
4	1.4	3.0	4.7	5.0	0.07	0.03	0.04	0.05
5	1.0	2.0	3.0	3.2	0.06	0.02	0.03	0.03
6	1.4	2.9	4.4	4.7	0.07	0.03	0.04	0.05
7	1.2	2.6	4.2	4.4	0.06	0.03	0.04	0.04
8	1.1	2.7	4.3	4.6	0.06	0.03	0.04	0.05
9	0.7	1.8	3.0	3.2	< 0.06	0.02	0.03	0.03
10	0.8	2.1	3.4	3.6	< 0.06	0.02	0.03	0.04
11	0.8	2.1	3.9	3.6	< 0.06	0.02	0.04	0.04
12	0.6	2.1	3.6	3.9	< 0.06	0.02	0.03	0.04
13	0.7	2.3	3.9	4.2	< 0.06	0.03	0.04	0.04

(1) Corrected to engine combustor inlet conditions and mixed flow turbofan engine exit conditions.

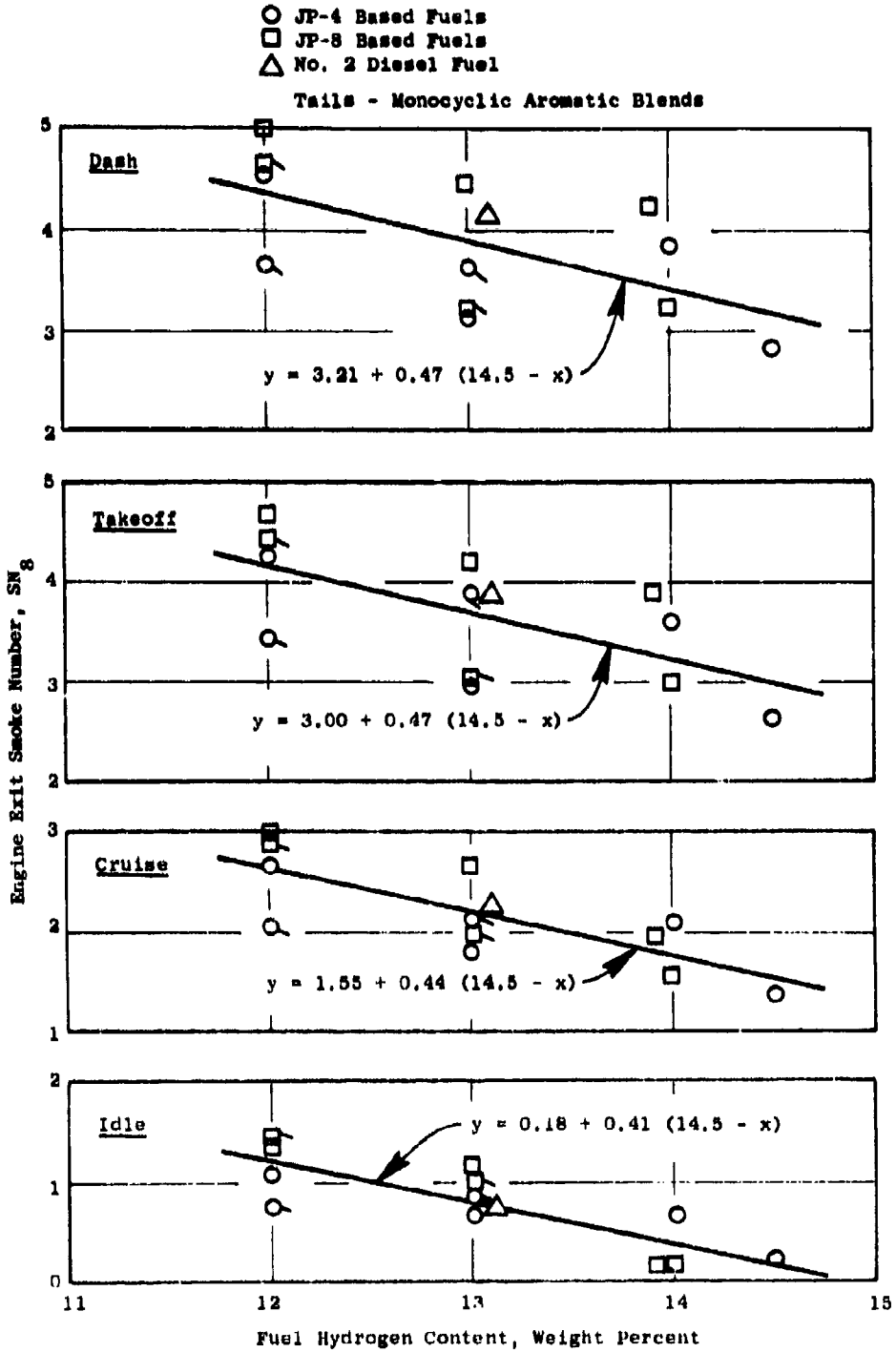

Figure 43. Effect of Fuel Hydrogen Content on Smoke Emission Levels.

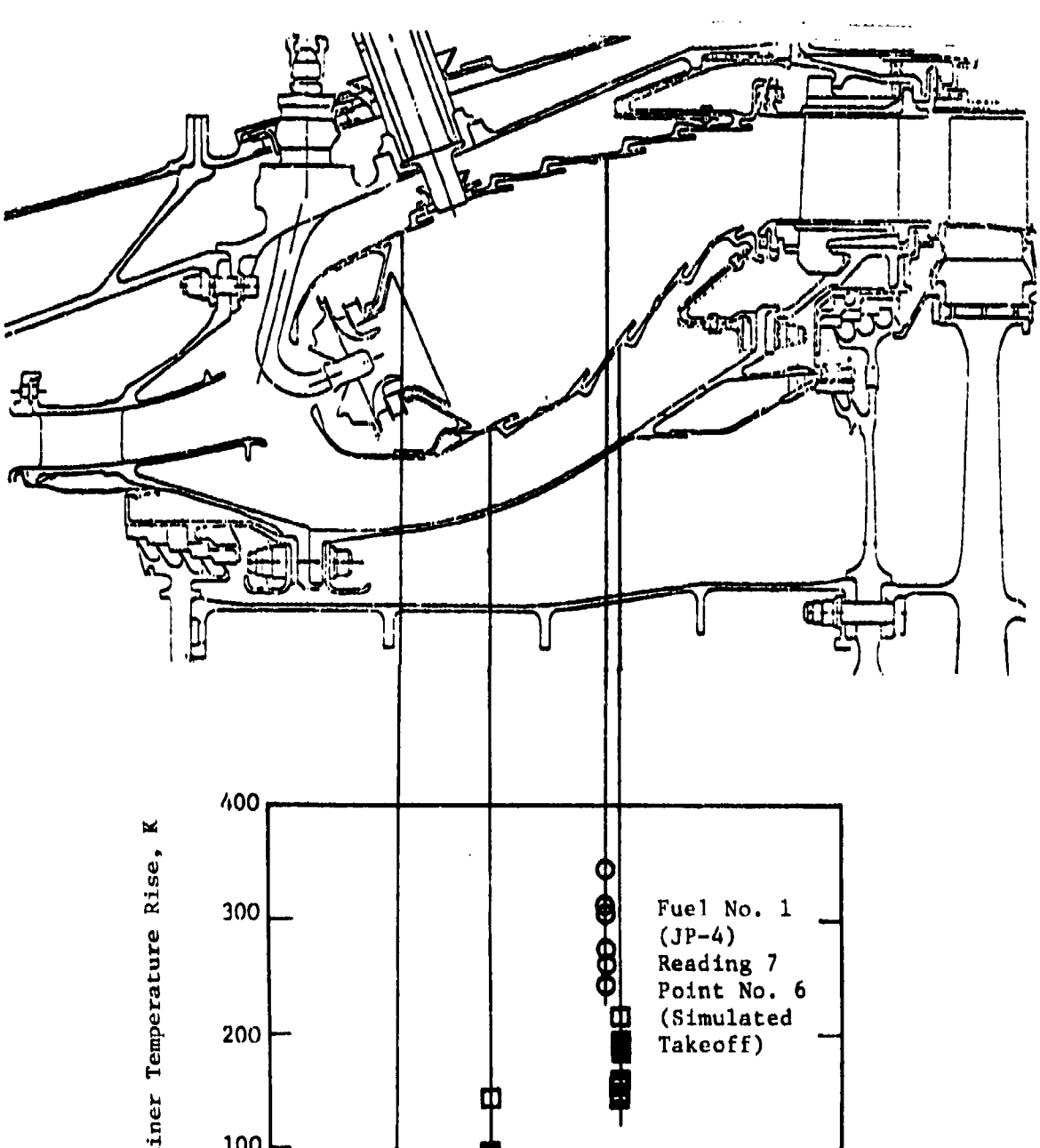

Figure 44. Typical Combustor Liner Temperature Distribution.

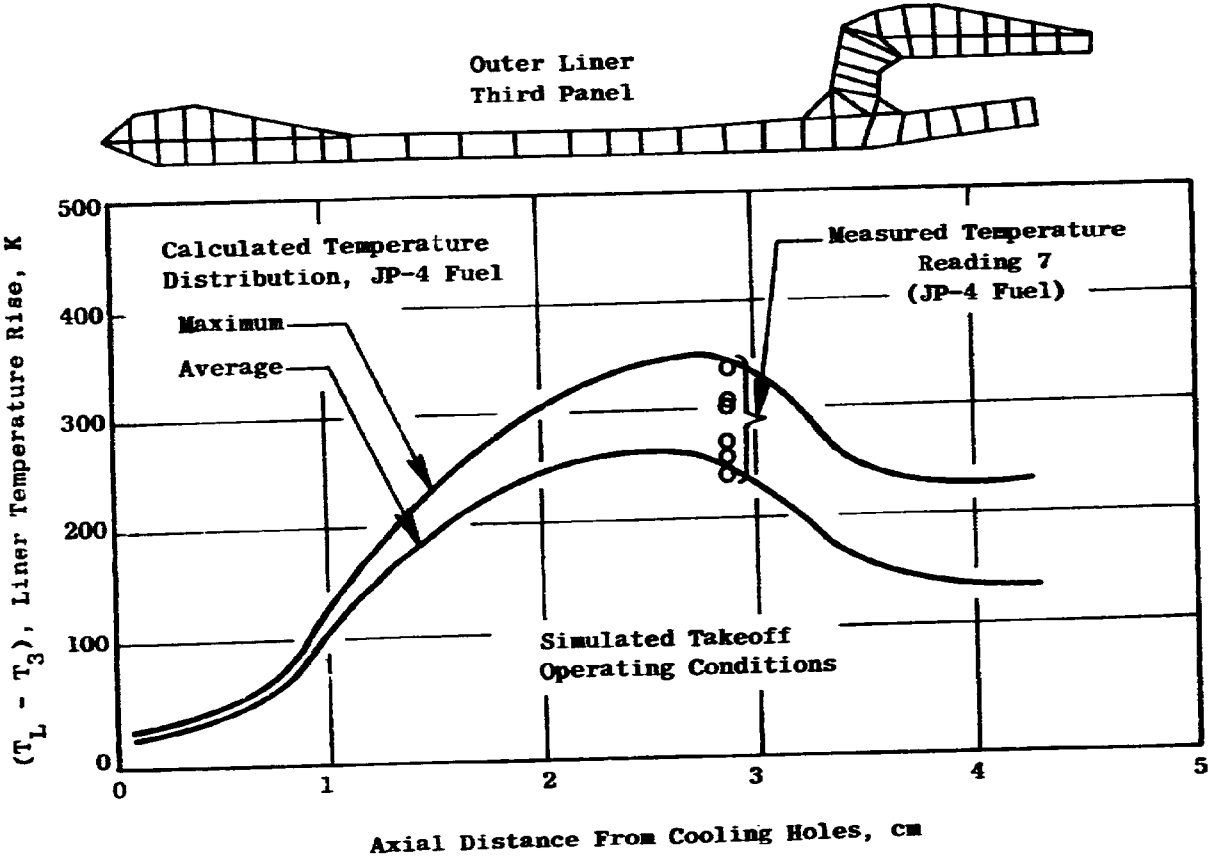

Figure 45. Typical Outer Liner Panel 3 Temperature Distribution.

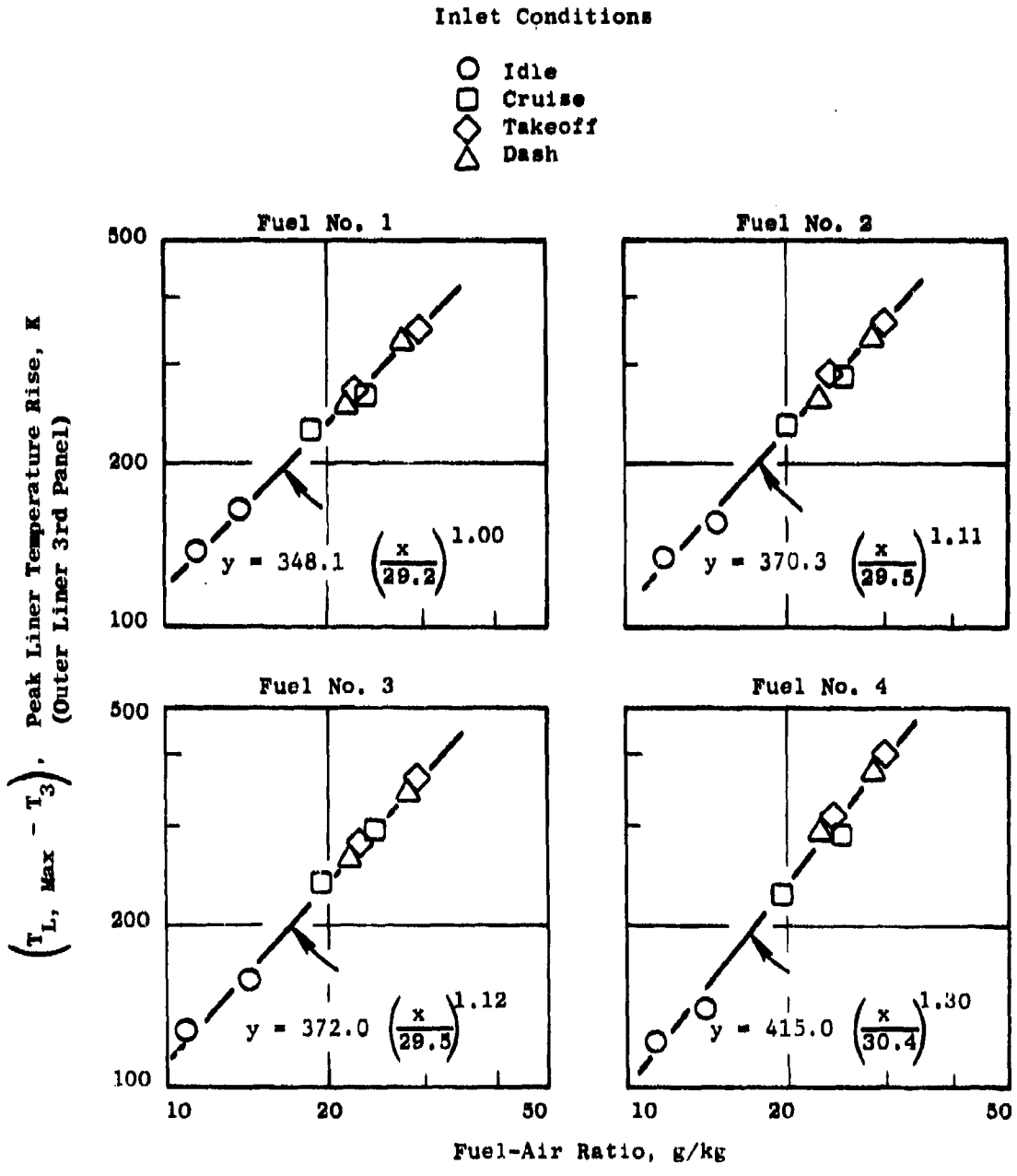

Figure 46. Effect of Operating Conditions on Rig Maximum Liner Temperature Rise.

Table 22. Summary of Liner Temperature Results.

Fuel Number	$(T_{Lmax} - T_3)$ Peak Liner Temperature Rise, K						
	Idle (Rig & Engine)	Cruise (1)		Takeoff (2)		Dash (3)	
		Rig	Engine	Rig	Engine	Rig	Engine
1	167	286	270	348	383	333	385
2	164	298	282	370	405	352	402
3	164	299	283	372	407	354	404
4	160	322	306	415	450	391	441
5	150	290	274	368	403	348	398
6	142	314	298	418	453	391	441
7	136	282	266	368	403	346	396
8	150	296	280	379	414	358	408
9	144	276	260	349	384	330	380
10	168	293	277	358	393	342	392
11	166	283	267	343	378	328	378
12	174	278	262	330	365	317	367
13	159	295	279	368	403	350	400

(1) $\Delta T_{Engine} = \Delta T_{Rig} - 16$, K due to backside cooling.

(2) $\Delta T_{Engine} = \Delta T_{Rig} + 35$, K due to backside cooling and pressure.

(3) $\Delta T_{Engine} = \Delta T_{Rig} + 50$, K due to backside cooling and pressure.

Table 22 summarizes both rig and predicted engine liner temperatures. Engine liner temperature rises at cruise were adjusted by 16 K due to backside cooling differences between the rig and engine. In the engine turbine cooling air provides additional backside cooling. The adjustment is based on computer estimates discussed further in Section VI.B. At takeoff and dash, adjustments of 35 K and 50 K were made to the rig data. These corrections included both backside cooling and pressure effects and were again estimated using the computer analysis. Peak rig liner temperature rise as a function of fuel hydrogen content and engine power level is shown in Figure 47. At takeoff and dash conditions, strong effects of hydrogen content are shown, but at cruise the effect is less, and at idle slightly reversed.

Shown in Reference 9 is the dimensionless liner temperature parameter $[(T_{L,\ max} - T_{L,\ max,\ JP\text{-}4})]/(T_{L,\ max,\ JP\text{-}4} - T_3)$ which correlates a wide variety of data involving rich combustion systems with pressure atomizing fuel injection systems designed by three different engine manufacturers. As shown in Figure 48, the current data indicate less sensitivity to fuel hydrogen content than do the data for the older, richer dome combustors.

5. Combustor Exit Profile and Pattern Factor

Combustor exit temperature distributions were measured in atmospheric discharge combustor rig tests as described in Section V.A.5. This atmospheric pressure test technique has been employed extensively at General Electric to develop the excellent temperature profile and pattern factor characteristics of large full annular combustion systems. In general, the effects of combustor inlet pressure level or fuel type on exit temperature distributions have been thought to be small, particularly for newer, large combustors. However, this program produced some surprises in that atmospheric pressure tests clearly showed a fuel effect.

Typical combustor exit temperature profiles from these tests are shown in Figure 49. Data for two fuels (JP-4 and JP-8) are included, and for each fuel repeat traverse data are included to show data consistency. The average profile is very repeatable, and no discernable fuel effect is evident, which is expected. The peak profiles, however, are less repeatable and a fuel effect is evident, which was unexpected. In this example, the pattern factor is about 0.09 higher with JP-8 fuel than with JP-4 fuel. Figure 50 shows that approximately this same pattern factor difference was measured at all test conditions. Results very similar to those shown in Figures 49 and 50 were obtained with all of the fuels, which are summarized in Table 23. As shown in Figure 51, pattern factor levels correlate quite well with the fuel atomization parameter.

This test series was the first time that fuel variations had been investigated in the F101 combustor atmospheric pressure pattern factor test rig, but fuel variations had been pattern factor tested many times in other combustor rigs including:

1) TF39/CF6 full-annular combustor rig at atmospheric pressure.

2) J79 single can high pressure test rig (Reference 1).

3) T700 full-annular combustor rig at high pressure. (Combustor design similar to F101)

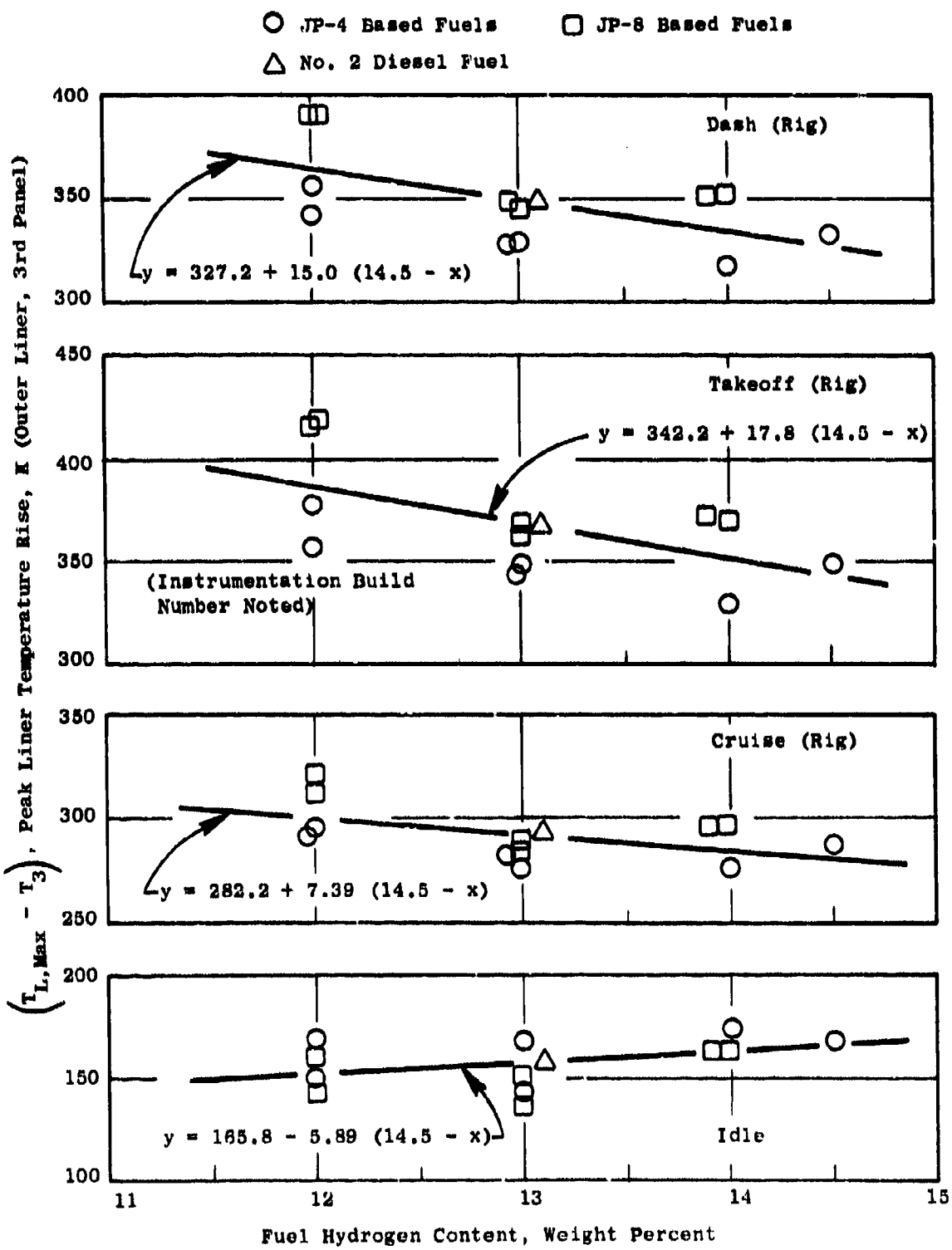

Figure 47. Effect of Fuel Hydrogen Content on Peak Liner Temperature Rise.

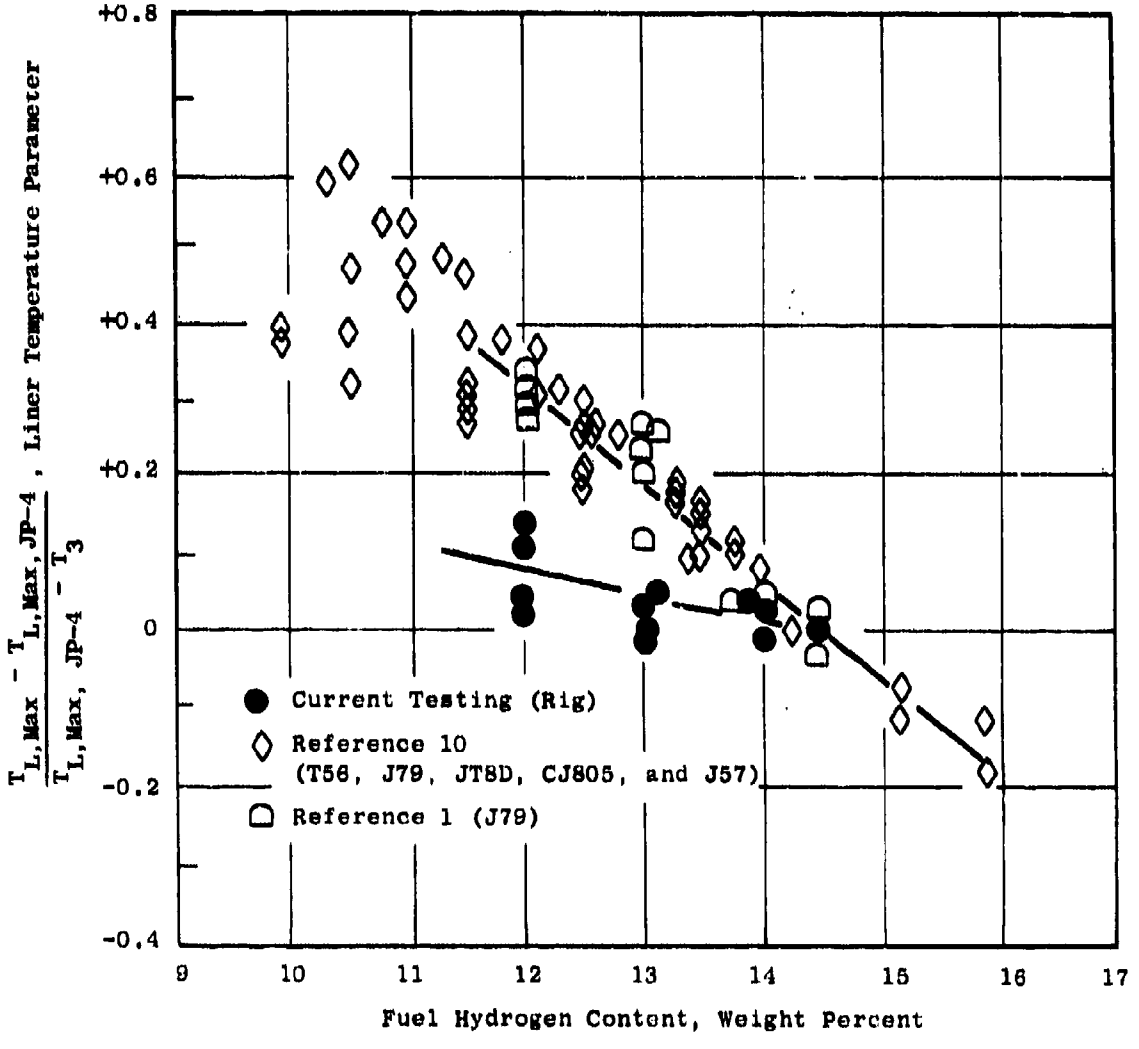

Figure 48. Effect of Fuel Hydrogen Content on Liner Temperature Parameter at Cruise Operating Conditions.

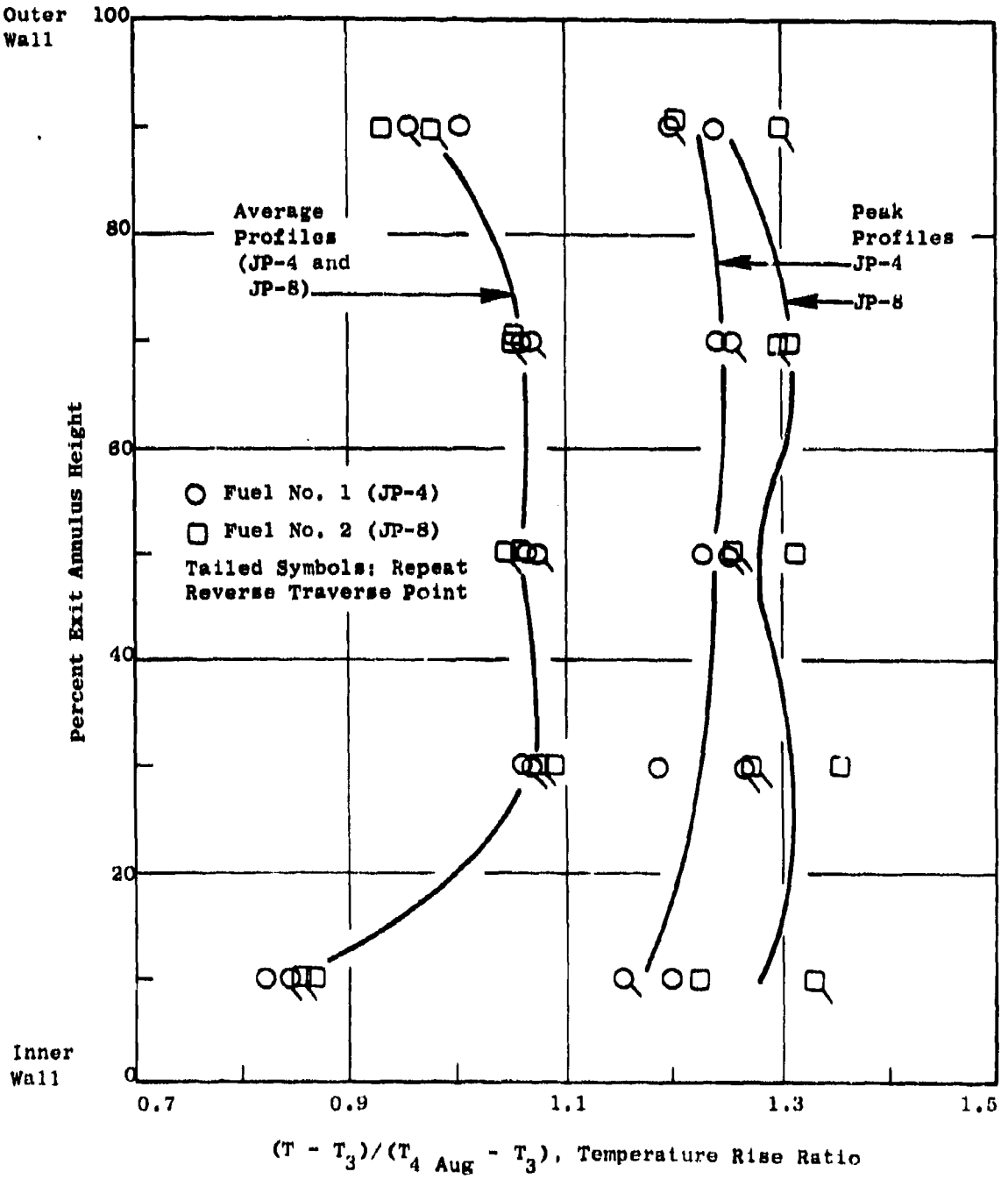

Figure 49. Typical Combustor Exit Temperature Profiles in Atmospheric Pressure Test.

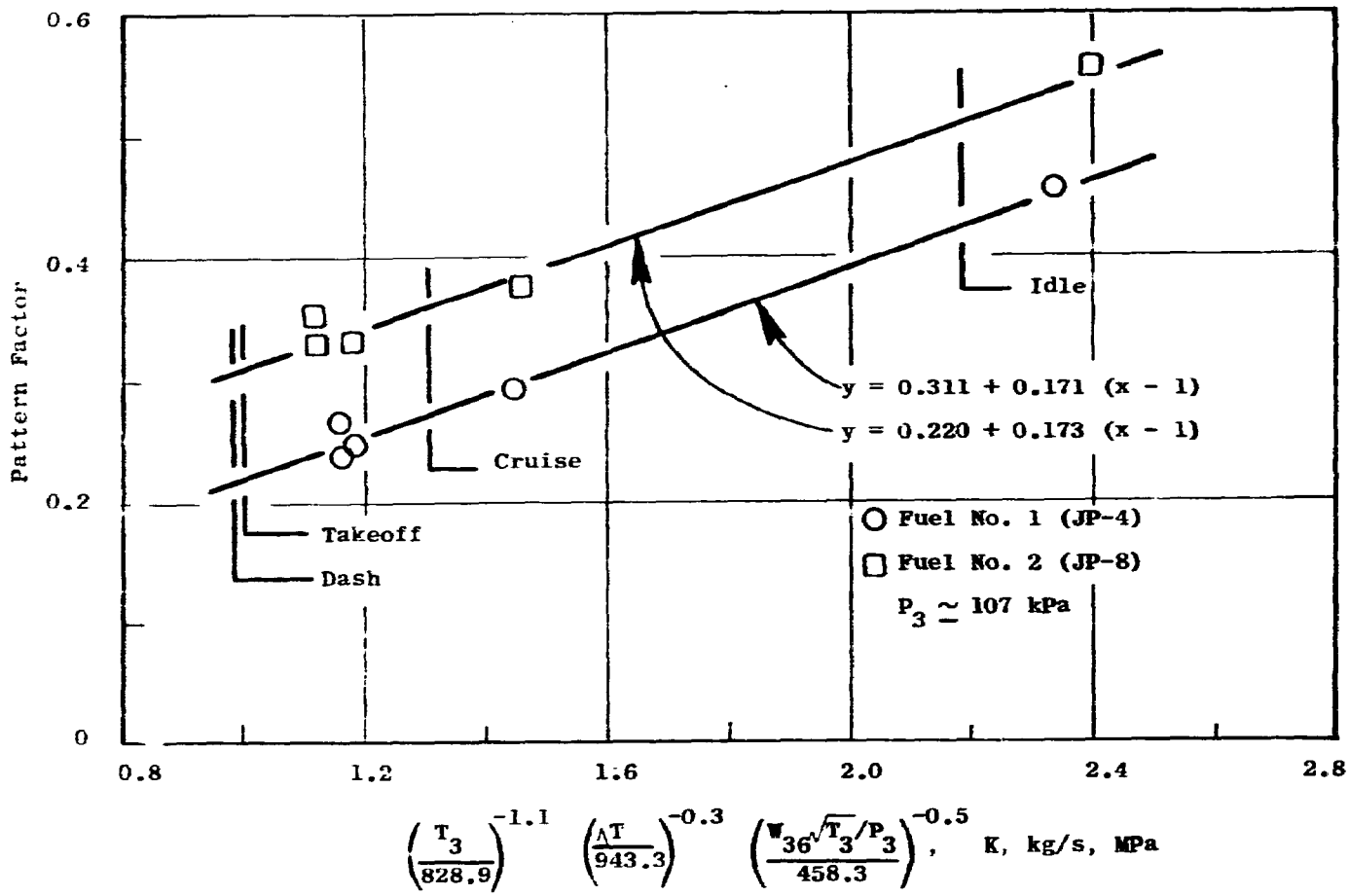

Figure 50. Effect of Combustor Operating Conditions on Pattern Factor in Atmospheric Pressure Tests.

Table 23. Summary of Pattern Factor and Radial Profile Test Results.

Fuel Number	Pattern Factor [1] $\left(T_{4,\,max} - T_{4,\,avg}\right) / \Delta T_{avg}$				Profile Factor $\Delta T_{max,\,profile} / \Delta T_{avg}$		
	Idle	Cruise	Takeoff	Dash	Idle	Cruise	Takeoff / Dash
1	0.425	0.274	0.220	0.216	1.085	1.063	1.073
2	0.513	0.364	0.311	0.307	1.083	1.072	1.089
3	0.636	0.370	0.274	0.268	1.077	1.068	1.076
4	0.725	0.393	0.274	0.266	1.081	1.068	1.092
5	0.670	0.360	0.249	0.241	1.135	1.092	1.101
6	0.833	0.425	0.279	0.269	1.131	1.119	1.134
7	0.493	0.329	0.270	0.266	1.094	1.075	1.088
8	0.461	0.273	0.205	0.200	1.087	1.069	1.077
9	0.484	0.285	0.214	0.209	1.076	1.066	1.078
10	0.644	0.307	0.186	0.178	1.119	1.101	1.103
11	0.508	0.292	0.215	0.210	1.111	1.098	1.103
12	0.475	0.282	0.212	0.208	1.105	1.090	1.100
13	0.630	0.372	0.279	0.273	1.093	1.082	1.101

[1] Corrected to engine T_3, ΔT, $\frac{W_c\sqrt{T}}{P_3}$ but at atmospheric discharge pressure.

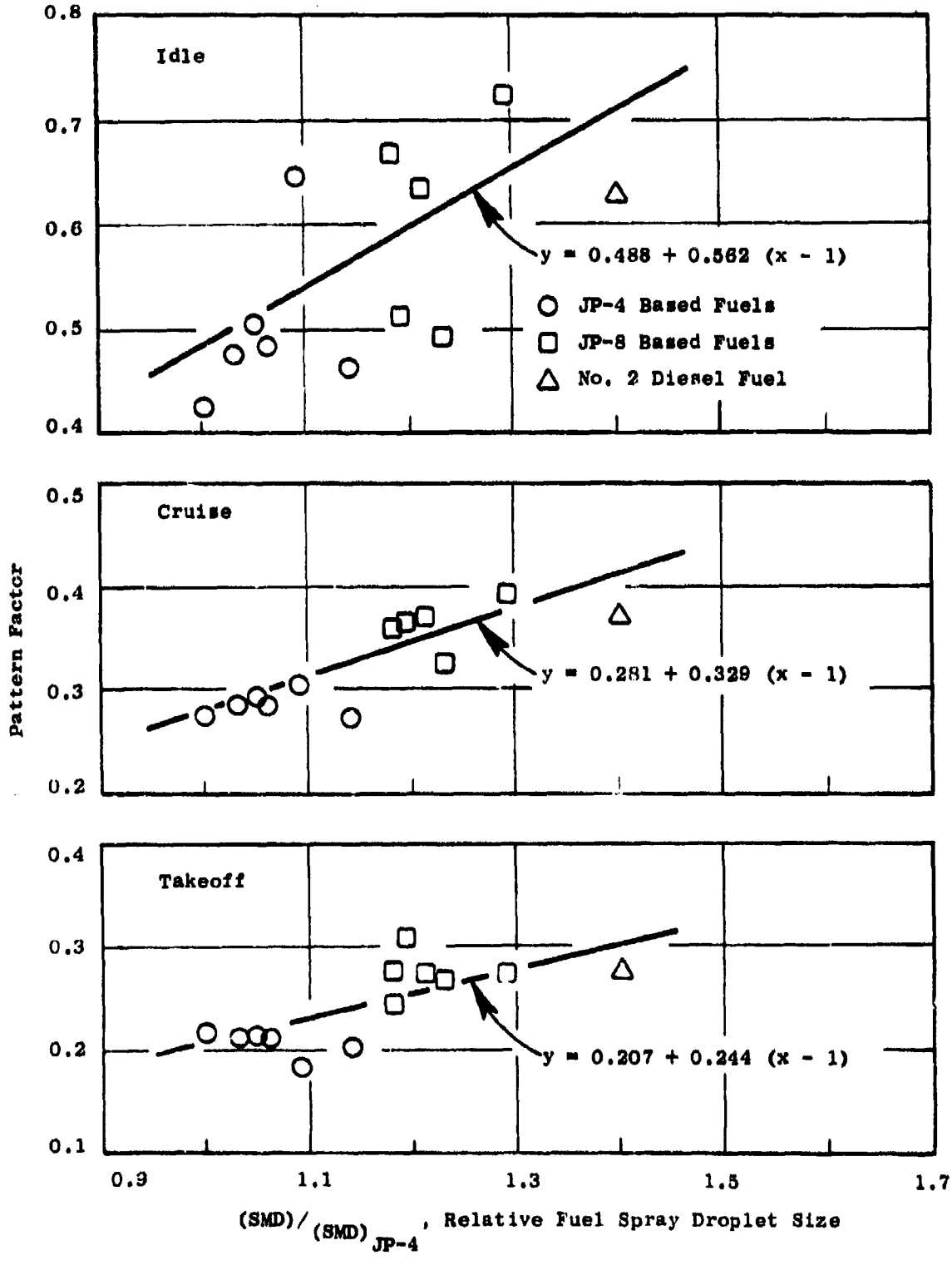

Figure 51. Effect of Fuel Spray Droplet Size on Pattern Factor in Atmospheric Pressure Test.

4) TF34 full-annular combustor rig at high pressure. (Combustor design similar to F101)

No fuel effects were detected in any of these other pattern factor rig tests. Further, all of these engines, including the F101, have been run with JP-4 and JP-5 (Jet A) fuel and no fuel effects on turbine stator vane condition have been detected. Therefore, it is concluded that the apparent effect of fuel properties on F101 pattern factor must be an atmospheric test phenomenon only which is evident because of the high loading in this design (high space rate and very low length-to-height ratio).

A possible explanation for the apparent effect of fuel atomization on pattern factor only in atmospheric pressure tests may be an effect of air density on spray droplet size in addition to the parameters contained in Equation 4. This correlation (from Reference 4) presumably does not contain an air density term because all of the experiments were conducted at atmospheric pressure, as have most atomization studies. However, it is generally concluded that droplet sizes decrease with increasing air density. In Reference 10, several droplet size correlations are presented which include air density with exponents ranging from -0.35 to -1.00. At full density F101 engine conditions droplet sizes may be small enough with both JP-4 and JP-5 fuels that pattern factor is controlled by other parameters.

6. Carbon Deposition

As discussed in Section V.B, high pressure combustor tests were run with procedures established to provide information as to the relative carbon deposition tendencies of each fuel. Each test began with a clean swirler and combustor dome, and was run the same total time (5.25 hours). At the completion of each test, airflow calibrations of the swirlers and total assembly were made which are presented in Table B-1 and summarized in Table 24. Photographs, which are included in Appendix B, were also made to document the carbon deposition tendencies. No massive deposits were found in any of the tests, and as shown in Figure 52, no significant flow area reduction was measured with any of the fuels. The only distress noted in this test series was a tendency for burning of the trailing edge of the flared dome extension insert with low hydrogen content fuels. The need for additional cooling in this region had previously been identified and has been incorporated into newer F101 combustor dome designs. These tests suggest that with reduced hydrogen content fuels some additional cooling may be required.

7. Cold Day Ground Starting and Idle Stability

Fifteen cold day ground start tests were conducted in the 54-degree sector combustor rig using procedures described in Section V.C.2. Detailed test results are listed in Appendix C, and typical results are illustrated in Figure 53. In each test, 2500 rpm engine motoring conditions were simulated, and lean lightoff and lean blowout limits were determined as a function of ambient (fuel and air) temperature in steps from test cell ambient down to the limit or to 239 K (-30° F). As shown in Figure 53, lightoffs were obtained down to 239 K with JP-4 fuel, but the required fuel-air ratio increased significantly. With the less volatile/more viscous fuels, cold day limits were encountered above 239 K. Results for all fuels are summarized in Table 25, and effects of fuel atomization and volatility on the cold day limits are illustrated in Figure 54. For this group of fuels, these two

Table 24. Summary of Carbon Deposition Test Results.

Fuel Number	Ae, Posttest / Ae, clean Effective Airflow Area Ratio		Splash Plate Burns	Flared Dome Extension Insert Burns
	Primary Swirler	Total Assembly		
1	0.953	0.970	No	No
2	0.955	0.955	No	No
3	0.973	0.965	No	No
4	0.980	0.976	No	Yes
5	1.063	0.981	No	No
6	1.002	0.977	No	Yes
7	0.968	0.934	No	No
8	0.900	0.972	No	No
9	0.946	0.980	No	No
10	1.000	0.994	No	No
11	0.971	1.003	No	No
12	0.968	0.978	No	No
13	0.989	0.960	No	No
Avg.	0.975	0.973		

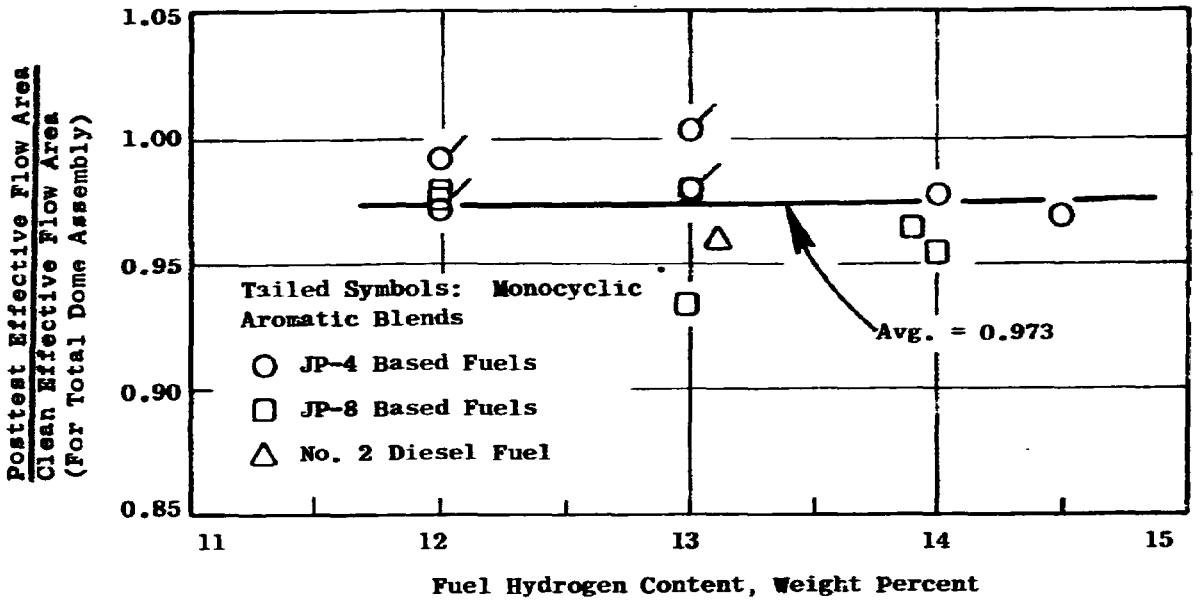

Figure 52. Effect of Fuel Hydrogen Content on Combustor Dome Assembly Flow Area Reduction Due to Carbon Deposition.

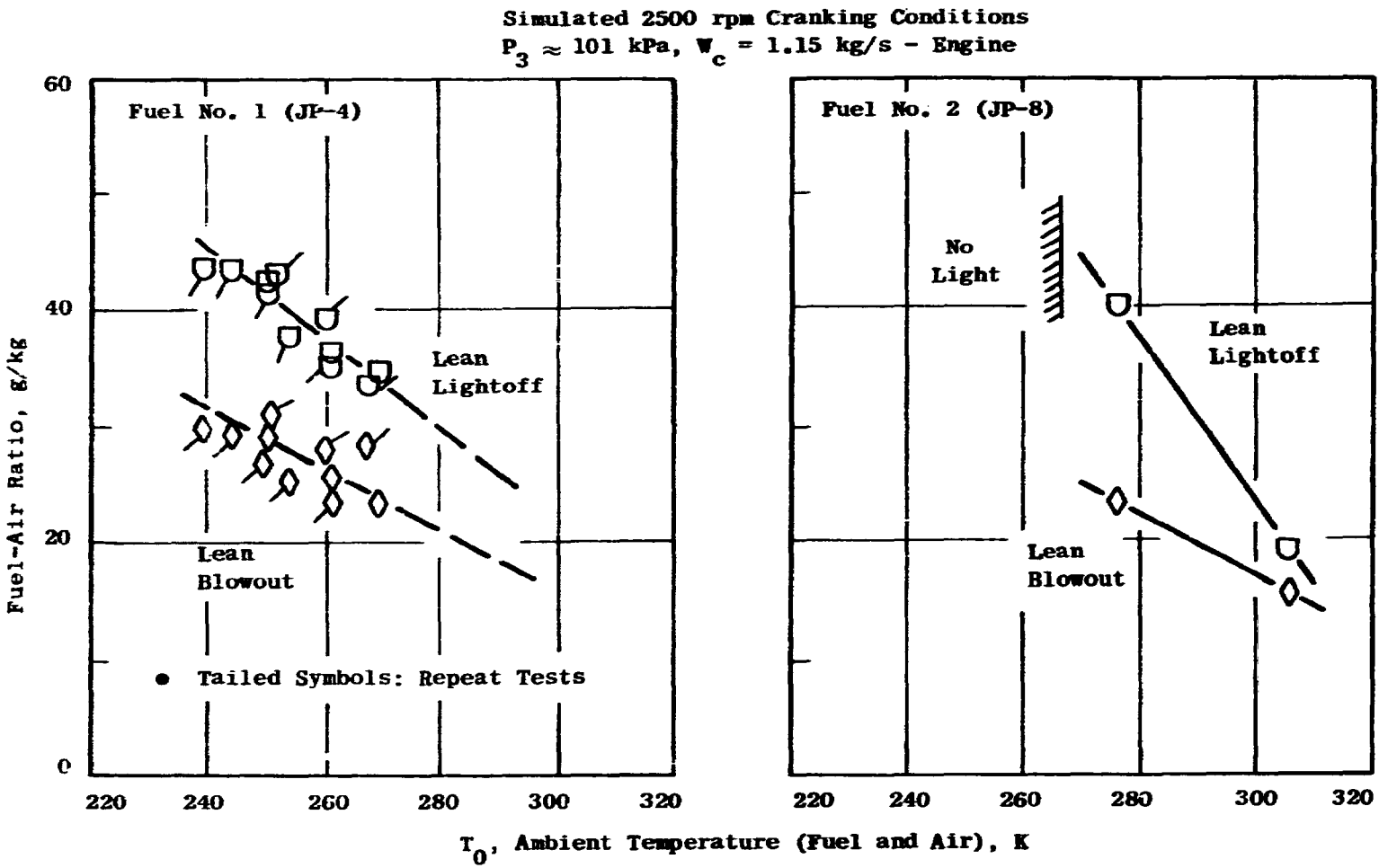

Figure 53. Typical Ground Start Characteristics.

Table 25. Summary of Ground Start Test Results.[1]

Fuel Number	Standard Day (288.2 K) Fuel-Air Ratio Limit, g/kg		Cold Day Limit[2] Ambient Temperature, K
	Lean Light-Off	Lean Blowout	
1	27	19	<239
1R	25	16	<239
2	34	20	266
3	35	20	279
4	40	24	272
5	34	22	267
6	37	27	268
7	39	33	278
8	38	26	260
9	41	26	256
10	43	23	273
11	36	28	244
12	29	24	<239
13	44	30	278
1RR	∿27	∿20	-

(1) Simulated 2500 rpm Cranking Conditions
$P_3 \approx 101$ kPa, $W_c = 1.15$ kg/s - engine.

(2) $T_3 = T_{fuel} = T_o$
$W_f \leq 50.4$ g/s - engine $\rightarrow$ $f_4 \leq 44$ g/kg.

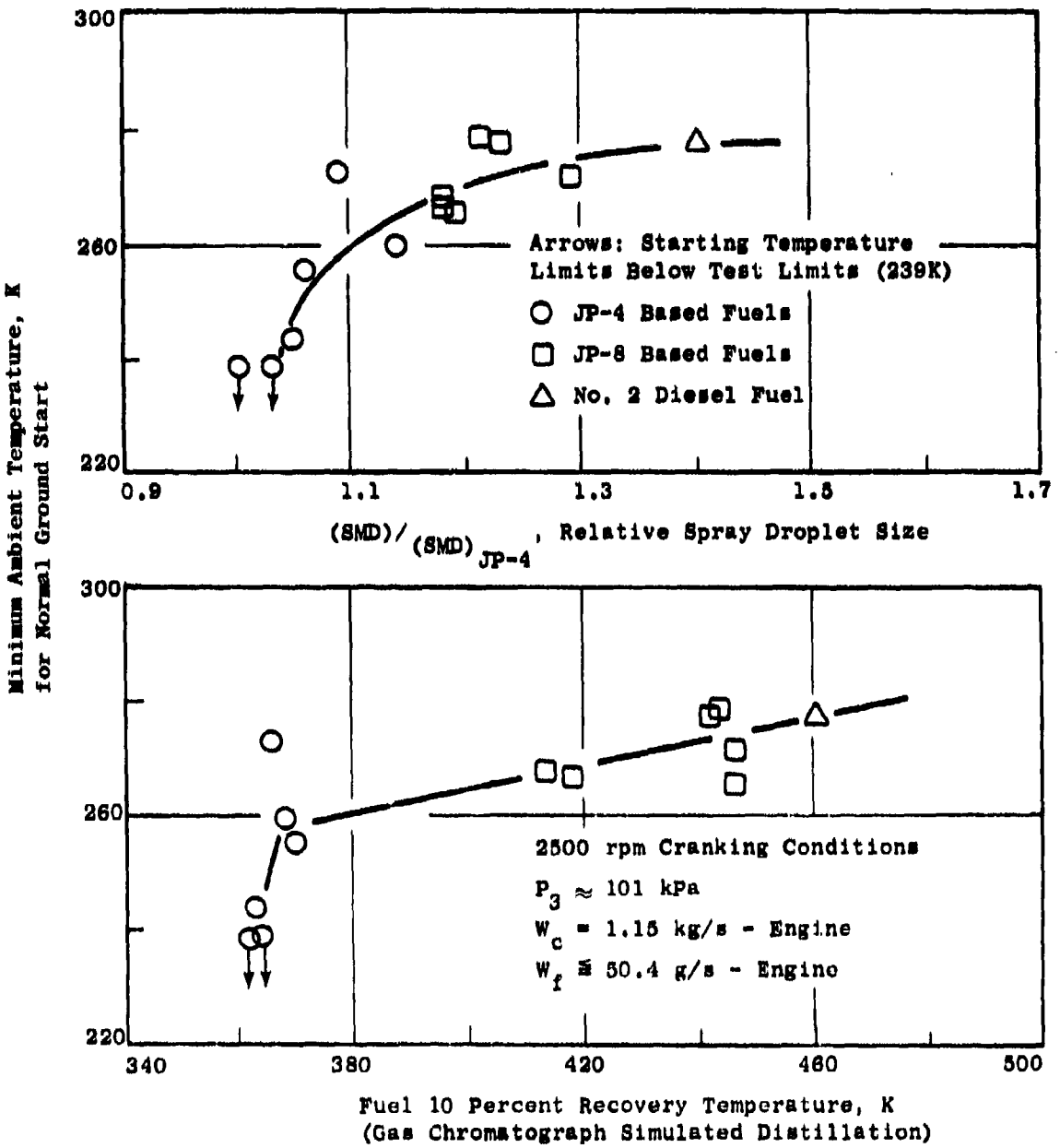

Figure 54. Effect of Fuel Atomization and Volatility on Cold Day Ground Starting Capability.

limits are illustrated in Figure 54. For this group of fuels, these two properties are highly correlated, but it appears that the cold day limit correlates somewhat better with the atomization parameter. No effect of fuel hydrogen content or aromatic type is evident.

In addition to the cold day ground start tests, altitude relight tests were conducted which are described in the following section, and lightoff/stability at simulated idle operating conditions were measured in the full-annular combustor tests. These idle stability data are summarized in Table 26. In contrast to the cold day start data, these idle data show hardly any effects of fuel properties, and the variations are attributed merely to data scatter.

8. Altitude Relight

Fourteen altitude relight tests were conducted in the 54-degree sector combustor rig using procedures described in Section V.C.2. Detailed results are listed in Appendix C, and trends are illustrated in Figures 55 and 56. Results are summarized in Figure 57 and Table 27.

Overall, as expected, very good altitude relight characteristics were found, and fuel effects were moderate. In Figure 55, measured minimum combustor inlet pressure limits for relight in the 54-degree sector rig are compared to the engine requirements corresponding to both open and closed exhaust nozzle windmilling conditions. Open nozzle conditions were generally utilized to increase the test severity, but the normal engine relight mode is with the exhaust nozzle closed, which increases the combustor inlet pressure making conditions more favorable for relight. As shown in Figure 55, the sector rig pressure limit line generally lies between the two engine requirement lines. With a highly volatile/low viscosity fuel (JP-4), the closed nozzle requirement is met with considerable margin at the higher airflow rates (flight Mach numbers). This sector rig tends to be pessimistic, relative to actual engine experience, but the difficulty in meeting even the closed nozzle requirement at low airflows (low flight Mach numbers) without starter assist is clearly indicated. With a less volatile/more viscous fuel (JP-8) relight at low airflows becomes even more difficult, which is also illustrated in Figure 55, but at high airflows, fuel type has little effect.

Relight maps, based on open exhaust nozzle windmilling conditions, for each of the test fuels are shown in Figure 56. The individual plots have been positioned in order of decreasing fuel hydrogen and decreasing fuel volatility (or increasing viscosity). The experimental limit curves always tend to be S-shaped with a maximum and a minimum at flight Mach numbers of about 0.75 and 1.00, respectively. There is virtually no effect of fuel hydrogen content, but fuel volatility/atomization effects are evident at low flight Mach numbers, which are summarized in Table 27 and Figure 57. The relative spray droplet size parameter (from Table 9) correlates the altitude relight limits at 0.50 and 0.75 flight Mach number quite well, but at flight Mach numbers of 1.00 and 1.25, the limits are virtually the same with all of the fuels.

9. Fuel Nozzle Fouling

Since the F101 engine combustion system incorporates low pressure drop air-blast fuel injection atomization, fuel nozzle fouling phenomena affect fuel flow metering characteristics rather than fuel spray quality or atomization characteristics.

Table 26. Summary of Idle Stability Test Results.

Test Fuel Number	P_3 Inlet Pressure, MPa	W_{36}, Combustor Airflow, kg/s	T_3, Inlet Temperature, K	Lightoff		Lean Blowout	
				W_f, Fuel Flow, g/s	f, Fuel-Air Ratio, g/kg	W_f, Fuel Flow, g/s	f, Fuel-Air Ratio, g/kg
1	0.106	2.25	458	33.3	14.8	14.7	6.5
2	0.106	2.25	452	31.2	13.9	11.7	5.2
3	0.107	2.24	473	30.1	13.4	12.7	5.7
4	0.107	2.39	472	30.7	12.8	4.5*	1.9*
5	0.107	2.41	466	33.9	14.1	14.0	5.8
6	0.107	2.42	468	38.4	15.9	12.5	5.2
7	0.108	2.41	469	27.1	11.2	13.6	5.6
8	0.108	2.41	466	27.6	11.5	13.4	5.6
9	0.107	2.37	473	35.4	14.9	13.1	5.5
10	0.108	2.43	462	32.6	13.4	17.1	7.0
11	0.108	2.41	453	38.3	15.9	15.7	6.5
12	0.107	2.23	460	31.0	13.9	13.9	6.2
13	0.107	2.40	427	29.5	12.3	12.0	5.0
Average				32.2	13.7	13.7	5.8
Std. Deviation				3.58	1.49	1.55	0.61
Normalized Deviation				0.111	0.109	0.114	0.105

* Suspect; excluded from statistical analysis.

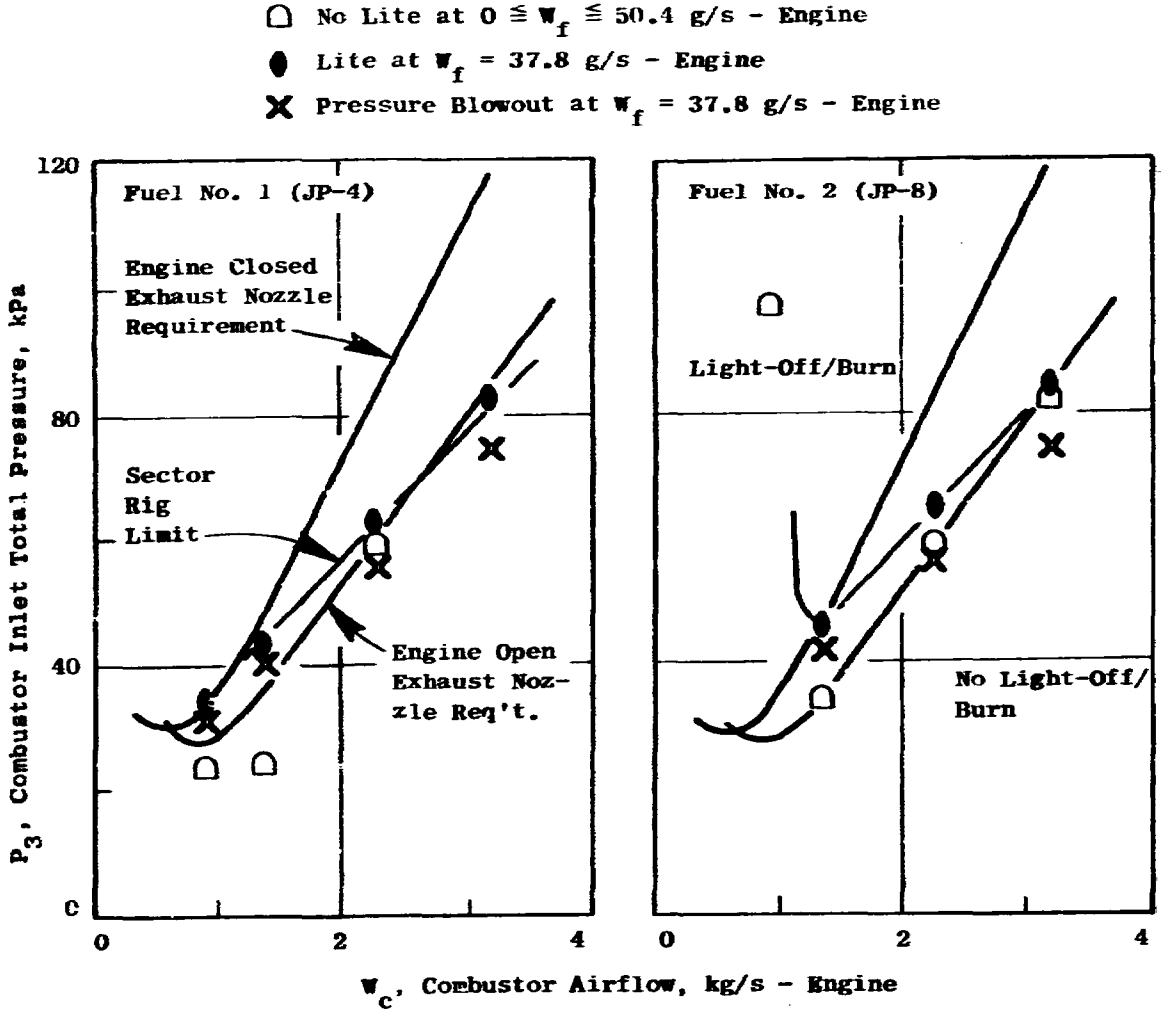

Figure 55. Effect of Combustor Inlet Conditions on Altitude Relight Limits.

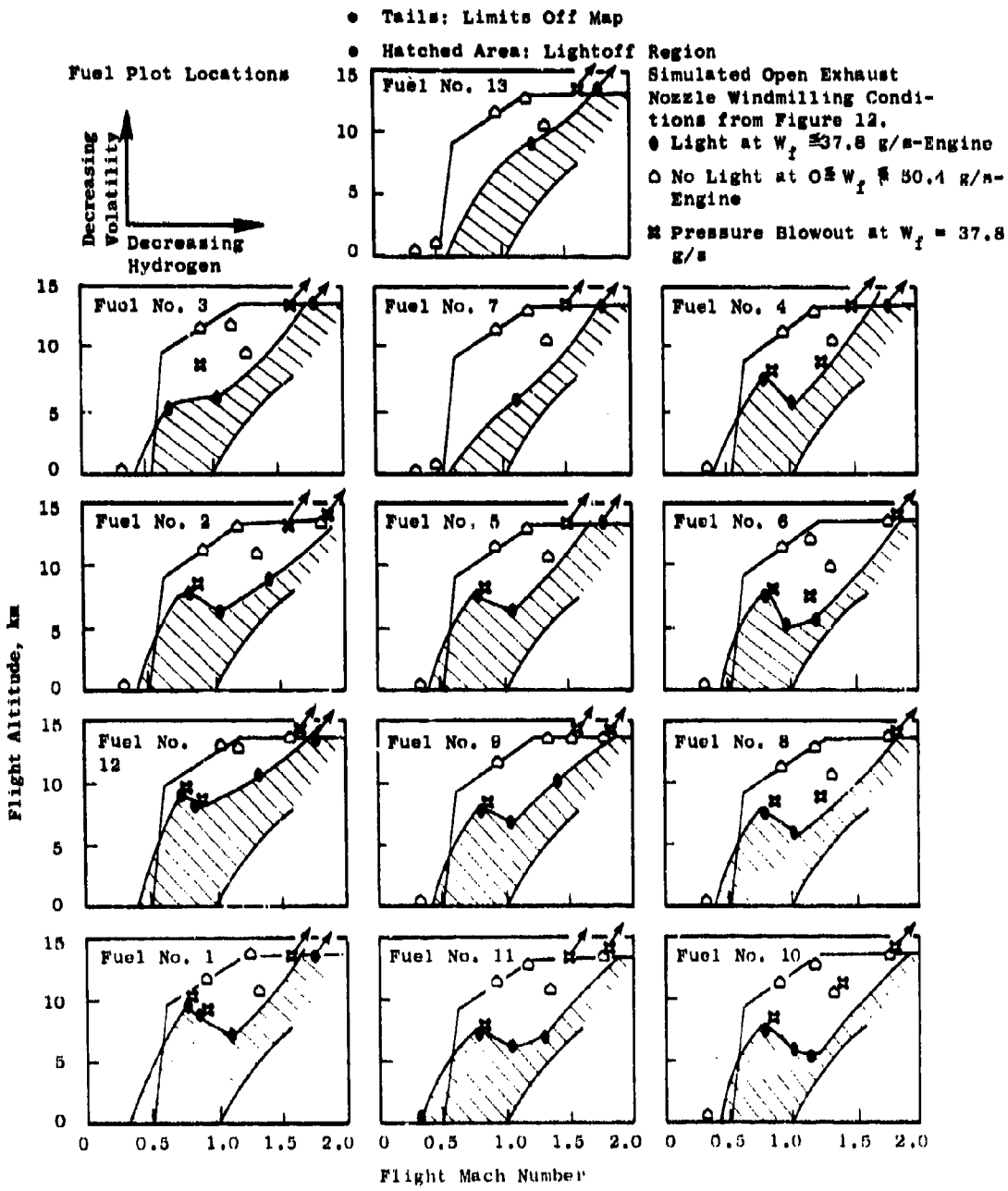

Figure 56. Altitude Relight Characteristics at Open Exhaust Nozzle Windmilling Conditions.

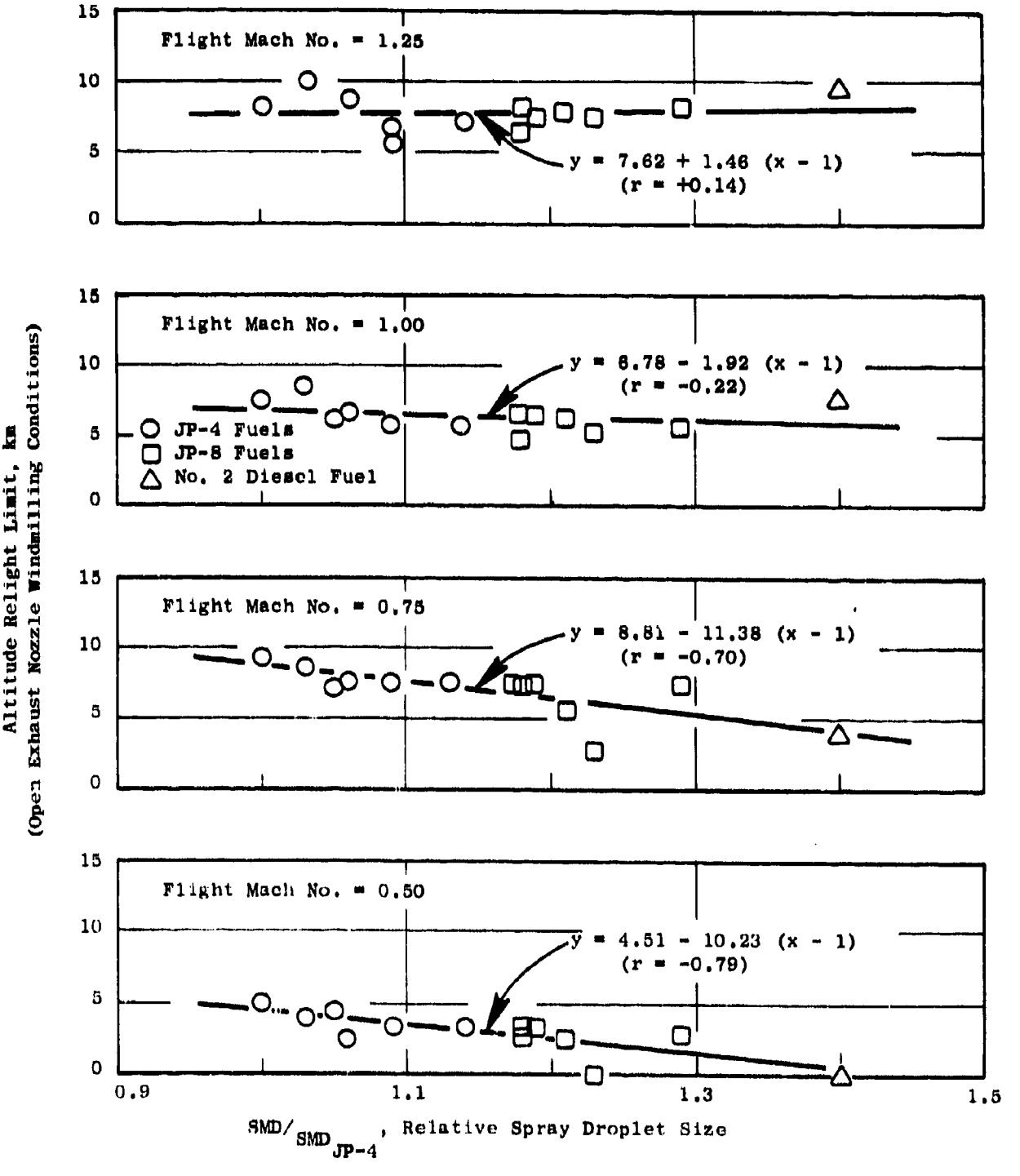

Figure 57. Effect of Fuel Atomization on Altitude Relight Limits (Open Exhaust Nozzle Windmilling Conditions).

Table 27. Summary of Altitude Relight Test Results

Fuel Number	Relight Altitude Limit, km (At Open Exhaust Nozzle Windmilling Conditions and Flight Mach Number =)			
	0.50	0.75	1.00	1.25
1	5.0	9.4	7.6	8.2
2	3.2	7.7	6.6	7.6
3	2.6	5.8	6.3	7.9
4	2.9	7.5	5.8	8.2
5	2.9	7.5	6.5	8.2
6	3.2	7.5	5.0	6.4
7	0	2.7	5.2	7.4
8	3.3	7.7	5.9	7.2
9	2.7	7.7	6.9	8.8
10	3.3	7.7	5.9	5.8
11	4.5	7.3	6.3	6.8
12	4.0	8.7	8.4	10.0
13	0	4.0	7.8	9.5

Figure 58 illustrates the types of flow characteristics deterioration which may occur. A fuel nozzle in good condition (pretest symbols) meets very close flow tolerances and exhibits virtually no flow hysteresis. After long engine service or hot fuel cyclic rig testing, gum deposits form which affect the metering valve action. For the post cyclic rig test flow calibration example shown, the valve cracking pressure has increased from 0.75 to 1.25 MPa, flow rates at 2.2 and 3.0 MPa have decreased about 4 percent, and descending pressure flow rates have increased about 8 and 103 percent at 1.2 and 0.8 MPa (hysteresis). Deterioration can therefore be characterized by either flow rate reduction or flow-hysteresis increase at selected nominal fuel nozzle pressure drop conditions. Two different metering deterioration parameters were calculated for analyses of the fuel nozzle fouling data:

$$\text{Flow Rate Reduction} = \left[\frac{(\text{Pretest Flow Rate})-(\text{Test Flow Rate})}{(\text{Pretest Flow Rate})}\right]_{\substack{\text{Ascending Pressure}\\ \text{Calibration}}} \quad (12)$$

and:

$$\text{Flow Hysteresis Increase} = \left(\frac{\text{Ascending Flow Rate}}{\text{Descending Flow Rate}}\right)_{\text{Pretest}} - \left(\frac{\text{Ascending Flow Rate}}{\text{Descending Flow Rate}}\right)_{\text{Test}} \quad (13)$$

The first type of deterioration indicator (ascending pressure flow rate reduction) could probably be related to relight ability (insufficient fuel in the vicinity of the ignitor). The second type of deterioration indicator (flow rate hysteresis) is probably more important in that variations in hysteresis of the twenty fuel nozzles can result in hot streaks and turbine distress at higher power operating conditions.

The extent of deterioration should be dependent upon fuel injector design features (clearances, finishes, spring forces, and manufacturing tolerances) as well as fuel properties (thermal stability rating), operating conditions (fuel temperature and flow rates, air temperature, and velocity, etc.) and exposure time.

Under normal engine operating conditions, the types of fuel nozzle fouling described above usually occur only after long use, which would require long tests and large fuel quantities to duplicate, which were beyond the original scope of this program. Therefore, short but severe tests described in Section V.D.1 were conducted in an effort to define the relative fouling tendencies of these 13 fuels. A total of 15 tests were conducted, and results are listed in Appendix D. After inconclusive tests with Fuels 1 and 2 (no significant flow calibration deterioration), the fuel temperature was increased from (436 to 478 K) to accelerate the fouling tendency. A summary of these later results is shown in Table 28. With the increased fuel temperature, noticeable deterioration at the first calibration point (0.83 MPa) occurred, by either definition, within this short (5-hour) test. However at the second calibration point (1.2 MPa), virtually no deterioration was detected.

Figure 59 is an attempt to relate the fuel nozzle fouling tendency in these tests to the laboratory fuel thermal stability rating of the fuels from Table 6. The expected trend would be more fouling with lower JFTOT breakpoint temperature.

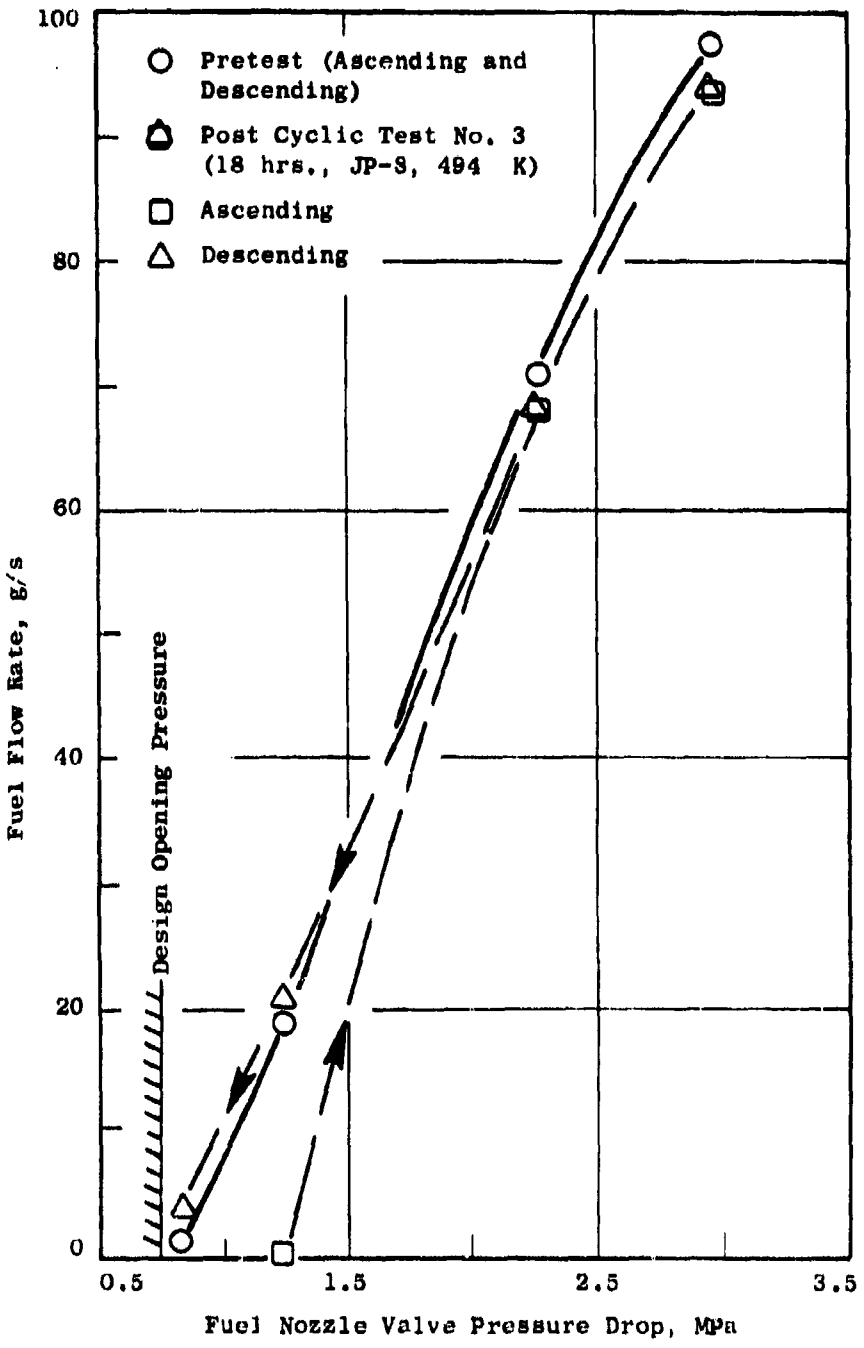

Figure 58. Effect of Hot Fuel Cyclic Testing on F101 Fuel Nozzle Metering Valve Flow Characteristics.

Table 28. Summary of Short Time Fuel Nozzle Fouling Test Results

(5-Hour Test at T_f = 478 K)

Fuel Number	Flow Rate Reduction, % (1) ΔP_f, MPa		Flow Hysteresis Increase, % (2) ΔP_f, MPa	
	0.827	1.241	0.827	1.241
1	22.2	3.3	20.2	4.0
2	2.7	2.1	25.2	7.0
3	36.4	2.1	45.2	1.6
4	7.1	-2.1	1.2	-1.0
5	29.5	3.6	2.9	-0.5
6	14.7	0	1.7	1.6
7	17.3	2.6	14.5	0
8	25.4	0.1	12.9	0
9	24.7	3.0	19.6	0
10	-6.2	0	-5.1	-1.1
11	-5.2	-0.3	-4.7	-0.5
12	3.9	2.3	13.2	2.6
13	28.0	0	18.8	-2.1
Avg.	15.2	1.3	12.7	0.9

(1) Defined by Equation 12
(2) Defined by Equation 13

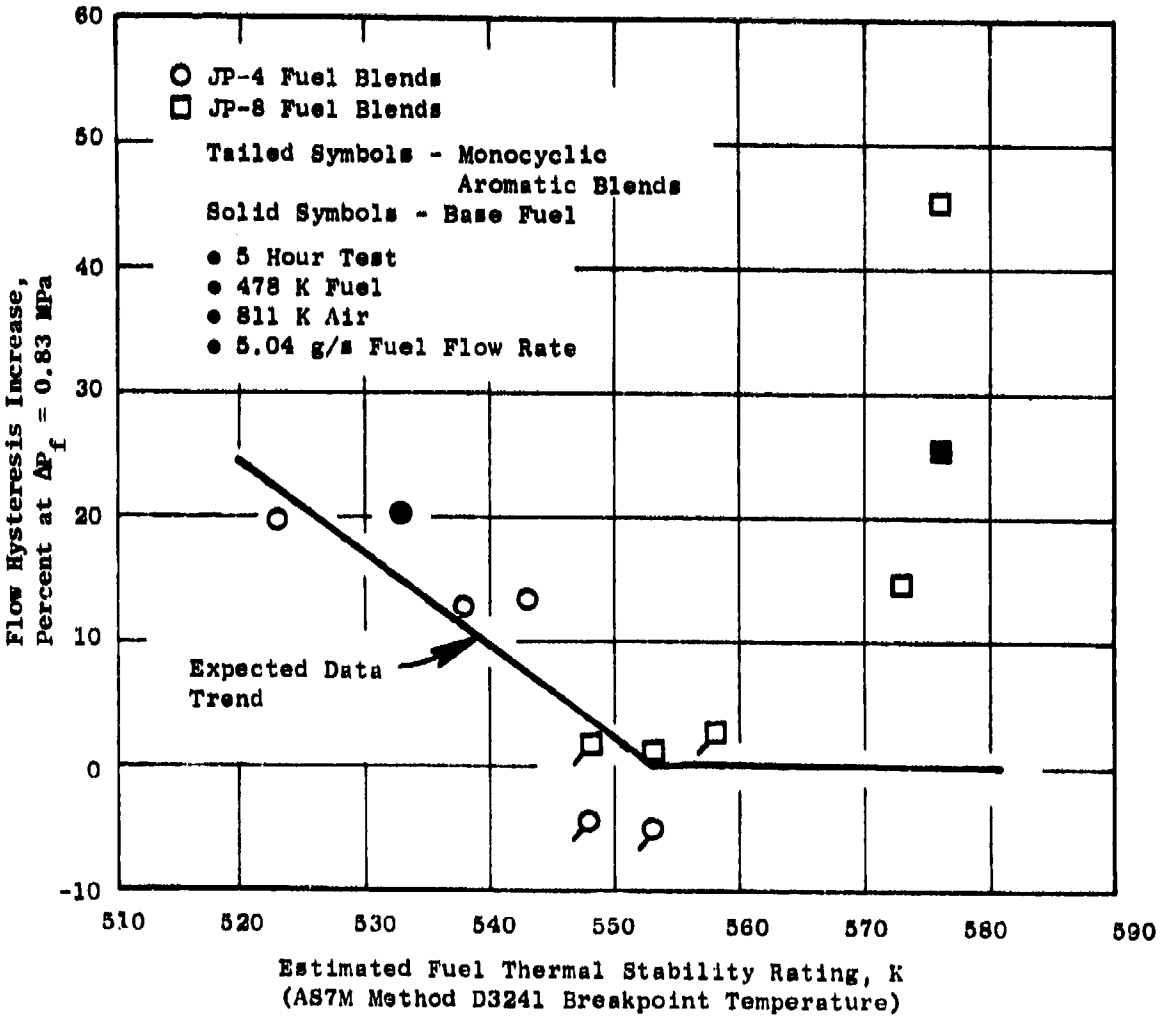

Figure 59. Effect of Fuel Thermal Stability Rating on Short Time Fuel Nozzle Fouling Tendancy.

However, the three fuels with the highest breakpoint temperature (Fuels 2, 3, and 7) do not fit the trend indicated by the other fuels. It was therefore concluded that the thermal stability variations in this set of fuels were probably not large enough to relate reliably to fuel nozzle fouling tendencies by these short tests. The program scope was then increased to include longer tests with selected fuels, which are described in the following section.

10. Fuel Nozzle Valve Gumming

As described above, it was concluded that longer tests were needed to characterize fuel nozzle fouling tendencies, so the program scope was revised to include a series of longer cyclic tests using the apparatus and procedure described in Section V.D.2. Eight tests were run using JP-4 and JP-8 fuels to determine the relative effects of fuel temperature and cyclic test time on fuel nozzle flow characteristics. Detailed data are listed in Appendix D, which are summarized in Table 29. Typical trends are illustrated in Figures 58 and 60, and summarized in Figure 61. As noted, the results summarized are for the upstream fuel nozzle valve in the test rig.

As shown in Table 29, each of the tests was run until significant flow calibration deterioration in the upstream fuel nozzle valve had occurred. Generally, the downstream valve flow calibration deterioration was less. At the lowest fuel temperature tested (436 K), deterioration was not great until near the end of the 100-hour test with either fuel. In all of the higher temperature tests, significant deterioration occurred quite soon (30 hours or less) and strong fuel temperature/fuel type effects were evident, as shown in Figure 60. In the higher temperature tests, the time between shutdowns for flow calibration was therefore reduced from 8 to 4 or 6 hours to determine more accurately the cyclic time required to produce a significant degree of flow calibration deterioration. However, as shown in Table 29, significant degrees of deterioration still often occurred before the first flow calibration. Therefore, life curves such as that shown in Figure 61 are difficult to construct with precision from these few tests. It is, however, evident from Figure 61 that life (time to produce a selected level of flow deterioration) tends to correlate with the temperature difference between the breakpoint by visual tube rating (JFTOT) and test fuel operating temperature of both fuels. A 20 K change in this parameter causes life to change by approximately a factor of 5. Thus, this correlation could be used to estimate the effect of either a change in fuel thermal stability rating or a change in engine operating conditions on life of this fuel system component.

B. Engine Systems Life Predictions

1. Combustion System Life Predictions

The analysis as described in Section V.F.2 was conducted assuming a nonluminous flame radiation level for Fuel 1 (current JP-4) and adjusting the film effectiveness level to achieve a match between the measured and calculated temperatures on the panels. Typical data match curves for Panel 3 outer liner are shown in Figure 62. Similar data match curves were prepared for each of the other fuels by maintaining a constant film effectiveness level and by adjusting the flame radiation to achieve the data match. This detailed approach permits the metal temperature distribution throughout the structure to be calculated with high accuracy providing the desired accurate input for the stress calculations.

Table 29. Summary of Long Time Fuel Valve Gumming Test Results (1)

Test Run Number	Fuel Type	Fuel Temperature, K	Test Duration, Hours	Test Time to Indicated Levels of Flow Metering Deterioration[1], Hours					
				Flow Rate[2] Reduction, % at ΔP_f = 0.83 MPa			Flow Hysteresis[3] Increase, % at ΔP_f = 1.24 MPa		
				25 % Reduction	50 % Reduction	100 % (Seizure)	5 % Increase	10 % Increase	20 % Increase
1	JP-4	436	100	88-96	88-96	>100	16-24	88-96	88-96
2	JP-8	436	100	<8	>100	>100	88-96	88-96	88-96
3	JP-8	494	18	<6	<6	<6	<6	<6	<6
4	JP-8	464	44	<6	<6	18-24	6	24-30	32-38
5	JP-4	464	32	<8	<8	8-16	<8	<8	16-24
6	JP-4	450	28	<4	12-20	12-20	<4	4-12	4-12
7	JP-4	456	24	<4	<4	8-12	<4	<4	4-8
8	JP-4	444	22[4]	>22	>22	>22	16-22	16-22	16-22

(1) Upstream test valve results only. Downstream valve results are similar but less deterioration.
(2) Defined by Equation 12.
(3) Defined by Equation 13.
(4) Test terminated because fuel supply exhausted.

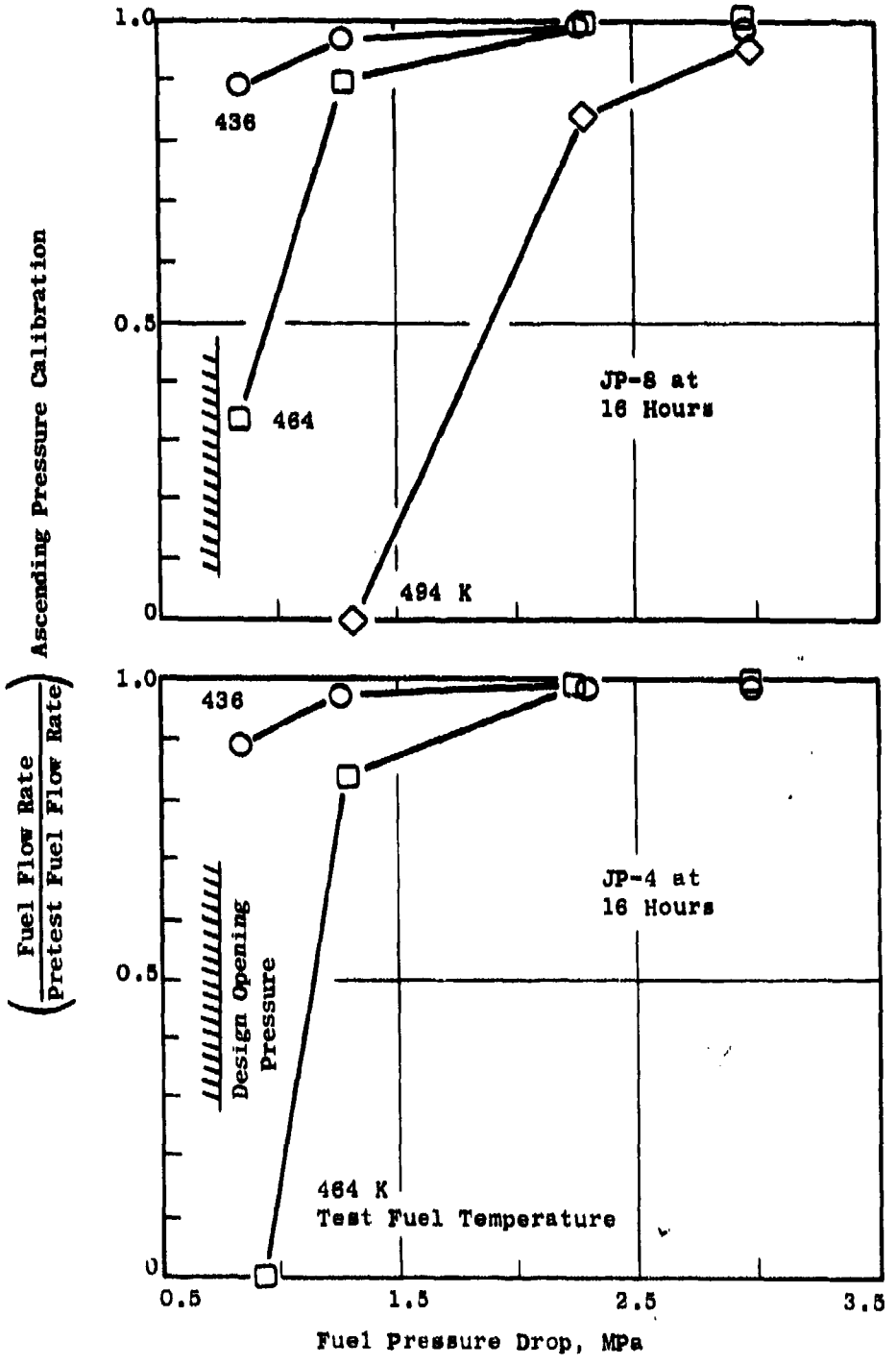

Figure 60. Effect of Fuel Type and Temperature on Fuel Nozzle Valve Performance.

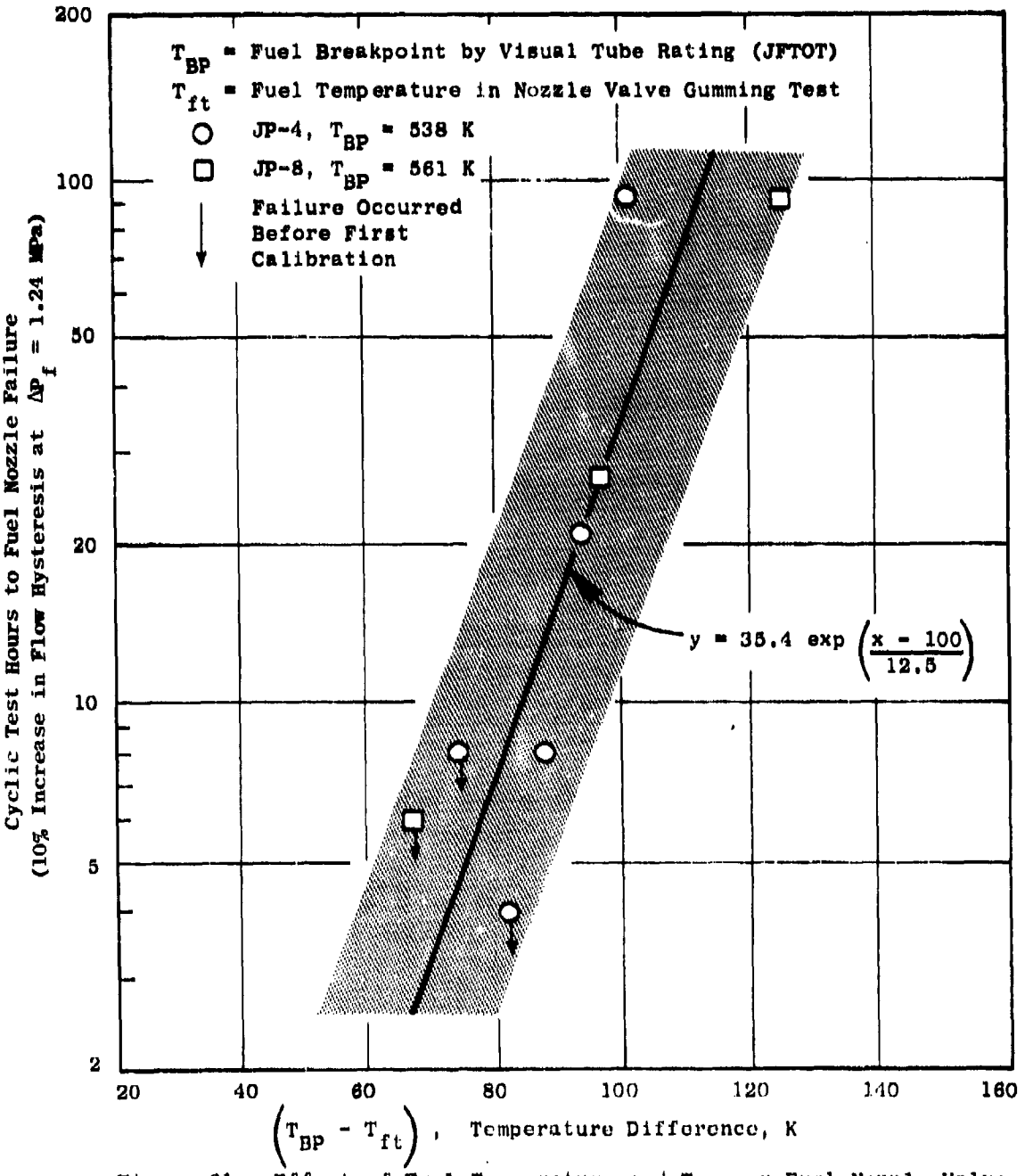

Figure 61. Effect of Fuel Temperature and Type on Fuel Nozzle Valve Life.

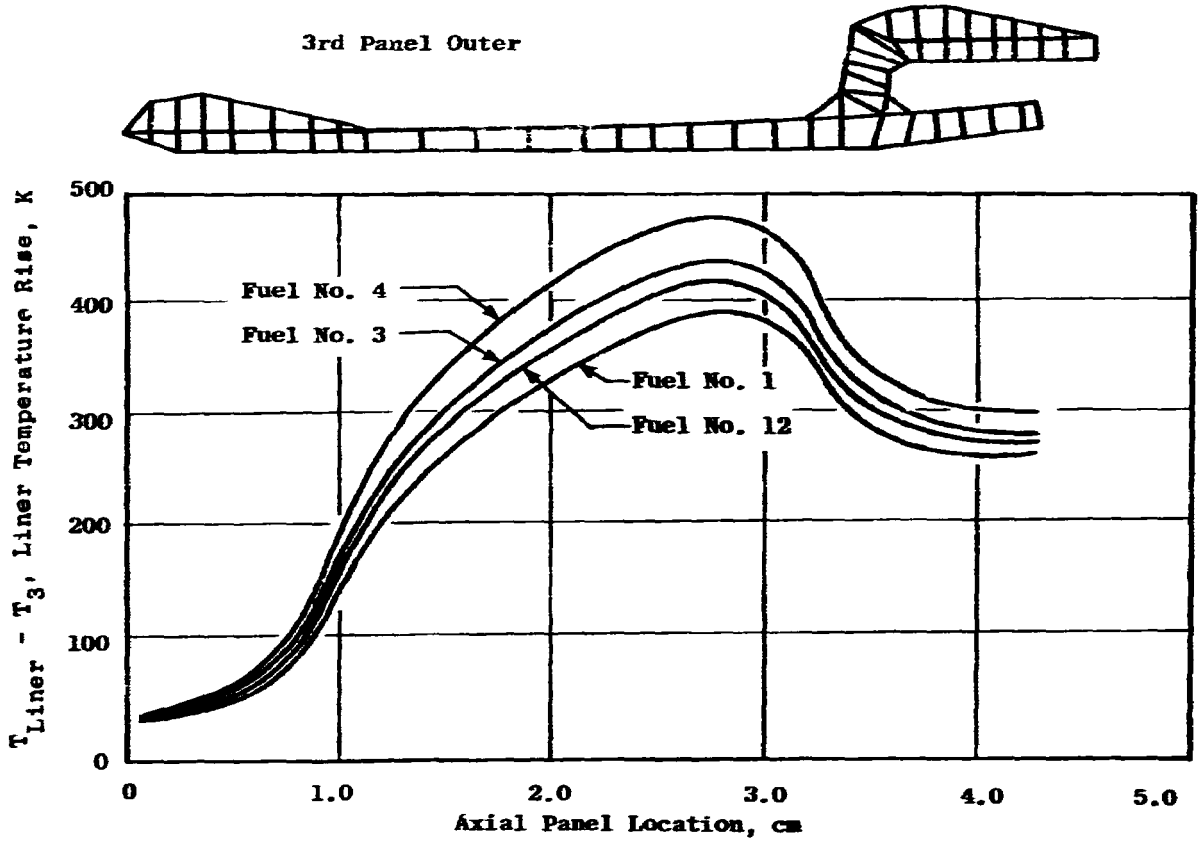

Figure 62. Panel 3 Outer Engine Maximum Temperature Distribution at Takeoff, Fuel No. 1, 3, 4 and 12.

The temperature profiles were used as input to the CLASS/MASS Computer Program and effective stress levels were calculated for the various fuels. The stress and temperature distributions were combined with available material property data (Figure 32) to predict cycles to crack initiation. The relative cyclic life for the various fuels is shown in Figure 63. The predicted cyclic life for fuels containing 12 weight percent hydrogen is less than half of the life predicted for the fuel containing 14.5 weight percent hydrogen. This decrease in life is due to two effects. The first and smaller effect is due to increases in effective stress levels because of increases in temperature gradients between the panel and the cooling slot. The second and more significant effect is due to the rapid decay in material properties in the predicted liner temperature range of 1200 to 1295 K.

The following table summarizes the life results:

Fuel Hydrogen Content, Weight Percent	Relative F101 Combustor Life
14.5 (Current JP-4)	1.00
14.0 (Current JP-8)	0.72
13.0 (ERBS Fuel, Ref. 2)	0.52
12.0 (Minimum, This Program)	0.47

2. Turbine System Life Predictions

The turbine vane heat load is made up of both convection and radiation and the relative levels vary around the perimeter of the vane. The leading edge of the vane has a view of the dome region and thus, a larger part of its heat load is dependent on radiation as compared to the trailing edge which receives radiation heating only from the gas path enclosed between the vanes. The radiation heating of the leading edge accounts for about 20 percent of the total heat load. This percentage decreases around the perimeter of the vane as a result of smaller dome view factors reaching a value of only about 8 - 10 percent of the total heat load for the trailing edge.

As discussed in Section V.F.3, the cooler combustion gases between the high temperature dome and the vane absorb in the wavelength bands for carbon dioxide and water and, thus, shield the vanes from upstream radiation in these bands. The luminous radiation from the dome regions of the spectrum, however, is not easily absorbed and increases the total heat load on the vane. Estimates were made of the increase in the total heat load and the corresponding increase in metal temperature. The temperature distributions were used to calculate stress levels which in turn were used to calculate the cycles to low cycle fatigue cracking. The predicted metal temperature increases for operation with fuels containing 12 weight percent hydrogen are shown in Figure 64.

It is predicted that the low cycle fatigue life at the leading edge is reduced by a factor of two when the fuel hydrogen content is reduced from 14.5 to 12 percent. This is approximately the same life factor found previously for the combustor liner. However, at its present stage of development the life of the turbine vane is limited primarily by cracking at the trailing edge, which is not affected at all by the flame luminosity. Until the life of the trailing edge

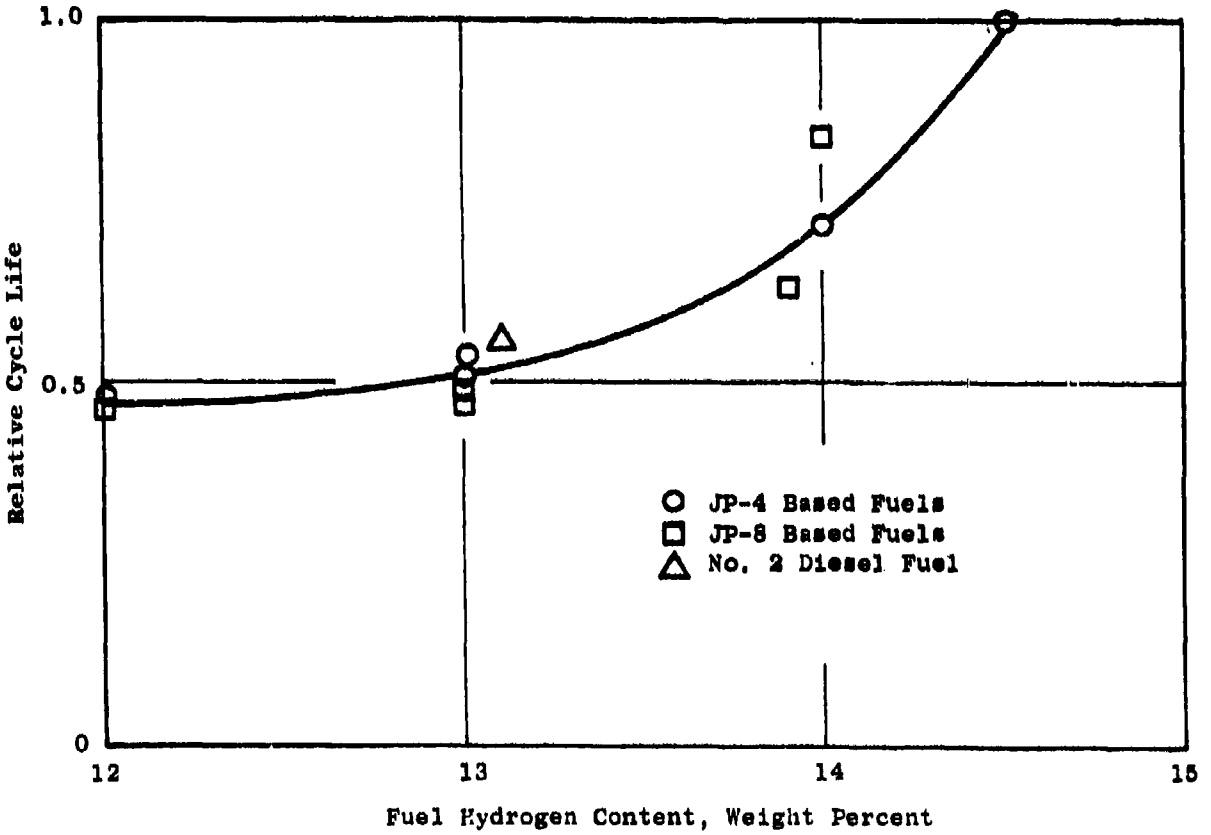

Figure 63. Predicted Effect of Fuel Hydrogen Content on Combustor Life.

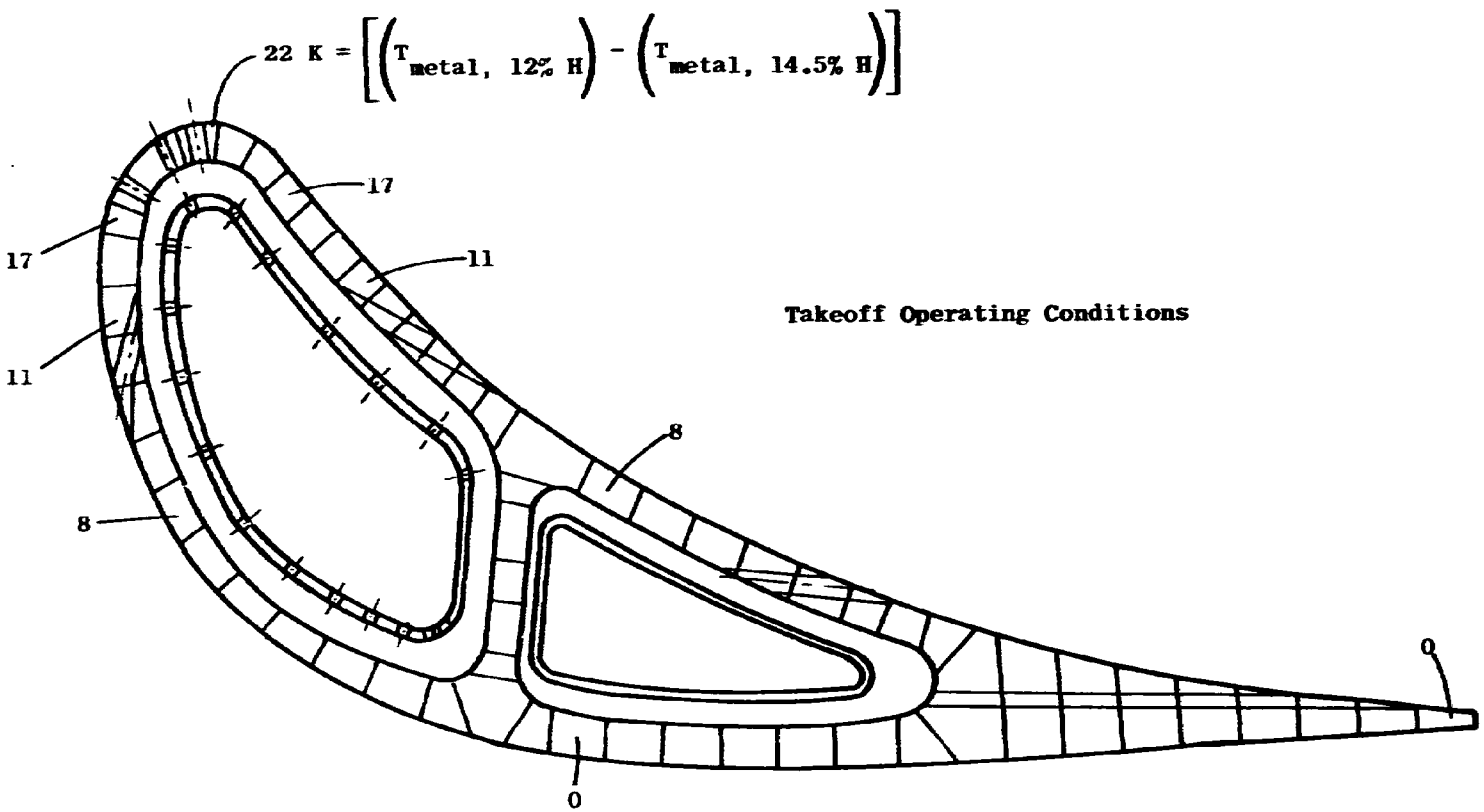

Figure 64. Predicted Turbine Stator Vane Temperature Increase With 12 Percent Hydrogen Fuel.

is improved to within 50 percent of the life of the leading edge, flame luminosity will not significantly alter the overall life of F101 turbine vanes.

C. Assessment of Results

The data and analyses presented in the previous section provide a summary of the effects of fuel property variations on the performance, emission and durability characteristics of the F101 combustion system, based on full-annular, sector and single-cup rig tests. The data are generally well ordered and in good agreement with previous data where comparisons could be made. Therefore, these data are thought to be a valuable addition to the USAF data bank. However, since these are all rig results, some direct verification by engine tests is recommended.

These data show that fuel hydrogen content is a key fuel property, with respect to high power performance/emissions and durability. In particular, smoke, liner temperature (and hence, combustor life) and NO_x emissions are predominantly fuel hydrogen content dependent. On the other hand, low power emissions and performance, such as idle CO and HC emissions, and ground start and altitude relight appear more dependent on fuel volatility and viscosity as they affect fuel atomization and evaporation characteristics. The F101 combustion system has excellent cold day ground start and altitude relight characteristics, but these data indicate that conversion from JP-4 to JP-8 as the primary USAF fuel will result in noticeable reductions in these starting capabilities.

The F101 fuel nozzle appears to be quite tolerant to fuel property changes with respect to short time fuel nozzle fouling. The short but harsh tests conducted in this program, however, were not very conclusive. The longer time fuel nozzle valve gumming tests suggest that JP-8 fuel may provide significantly longer life than JP-4. It appears that some of the concerns regarding future fuel characteristics are: to what extent the thermal stability ratings will change, how significant are current procedures for rating fuel thermal stability, and how much engine fuel supply/injection system performance will be affected. Additional studies in these areas are therefore needed.

Section VII

CONCLUSIONS AND RECOMMENDATIONS

Based on the F101 combustion system experiments and analyses conducted in this program, the following conclusions and recommendations are made:

A. Conclusions

1) Fuel hydrogen content strongly affects smoke emissions, liner temperature and NO_x emissions. Hydrogen content is, therefore, probably the single most important fuel property, particularly with respect to high power performance and emission characteristics and combustor durability (life).

2) Fuel volatility (as indicated by initial boiling range) and viscosity effects became evident at low power operating conditions. Cold day starting and altitude relight capability are highly dependent upon these properties.

3) Within the range tested, neither aromatic type (monocyclic or bicyclic) nor final boiling range produced any significant effect on combustion characteristics.

4) Combustor exit temperature distributions in the atmospheric discharge tests conducted in this program showed a strong effect of fuel viscosity (droplet size) on exit pattern factor. This effect, however, is probably not present in the high pressure engine environment.

5) None of the fuel properties produced any measureable harmful carbon deposition within the short but severe tests which were conducted.

B. Recommendations

1) F101 engine tests with selected fuels are recommended to verify the trends established in these rig tests.

2) Although the current testing showed no adverse fuel effects on fuel system components at normal operating temperatures, more sophisticated long term tests are needed to determine the effects of fuel thermal stability on fuel supply/injection system components and to establish quantitative correlations with thermal stability ratings.

REFERENCES

1. Gleason, C. C., Oller, T. L., Shayeson, M. W., and Bahr, D. W., "Evaluation of Fuel Character Effects on J79 Engine Combustion Systems," AFAPL TR-79-2015, June 1979.

2. Longwell, J. P., "Jet Aircraft Hydrocarbon Fuels Technology," NASA CP-2033, January 1978.

3. Colley, W. C., et al, "Development of Emissions Measurement Techniques for Afterburning Turbine Engines; Supplement 2 - Afterburner Plume Computer Program User's Manual," Air Force Aero Propulsion Laboratory, AFAPL-TR-75-52, Supplement 2, (General Electric Report R75AEG459), October 1975.

4. Rizkalla, A. A., Lefebvre, A. H., "Influence of Liquid Properties on Airblast Atomizer Spray Characteristics," ASME Paper 74-GT-1, April 1974.

5. "Aircraft Gas Turbine Engine Exhaust Smoke Measurement," Aerospace Recommended Practice 1179, SAE, 1970.

6. "Procedure for the Continuous Sampling and Measurement of Gaseous Emissions from Aircraft Turbine Engines," Aerospace Recommended Practice 1256, SAE, 1971.

7. Gleason, C. C., Rogers, D. W., and Bahr, D. W., "Experimental Clean Combustor Program, Phase II Final Report," NASA CR-134971, August 1976.

8. Gleason, C. C. and Bahr, D. W., "Experimental Clean Combustor Program Alternate Fuels Addendum, Phase II Final Report," NASA CR-134972, January 1976.

9. Moses, C. A. and Naegeli, D. W., "Effects of High Availability Fuels on Combustor Properties," AFAPL-101, January 1978.

10. Blazowski, W. S. and Jackson, T. A., "Evaluation of Future Jet Fuel Combustion Characteristics," AFAPL-TR-77-93, July 1978.

11. Jasuja, A. K., "Atomization of Crude and Residual Fuel Oils," ASME Paper 78-GT-83, April 1978.

12. Shaffernocker, W. M. and Stanforth, C. M., "Smoke Measurement Techniqes," SAE Paper C80346, April 1968.

APPENDIX A

FULL-ANNULAR TEST DATA

Table A-1 presents a summary of the key reduced data from the high pressure performance and emission tests. Additional computed parameters are listed in Table A-2.

Table A-3 presents the analyses of the idle CO and HC emission data. A logarithmic curve fit of the test data for each fuel was performed (see Figures 34 and 37) from which the quoted engine idle emission indices were calculated. At higher engine power test conditions, CO emission levels were very low, particularly after corrections from rig to engine pressure levels were made (Table A-4). Hydrocarbon emission levels at all higher power rig conditions were essentially zero.

The NO_x emissions data were correlated as shown in Table A-5. A linear regression curve fit of the test data for each fuel was performed (see Figure 39) from which the quoted engine emission indices were calculated.

The engine exit smoke data were correlated as shown in Table A-6. Again, a linear regression curve fit of the test data for each fuel was performed (see Figures 42 and 43) from which the quoted smoke levels were calculated.

Detailed liner temperature data are listed in Table A-7 (inner liner) and Table A-8 (outer liner). The data are presented as liner temperature rise (T_L-T_3). The thermocouple locations indicated correspond to those shown in Table 12 and Figures 22-25. The peak liner temperatures always occurred on the third panel of the outer liner and were correlated (see Figures 46 and 47) as shown in Table A-9.

Detailed data from the atmospheric pressure pattern factor tests is listed in Table A-10. The pattern factor data were correlated (see Figures 50 and 51) as shown in Table A-11.

Table A-1. Performance and Emission Data Summary.

Reading Number	Point Number	Fuel Number	W_a, Combustor Airflow, kg/s	P_3, Inlet Total Pressure, MPa	T_{t3}, Inlet Total Temperature, K	f_m, Metered Fuel-Air Ratio, g/kg	T_f, Fuel Temperature, K	W_f, Fuel Flow Rate, g/s	ΔP_f, Fuel Nozzle Pressure Drop, MPa	A_{f_e}, Fuel Nozzle Effective Area, mm^2	h_3, Inlet Air Humidity, g/kg	$\Delta P_3/P_3$, Total Pressure Drop, %	$(T_{L,max}-T_3)$, Peak Liner Temp. Rise, K	EI_{CO}, CO Emission Index, g/kg	EI_{HC}, HC Emission Index, g/kg	EI_{NO_x}, NO_x Emission Index, g/kg	f_s, Sample Fuel-Air Ratio, g/kg	η_{CB}, Gas Sample Combustion Efficiency, %	SN_g, Combustor Exit Smoke Number
2	1	1	8.48	0.394	467	11.5	295	97.5	0.786	2.84	1.1	5.00	244	49.6	10.9	2.7	11.1	97.76	0.0
3	2	1	8.71	0.394	469	13.8	294	120.2	0.772	3.48	1.1	5.59	249	30.2	2.0	3.2	13.7	99.10	0.0
4	3	1	17.01	1.016	678	18.6	295	316.4	0.958	8.34	1.1	5.31	227	2.3	0.1	11.3	18.8	99.94	4.0
5	4	1	17.15	0.982	676	23.1	294	396.1	1.048	9.98	1.1	5.27	264	2.0	0.1	9.8	23.7	99.95	4.0
6	5	1	20.37	1.256	811	22.2	293	452.1	1.096	11.08	1.1	5.66	262	1.1	0.0	20.3	22.0	99.97	7.0
7	6	1	19.60	1.253	811	28.9	291	566.3	1.227	13.10	1.1	5.98	343	1.6	0.0	19.8	27.6	99.96	6.0
8	8	1	19.87	1.250	812	27.3	291	542.4	1.200	12.73	1.1	5.69	333	1.5	0.0	19.8	27.2	99.96	5.0
9	7	1	20.00	1.250	815	21.7	292	434.1	1.076	10.73	1.1	6.15	258	1.0	0.0	21.1	21.6	99.97	7.0
10	7	2	19.91	1.247	818	22.0	292	438.2	1.069	10.54	1.1	6.00	269	1.0	0.0	22.5	21.5	99.97	6.0
11	8	2	19.60	1.247	816	28.1	291	550.6	1.200	12.54	1.1	5.88	351	1.6	0.0	20.4	27.7	99.96	8.0
12	6	2	19.73	1.254	815	29.2	290	576.2	1.227	12.95	1.1	5.92	364	2.2	0.0	20.4	29.1	99.95	6.0
13	5	2	19.96	1.255	815	23.1	291	461.0	1.096	10.97	1.1	5.45	292	1.2	0.0	21.3	24.0	99.97	5.0
14	4	2	16.56	0.976	676	24.2	292	400.7	1.034	9.87	1.1	5.05	292	2.3	0.0	9.9	24.8	99.94	6.0
15	3	2	16.78	0.979	673	19.3	292	323.9	0.951	8.28	1.1	4.61	236	2.4	0.0	11.1	19.9	99.94	7.0
16	2	2	8.62	0.392	465	14.3	292	123.2	0.772	3.48	1.1	5.70	272	24.6	0.6	3.8	16.5	99.37	3.0
17	1	2	8.66	0.395	465	11.6	291	100.5	0.745	2.88	1.1	5.60	209	34.1	3.1	3.5	12.7	98.89	0.0
18	2	3	8.57	0.395	468	14.2	289	121.7	0.779	3.44	1.1	5.65	220	23.8	0.7	3.8	16.7	99.37	0.0
19	1	3	8.62	0.395	468	10.9	289	93.9	0.745	2.71	1.1	5.87	216	39.5	4.9	3.4	11.9	98.59	----
20	3	3	16.60	0.982	683	19.4	288	322.1	0.965	8.19	1.1	5.17	233	2.2	0.1	11.5	19.6	99.94	8.0
21	4	3	16.78	0.979	677	24.0	289	402.8	1.048	9.83	1.1	4.89	290	2.2	0.1	9.8	24.3	99.94	5.0
22	5	3	20.14	1.255	819	22.8	289	459.2	1.096	10.97	1.1	5.31	281	1.2	0.0	20.7	22.2	99.97	9.0
23	6	3	20.18	1.261	824	28.5	289	575.3	1.220	12.95	1.1	5.30	369	1.7	0.0	20.6	30.4	99.96	9.0
24	7	3	19.78	1.247	825	21.9	290	433.1	1.069	10.47	1.1	5.48	264	1.0	0.0	22.2	23.0	99.97	7.0
25	8	3	19.96	1.251	826	27.6	289	550.8	1.200	12.56	1.1	5.96	347	1.6	0.0	20.5	28.9	99.96	11.0
35	7	4	19.86	1.245	843	22.7	292	451.2	1.321	9.48	1.5	5.46	293	1.1	0.0	26.5	22.2	99.97	6.9
34	8	4	20.02	1.241	842	28.2	291	564.9	1.447	11.34	1.5	5.46	387	1.5	0.0	24.5	27.4	99.96	13.8
36	6	4	20.03	1.249	823	29.5	292	591.3	1.474	11.76	1.5	5.18	406	1.6	0.0	22.1	29.8	99.96	15.6
37	5	4	19.70	1.254	829	24.0	291	473.7	1.335	9.90	1.5	5.30	311	1.2	0.0	24.3	23.5	99.97	6.6
38	4	4	16.93	0.979	674	24.4	292	412.8	1.274	8.83	1.5	4.92	301	2.4	0.0	12.5	23.6	99.94	13.2
39	3	4	17.17	0.975	683	19.2	292	329.5	1.184	7.31	1.5	5.12	288	2.6	0.0	14.4	18.6	99.94	5.2
40	2	4	8.65	0.388	470	14.0	291	121.0	0.956	3.03	1.5	5.93	180	40.5	3.1	3.9	13.4	98.73	7.1
41	1	4	8.80	0.390	470	11.2	290	98.3	0.901	2.50	1.5	5.86	153	60.3	11.3	4.0	10.9	97.43	9.0

Table A-1. Performance and Emission Data Summary (Continued).

Reading Number	Point Number	Fuel Number	W_a, Combustor Airflow, kg/s	P_3, Inlet Total Pressure, MPa	T_3, Inlet Total Temperature, K	f_m, Metered Fuel-Air Ratio, g/kg	T_f, Fuel Temperature, K	W_f, Fuel Flow Rate, g/s	ΔP_f, Fuel Nozzle Pressure Drop, MPa	A_{fe}, Fuel Nozzle Effective Area, mm^2	h_3, Inlet Air Humidity, g/kg	$\Delta P_T/P_3$, Total Pressure Drop, %	$(T_{L,max}-T_3)$, Peak Liner Temperature Rise, K	EI_{CO}, CO Emission Index, g/kg	EI_{HC}, HC Emission Index, g/kg	EI_{NO_x}, NO_x Emission Index, g/kg	f_s, Sample Fuel-Air Ratio, g/kg	η_{CB}, Gas Sample Combustion Efficiency, %	SN_1, Combustor Unit Smoke Number
44	7	5	20.21	1 257	850	22.1	289	447.3	1.316	9.62	1.5	5.53	266	1.2	0.0	26.9	21.4	99.97	6.1
42	5	5	20.17	1.258	831	23.2	289	467.0	1.345	9.93	1.5	5.38	281	1.0	0.0	24.5	22.3	99.98	6.9
43	6	5	20.05	1.256	828	29.2	289	584.5	1.465	11.91	1.5	5.29	366	1.7	0.0	22.6	28.3	99.96	7.1
45	8	5	20.35	1.256	851	27.5	289	560.4	1.445	11.50	1.5	5.49	347	1.6	0.0	21.8	27.0	99.96	6.9
46	4	5	16.87	0.979	676	24.3	290	410.5	1.259	9.03	1.5	4.93	263	2.6	0.0	19.6	23.5	99.94	7.7
47	3	5	16.81	0.977	676	19.6	290	328.8	1.161	7.53	1.5	4.89	213	2.5	0.0	13.2	18.4	99.94	5.4
48	2	5	8.80	0.389	466	13.8	291	121.5	0.914	3.14	1.5	5.86	154	36.1	3.3	4.6	13.4	98.82	5.3
49	1	5	9.82	0.389	468	11.2	291	98.7	0.884	2.59	1.5	5.78	134	54.4	11.6	4.0	10.9	97.55	4.6
26	1	6	8.55	0.392	467	11.4	291	97.6	0.896	2.53	1.5	5.50	148	69.1	17.2	4.4	9.3	96.63	5.5
27	2	6	8.53	0.393	469	14.5	291	123.6	0.928	3.14	1.5	5.50	166	41.6	3.7	4.6	12.6	98.63	6.0
28	3	6	16.31	0.974	680	20.2	290	330.0	1.173	7.46	1.4	4.95	224	2.4	0.0	12.3	20.1	99.94	10.1
29	4	6	16.47	0.974	679	25.8	290	424.9	1.277	9.22	1.4	4.89	290	2.3	0.0	10.8	25.8	99.94	9.6
30	5	6	19.84	1.246	829	23.9	292	475.1	1.348	10.02	1.4	5.31	316	1.1	0.0	24.7	23.8	99.97	8.5
31	6	6	20.14	1.251	829	29.3	292	590.4	1.479	11.89	1.4	5.28	402	1.5	0.0	23.1	29.4	99.96	14.8
32	7	6	20.13	1.245	844	22.4	292	451.5	1.318	9.63	1.5	5.29	285	1.1	0.0	27.7	22.0	99.97	8.5
33	8	6	19.86	1.215	843	28.5	291	565.1	1.447	11.50	1.5	5.77	375	1.5	0.0	24.4	27.4	99.96	9.3
50	1	7	8.90	0.392	470	10.9	297	97.3	0.837	2.61	4.3	5.85	144	64.7	19.7	2.9	10.5	96.49	5.9
51	2	7	8.84	0.390	469	13.9	297	122.6	0.879	3.21	4.3	6.55	167	39.8	4.4	3.4	13.3	98.61	8.0
52	3	7	16.81	0.977	680	19.5	296	327.5	1.120	7.60	4.5	5.50	234	2.3	0.0	11.8	18.5	99.94	7.0
53	4	7	17.41	0.981	678	23.4	296	408.0	1.211	9.11	4.5	5.33	271	2.3	0.0	10.0	23.0	99.95	7.7
54	5	7	20.37	1.260	829	22.9	294	466.6	1.284	10.10	2.0	6.40	268	1.4	0.0	22.9	21.4	99.97	8.4
55	6	7	20.45	1.262	826	28.5	293	582.9	1.413	12.03	2.0	5.35	354	2.2	0.0	20.9	26.6	99.95	13.6
56	7	7	19.83	1.248	850	22.5	296	446.3	1.258	9.77	2.0	6.16	258	1.4	0.0	25.7	20.3	99.97	8.8
57	8	7	20.03	1.255	850	28.0	294	561.4	1.397	11.66	2.0	6.16	344	1.7	0.0	23.5	25.8	99.96	8.0
58	8	8	20.22	1.251	850	27.5	293	555.1	1.379	11.58	2.0	6.24	344	1.6	0.0	24.1	25.8	99.96	10.2
59	7	8	20.34	1.254	851	22.0	294	446.7	1.256	9.77	2.0	6.36	260	1.1	0.0	27.0	20.2	99.97	8.6
60	6	8	20.25	1.262	827	28.8	293	582.7	1.412	12.01	2.0	5.48	369	1.9	0.0	22.0	26.5	99.96	12.3
61	5	8	20.13	1.264	830	23.1	294	464.4	1.270	10.10	2.0	5.44	275	1.1	0.0	24.4	20.9	99.97	4.7
62	4	8	16.93	0.982	674	24.4	295	413.9	1.212	9.22	2.0	4.90	302	2.5	0.0	11.4	23.2	99.94	9.5
63	3	8	17.01	0.985	677	19.5	295	332.3	1.118	7.71	2.0	5.09	245	2.5	0.0	13.6	18.3	99.94	4.2
64	2	8	8.84	0.393	466	14.2	295	125.2	0.873	3.29	2.0	6.21	177	36.2	2.4	4.2	13.3	98.91	5.5
65	1	8	9.01	0.395	466	11.1	295	100.4	0.841	2.69	2.0	6.51	148	63.7	21.9	3.4	10.7	96.31	6.6
66	5	9	20.49	1.263	831	22.8	293	467.4	1.291	10.27	2.0	6.06	263	1.2	0.0	26.3	21.3	99.97	4.2
67	6	9	20.20	1.266	832	28.8	293	582.0	1.431	12.15	2.0	6.08	350	2.0	0.0	24.2	26.9	99.95	8.4
68	8	9	20.13	1.259	843	27.6	293	556.5	1.389	11.79	2.0	5.85	329	1.7	0.0	25.0	26.0	99.96	7.5
69	7	9	20.16	1.256	847	22.1	294	446.3	1.261	9.93	2.0	6.11	247	1.0	0.0	28.3	20.3	99.98	3.6
70	4	9	16.94	0.990	681	24.1	294	409.0	1.218	9.26	2.1	5.73	278	2.4	0.0	11.1	22.1	99.94	7.7
'	3	9	17.36	0.991	677	18.9	295	327.4	1.120	7.73	2.1	5.76	226	2.6	0.0	13.4	17.5	99.94	2.2

Table A-1. Performance and Emission Data Summary (Concluded).

Reading Number	Point Number	Fuel Number	W_c, Combustor Airflow, kg/s	P_3, Inlet Total Pressure, MPa	T_3, Inlet Total Temperature, K	f_m, Metered Fuel-Air Ratio, g/kg	T_f, Fuel Temperature, K	W_f, Fuel Flow Rate, g/s	ΔP_f, Fuel Nozzle Pressure Drop, MPa	A_{Eg}, Fuel Nozzle Effective Area, mm^2	h_3, Inlet Air Humidity, g/kg	$\Delta P_T/P_3$, Total Pressure Drop, %	$\Delta T_{L,max}-T_3$), Peak Liner Temperature Rise, K	EI_{CO}, CO Emission Index, g/kg	EI_{HC}, HC Emission Index, g/kg	EI_{NO_x}, NO_x Emission Index, g/kg	f_s, Sample Fuel-Air Ratio, g/kg	η_{GS}, Gas Sample Combustion Efficiency, %	SN_s, Combustor Exit Smoke Number
72	2	9	8.82	0.396	469	13.8	295	122.0	0.869	3.27	2.1	5.74	166	34.7	2.3	4.1	12.8	98.94	3.9
73	1	9	8.94	0.396	466	11.0	295	98.8	0.837	2.70	2.1	6.36	142	62.9	13.7	3.6	10.4	97.13	4.2
99	2	10	8.71	0.388	464	14.0	299	122.1	0.860	3.27	3.7	5.64	163	35.4	2.3	3.6	13.4	98.92	4.6
100	1	10	8.58	0.388	466	11.3	299	96.9	0.827	2.65	3.7	5.71	137	54.6	16.4	3.5	10.9	97.05	4.3
103	5	10	19.69	1.252	826	23.6	298	465.0	1.289	10.17	3.5	5.25	279	1.1	0.0	23.8	21.5	99.97	6.6
104	6	10	20.08	1.251	826	28.9	298	581.2	1.440	12.03	3.5	5.22	363	1.8	0.0	22.9	26.9	99.96	9.8
105	7	10	19.87	1.244	849	22.3	298	443.6	1.261	9.81	3.5	5.45	266	1.1	0.0	26.2	20.2	99.97	3.7
106	8	10	19.57	1.245	844	28.1	298	550.3	1.399	11.56	3.5	5.35	345	1.5	0.0	24.5	25.3	99.96	4.6
101	3	10	16.87	0.975	676	19.3	310	326.1	1.126	7.64	3.7	5.18	226	2.6	0.0	12.0	18.0	99.94	3.6
102	4	10	17.22	0.974	677	23.6	298	405.7	1.216	9.14	3.6	5.18	276	2.3	0.0	10.6	22.0	99.94	4.7
91	5	11	19.96	1.253	829	22.9	298	457.4	1.287	10.16	4.0	5.32	262	1.2	0.0	22.0	21.3	99.97	9.1
92	6	11	19.36	1.251	823	29.6	298	573.5	1.438	12.05	4.0	5.32	354	1.7	0.0	20.4	27.1	99.96	9.1
93	7	11	19.61	1.243	845	22.3	299	436.5	1.260	9.80	4.0	5.52	251	1.2	0.0	23.6	20.2	99.97	5.9
94	8	11	19.99	1.243	845	27.4	298	547.5	1.407	11.63	3.9	5.66	334	1.5	0.0	22.6	25.5	99.96	6.2
95	4	11	16.44	0.976	674	24.4	298	400.3	1.211	9.16	3.8	4.84	273	2.2	0.0	10.0	22.1	99.95	4.9
96	3	11	16.91	0.977	676	18.9	298	320.3	1.119	7.63	3.8	5.07	221	2.3	0.0	11.2	17.8	99.95	2.7
97	2	11	8.68	0.385	465	14.0	299	121.5	0.862	3.30	3.7	5.98	159	33.8	1.9	3.5	13.3	99.02	4.7
98	1	11	8.61	0.386	467	11.2	299	96.6	0.827	2.68	3.7	5.87	137	54.0	14.7	3.3	10.7	97.26	4.0
83	8	12	19.99	1.247	846	27.0	298	540.8	1.404	11.61	4.3	5.68	321	1.3	0.0	21.7	25.2	99.97	9.8
84	7	12	19.51	1.240	844	22.2	298	432.3	1.265	9.77	4.3	5.74	244	1.0	0.0	21.9	19.8	99.98	4.3
85	6	12	19.53	1.257	824	28.8	298	562.2	1.431	11.95	4.3	5.32	342	1.4	0.0	19.3	26.1	99.97	6.9
86	5	12	20.03	1.255	828	22.4	298	449.2	1.282	10.09	4.3	5.18	260	1.1	0.0	20.6	20.7	99.97	5.5
87	4	12	16.75	0.980	676	23.5	299	392.9	1.210	9.09	4.2	4.99	260	2.1	0.0	9.4	21.8	99.95	5.4
88	3	12	16.84	0.977	675	18.9	299	318.0	1.121	7.64	4.2	5.01	221	2.3	0.0	10.3	17.7	99.95	4.6
89	2	12	8.53	0.389	465	14.0	299	119.3	0.866	3.26	4.1	5.29	166	29.3	1.4	3.4	13.5	99.17	3.6
90	1	12	8.57	0.389	465	11.2	299	96.0	0.828	2.68	4.1	5.47	152	48.2	11.8	3.1	11.0	97.69	2.2
74	1	13	8.47	0.386	465	11.6	300	98.4	0.853	2.62	5.3	5.69	133	54.8	10.7	3.4	11.6	97.63	3.1
75	2	13	8.56	0.388	467	14.2	300	121.7	0.876	3.19	5.1	5.62	156	38.4	3.2	3.6	13.9	98.78	4.1
76	3	13	16.65	0.973	672	19.3	302	322.1	1.126	7.46	4.9	4.85	221	2.4	0.0	11.1	17.9	99.94	5.5
77	4	13	17.02	0.978	676	23.5	303	399.6	1.219	8.90	4.8	5.13	272	2.2	0.0	9.5	22.2	99.94	5.6
78	5	13	19.99	1.253	828	22.9	304	458.7	1.288	9.96	4.5	5.51	269	1.1	0.0	21.5	21.2	99.97	7.3
79	6	13	20.19	1.254	829	28.2	304	568.8	1.426	11.72	4.5	5.62	349	1.5	0.0	20.2	26.3	99.96	9.8
80	7	13	20.01	1.248	844	21.8	304	435.7	1.264	9.53	4.4	5.69	260	1.2	0.0	21.3	20.0	99.97	6.6
81	8	13	19.99	1.247	844	27.3	304	546.3	1.402	11.35	4.4	5.62	345	1.5	0.0	22.3	25.2	99.96	6.2
82	7	13	19.87	1.242	846	22.0	304	437.6	1.264	9.57	4.3	5.67	263	1.1	0.0	23.7	19.8	99.97	4.7

Table A-2. Additional Performance Data.

Fuel Number	Reading Number	SN_g, Engine Exit Smoke Number	V_r, Reference Velocity, m/s	fs/fm, Ratio of Sample to Metered Fuel-Air Ratio	S_s, Smoke Severity Operating Parameter	S_{NOx}, NO_x Severity Operating Parameter
1	2	0.	17.8	0.965	0.0413	0.1170
	3	0.	18.3	0.993	0.0578	0.1307
	4	0.9	20.1	1.011	0.1678	0.4370
	5	0.9	20.9	1.026	0.2364	0.3849
	6	1.8	23.3	0.991	0.2162	0.7818
	7	1.6	22.4	0.955	0.2919	0.7726
	8	1.3	22.9	0.996	0.2887	0.7629
	9	1.8	23.1	0.995	0.2045	0.8160
2	10	1.6	23.1	0.977	0.2008	0.8199
	11	2.1	22.7	0.986	0.2910	0.7814
	12	1.5	22.7	0.997	0.3159	0.7797
	13	1.2	23.0	1.039	0.2395	0.7923
	14	1.5	20.3	1.025	0.2436	0.3851
	15	1.7	20.4	1.031	0.1789	0.4269
	16	0.3	18.1	1.154	0.0765	0.1301
	17	0	18.1	1.095	0.0521	0.1149
3	18	0	18.0	1.176	0.0769	0.1334
	19	0	18.1	1.092	0.0466	0.1187
	20	2.0	20.5	1.010	0.1695	0.4486
	21	1.2	20.6	1.013	0.2393	0.3836
	22	2.4	23.3	0.974	0.2134	0.8036
	23	2.2	23.4	1.067	0.3043	0.7973
	24	1.7	23.2	1.050	0.2179	0.8513
	25	2.7	23.3	1.047	0.3097	0.8019
4	35	2.2	23.8	0.973	0.2007	0.8983
	34	3.7	24.0	0.971	0.2775	0.8525
	36	4.1	23.4	1.009	0.3269	0.7965
	37	2.1	23.1	0.977	0.2231	0.8325
	38	3.6	20.6	0.967	0.2326	0.3785
	39	1.7	21.3	0.971	0.1615	0.4312
	40	1.0	18.6	0.961	0.0550	0.1302
	41	1.6	18.8	0.978	0.0411	0.1096

Table A-2. Additional Performance Data. (Continued)

Fuel Number	Reading Number	SN_g, Engine Exit Smoke Number	V_r, Reference Velocity m/s	fs/fm, Ratio of Sample to Metered Fuel-Air Ratio	S_s, Smoke Severity Operating Parameter	S_{NOx}, NO_x Severity Operating Parameter
5	44	2.0	24.2	0.966	0.1918	0.9328
	42	2.3	23.6	0.965	0.2108	0.8454
	43	1.9	23.4	0.972	0.3042	0.8172
	45	1.8	24.4	0.979	0.2732	0.8842
	46	2.0	20.6	0.964	0.2225	0.3818
	47	1.8	20.6	0.940	0.1581	0.4274
	48	0.7	18.7	0.969	0.0567	0.1257
	49	0.8	18.7	0.971	0.0418	0.1077
6	26	1.1	18.0	0.812	0.0319	0.1145
	27	0.9	18.0	0.870	0.0499	0.1328
	28	3.1	20.2	0.996	0.1734	0.4399
	29	2.6	22.9	0.977	0.2162	0.3946
	30	2.7	23.4	0.992	0.2283	0.8206
	31	4.0	23.6	1.004	0.3189	0.8614
	32	2.8	24.2	0.979	0.2003	0.8958
	33	2.5	24.4	0.964	0.2719	0.8365
7	50	1.0	18.9	0.963	0.0394	0.1023
	51	1.1	18.8	0.956	0.0559	0.1207
	52	0.7	20.7	0.947	0.1580	0.4106
	53	2.1	21.3	0.980	0.2283	0.3592
	54	2.9	23.7	0.933	0.2010	0.8210
	55	3.9	23.7	0.934	0.2814	0.7938
	56	3.1	23.9	0.900	0.1733	0.9195
	57	2.2	24.0	0.921	0.2521	0.8841
8	58	2.9	24.3	0.939	0.2535	0.8719
	59	3.0	24.5	0.921	0.1765	0.9211
	60	3.5	23.5	0.921	0.2766	0.8021
	61	1.7	23.4	0.904	0.1917	0.8746
	62	2.5	20.6	0.943	0.2271	0.3763
	63	1.3	20.7	0.938	0.1590	0.4247
	64	0.8	18.6	0.941	0.0566	0.1266
	65	1.1	18.9	0.961	0.0418	0.1064

Table A-2. Additional Performance Data, (Continued)

Fuel Number	Reading Number	SN_g, Engine Exit Smoke Number	V_r, Reference Velocity, m/s	fs/fm, Ratio of Sample to Metered Fuel-Air Ratio	S_s, Smoke Severity Operating Parameter	S_{NOx}, NO_x Severity Operating Parameter
9	66	1.4	23.9	0.934	0.2003	0.8327
	67	2.4	23.5	0.932	0.2800	0.8244
	68	2.1	23.9	0.941	0.2593	0.8589
	69	1.2	24.1	0.917	0.1777	0.9177
	70	2.1	20.6	0.917	0.2009	0.4205
	71	0.7	21.0	0.931	0.1522	0.4276
	72	0.5	18.5	0.923	0.0530	0.1282
	73	0.7	18.6	0.943	0.0398	0.1073
10	99	0.6	13.4	0.953	0.0564	0.1226
	100	0.7	18.2	0.965	0.0405	0.1067
	103	2.3	23.0	0.912	0.1961	0.8224
	104	2.8	23.5	0.980	0.2797	0.7762
	105	1.3	24.0	0.905	0.1742	0.8903
	106	1.2	23.5	0.900	0.2402	0.8514
	101	1.2	20.7	0.929	0.1534	0.4175
	102	1.8	21.2	0.933	0.2110	0.3616
11	91	3.2	23.4	0.930	0.1950	0.8044
	92	2.5	22.5	0.916	0.2742	0.7864
	93	2.1	23.6	0.907	0.1713	0.8795
	94	1.7	24.1	0.932	0.2476	0.8265
	95	1.3	20.1	0.907	0.2044	0.3711
	96	0.9	20.7	0.939	0.1514	0.4145
	97	0.6	18.6	0.950	0.0552	0.1220
	98	0.7	18.4	0.953	0.0393	0.1053
12	83	2.8	24.0	0.930	0.2432	0.8589
	84	1.5	23.5	0.895	0.1654	0.8762
	85	2.0	22.7	0.905	0.2616	0.7834
	86	2.0	23.4	0.923	0.1880	0.8073
	87	1.5	20.5	0.931	0.2035	0.3721
	88	1.6	20.6	0.937	0.1498	0.4119
	89	0.5	18.1	0.963	0.0558	0.1009
	90	0.4	18.1	0.982	0.0412	0.1058

Table A-2. Additional Performance Data, (Concluded)

Fuel Number	Reading Number	SN_8, Engine Exit Smoke Number	V_r, Reference Velocity, m/s	fs/fm, Ratio of Sample to Metered Fuel-Air Ratio	S_s, Smoke Severity Operating Parameter	SNO_x, NO_x Severity Operating Parameter
13	74	0.5	18.1	0.998	0.0439	0.1055
	75	0.5	18.3	0.930	0.0580	0.1219
	76	1.9	20.4	0.926	0.1475	0.4004
	77	1.5	20.8	0.947	0.2123	0.3711
	78	2.6	23.4	0.924	0.1943	0.7913
	79	2.8	23.6	0.932	0.2708	0.7702
	80	2.3	24.0	0.920	0.1728	0.8709
	81	1.8	24.0	0.321	0.2441	0.8215
	82	1.7	24.0	0.893	0.1630	0.8730

Table A-3. Idle CO and HC Emission Test Data Correlation.

$$EI = b\left(\frac{f_s}{14.0}\right)^m$$

Fuel Number	f_I, Ideal Fuel-Air Ratio at Idle, g/kg	CO Emission Correlation (1)			HC Emission Correlation (2)		
		m, Slope	b, Intercept, g/kg	EI_{CO}, Idle, g/kg (Calculated from Correlation @ f_I)	m, Slope	b, Intercept, g/kg	EI_{HC}, Idle, g/kg Calculated from Correlation @ f_I
1	14.00	-2.36	28.70	28.70	-8.06	1.68	1.68
2	14.13	-1.25	30.20	29.85	-6.27	1.68	1.59
3	14.13	-1.50	31.00	30.55	-5.74	1.93	1.83
4	14.55	-1.93	37.22	34.56	-6.26	2.36	1.85
5	14.29	-1.99	33.09	31.77	-6.09	2.53	2.23
6	14.49	-1.67	34.88	32.94	-4.92	2.60	2.20
7	14.34	-2.06	35.82	34.09	-6.34	3.18	2.73
8	14.46	-2.60	31.68	29.13	-10.16	1.42	1.03
9	14.32	-2.86	26.84	25.16	-8.59	1.06	0.88
10	14.47	-2.10	32.29	30.13	-9.51	1.52	1.11
11	14.30	-2.15	30.26	28.91	-9.41	1.17	0.96
12	14.08	-2.43	26.82	26.45	-10.41	0.96	0.90
13	14.30	-1.97	37.86	36.32	-6.67	3.05	2.65

(1) Curve-fit examples shown in Figure 34.

(2) Curve-fit examples shown in Figure 37.

Table A-4. High Power CO Emission Data Corrections.

$$EI_{CO'engine} = EI_{CO'rig} \left(\frac{P_{3,\,rig}}{P_{3,\,engine}} \right)^{1.5}$$

Fuel Number	CO Emission Index, g/kg				
	Cruise[1] (Rig & Engine)	Takeoff[2]		Dash[3]	
		Rig	Engine	Rig	Engine
1	2.0	1.6	0.5	1.5	0.3
2	2.3	2.2	0.7	1.6	0.4
3	2.2	1.7	0.5	1.6	0.4
4	2.4	1.6	0.5	1.5	0.3
5	2.6	1.7	0.5	1.6	0.4
6	2.3	1.5	0.5	1.5	0.3
7	2.3	2.2	0.7	1.7	0.4
8	2.5	1.9	0.6	1.6	0.4
9	2.4	2.0	0.6	1.7	0.4
10	2.3	1.8	0.6	1.5	0.3
11	2.2	1.7	0.5	1.5	0.3
12	2.1	1.4	0.4	1.3	0.3
13	2.2	1.5	0.5	1.5	0.3

(1) $P_{3,\,rig} / P_{3,\,engine} = 1.000$

(2) $P_{3,\,rig} / P_{3,\,engine} = 0.461$

(3) $P_{3,\,rig} / P_{3,\,engine} = 0.364$

Table A-5. NO_x Emission Test Data Correlation.

a) Correlation with Combustor Operating Conditions

$$EI_{NOx} = mS_{NOx} + b$$

where:

$$S_{NOx} = \left(\frac{23.5}{V_r}\right)\left(\frac{P_3}{2.718}\right)^{0.37}\left|\phi(f)\right|\left\{\exp\left[\left(\frac{T_3-828.7}{191.7}\right)+\left(\frac{6.29-h}{53.2}\right)\right]\right\}$$

and $\phi(f)$ is defined in Section V. F. 1.

Fuel Number	Number of Data Points	m, Slope, g/kg	b, Intercept, g/kg	r, correlation coefficient	EI_{NOx}, g/kg (Calculated from Operating Conditions Correlation at S_{NOx} = 0.1205, 0.3491, 1.000, and 1.1756)			
					Idle 0.1205	Cruise 0.3491	Takeoff 1.000	Dash 1.1756
1	8	26.21	-0.27	0.9999	2.89	8.88	25.94	30.55
2	8	26.34	+0.18	0.9986	3.36	9.38	26.52	31.15
3	8	25.44	+0.27	0.9997	3.33	9.15	25.71	30.17
4	8	27.68	+1.18	0.9961	4.52	10.85	28.87	33.73
5	8	26.22	+1.18	0.9910	4.34	10.33	27.40	32.00
6	8	28.65	+0.37	0.9929	3.83	10.38	29.02	34.05
7	8	26.98	+0.26	0.9984	3.51	9.68	27.24	31.98
8	8	27.19	+0.92	0.9974	4.19	10.41	28.11	32.88
9	8	30.26	-0.11	0.9960	3.54	10.45*	30.15*	35.46*
10	8	28.93	+0.16	0.9997	3.65	10.26	29.09	34.17
11	8	26.40	+0.33	0.9992	3.51	9.54	26.73	31.37
12	8	24.37	+0.56	0.9994	3.50	9.07	24.93	29.21
13	9	25.73	+0.52	0.9959	3.62	9.50	26.25	30.77

b) Correlation with Fuel Hydrogen Content

$$EI_{NOx} = b\left(\frac{H}{14.5}\right)^m$$

Engine Power Level	Idle	Cruise*	Takeoff*	Dash*
b, Intercept, g/kg	3.15	8.90	25.22	29.63
m, Slope	-1.376	-0.863	-0.670	-0.653
r, Correlation Coefficient	-0.762	-0.925	-0.913	-0.901

* Fuel 9 excluded from curve fit (calibration span setting suspect).

Table A-6. Smoke Emission Test Data Correlation.

a) Correlation With Combustor Operating Conditions

$$SN_8 = b + m \left[\ln(S_s)\right]$$

where:

$$S_s = \left[\left(\frac{P_3}{2.718}\right)\left(\frac{f_\mu}{29.2}\right)\left(\frac{828.7}{T_3}\right)^{1.5}\left(\frac{W_c/P_3}{15.92}\right)\right]$$

Fuel Number	Number of Data Points	m, Slope	b, Intercept	r, Correlation Coefficient	SN_8 (Calculated from Operating Conditions Correlation at S_s = 0.0590, 0.2368, 1.000, and 1.2807)			
					Idle (0.0590)	Cruise (0.2368)	Takeoff (1.0000)	Dash (1.2807)
1	8	0.853	2.62	0.869	0.21	1.39	2.62	2.83
2	8	1.006	3.01	0.911	0.16	1.56	3.01	3.26
3	8	1.329	3.88	0.885	0.12	1.96	3.88	4.21
4	8	1.179	4.69	0.789	1.36	2.99	4.69	4.99
5	8	0.723	3.03	0.907	0.98	1.98	3.03	3.21
6	8	1.052	4.41	0.875	1.43	2.89	4.41	4.67
7	8	1.068	4.19	0.683	1.16	2.65	4.19	4.45
8	8	1.144	4.30	0.804	1.07	2.66	4.30	4.59
9	8	0.810	2.96	0.799	0.67	1.80	2.96	3.16
10	6	0.931	3.41	0.826	0.77	2.07	3.41	3.64
11	8	0.899	3.89	0.691	0.84	2.09	3.89	3.61
12	8	1.047	3.60	0.907	0.64	2.10	3.60	3.86
13	9	1.113	3.88	0.863	0.73	2.28	3.88	4.16

b) Correlation with Fuel Hydrogen Content

$$SN_8 = b + m\,(14.5-H)$$

Engine Power Level	Idle	Cruise	Takeoff	Dash
b, Intercept	0.179	1.546	2.999	3.206
m, Slope	+0.4115	+0.4382	+0.4675	+0.4715
r, Correlation Coefficient	+0.833	+0.776	+0.634	+0.607

Table A-7. Detailed Inner Liner Temperature Data.

Fuel Number	Reading Number	$(T_L - T_1)$ Inner Liner Temperature Rise, K																	
		Inner Panel 1 Located at Angles						Inner Panel 2 Located at Angles											
		306	315	324	333	342	351	302	304	308	310	320	322	324	326	328	336	340	346
1	2	35	34	19	144	35	45		61		61	62	76	80	76	62	54	54	
	3	36	38	21	140	44	52		64		66	68	82	87	84	69	54	55	
	4	58	61	43	136	62	69		112		102	109	129	122	111	85	86	81	
	5	64	59	48	136	67	76		136		119	118	139	133	119	91	98	93	
	6	77	64	50	157	79	81		166		148	136	162	148	136	106	106	100	
	7	91	89	72	147	100	95		219		197	168	186	189	181	144	156	149	
	8	88	81	66	149	97	92		209		186	152	176	177	168	134	147	139	
	9	73	57	48	143	80	78		155		140	119	142	148	132	103	104	97	
2	10	80	62	58	149	86	82		179		157	126	149	142	140	110	114	106	
	11	94	90	74	140	107	96		229		208	170	195	195	186	152	170	163	
	12	96	94	81	166	113	152		242		223	187	212	212	203	167	187	181	
	13	87	68	59	164	93	88		198		177	141	163	162	153	121	133	124	
	14	72	68	56	196	85	81		164		144	127	157	150	137	108	122	116	
	15	65	57	46	168	72	68		131		119	115	134	130	119	93	94	89	
	16	38	42	26	217	52	51		65		65	72	86	90	86	70	66	63	
	17	39	39	28	209	48	46		64		68	63	77	82	79	64	57	56	
3	18	36	42	24	221	51	49		65		66	73	88	92	88	71	65	63	
	19	36	37	21	218	46	48		59		60	62	76	81	78	63	53	52	
	20	65	57	44	166	69	67		131		118	114	135	131	119	91	92	86	
	21	73	69	55	177	82	81		166		151	136	156	149	136	107	117	112	
	22	83	67	54	148	87	84		183		166	134	157	154	144	113	122	116	
	23	97	96	81	166	112	96		237		227	188	213	211	201	164	191	188	
	24	80	60	51	152	83	81		171		154	129	152	148	137	108	114	108	
	25	96	87	74	160	107	96		226		211	174	197	196	186	151	172	166	
4	35	98	88	80	113	105	80	74	242	227	236	183	197	200	197	176	159	173	160
	34	103	116	96	126	138	95	102	309	316	307	368	275	279	277	253	252	268	248
	36	101	118	98	133	135	99	110	306	325	314	276	233	304	304	278	275	209	273
	37	108	93	85	124	119	86	86	353	257	245	204	219	220	317	194	188	201	184
	38	95	95	84	110	108	85	104	237	239	226	192	211	214	211	186	176	189	187
	39	80	81	66	82	77	63	67	174	170	164	132	150	152	148	128	105	115	109
	40	39	52	32	43	48	43	36	73	77	82	73	85	90	93	83	63	67	62
	41	33	42	28	32	36	35	24	59	63	67	59	71	76	79	72	49	56	43
5	44	82	71	55	89	83	62	34	186	187	181	118	133	149	151	133	121	135	124
	42	85	76	63	92	90	66	54	204	204	196	134	123	161	165	143	134	148	136
	43	93	97	86	113	115	85	85	261	276	269	203	222	238	244	218	222	236	219
	45	94	93	83	114	115	115	84	77		267	259	200	216	227	205	206	220	203
	46	75	81	61	87	87	66	67	177	180	174	131	111	159	158	135	123	133	127
	47	59	69	48	70	68	51	85	123	125	123	91	80	123	126	107	87	96	89
	48	32	51	24	39	48	43	22	56	62	69	60	75	83	84	72	63	66	58
	49	31	41	22	30	39	35	17	52	57	69	52	67	74	76	63	53	57	49
6	26	37	40	15	24	31	34	27	77	72	72	49	57	63	66	58	49	58	51
	27	33	45	18	34	41	40	34	85	80	80	57	65	71	74	66	64	72	65
	28	61	54	41	69	57	57	36	142	144	139	111	125	126	120	105	93	105	95
	29	93	88	69	95	86	72	72	232	229	221	172	183	179	175	156	142	159	145
	30	99	97	76	100	97	77	83	254	254	245	198	202	197	191	172	160	175	160
	31	99	120	90	113	123	83	105	300	315	305	256	271	275	276	253	254	270	247
	32	91	80	68	106	91	73	68	222	220	210	164	177	177	175	157	140	155	143
	33	99	103	86	122	121	88	97	287	299	290	240	254	254	251	229	231	245	225
7	50	30	41	20	21	35	45	37	55	55	64	49	60	66	70	61	47	53	47
	51	31	46	26	31	45	52	43	63	61	70	56	66	73	77	66	60	68	59
	52	65	67	41	63	67	64	33	130	140	137	93	115	121	120	101	91	100	92
	53	78	77	56	83	87	79	58	185	188	180	196	154	158	156	182	122	132	125
	54	89	78	61	99	100	77	16	213	211	205	145	155	164	173	146	142	152	139
	55	96	105	85	121	123	98	28	269	281	275	214	228	248	250	224	236	246	227
	56	86	77	57	100	94	77		196	198	196	133	145	154	158	139	135	146	134
	57	98	102	83	125	126	101	83	268	278	274	212	223	246	242	216	229	240	220

Table A-7. Detailed Inner Liner Temperature Data (Concluded).

Fuel Number	Reading Number	$(T_L - T_3)$ Inner Liner Temperature Rise, K																	
		Inner Panel 1 Located at Angles						Inner Panel 2 Located at Angles											
		306	315	324	333	342	351	302	304	308	310	320	322	324	326	328	336	340	346
8	58	106	112	94	134	126	105	42	297	294	298	238	248	253	266	242	256	266	242
	59	101	86	66	111	106	93	71	225	223	219	144	156	166	173	156	156	168	150
	60	104	115	96	136	136	103	55	298	312	307	250	264	276	283	259	275	289	281
	61	103	90	74	116	116	90	27	244	245	237	163	176	185	191	170	181	196	171
	62	94	96	77	119	108	93	88	239	240	231	179	194	200	202	177	188	203	186
	63	82	81	57	90	82	73	54	175	175	172	119	136	145	148	129	120	171	117
	64	45	52	32	49	51	56	56	60	83	87	66	79	90	93	83	67	73	64
	65	40	37	23	32	34	46	41	63	69	74	47	60	70	75	66	50	56	49
9	66	92	82	65	105	96	75	26	225	218	214	153	162	167	169	148	152	168	144
	67	98	109	86	126	123	96	94	276	283	277	220	232	244	252	227	245	261	232
	68	93	103	83	128	121	95	37	268	270	264	208	219	228	234	210	224	239	203
	69	89	76	57	104	90	73	10	195	200	195	124	137	149	155	138	143	160	136
	70	82	82	58	104	91	77	56	184	194	187	129	144	155	159	137	139	152	135
	71	64	71	45	83	70	61	23	122	127	127	89	104	116	121	106	98	112	96
	72	38	53	29	40	740	51	42	63	67	69	58	72	82	84	72	64	71	63
	73	35	41	23	29	567	43	34	54	59	62	47	61	70	73	64	49	58	51
10	99	56	67	50	26	43	39			64	65	52	83		71	57	54		
	100	46	55	42	20	36	31			53	59	60	58		54	41	45		
	103	85	136	112	63	85	96		44	166	175	170	183		158	157	205		
	104	106	158	124	82	114	98		103	248	255	251	273		232	231	246		
	105	77	131	107	63	80	93		35	155	164	156	172		146	142	187		
	106	104	154	125	38	107	101		33	233	241	231	253		211	214	239		
	101	53	84	71	39	64	64		7	85	83	101	117		102	89	116		
	102	75	110	91	57	78	81		34	134	140	141	161		146	136	171		
11	91	74	114	101	57	77	86		46	134	140	143	169		138	131	175		
	92	96	133	117	80	102	91		70	213	218	218	233		202	200	222		
	93	68	108	97	52	72	83		29	125	131	136	150		125	118	153		
	94	96	133	118	73	98	54		78	199	206	202	222		187	186	216		
	95	71	101	87	58	74	72		3	116	121	128	148		128	115	143		
	96	53	79	72	39	64	57			78	81	98	115		100	85	93		
	97	51	58	46	24	43	31			56	56	69	81		68	54	48		
	98	48	46	33	18	36	29			47	46	59	68		54	41	42		
12	83	91	126	121	72	86	86		75	163	173	178	196		168	165	187		
	84	84	97	100	48	66	72		42	107	111	125	136		111	98	128		
	85	88	132	116	69	86	80		61	172	178	182	202		172	169	136		
	86	66	99	101	48	65	72		50	115	120	130	142		118	106	140		
	87	66	91	83	46	69	61			97	101	114	134		118	102	116		
	88	52	76	67	37	61	48			72	75	95	113		98	80	82		
	89	50	54	44	23	41	30			53	54	66	78		67	53	48		
	90	43	38	36	19	35	29			42	42	59	60		58	44	44		
13	74	42	41	31	16	34	35		61	47	45	60	68		54	41	54		
	75	42	44	35	19	39	35		67	52	50	69	75		64	51	58		
	76	55	77	69	39	61	63		98	80	83	103	120		110	97	114		
	77	73	97	86	52	72	74		131	116	120	134	154		142	129	151		
	78	76	111	105	59	76	82		86	140	147	145	161		142	136	172		
	79	95	132	115	78	102	88		180	203	210	210	232		193	198	203		
	80	73	110	120	59	76	84		135	135	142	141	155		137	132	163		
	81	98	136	129	81	101	92		113	201	208	205	226		194	194	213		
	82	72	110	111	58	74	83		55	141	142	140	155		134	127	163		

Table A-8. Detailed Outer Liner Temperature Data.

Fuel Number	Reading Number	$(T_L - T_3)$ Outer Liner Temperature Rise, K													
		Outer Panel 1 Located at Angles (deg.)							Outer Panel 2 Located at Angles (deg.)						
		9	18	27	36	45	108	117	14	18	32	36	86	90	104	108
1	2				9	23	13	30	127	81	113	137			109	109
	3				13	30	17	30	157	102	142	169			128	192
	4				19	48	26	48	178	162	206	227			171	168
	5				26	61	29	68	211	201	247	264			204	191
	6				27	69	33	66	235	212	239	266			208	193
	7				41	84	47	89	309	276	314	243			261	244
	8				40	78	44	84	294	264	299	333			249	229
	9				27	61	33	63	232	205	229	258			199	191
2	10				31	63	35	66	239	216	289	260			201	191
	11				46	85	50	91	317	285	313	351			263	243
	12				48	90	54	98	326	301	326	364			283	261
	13				37	71	40	74	261	236	263	292			216	206
	14				37	71	39	60	240	228	259	292			231	201
	15				27	51	30	54	187	175	209	236			186	168
	16				21	31	19	33	134	122	140	159			145	124
	17				16	24	16	31	112	99	112	135			123	109
3	18				17	28	18	29	133	121	124	157			138	129
	19				12	22	14	26	103	92	104	127			113	165
	20				22	48	28	52	176	165	208	233			182	173
	21				34	67	38	68	229	224	255	291			239	213
	22				34	67	38	74	253	226	253	281			224	211
	23				42	89	54	102	334	304	329	367			297	269
	24				31	63	35	68	237	213	331	264			202	198
	25				47	86	51	96	314	293	312	347			271	251
4	35	47			55	19	51	76	222	293	209	262	245	91	259	200
	34	64			64	44	72	104	320	387	297	345	333	187	336	231
	36	67			64	51	74	106	337	406	303	369	352	160	359	314
	37	51			61	29	37	82	241	311	226	235	261	105	272	215
	38	57			62	47	59	78	238	292	229	301	253	157	220	234
	39	39			44	20	44	62	163	228	169	223	193	108	223	167
	40	37			28	19	29	28	111	140	104	157	118	105	180	126
	41	32			20	10	17	21	93	121	85	134	93	90	153	100
5	44	38			37		39	65	194	266	177	229	224	77	243	204
	42	39			40	9	43	68	206	281	193	243	239	84	263	222
	43	53			54	36	63	92	292	366	273	326	315	135	335	299
	45	54			55	28	61	93	281	347	257	310	301	114	308	277
	46	45			46	28	44	74	202	262	193	263	234	137	247	213
	47	32			32	7	34	58	141	213	152	206	187	105	204	167
	48	34			22	15	19	27	100	133	97	145	115	108	154	110
	49	31			17	9	16	24	83	120	79	127	98	99	134	96
6	26	13			8	1	16	18	69	108	57	102	83	88	142	104
	27	18			14	9	18	22	87	129	84	133	111	102	166	116
	28	23			27	1	31	50	140	211	149	214	174	81	224	160
	29	46			47	20	44	72	223	292		261	234	83	258	198
	30	50			53	28	51	80	244	316	224	285	251	93	275	218
	31	63			57	47	68	103	333	402	233	361	333	145	351	305
	32	43			46	11	44	70	213	285	203	252	233	79	252	190
	33	60			59	39	65	98	312	375	279	333	316	125	325	273
7	50	15			9	22	13	19	74	101	62	114	95	89	144	100
	51	18			14	29	16	23	89	121	85	139	123	102	167	122
	52	22			30		33	48	123	196	139	217	183	92	236	183
	53	33			42	16	44	62	178	245	179	271	228	124	270	217
	54	39			43		43	74	199	263	189	257	233		260	225
	55	54			56		64	97	294	354	271	340	320		332	308
	56	39			42		41	71	192	258	179	243	223		250	215
	57	55			59		64	97	287	344	266	325	209		320	295

Table A-8. Detailed Outer Liner Temperature Data (Concluded).

Fuel Number	Reading Number	$(T_L - T_3)$ Outer Liner Temperature Rise, K													
		Outer Panel 1 Located at Angles (deg.)							Outer Panel 2 Located at Angles (deg.)							
		9	18	27	36	45	108	117	14	18	32	36	86	90	104	108
8	58	59			66		71	98	298	344	268	322	303		320	295
	59	43			52		49	75	210	260	194	255	223		255	220
	60	63			67	4	76	101	330	369	292	346	323		347	336
	61	47			58		54	77	233	275	212	256	229		268	225
	62	53			62	34	64	72	230	276	237	288	243	49	302	256
	63	38			48	13	48	54	169	215	178	219	177	20	265	193
	64	41			34	42	28	32	117	137	117	157	112	106	177	183
	65	31			21	28	18	24	93	114	87	128	86	88	142	107
9	66	38			45		45	69	209	259	195	252	215		263	232
	67	54			57		67	90	306	350	283	329	292		333	309
	68	52			58		63	89	287	329	264	305	272		312	285
	69	38			44		42	68	203	247	180	236	202		246	215
	70	42			48	12	51	61	199	243	202	254	207	23	278	229
	71	30			34		37	45	149	196	155	200	157	12	226	176
	72	33			27	32	22	27	100	129	103	141	107	90	166	121
	73	28			19	25	17	22	85	112	80	123	85	82	142	100
10	99	42	32	31	35	44	24	32	118		128	163	57		153	130
	100	35	26	23	23	32	17	26	93		101	136	48		137	94
	102	48	32	50	62	82	53	88	226	202	227	273	187		273	231
	104	64	46	75	72	109	79	114	327	292	321	363	232	24	253	315
	105	46	28	45	57	76	47	81	209	172	208	253	168		264	209
	106	63	42	69	75	105	73	110	303	272	294	345	222		331	289
	101	29	17	29	34	54	34	52	140	81	152	207	111		226	175
	102	42	30	51	52	77	52	72	200	158	217	276	156		271	221
11	91	44	24	42	52	78	46	76	213	182	213	292	163		262	214
	92	58	36	58	66	102	70	106	303	267	304	354	211	3	333	295
	93	43	22	39	47	71	42	71	200	165	196	242	147		251	199
	94	59	38	62	69	100	65	102	286	250	279	334	205		314	265
	95	45	32	51	51	75	49	69	196	139	212	272	139		254	211
	96	33	21	32	36	55	33	52	140	81	163	214	97		221	165
	97	40	30	29	31	42	22	32	103		124	159	52		153	120
	98	32	24	22	23	32	16	27	90		102	137	45		136	83
12	83	61	36	60	63	96	59	104	266	205	266	321	177		275	252
	84	43	21	36	43	69	39	71	195	146	188	244	122		235	177
	85	56	34	61	59	95	56	100	273	238	274	342	180		287	240
	86	41	21	38	42	72	38	73	197	160	200	260	133		238	173
	87	45	28	47	42	69	38	70	178	134	193	260	116		217	183
	88	34	20	30	33	54	32	57	140	102	162	221	84		194	147
	89	39	28	27	31	41	21	28	106		124	166	52		161	121
	90	34	24	22	25	34	17	26	92		109	152	47		144	100
13	74	18	11	16	17	25	16	27	77	112	87	133	57		129	91
	75	21	12	19	22	34	21	30	89	123	104	148	61		156	115
	76	26	17	31	34	56	34	59	129	193	159	221	118		204	155
	77	38	26	48	47	75	46	78	187	244	204	272	148		233	206
	78	42	25	44	50	78	45	88	203	264	203	269	164		241	204
	79	57	35	67	65	102	65	113	284	343	288	349	204		299	221
	80	44	26	43	52	78	45	84	200	254	201	260	155		236	192
	81	61	39	67	71	103	65	113	280	330	282	345	207		288	267
	82	48	25	42	51	76	44	83	200	253	200	263	152		234	192

Table A-9. Peak Liner Temperature Data Correlation.

a) Correlation with Combustor Operating Conditions[1]

$$\left(T_{L\,max} - T_3 \right) = b \left(\frac{f}{29.2} \right)^m$$

Fuel Number	m, Slope	b, Intercept, K	r, Correlation Coefficient	f_{TO}, Ideal Fuel-Air Ratio at Takeoff	$(T_{L\,max} - T_3)$, K (Calculated from Operating Conditions Correlation at f/f_{TO} = 0.4795, 0.8219, 1.000 and 0.9555)			
					Idle (0.4795)	Cruise (0.8219)	Takeoff (1.000)	Dash (0.9555)
1	1.003	348.1	0.998	29.20	166.6	286.0	348.1	332.6
2	1.107	366.6	0.998	29.47	164.1	298.0	370.3	352.1
3	1.118	368.1	0.998	29.48	163.6	298.8	372.0	353.5
4	1.300	394.4	0.994	30.35	159.6	321.6	415.0	391.1
5	1.218	358.4	0.989	29.80	150.2	289.7	367.9	348.1
6	1.469	397.7	0.990	30.22	142.1	313.6	418.3	391.2
7	1.352	356.0	0.992	29.92	136.1	282.1	367.7	345.8
8	1.260	363.7	0.994	30.17	150.1	296.0	379.0	357.9
9	1.205	339.6	0.990	29.87	143.9	275.5	349.0	330.4
10	1.033	346.0	0.990	30.17	167.6	292.5	358.2	341.7
11	0.987	335.7	0.992	29.83	166.1	282.7	343.1	328.0
12	0.868	327.6	0.986	29.36	174.1	277.9	329.5	316.7
13	1.141	359.2	0.994	29.82	159.2	294.5	368.4	349.7

b) Correlation With Fuel Hydrogen Content

$$(T_{L\,max} - T_3) = b + m\,(14.5 - H)$$

Engine Power Level	Idle	Cruise	Takeoff	Dash
b, Intercept	165.8	282.2	342.2	327.2
m, Slope	-5.89	+7.39	+17.79	+14.99
r, Correlation Coefficient	-0.441	+0.482	+0.605	+0.591

(1) Examples shown in Figure 46.

Table A-10. Combustor Exit Temperature Distribution Data.

Fuel Number	Reading Number	P_3, Inlet Total Pressure, MPa	T_3, Inlet Total Temperature, K	W_a, Combustor Airflow, kg/s	f_m, Metered Fuel-Air Ratio, g/kg	T_f, Fuel Temperature, K	W_f, Fuel Flow Rate, g/s	ΔP_f, Fuel Nozzle Pressure Drop, MPa	A_{fa}, Fuel Nozzle Effective Area, mm^2	$\Delta P_T/P_3$, Combustor Pressure Drop, %	$\Delta T_{avg.}$, Combustor Temperature Rise, K	η_{TC}, Thermal Combustion Efficiency, %	PF, Pattern Factor	PrF, Profile Factor	$(T_{local} - T_3)/\Delta T_{avg.}$ Temperature Rise Ratio										S_{TP}, Pattern Factor Severity Parameter
															Average Profile					Peak Profile						
															Tip 1	2	3	4	Root 5	Tip 1	2	3	4	Root 5	
3	2	0.108	478.	2.209	14.0	288.	30.9	0.21	1.715	6.64	495.	92.35	0.665	0.077	0.939	1.044	1.076	1.077	0.864	1.542	1.665	1.523	1.445	1.303	2.251
	3	0.108	678.	1.837	22.9	291.	42.1	0.43	1.604	5.97	694.	95.98	0.366	0.038	0.968	1.046	1.068	1.063	0.855	1.231	1.279	1.311	1.366	1.260	1.391
	4	0.107	812.	1.383	28.1	291.	38.9	0.35	1.632	5.25	662.	65.84	0.354	0.073	0.975	1.053	1.073	1.055	0.844	1.354	1.292	1.292	1.328	1.246	1.269
	5	0.107	822.	1.592	24.2	292.	38.5	0.35	1.631	5.49	650.	78.52	0.321	0.065	0.974	1.048	1.065	1.062	0.851	1.321	1.294	1.288	1.321	1.255	1.170
	6	0.107	826.	1.633	26.3	292.	43.8	0.47	1.583	5.38	713.	78.51	0.314	0.060	0.976	1.052	1.056	1.060	0.856	1.314	1.290	1.271	1.293	1.290	1.116
	7	0.107	826.	1.642	26.5	291.	43.5	0.47	1.587	5.50	707.	78.78	0.334	0.076	0.962	1.055	1.061	1.076	0.865	1.221	1.314	1.334	1.330	1.187	1.116
2	8	0.107	828.	1.642	26.4	291.	43.3	0.46	1.601	5.63	703.	78.61	0.354	0.089	0.930	1.056	1.061	1.089	0.865	1.197	1.309	1.312	1.354	1.226	1.114
	9	0.107	829.	1.606	26.9	291.	43.2	0.46	1.593	5.53	710.	77.96	0.330	0.071	0.977	1.050	1.046	1.071	0.855	1.298	1.308	1.250	1.267	1.330	1.121
	10	0.106	828.	1.510	25.7	289.	38.8	0.35	1.628	5.07	652.	74.25	0.331	0.078	0.966	1.052	1.044	1.078	0.861	1.287	1.331	1.324	1.290	1.327	1.183
	11	0.106	676.	1.619	26.1	289.	42.3	0.43	1.608	5.48	723.	78.87	0.374	0.072	0.951	1.044	1.046	1.072	1.887	1.204	1.237	1.283	1.296	1.374	1.456
	12	0.107	459.	2.214	14.4	288.	31.9	0.21	1.709	6.48	467.	84.20	0.556	0.083	0.903	1.044	1.074	1.083	0.896	1.347	1.556	1.508	1.439	1.436	2.405
1	13	0.107	814.	1.583	24.3	286.	38.5	0.36	1.721	5.70	660.	79.30	0.244	0.069	0.999	1.065	1.069	1.058	0.808	1.219	1.244	1.244	1.186	1.166	1.193
	14	0.106	813.	1.606	24.9	286.	40.0	0.40	1.628	5.51	687.	80.82	0.238	0.063	1.001	1.057	1.063	1.059	0.820	1.238	1.237	1.228	1.187	1.199	1.157
	15	0.106	814.	1.615	24.8	287.	40.0	0.40	1.626	5.49	680.	80.37	0.267	0.073	0.953	1.065	1.073	1.065	0.844	1.196	1.254	1.250	1.267	1.151	1.156
	16	0.107	674.	1.678	24.8	287.	41.6	0.43	1.692	5.60	715.	81.87	0.293	0.063	0.961	1.050	1.060	1.063	0.866	1.177	1.260	1.241	1.228	1.293	1.448
	17	0.107	464.	2.254	13.5	286.	30.4	0.19	1.781	6.44	471.	90.83	0.454	0.085	0.901	1.046	1.085	1.080	0.889	1.369	1.385	1.454	1.364	1.402	2.343
4	19	0.107	472.	2.392	13.7	290.	32.8	0.22	1.703	7.30	466.	88.62	0.729	0.081	0.877	1.043	1.080	1.081	0.920	1.397	1.729	1.566	1.484	1.439	2.214
	20	0.107	673.	1.998	23.7	292.	47.3	0.53	1.574	7.45	732.	87.93	0.434	0.068	0.943	1.045	1.068	1.061	1.882	1.199	1.343	1.335	1.304	1.211	1.316
	22	0.107	830.	1.719	24.2	295.	41.5	0.38	1.636	6.96	678.	82.50	0.314	0.087	0.962	1.059	1.087	1.065	0.827	1.168	1.287	1.314	1.246	1.195	1.035
	23	0.107	831.	1.707	27.7	295.	47.3	0.52	1.594	7.01	753.	80.86	0.279	0.082	0.959	1.057	1.082	1.063	0.839	1.174	1.279	1.276	1.245	1.186	1.063
	24	0.107	831.	1.706	27.7	295.	47.3	0.52	1.594	6.90	754.	80.93	0.283	0.092	0.958	1.060	1.092	1.068	0.823	1.263	1.269	1.247	1.283	1.132	1.062
5	25	0.107	832.	1.718	23.3	297.	40.1	0.36	1.650	7.00	669.	84.31	0.287	0.100	0.929	1.066	1.100	1.078	0.827	1.200	1.265	1.287	1.265	1.171	1.093
	26	0.107	832.	1.717	26.8	297.	46.0	0.50	1.607	7.07	745.	0.254	0.094	82.69	0.957	1.064	1.094	1.071	0.814	1.193	1.248	1.254	1.242	1.162	1.061
	27	0.107	831.	1.732	26.5	298.	45.9	0.50	1.609	7.10	739.	82.87	0.285	0.101	0.940	1.066	1.101	1.075	0.818	1.218	1.241	1.285	1.262	1.137	1.062
	28	0.107	680.	1.879	23.6	297.	44.4	0.46	1.619	6.72	745.	90.09	0.362	0.093	0.915	1.058	1.093	1.083	0.851	1.236	1.362	1.318	1.315	1.197	1.328
	29	0.107	467.	2.414	13.8	297.	33.3	0.22	1.747	6.91	480.	90.82	0.680	0.135	0.818	1.070	1.038	1.135	0.939	1.368	1.680	1.520	1.512	1.355	2.208
6	30	0.107	823.	1.710	23.9	296.	40.8	0.36	1.668	6.63	695.	85.58	0.406	0.134	0.913	1.057	1.134	1.073	0.824	1.183	1.233	1.406	1.268	1.139	1.099
	31	0.107	830.	1.711	27.4	296.	46.8	0.51	1.614	6.90	57.	82.41	0.240	0.088	0.965	1.056	1.088	1.072	0.840	1.192	1.240	1.208	1.235	1.145	1.060
	32	0.107	831.	1.714	27.3	296.	46.8	0.51	1.612	6.92	752.	81.98	0.263	0.108	0.932	1.065	1.108	1.076	0.819	1.212	1.227	1.263	1.253	1.160	1.059
	33	0.106	677.	1.868	23.8	296.	44.5	0.45	1.635	6.57	758.	91.00	0.477	0.119	0.910	1.044	1.119	1.072	0.855	1.208	1.324	1.477	1.283	1.197	1.327
	34	0.107	469.	2.420	15.5	295.	37.5	0.29	1.701	6.96	540.	91.72	0.790	0.131	0.828	1.075	1.031	1.131	0.934	1.333	1.531	1.790	1.441	1.400	2.119
7	46	0.108	823.	1.736	24.1	292.	41.8	0.36	1.717	7.16	674.	82.08	0.302	0.085	0.946	1.049	1.085	1.068	0.852	1.240	1.223	1.273	1.302	1.254	1.108
	47	0.108	830.	1.727	27.5	292.	47.4	0.49	1.666	7.28	742.	80.28	0.286	0.081	0.946	1.048	1.081	1.067	0.858	1.214	1.213	1.264	1.284	1.230	1.067
	48	0.108	830.	1.724	27.5	293.	47.4	0.49	1.667	7.26	740	79.96	0.283	0.088	0.954	1.056	1.088	1.069	0.833	1.179	1.274	1.273	1.283	1.182	1.069
	49	0.108	676.	1.919	23.6	293.	45.3	0.43	1.686	7.18	719.	86.61	0.320	0.075	0.918	1.041	1.075	1.070	0.896	1.244	1.253	1.268	1.320	1.258	1.346
	50	0.108	469.	2.407	14.1	294.	34.0	0.21	1.828	7.35	471.	86.70	0.505	0.094	0.846	1.052	1.094	1.089	0.919	1.505	1.446	1.428	1.488	1.457	2.256

Table A-10. Combustor Exit Temperature Distribution Data (Concluded).

Fuel Number	Reading Number	P_3, Inlet Total Pressure, MPa	T_3, Inlet Total Temperature, K	W_c, Combustor Airflow, kg/s	f_m, Metered Fuel-Air Ratio, g/kg	T_F, Fuel Temperature, K	W_f, Fuel Flow Rate, g/s	ΔP_f, Fuel Nozzle Pressure Drop, MPa	A_{fe}, Fuel Nozzle Effective Area, mm^2	$\Delta P_T/P_3$, Combustor Pressure Drop, %	$\Delta T_{avg.}$, Combustor Temperature Rise, K	η_{TC}, Thermal Combustion Efficiency, %	PF, Pattern Factor	PrF, Profile Factor	$(T_{local} - T_3)/\Delta T_{avg.}$ Temperature Rise Ratio										S_{prf}, Pattern Factor Severity Parameter
															Average Profile					Peak Profile					
															Tip 1	2	3	4	Root 5	Tip 1	2	3	4	Root 5	
A	41	0.107	829.	1.722	24.1	291.	41.6	0.22	2.189	7.22	660.	80.19	0.222	0.077	0.985	1.072	1.077	1.026	0.830	1.151	1.222	1.189	1.179	1.101	1.103
	42	0.107	830.	1.722	27.7	291.	47.7	0.33	2.028	7.28	736.	78.93	0.241	0.073	0.986	1.068	1.073	1.038	0.835	1.170	1.241	1.199	1.194	1.069	1.069
	43	0.107	829.	1.761	27.1	291.	47.6	0.49	1.662	7.30	735.	80.54	0.196	0.077	0.997	1.072	1.077	1.040	0.813	1.194	1.196	1.187	1.175	1.151	1.060
	44	0.107	676.	1.844	24.6	290.	45.4	-0.06	4.448	7.00	727.	84.02	0.292	0.069	0.943	1.050	1.069	1.053	0.884	1.160	1.229	1.244	1.292	1.155	1.364
	45	0.108	466.	2.415	14.1	291.	34.0	0.21	1.811	7.49	465.	86.12	0.474	0.087	0.851	1.039	1.085	1.087	0.938	1.461	1.438	1.435	1.475	1.347	2.250
9	35	0.107	475.	2.368	14.5	293.	34.3	0.18	1.979	7.54	498.	89.87	0.482	0.076	0.909	1.034	1.074	1.076	1.907	1.482	1.408	1.419	1.472	1.398	2.179
	36	0.107	677.	1.950	23.8	292.	46.4	0.42	1.747	7.48	709.	84.56	0.297	0.066	0.976	1.047	1.066	1.056	0.855	1.184	1.221	1.246	1.297	1.174	1.337
	37	0.107	821.	1.726	24.7	292.	42.5	0.35	1.769	7.24	651.	77.12	0.245	0.073	0.998	1.072	1.073	1.033	0.825	1.156	1.245	1.198	1.165	1.109	1.125
	38	0.107	831.	1.707	25.2	291.	43.0	0.35	1.764	7.17	659.	76.74	0.231	0.074	0.997	1.072	1.074	1.033	0.824	1.157	1.231	1.183	1.163	1.083	1.109
	39	0.107	831.	1.699	28.8	291.	49.0	0.50	1.695	7.25	735.	75.67	0.249	0.073	0.998	1.071	1.073	1.034	0.824	1.159	1.249	1.195	1.166	1.083	1.075
	40	0.107	832.	1.734	28.2	291.	49.0	0.50	1.694	7.24	731.	76.79	0.213	0.078	1.008	1.076	1.078	1.037	0.800	1.200	1.213	1.194	1.169	1.129	1.065
10	68	0.108	827.	1.815	27.6	294.	50.1	0.58	1.625	7.94	742.	79.71	0.220	0.097	1.003	1.095	1.097	1.022	0.786	1.173	1.220	1.216	1.214	1.156	1.030
	69	0.108	829.	1.856	27.0	294.	50.1	0.59	1.622	7.93	738.	81.10	0.210	0.107	0.988	1.098	1.102	1.029	0.783	1.194	1.199	1.210	1.204	1.106	1.035
	70	0.108	832.	1.861	22.2	293.	41.3	0.35	1.720	7.88	636.	83.71	0.202	0.103	0.979	1.100	1.103	1.032	0.786	1.200	1.197	1.202	1.198	1.113	1.025
	71	0.107	677.	1.879	24.0	294.	45.0	0.44	1.689	7.09	704.	83.43	0.312	0.101	0.941	1.076	1.101	1.063	0.819	1.226	1.228	1.312	1.300	1.194	1.342
	73	0.108	463.	2.452	13.7	295.	33.6	0.19	1.895	7.92	452.	85.61	0.685	0.119	0.884	1.069	1.119	1.083	0.844	1.268	1.385	1.685	1.436	1.432	2.276
11	63	0.108	467.	2.414	13.7	294.	33.0	0.19	1.885	7.69	454.	86.28	0.520	0.111	0.911	1.062	1.111	1.078	0.838	1.274	1.392	1.520	1.517	1.428	2.267
	64	0.107	683.	1.925	23.0	294.	44.3	0.44	1.682	7.34	690.	85.01	0.346	0.098	0.972	1.072	1.098	1.057	0.801	1.230	1.256	1.315	1.346	1.194	1.340
	65	0.108	824.	1.767	24.2	294.	42.8	0.35	1.764	7.63	635.	76.56	0.217	0.102	0.992	1.095	1.102	1.028	0.782	1.202	1.204	1.217	1.204	1.108	1.119
	66	0.108	826.	1.806	28.9	294.	52.2	0.59	1.661	7.83	742.	76.11	0.230	0.103	0.987	1.095	1.103	1.033	0.783	1.211	1.215	1.230	1.222	1.105	1.053
	67	0.108	826.	1.800	29.3	294.	52.7	0.61	1.656	7.80	748.	75.94	0.216	0.099	1.000	1.095	1.099	1.026	0.781	1.190	1.212	1.216	1.205	1.150	1.033
12	57	0.107	828.	1.725	28.2	297.	48.6	0.60	1.600	7.42	748.	78.92	0.224	0.095	1.028	1.093	1.095	1.020	0.764	1.177	1.220	1.217	1.208	1.153	1.089
	58	0.108	828.	1.749	27.7	297.	48.4	0.59	1.609	7.52	758.	81.47	0.256	0.099	1.022	1.090	1.100	1.023	0.765	1.207	1.210	1.250	1.256	1.130	1.062
	59	0.107	829.	1.746	23.8	298.	41.5	0.39	1.683	7.40	669.	82.52	0.215	0.099	1.009	1.089	1.099	1.029	0.774	1.200	1.189	1.211	1.215	1.122	1.036
	60	0.107	675.	1.868	23.6	297.	43.7	0.44	1.670	7.02	717.	86.29	0.285	0.090	0.973	1.070	1.090	1.051	0.816	1.220	1.217	1.282	1.285	1.166	1.373
	61	0.107	460.	2.231	14.5	296.	32.3	0.20	1.857	7.28	651.	80.69	0.526	0.105	0.903	1.056	1.105	1.082	0.855	1.282	1.400	1.526	1.480	1.463	2.400
13	51	0.107	426.	2.405	14.0	300.	33.6	0.22	1.747	7.39	618.	76.56	0.759	0.093	0.908	1.047	1.093	1.079	0.873	1.371	1.509	1.634	1.759	1.635	2.624
	53	0.107	656.	1.889	23.6	300.	44.5	0.47	1.602	7.62	706.	85.28	0.386	0.082	0.971	1.045	1.082	1.056	0.845	1.256	1.276	1.364	1.386	1.244	1.335
	54	0.107	830.	1.735	23.7	299.	41.1	0.38	1.641	7.44	656.	81.18	0.341	0.101	0.982	1.063	1.101	1.038	0.816	1.210	1.270	1.341	1.340	1.244	1.102
	55	0.108	828.	1.760	28.3	299.	49.7	0.59	1.588	7.62	754.	79.35	0.277	0.100	0.986	1.066	1.100	1.046	0.802	1.201	1.223	1.277	1.267	1.208	1.058
	56	0.108	828.	1.781	27.9	299.	49.6	0.59	1.580	7.74	755.	80.66	0.277	0.095	0.995	1.069	1.095	1.041	0.800	1.213	1.232	1.268	1.277	1.249	1.052

Table A-11. Pattern Factor Test Data Correlation.

a) Correlation with Combustor Operating Conditions

$$PF = b + m\,(S_{PF} - 1)$$

where:

$$S_{PF} = \left(\frac{T_3}{828.9}\right)^{-1.1} \left(\frac{\Delta T}{943.3}\right)^{-0.3} \left(\frac{W_c\sqrt{T_3}/P_3}{458.3}\right)^{-0.5}$$

Fuel Number	Number of Data Points	m, Slope	b, Intercept	r, Correlation Coefficient	PF (Calculated from Operating Conditions Correlation at S_{PF} = 0.979, 1.000, 1.312 and 2.181)			
					Idle (0.979)	Cruise (1.000)	Takeoff (1.312)	Dash (2.181)
1	5	0.1733	0.2199	0.991	0.425	0.274	0.220	0.216
2	5	0.1711	0.3110	0.987	0.513	0.364	0.311	0.307
3	6	0.3065	0.2742	0.992	0.636	0.370	0.274	0.268
4	5	0.3819	0.2742	0.992	0.725	0.393	0.274	0.266
5	5	0.3565	0.2487	0.998	0.670	0.360	0.249	0.241
6	5	0.4697	0.2793	0.961	0.833	0.425	0.279	0.269
7	5	0.1888	0.2703	0.995	0.493	0.329	0.270	0.266
8	5	0.2169	0.2049	0.990	0.461	0.273	0.205	0.200
9	6	0.2282	0.2142	0.993	0.484	0.285	0.214	0.209
10	5	0.3874	0.1864	0.998	0.644	0.307	0.186	0.178
11	5	0.2485	0.2148	0.977	0.508	0.292	0.215	0.210
12	5	0.2219	0.2124	0.990	0.475	0.282	0.212	0.208
13	5	0.2967	0.2789	0.995	0.630	0.372	0.279	0.273

b) Correlation With Relative Fuel Spray Droplet Size

$$PF = b + m\left[\left(\frac{SMD}{SMD_{JP-4}}\right) - 1\right]$$

Engine Power Level	Idle	Cruise	Takeoff	Dash
b, Intercept	0.4881	0.2809	0.2067	0.2016
m, Slope	0.5617	0.3287	0.2444	0.2389
r, Correlation Coefficient	0.521	0.731	0.721	0.708

APPENDIX B

CARBON DEPOSITION DATA

Tests to determine relative levels of carbon deposition were conducted as described in Section V.2. After each carbon deposition test, the swirl cup was flow calibrated. Results of these flow calibrations are presented in Table B-1. Also after each test, carbon deposition was observed and photographically documented. These posttest photos of the swirl cup condition are presented in Figures B-1 through B-13.

As shown in Table B-1, none of the fuels produced enough carbon deposition to cause any significant blockage or reduction in swirler flow area. Figures B-1 through B-13 further show that nowhere in the dome was there any significant deposition in any of the tests. In two of the tests, however, some distress was detected which is evident in Figures B-4 and B-6. In these two photos, burnout on the flared dome extension insert occurred. The burned region extended from the insert trailing edge forward approximately 0.5 cm from about 2 to 4 o'clock, aft looking forward. The need for increased cooling around this flared extension has been identified previously, and increased cooling has been incorporated into newer F101 combustor dome designs.

Table B-1. Carbon Deposition Test Swirl Cup Airflow Calibration Results.

Airflow Calibration Date	Combustor Dome Assembly Condition	Test Fuel Number	A_e, Effective Area, cm^2					$\frac{A_e, \text{Postrun}}{A_e, \text{Clean}}$	
			Primary Swirler	Secondary Swirler	Both Swirlers	Splash Cooling	Total Assembly	Primary Swirler	Total Assembly
11/16/77	Clean	-	-	-	1.755	-	2.903	-	-
1/13/78	Postrun 1	1	0.633	0.965	-	1.271	2.797	0.953	0.970
1/25/78	Postrun 2	2	0.634	1.001	-	1.199	2.752	0.955	0.955
2/02/78	Postrun 3	3	0.646	1.029	-	1.223	2.783	0.973	0.965
2/10/78	Postrun 4	4	0.651	1.072	-	1.253	2.813	0.980	0.976
2/16/78	Postrun 5	5	0.706	1.041	-	1.289	2.829	1.063	0.981
3/03/78	Postrun 6	6	0.665	1.015	-	1.314	2.816	1.002	0.977
5/18/78	Clean	-	0.717	1.098	1.705	1.358	3.173	-	-
5/23/78	Postrun 7	9	0.628	1.050	1.657	1.249	2.825	0.946	0.980
5/26/78	Postrun 8	8	0.597	1.030	1.637	1.123	2.801	0.900	0.972
5/31/78	Postrun 9	7	0.643	1.032	1.475	1.287	2.692	0.968	0.934
5/31/78	Clean	-	0.639	1.027	1.461	1.290	2.623	-	-
6/14/78	Clean	-	0.636	1.045	1.653	1.243	2.828	-	-
6/19/78	Postrun 10	13	0.657	0.999	1.643	1.197	2.768	0.989	0.960
6/20/78	Postrun 11	12	0.643	1.011	1.661	1.237	2.819	0.968	0.978
6/23/78	Postrun 12	11	0.645	1.077	1.712	1.285	2.892	0.971	1.003
6/30/78	Postrun 13	10	0.664	1.053	1.694	1.226	2.865	1.000	0.994
Average, Clean			0.664	1.057	1.644	1.297	2.882	-	-
Average, Postrun			0.647	1.029	-	1.243	2.804	0.974	0.973

Figure B-1. Posttest Photograph of Swirl Cup After Carbon Deposition Test of Fuel 1.

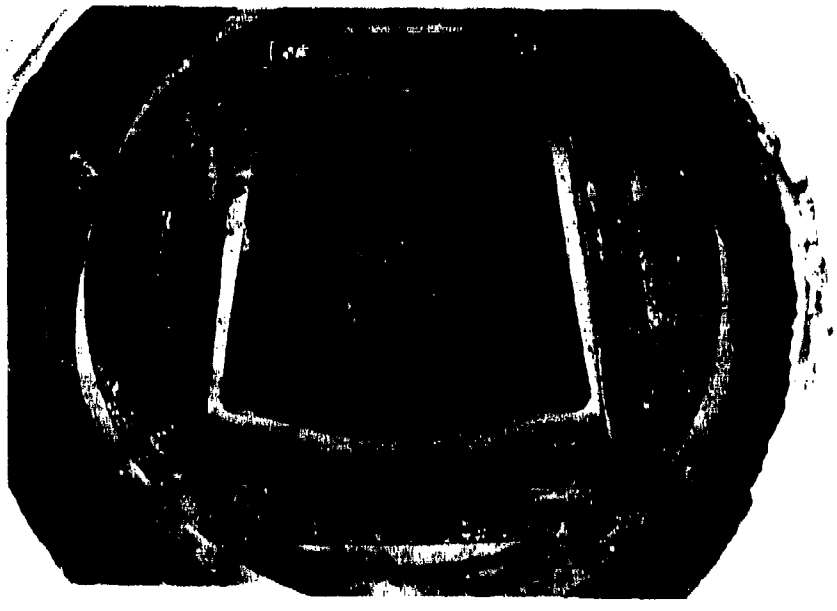

Figure B-2. Posttest Photograph of Swirl Cup After Carbon Deposition Test of Fuel 2.

Figure B-3. Posttest Photograph of Swirl Cup After Carbon Deposition Test of Fuel 3.

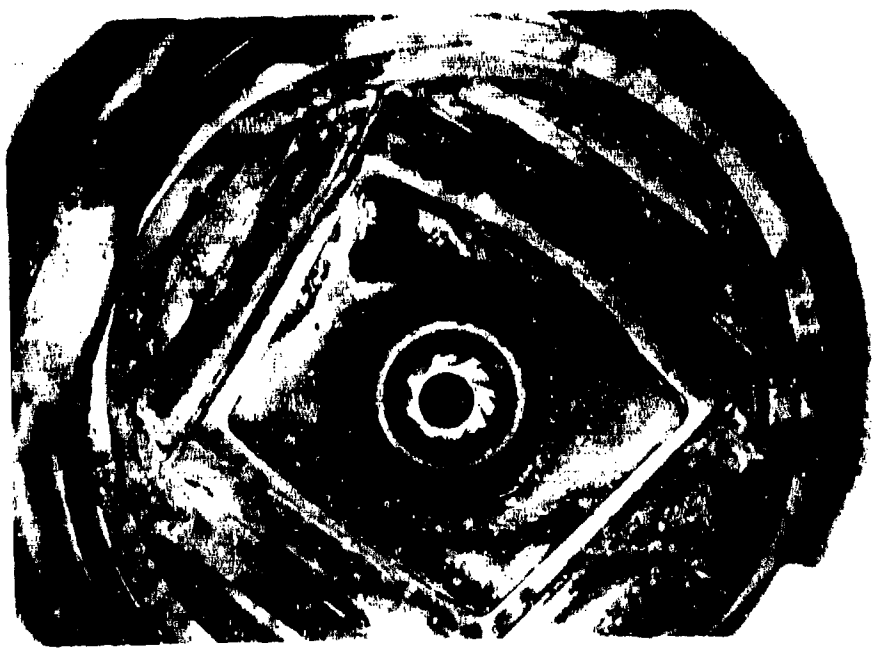

Figure B-4. Posttest Photograph of Swirl Cup After Carbon Deposition Test of Fuel 4.

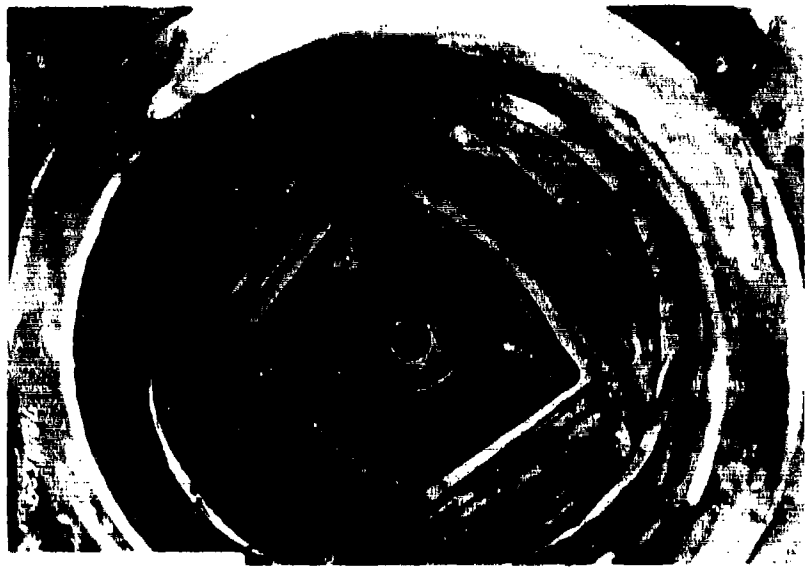

Figure B-5. Posttest Photograph of Swirl Cup After Carbon Deposition Test of Fuel 5.

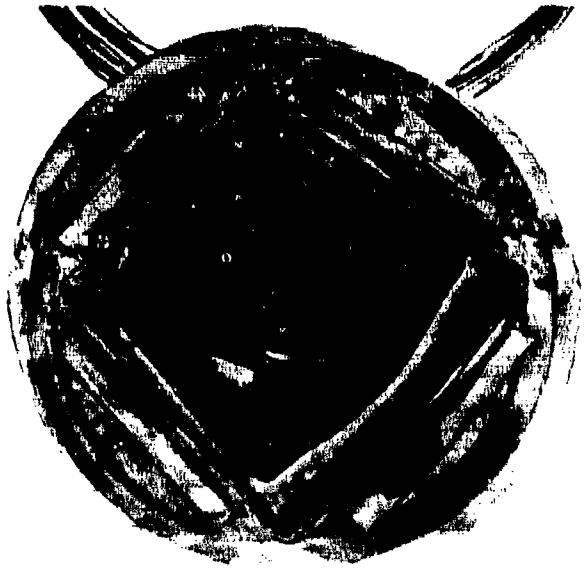

Figure B-6. Posttest Photograph of Swirl Cup After Carbon Deposition Test of Fuel 6.

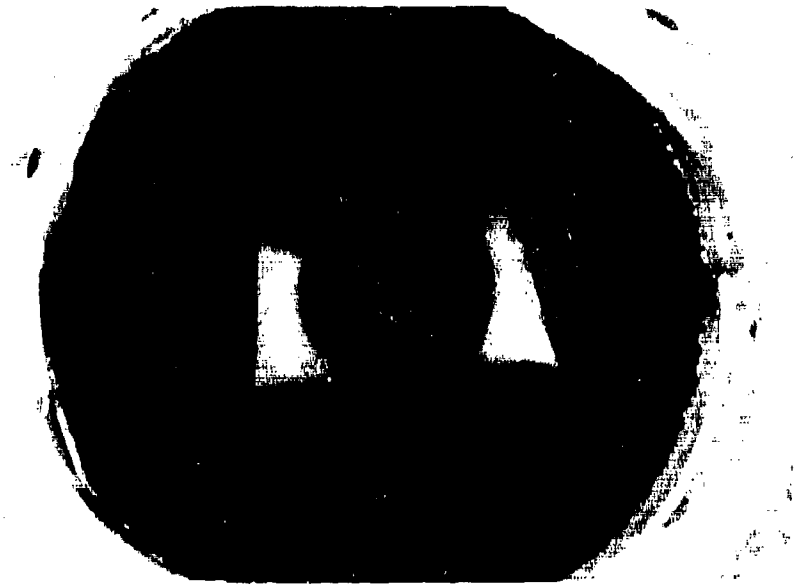

Figure B-7. Posttest Photograph of Swirl Cup After Carbon Deposition Test of Fuel 7.

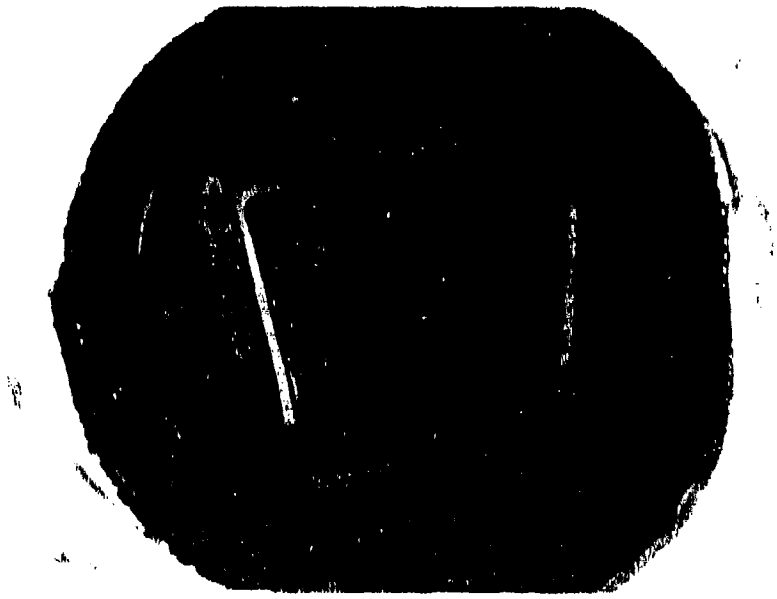

Figure B-8. Posttest Photograph of Swirl Cup After Carbon Deposition Test of Fuel 8.

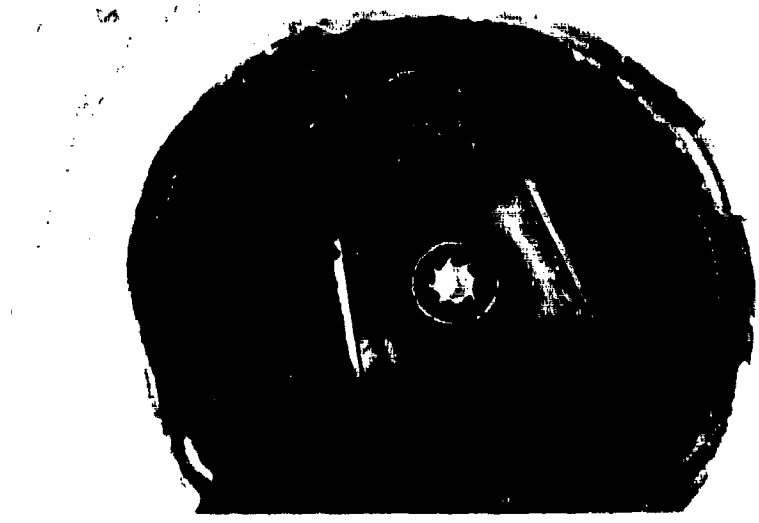

Figure B-9. Posttest Photograph of Swirl Cup After Carbon Deposition Test of Fuel 9.

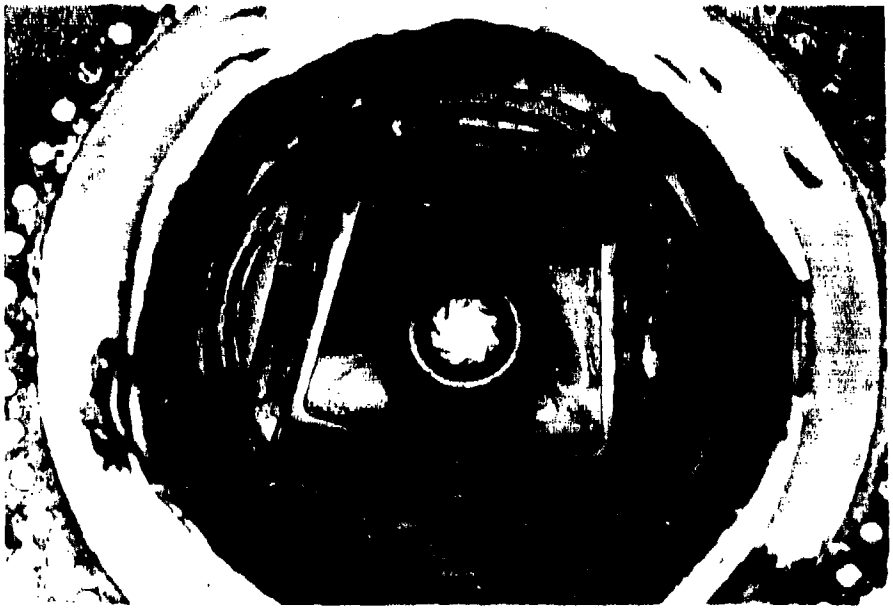

Figure B-10. Posttest Photograph of Swirl Cup After Carbon Deposition Test of Fuel 10.

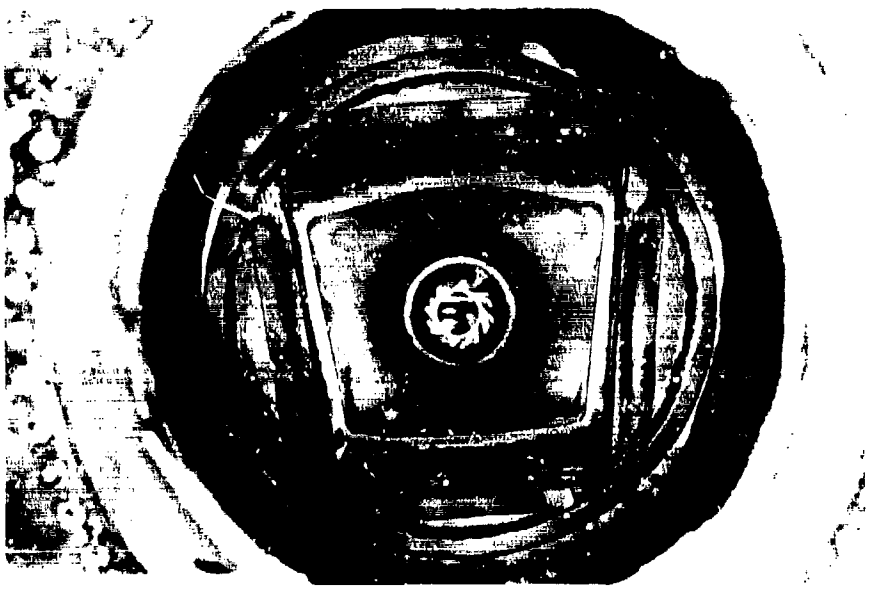

Figure B-11. Posttest Photograph of Swirl Cup After Carbon Deposition Test of Fuel 11.

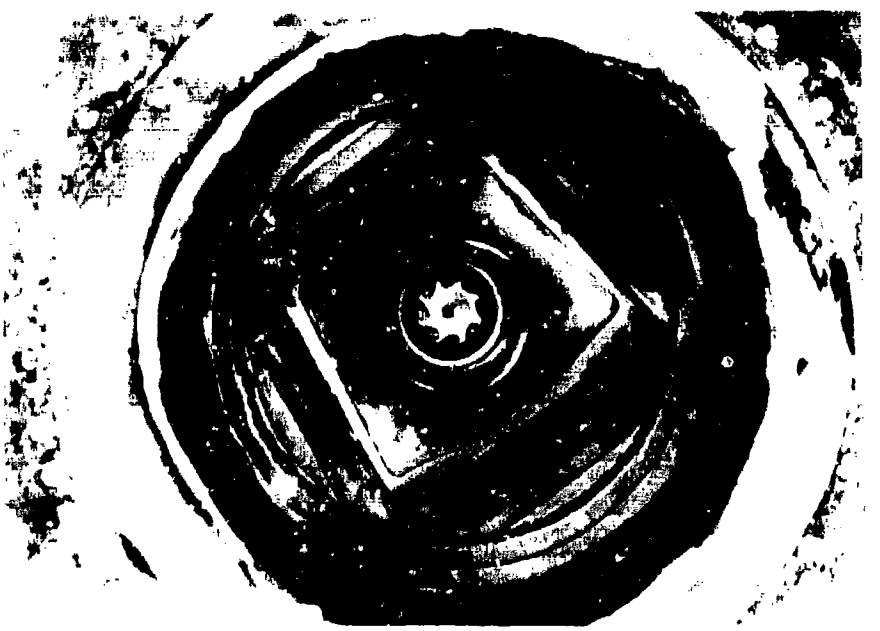

Figure B-12. Posttest Photograph of Swirl Cup After Carbon Deposition Test of Fuel 12.

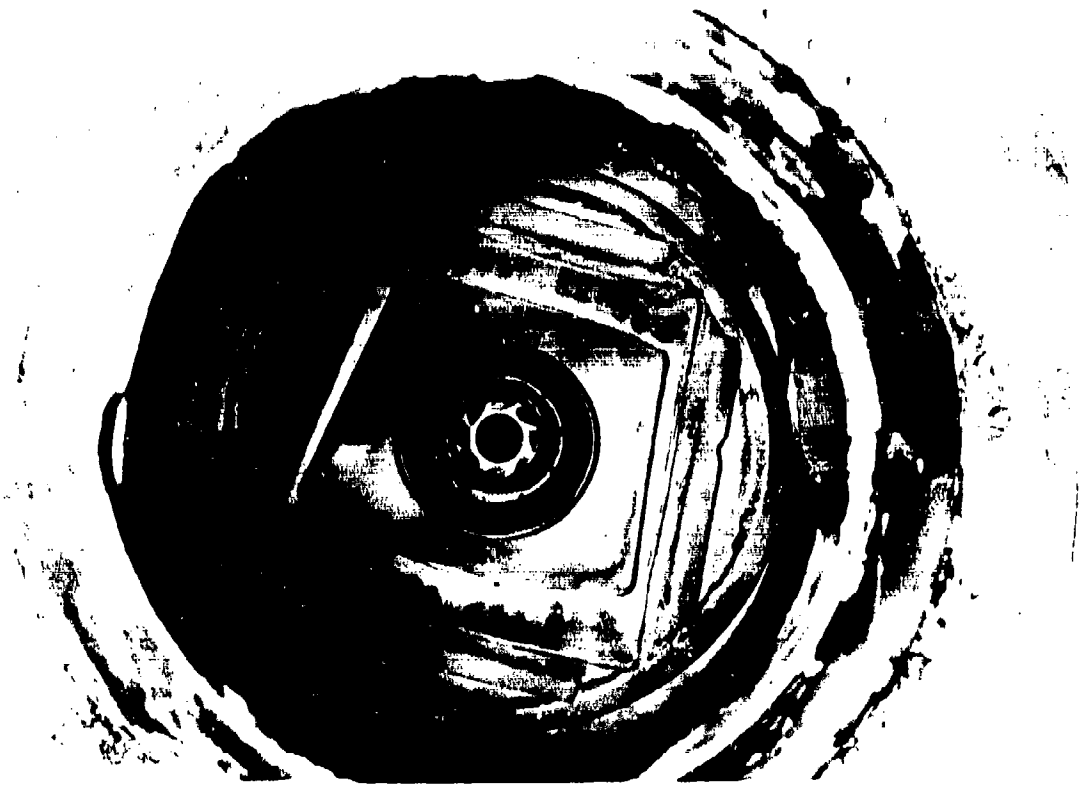

Figure B-13. Posttest Photograph of Swirl Cup After Carbon Deposition Test of Fuel 14.

APPENDIX C

LOW PRESSURE TEST DATA

Two types of tests were conducted in the low pressure combustor test rig: altitude relight tests and cold day start tests. Apparatus and procedures which were used are described in Section V.C.

Detailed results of the altitude relight tests are presented in Tables C-1 through C-7. Listed are the combustor operating conditions from which the simulated flight conditions were determined, and in the remarks column, the type of data point is indicated (LIGHT = maximum altitude relight capability at normal minimum fuel flow rate, PBO = pressure blowout, LLO = lean lightoff, LBO = lean blowout.

Detailed results of the cold day ground start tests are listed in Tables C-8 and C-9. At each combustor operating condition shown, lean lightoff and lean blowout fuel-air ratios were determined which are listed.

Table C-1. Altitude Relight Test Results, Fuel Number 1.

Fuel No.	Simulated Flight Condition (Open Nozzle)		Combustor Operating Conditions						Lightoff Attempt		Remarks			
	Alt km	M_P	T_F K	T_3 K	P_3 kPa	W_c (engine) kg/s	$\frac{\Delta P}{P}$ %	$\frac{PT}{V}$ MPa-K m/s	W_f (engine) g/s	f g/kg	Light	FBO	LLO	LBO
Base Test														
1	13.0	1.05	250.9	259.9	24.1	0.91	11.07	0.43	37.8	41.7	No			
1	9.6	.76	250.7	259.6	33.8	0.91	–	0.86	37.8	41.7	Yes			
1	9.7	.77	250.7	259.4	33.1	0.91	–	0.82	37.8	41.7		X		
1	9.6	.76	250.9	259.9	33.8	0.91	–	0.86	34.4	38.0			X	
1	9.6	.76	252.4	259.7	33.8	0.91	–	0.86	23.1	25.5				X
1	–	–	268.7	268.2	24.4	1.36	25.95	0.57	37.8	27.8	No			
1	8.5	.86	265.4	267.0	43.4	1.36	6.75	0.94	37.8	27.8	Yes			
1	9.1	.90	266.2	267.0	41.6	1.36	–	0.87	37.8	27.8		X		
1	8.5	.86	269.5	266.6	43.4	1.36	–	0.94	21.4	15.8			X	
1	8.5	.86	269.2	266.6	43.4	1.36	–	0.94	17.4	12.8				X
1	10.8	1.32	289.3	297.4	59.3	2.27	10.96	1.06	37.8	16.7	No			
1	7.2	1.11	271.4	297.7	62.7	2.27	10.04	1.18	37.8	16.7	Yes			
1	–	–	287.8	297.9	55.8	2.27	–	0.93	37.8	16.7		X		
1	7.2	1.11	288.2	297.7	62.7	2.27	–	1.18	49.9	19.8			X	
1	7.2	1.11	288.4	297.7	62.7	2.27	–	1.18	19.7	8.7				X
1	–	–	289.8	297.7	82.9	3.18	10.82	1.47	37.8	11.9	Yes			
1	–	–	290.4	297.6	75.1	3.18	–	1.21	37.8	11.9		X		
1	–	–	291.2	297.1	82.9	3.18	–	1.47	34.4	10.8			X	
1	–	–	291.2	297.1	82.9	3.18	–	1.47	26.0	8.2				X
Repeat Test														
1	13.0	1.05	252.1	251.7	24.2	0.91	9.69	0.44	37.8	41.7	No			
1	9.7	.77	249.9	251.7	33.1	0.91	5.00	0.82	37.8	41.7	Yes			
1	10.0	.80	251.6	249.7	31.9	0.91	–	0.76	37.8	41.7		X		
1	9.7	.77	251.3	252.7	33.1	0.91	–	0.82	33.0	36.4			X	
1	9.7	.77	251.5	258.5	33.1	0.91	–	0.82	23.8	26.2				X
1	13.2	1.18	265.4	267.0	34.4	1.36	11.16	0.59	37.8	27.8	No			
1	8.5	.66	270.9	268.4	43.3	1.36	6.93	0.94	37.8	27.8	Yes			
1	9.1	.90	268.1	267.6	41.6	1.36	–	0.87	37.8	27.8		X		
1	8.5	.86	267.8	268.3	43.3	1.36	–	0.94	22.3	16.4			X	
1	8.5	.86	267.3	267.9	43.3	1.36	–	0.94	20.2	14.8				X
1	10.8	1.32	298.2	301.5	59.3	2.27	11.72	1.06	37.8	16.7	No			
1	7.1	1.10	295.9	299.1	63.0	2.27	10.24	1.19	37.8	16.7	Yes			
1	8.8	1.19	295.9	298.8	60.7	2.27	–	1.11	37.8	16.7		X		
1	7.1	1.10	297.5	296.7	63.0	2.27	–	1.19	20.2	8.9			X	
1	7.1	1.10	297.1	297.1	63.0	2.27	–	1.19	17.9	7.9				X
1	–	–	297.5	294.9	82.2	3.18	11.69	1.45	37.8	11.9	Yes			
1	–	–	296.5	294.4	76.5	3.18	–	1.25	37.8	11.9		X		
1	–	–	297.3	293.5	82.2	3.18	–	1.45	32.2	10.1			X	
1	–	–	297.1	293.7	82.2	3.18	–	1.45	26.5	8.3				X

Table C-2. Altitude Relight Test Results, Fuels 2 and 3.

Fuel No.	Simulated Flight Condition (Open Nozzle)		Combustor Operating Conditions						Lightoff Attempt		Remarks			
	Alt km	M_P	T_F K	T_3 K	P_3 kPa	W_c (engine) kg/s	$\frac{\Delta P}{P}$ %	$\frac{PT}{V}$ MPa-K/m/s	W_f (engine) g/s	f g/kg	Light	PBO	LLO	LBO
2	0.2	0.31	254.1	252.6	97.5	0.91	0.55	7.14	50.4	55.6	No			
2	13.2	1.18	270.9	268.7	34.4	1.36	11.99	0.59	37.8	27.8	No			
2	7.8	0.80	268.2	268.2	46.5	1.36	6.09	1.08	37.8	27.8	Yes			
2	8.6	0.87	267.6	269.3	43.1	1.36	–	0.93	37.8	27.8		X		
2	7.8	0.80	267.6	269.7	46.5	1.36	–	1.08	26.0	19.1			X	
2	7.8	0.80	267.1	269.1	46.5	1.36	–	1.08	20.1	14.8				X
2	11.0	1.33	293.2	296.8	59.2	2.27	11.26	1.05	37.8	16.7	No			
2	6.4	1.04	293.9	296.4	65.6	2.27	9.19	1.29	37.8	16.7	Yes			
2	–	–	291.9	296.6	57.6	2.27	–	1.00	37.8	16.7		X		
2	6.4	1.04	295.4	296.4	65.6	2.27	–	1.29	20.2	8.9			X	
2	6.4	1.04	294.8	296.4	65.6	2.27	–	1.29	15.3	6.7				X
2	–	–	293.7	297.6	82.8	3.18	11.40	1.47	37.8	11.9	No			
2	9.0	1.41	293.7	297.6	84.1	3.18	11.00	1.52	37.8	11.9	Yes			
2	–	–	292.6	297.4	75.8	3.18	–	1.23	37.8	11.9		X		
2	9.0	1.41	293.2	297.1	84.1	3.18	–	1.52	28.6	9.0			X	
2	9.0	1.41	292.8	297.1	84.1	3.18	–	1.52	21.8	6.9				X
3	0.1	0.31	251.1	251.2	97.9	0.91	0.32	7.17	37.8	41.7	No			
3	11.9	1.14	268.7	269.2	35.4	1.36	11.34	0.63	37.8	27.8	No			
3	5.2	0.65	268.4	270.7	60.9	1.36	6.54	1.86	37.8	27.8	Yes			
3	8.8	0.88	268.9	266.9	42.4	1.36	–	0.90	37.8	27.8		X		
3	5.2	0.66	268.6	268.8	60.9	1.36	–	1.86	32.8	24.1			X	
3	5.2	0.66	268.9	268.3	60.9	1.36	–	1.86	23.5	17.3				X
3	9.6	1.25	298.4	298.5	60.0	2.27	11.16	1.08	37.8	16.7	No			
3	6.1	1.02	298.4	298.7	66.4	2.27	8.97	1.32	37.8	16.7	Yes			
3	–	–	295.4	298.7	58.5	2.27	–	1.03	37.8	16.7		X		
3	6.1	1.02	296.2	298.7	66.4	2.27	–	1.32	24.4	10.7			X	
3	6.1	1.02	295.8	298.7	66.4	2.27	–	1.32	19.3	8.5				X
3	–	–	298.4	299.6	83.4	3.18	11.01	1.49	37.8	11.9	Yes			
3	–	–	298.2	299.8	75.6	3.18	–	1.22	37.8	11.9		X		
3	–	–	295.6	299.4	83.4	3.18	–	1.49	36.0	11.3			X	
3	–	–	296.2	299.5	83.4	3.18	–	1.49	25.2	7.9				X

Table C-3. Altitude Relight Test Results, Fuels 4 and 5.

Fuel No.	Simulated Flight Condition (Open Nozzle)		Combustor Operating Conditions						Lightoff Attempt		Remarks			
	Alt km	M_P	T_F K	T_3 K	P_3 kPa	W_c (engine) kg/s	$\frac{\Delta P}{P}$ %	$\frac{PT}{V}$ MPa-K/s	W_f (engine) g/s	f g/kg	Light	PBO	LLO	LBO
4	13.0	1.05	254.3	251.2	24.2	0.91	10.50	0.44	54.2	59.7	No			
4	0.2	0.33	251.1	251.2	97.2	0.91	0.65	7.10	37.8	41.7	No			
4	12.8	1.17	268.4	267.6	34.6	1.36	11.08	0.60	37.8	59.7	No			
4	7.5	0.78	268.6	267.6	47.9	1.36	5.42	1.15	37.8	59.7	Yes			
4	8.1	0.83	268.9	268.0	44.8	1.36	–	1.01	37.8	59.7		X		
4	7.5	0.78	269.5	267.8	47.9	1.36	–	1.15	32.0	23.5			X	
4	7.5	0.78	268.6	267.7	47.9	1.36	–	1.15	23.5	17.3				X
4	10.6	1.32	282.8	294.6	59.4	2.27	11.03	1.06	37.8	16.7	No			
4	5.9	1.00	283.4	294.8	67.4	2.27	8.34	1.36	37.8	16.7	Yes			
4	9.1	1.21	284.6	294.8	60.4	2.27	–	1.09	37.8	16.7		X		
4	5.9	1.00	284.8	294.8	67.4	2.27	–	1.36	24.3	10.7			X	
4	5.9	1.00	283.4	294.8	67.4	2.27	–	1.36	19.1	8.4				X
4	–	–	286.5	295.4	82.6	3.18	11.02	1.46	37.8	11.9	No			
4	6.6	1.25	287.1	295.4	86.0	3.18	10.19	1.58	37.8	11.9	Yes			
4	–	–	289.8	295.1	77.7	3.18	–	1.29	37.8	11.9		X		
4	6.6	1.25	289.2	295.1	86.0	3.18	–	1.58	31.8	10.0			X	
4	6.6	1.25	287.1	295.1	86.0	3.18	–	1.58	23.4	7.3				X
5	13.0	1.05	252.1	252.4	24.2	0.91	10.06	0.44	59.6	65.8	No			
5	13.0	1.18	268.9	268.2	34.5	1.36	12.35	0.60	37.8	27.8	No			
5	7.6	0.79	268.2	268.4	47.6	1.36	6.14	1.14	37.8	27.8	Yes			
5	8.3	0.84	268.4	267.7	44.2	1.36	–	0.98	37.8	27.8		X		
5	7.6	0.79	270.4	267.0	47.6	1.36	–	1.14	25.2	18.5			X	
5	7.6	0.79	268.2	268.4	47.6	1.36	–	1.14	21.3	15.6				X
5	10.8	1.32	287.8	298.7	59.3	2.27	10.98	1.06	37.8	16.7	No			
5	6.5	1.05	288.7	298.1	64.9	2.27	9.03	1.26	37.8	16.7	Yes			
5	–	–	290.8	299.5	58.7	2.27	–	0.50	37.8	16.7		X		
5	6.5	1.05	291.5	299.4	64.9	2.27	–	1.26	23.9	10.5			X	
5	6.5	1.05	288.7	298.1	64.9	2.27	–	1.26	19.5	8.6				X
5	–	–	289.8	300.2	83.0	3.18	10.94	1.48	37.8	11.9	No			
5	–	–	289.8	300.5	83.3	3.18	10.76	1.49	37.8	11.9	Yes			
5	–	–	288.4	300.5	76.8	3.18	–	1.26	37.8	11.9		X		
5	–	–	289.3	300.5	83.3	3.18	–	1.49	31.9	10.0			X	
5	–	–	289.8	300.5	83.3	3.18	–	1.49	24.8	7.8				X

Table C-4. Altitude Relight Test Results, Fuels 6 and 7.

Fuel No.	Simulated Flight Condition (Open Nozzle)		Combustor Operating Conditions						Lightoff Attempt		Remarks			
	Alt km	Mp –	T_F K	T_3 K	P_3 kPa	W_c (engine) kg/s	$\frac{\Delta P}{P}$ %	$\frac{PT}{V}$ $\frac{MPa-K}{m/s}$	W_f (engine) g/s	f g/kg	Light	PBO	LLO	LBO
6	12.9	1.01	253.7	251.5	24.5	0.91	10.36	0.452	65.9	72.7	No			
6	0.3	0.32	251.5	233.7	96.5	0.91	0.62	7.017	37.8	41.5	No			
6	12.2	1.15	265.9	266.8	34.9	1.36	11.56	0.612	37.8	27.8	No			
6	7.5	0.78	268.2	268.2	48.1	1.36	5.69	1.163	37.8	27.8	Yes			
6	8.2	0.82	268.2	268.9	45.0	1.36	–	1.108	37.8	27.8		X		
6	7.5	0.78	268.2	268.9	48.1	1.36	–	1.163	33.6	24.7			X	
6	7.5	0.78	269.3	268.4	48.1	1.36	–	1.163	22.0	16.2				X
6	10.0	1.30	283.7	289.7	59.8	2.27	11.04	1.076	37.8	16.7	No			
6	5.2	0.95	284.3	289.7	70.5	2.27	7.77	1.496	37.8	16.7	Yes			
6	7.6	1.13	285.9	289.7	61.9	2.27	–	1.155	37.8	16.7		X		
6	5.2	0.95	285.9	289.7	70.5	2.27	–	1.496	22.2	9.8			X	
6	5.2	0.95	285.9	289.7	70.5	2.27	–	1.496	19.6	8.6				X
6	–	–	285.4	288.8	82.7	3.18	10.86	1.470	37.8	11.7	No			
6	5.9	1.18	285.4	288.8	87.4	3.18	9.80	1.642	37.8	11.7	Yes			
6	–	–	285.4	288.8	90.6	3.18	–	1.398	37.8	11.7		X		
6	5.9	1.18	285.4	288.8	87.4	3.18	–	1.642	29.0	9.1			X	
6	5.9	1.18	285.4	288.8	87.4	3.18	–	1.642	25.2	7.9				X
7	13.0	1.05	255.4	252.1	24.1	0.91	9.57	0.438	55.3	61.0	No			
7	0.2	.31	252.1	257.3	97.1	0.91	0.54	7.104	37.8	41.5	No			
7	13.0	1.18	272.0	267.7	34.5	1.36	10.54	0.598	55.3	40.7	No			
7	0.8	.46	270.9	266.2	98.2	1.36	1.15	4.846	37.8	27.8	No			
7	10.6	1.32	301.7	312.5	59.4	2.27	10.94	1.062	55.3	24.4	No			
7	5.9	1.09	301.7	312.5	63.6	2.27	10.94	1.218	37.8	16.7	No			
7	5.9	1.09	301.7	312.5	63.5	2.27	9.51	1.214	37.8	16.7	Yes			
7	–	–	301.7	312.5	58.4	2.27	–	1.027	37.8	16.7		X		
7	7.0	1.09	304.2	312.5	63.5	2.27	–	1.214	40.3	17.8			High	
7	7.0	1.09	304.5	312.5	63.5	2.27	–	1.214	29.1	12.8				X
7	–	–	304.3	310.7	82.9	3.18	10.69	1.477	50.4	15.9	High			
7	–	–	305.4	310.7	77.3	3.18	–	1.284	37.8	11.7		X		
7	–	–	305.4	310.7	83.4	3.18	–	1.495	38.2	12.0			X	
7	–	–	305.4	310.7	83.4	3.18	–	1.495	32.3	10.2				X

Table C-5. Altitude Relight Test Results, Fuels 8 and 9.

Fuel No.	Simulated Flight Condition (Open Nozzle)		Combustor Operating Conditions						Lightoff Attempt		Remarks			
	Alt. km	Mp –	T_F K	T_3 K	P_3 kPa	W_c (engine) kg/s	$\frac{\Delta P}{P}$ %	$\frac{PT}{V}$ MPa-K / m/s	W_f (engine) g/s	f g/kg	Light	PBO	LLO	LBO
8	14.0	1.14	255.5	249.8	23.7	0.91	10.91	0.42	50.4	55.6	No			
8	0.3	0.32	249.8	250.0	96.7	0.91	0.57	7.02	50.4	55.6	No			
8	13.0	1.18	268.4	268.4	34.5	1.36	10.98	0.60	50.4	37.1	No			
8	7.5	0.78	269.8	267.2	47.8	1.36	5.39	1.14	37.8	27.8	Yes			
8	8.5	0.85	267.6	267.7	43.6	1.36	–	0.955	37.8	27.8		X		
8	7.5	0.78	268.2	267.4	47.7	1.36	–	1.14	39.1	28.7			High	
8	7.5	0.78	268.6	267.2	47.7	1.36	–	1.14	29.7	21.9				X
8	10.5	1.31	294.5	298.4	59.5	2.27	10.56	1.07	50.4	22.2	No			
8	5.9	1.00	295.0	301.2	67.7	2.27	8.04	1.37	37.8	16.7	Yes			
8	8.9	1.20	295.4	303.4	60.6	2.27	–	1.10	37.8	16.7		X		
8	5.8	1.00	295.0	301.7	67.7	2.27	–	1.37	41.8	18.5			High	
8	5.8	1.00	295.4	302.4	67.7	2.27	–	1.37	28.6	12.6				X
8	–	–	289.3	308.9	82.7	3.17	10.03	1.47	50.4	15.9	High			
8	–	–	291.2	309.0	71.8	3.17	–	1.11	28.1	8.9		X		
8	–	–	291.5	309.2	82.7	3.17	–	1.47	41.0	12.9			High	
8	–	–	290.4	309.2	82.7	3.17	–	1.47	16.8	5.3				X
9	15.2	1.18	251.8	249.9	23.2	0.91	12.03	0.40	50.4	55.6	No			
9	0.3	0.32	251.8	249.9	95.1	0.91	0.58	6.79	50.4	55.6	No			
9	–	–	267.3	268.1	33.8	1.36	12.3	0.57	50.4	37.1	No			
9	7.8	0.80	268.9	266.7	46.4	1.36	6.0	1.08	37.8	27.8	Yes			
9	8.4	0.81	268.0	268.2	43.9	1.36	–	0.97	37.8	27.8		X		
9	7.8	0.80	268.0	268.2	46.4	1.36	–	1.08	42.0	30.9			High	
9	7.8	0.80	267.8	267.5	46.4	1.36	–	1.08	32.8	24.1				X
9	–	–	290.8	307.3	58.6	2.27	10.74	1.03	50.4	22.2	No			
9	6.7	1.02	290.9	308.7	64.4	2.27	8.80	1.25	37.8	16.6	Yes			
9	–	–	291.9	310.0	57.3	2.27	–	0.99	37.8	16.6		X		
9	6.7	1.02	291.7	308.9	64.4	2.27	–	1.25	40.3	17.8			High	
9	6.7	1.02	291.2	309.5	64.4	2.27	–	1.25	24.7	10.9				X
9	–	–	292.0	314.8	83.0	3.18	10.02	1.48	50.4	15.9	High			
9	5.8	1.18	292.3	315.6	87.7	3.18	8.93	1.65	37.8	11.9	Yes			
9	–	–	292.8	315.9	80.0	3.18	–	1.37	37.8	11.9		X		
9	5.8	1.18	292.5	315.6	87.7	3.18	–	1.65	38.6	12.2			High	
9	5.8	1.18	292.3	315.6	87.7	3.18	–	1.65	32.8	10.3				X

Table C-6. Altitude Relight Test Results, Fuels 10 and 11.

Fuel No.	Simulated Flight Condition (Open Nozzle)		Combustor Operating Conditions						Lightoff Attempt		Remarks			
	Alt, km	Mp -	T_F K	T_3 K	P_3 kPa	W_c (engine) kg/s	$\frac{\Delta P}{P}$ %	$\frac{PT}{V}$ $\frac{MPa-K}{m/s}$	W_f (engine) g/s	f g/kg	Light	PBO	LLO	LBO
10	13.0	1.05	250.9	252.9	24.2	0.91	10.64	0.44	50.4	55.6	No			
10	0.5	0.32	250.9	249.6	94.0	0.91	0.57	6.44	50.4	55.6	No			
10	12.8	1.17	268.2	267.4	34.6	1.36	11.43	0.60	50.4	37.1	No			
10	7.5	0.78	269.5	269.2	48.2	1.36	5.56	1.17	37.8	27.8	Yes			
10	8.5	0.85	267.1	269.4	43.6	1.36	–	0.96	37.8	27.8		X		
10	7.5	0.78	267.3	270.4	48.2	1.36	–	1.17	38.3	28.2			High	
10	7.5	0.78	267.5	269.5	48.2	1.36	–	1.17	31.0	22.8				X
10	10.5	1.31	301.2	317.3	59.5	2.27	10.50	1.07	50.4	22.2	No			
10	5.9	1.00	302.6	318.1	67.4	2.27	8.12	1.37	37.8	16.7	Yes			
10	11.3	1.33	304.5	318.9	59.8	2.27	–	1.05	37.8	16.7		X		
10	5.9	1.00	304.5	318.9	67.4	2.27	–	1.37	39.0	17.2			High	
10	5.9	1.00	304.5	318.2	67.4	2.27	–	1.37	28.5	12.6				X
10	–	–	300.1	320.8	82.9	3.18	10.10	1.48	50.4	15.8	High			
10	5.4	0.34	302.1	321.2	88.4	3.18	8.79	1.68	37.8	11.9	Yes			
10	–	–	303.1	322.1	78.3	3.18	–	1.32	37.8	11.9		X		
10	5.4	0.34	302.6	321.5	88.4	3.18	–	1.68	40.3	12.7			High	
10	5.4	0.34	302.3	321.4	88.4	3.18	–	1.58	33.1	10.4				X
11	12.8	1.01	251.5	252.6	24.7	0.91	9.67	0.46	50.4	55.6	No			
11	0.5	0.32	252.2	248.4	94.3	0.91	0.57	6.68	50.4	55.6	Yes			
11	0.5	0.32	251.3	251.0	94.3	0.91	–	6.68	40.3	44.3				High
11	12.8	1.17	266.7	267.4	34.6	1.36	12.70	0.60	50.4	37.1	No			
11	7.3	0.77	269.8	266.6	48.9	1.36	5.52	1.20	37.8	27.8	Yes			
11	7.7	0.80	269.5	268.9	46.7	1.36	–	1.10	37.8	27.8		X		
11	7.3	0.77	268.9	266.7	48.9	1.36	–	1.20	34.9	25.7				X
11	10.6	1.32	303.2	308.9	59.4	2.27	10.11	1.06	50.4	22.2	No			
11	6.3	1.03	304.8	309.6	65.9	2.27	8.13	1.31	37.8	16.7	Yes			
11	–	–	305.9	309.8	58.9	2.27	–	1.04	37.8	16.7		X		
11	6.3	1.03	305.1	309.8	65.9	2.27	–	1.31	35.2	15.5				X
11	–	–	301.4	312.3	82.7	3.18	8.57	1.47	50.4	15.8	High			
11	7.0	1.26	303.4	312.6	85.7	3.18	8.96	1.58	37.8	11.9	Yes			
11	–	–	305.4	312.6	81.3	3.18	–	1.42	37.8	11.9		X		
11	7.0	1.25	303.9	312.6	85.7	3.18	–	1.58	35.9	11.3				X

Table C-7. Altitude Relight Test Results, Fuels 12 and 13.

Fuel No.	Simulated Flight Condition (Open Nozzle)		Combustor Operating Conditions						Lightoff Attempt		Remarks			
	Alt km	Mp –	T_F K	T_3 K	P_3 kPa	W_c (engine) kg/s	$\frac{\Delta P}{P}$ %	$\frac{PT}{V}$ $\frac{MPa-K}{m/s}$	W_f (engine) g/s	f g/kg	Light	FBO	LLO	LBO
12	13.1	1.06	252.1	252.5	24.0	0.91	11.90	0.43	50.4	55.4	No			
12	9.0	0.74	251.8	252.5	35.1	0.91	5.02	0.93	37.8	41.5	Yes			
12	9.1	0.75	251.3	252.5	34.2	0.91	–	0.88	37.8	41.5		X		
12	9.0	0.74	252.5	252.5	35.1	0.91	–	0.93	31.5	34.6				X
12	12.8	1.17	267.6	268.3	34.6	1.36	11.94	0.60	50.4	37.1	No			
12	8.1	0.82	268.4	267.4	45.1	1.36	6.58	1.02	37.8	27.8	Yes			
12	8.6	0.87	268.4	268.0	43.0	1.36	–	0.93	37.8	27.8		X		
12	8.1	0.82	268.2	267.4	45.1	1.36	–	1.02	31.9	23.5				X
12	10.6	1.32	298.2	318.5	59.4	2.27	10.78	1.06	37.8	16.7	Yes			
12	–	–	300.6	318.4	56.6	2.27	–	0.96	37.8	16.7		X		
12	10.0	1.30	300.9	318.4	59.8	2.27	–	1.08	31.9	14.1				X
12	–	–	301.2	316.5	82.8	3.18	9.53	1.47	37.8	11.9	Yes			
12	–	–	302.1	316.5	73.8	3.18	–	1.17	37.8	11.9		X		
12	–	–	302.1	316.2	78.8	3.18	–	1.17	37.4	11.8			X	
12	–	–	302.3	316.2	78.8	3.18	–	1.17	34.9	11.0				X
13	12.9	1.01	252.6	251.1	24.5	0.91	10.54	0.45	50.4	55.4	No			
13	0.5	0.32	251.5	249.4	94.4	0.91	0.59	6.69	50.4	55.4	No			
13	12.7	1.16	269.3	268.9	34.7	1.36	12.76	0.61	50.4	37.1	No			
13	1.0	0.47	269.3	266.6	55.0	1.36	1.26	4.54	50.4	37.1	No			
13	10.6	1.32	302.6	326.2	59.4	2.27	10.78	1.06	50.4	22.2	No			
13	9.1	1.21	303.9	326.7	60.3	2.27	10.45	1.09	37.8	16.7	Yes			
13	–	–	304.8	327.5	55.7	2.27	–	0.93	37.8	16.7		X		
13	9.1	1.21	304.3	327.2	60.3	2.27	–	1.09	37.7	16.6			X	
13	9.1	1.21	305.1	327.1	60.3	2.27	–	1.09	25.2	11.1				X
13	–	–	300.1	328.6	82.8	3.18	9.60	1.47	37.8	11.9	Yes			
13	–	–	299.5	329.5	69.7	3.18	–	1.04	37.8	11.9		X		
13	–	–	305.9	330.1	76.7	3.18	–	1.26	36.5	11.5			X	
13	–	–	300.6	328.7	82.8	3.18	–	1.47	28.1	8.9				X

Table C-8. Ground Start Test Results, Fuels 1-8.

Fuel No.	Combustor Operating Conditions					Lean Blowout		Lean Lightoff	
	T_F	T_3	P_3	W_c (engine)	$\frac{\Delta P}{P}$	W_f (engine)	f	W_f (engine)	f
	K	K	kpa	kg/s	%	g/s	g/kg	g/s	g/kg
1	265.4	267.4	101.3	1.149	0.87	27.1	23.6	89.9	34.7
	260.8	261.3	101.3	1.149	0.82	29.4	25.6	40.3	35.1
	250.2	250.1	101.3	1.149	0.79	33.6	29.2	49.0	42.6
	243.7	244.5	101.3	1.149	0.76	-	-	>50.4	>43.9
1R	260.9	260.4	101.7	1.149	0.87	27.3	23.8	41.6	36.2
	254.6	253.9	101.7	1.149	0.86	29.4	25.6	43.7	38.0
	250.7	250.2	101.7	1.149	0.85	31.1	27.0	48.1	41.9
	244.3	244.3	101.6	1.149	0.80	33.5	29.2	50.4	43.9
	240.4	239.3	101.6	1.149	0.82	34.4	30.0	50.4	43.9
1RR	264.7	267.3	100.9	1.149	0.77	32.7	28.4	39.0	33.8
	259.2	260.4	100.9	1.149	0.66	32.3	28.1	45.2	39.3
	262.5	250.6	100.9	1.149	0.66	36.0	31.4	49.6	43.1
2	304.7	310.4	101.1	1.149	0.98	18.3	15.9	22.3	19.4
	275.9	278.2	101.0	1.149	0.90	27.2	23.7	46.9	40.8
	265.8	265.9	101.0	1.149	0.93	-	-	>50.4	>43.9
3	296.7	301.3	101.8	1.149	0.94	23.1	20.1	39.1	34.0
	278.9	278.7	101.0	1.149	0.90	-	-	>50.4	>43.9
4	296.5	305.1	101.5	1.149	0.98	22.9	20.0	38.6	33.6
	277.6	276.9	101.5	1.149	0.90	30.8	26.8	51.7	45.0
	272.3	272.2	101.5	1.149	0.89	-	-	>50.4	>43.9
5	296.7	298.0	100.8	1.149	0.94	22.7	19.7	33.6	29.2
	277.3	277.4	100.8	1.149	0.91	27.7	24.1	50.4	43.9
	273.2	272.6	100.8	1.149	0.88	30.7	26.7	51.2	44.6
	266.5	267.4	100.7	1.149	0.82	-	-	>50.4	>43.9
6	298.1	296.2	100.0	1.149	1.00	22.3	19.4	37.6	32.7
	276.5	277.6	100.0	1.149	0.93	29.0	25.2	50.4	43.9
	270.4	272.6	100.0	1.149	0.88	31.1	27.0	49.6	43.1
	265.1	265.9	99.9	1.149	0.83	-	-	>50.4	>43.9
7	307.1	327.9	101.1	1.149	0.99	27.0	23.5	39.3	34.2
	279.5	276.4	100.9	1.149	0.84	-	-	>50.4	>43.9
8	308.4	305.2	101.0	1.149	0.89	26.8	23.3	38.6	33.6
	275.4	277.7	101.0	1.149	0.83	31.9	27.8	47.7	41.5
	272.6	272.4	100.9	1.149	0.81	32.8	28.5	50.4	43.9
	266.2	266.1	100.9	1.149	0.79	34.9	30.3	52.3	45.5
	262.5	260.8	100.9	1.149	0.77	-	-	>51.5	>44.8

Table C-9. Ground Start Test Results, Fuels 9-13.

Fuel No.	Combustor Operating Conditions					Lean Blowout		Lean Lightoff	
	T_F	T_3	P_3	W_c (engine)	$\frac{\Delta P}{P}$	W_f (engine)	f	W_f (engine)	f
	K	K	kpa	kg/s	%	g/s	g/kg	g/s	g/kg
9	299.5	307.8	101.5	1.149	0.90	15.9	13.8	42.0	36.5
	274.8	279.8	101.5	1.149	0.77	20.0	17.4	50.0	43.5
	269.8	273.7	101.5	1.149	0.79	26.0	22.7	51.2	44.6
	263.7	267.0	101.5	1.149	0.74	30.2	26.3	50.6	44.0
	260.3	261.2	101.5	1.149	0.76	38.6	33.6	50.4	43.9
	255.4	256.3	101.4	1.149	0.78	-	-	>50.4	>43.9
10	302.8	318.8	100.9	1.149	0.86	13.4	11.7	39.6	34.5
	277.6	277.6	100.8	1.149	0.80	31.5	27.4	52.1	45.3
	270.6	273.2	100.7	1.149	0.75	-	-	>52.5	>45.7
11	302.6	309.3	101.4	1.149	0.86	25.2	21.9	38.6	33.6
	278.1	277.4	101.3	1.149	0.77	37.4	32.5	43.3	37.6
	270.4	272.1	101.3	1.149	0.77	36.8	32.0	42.8	37.3
	267.8	265.6	101.4	1.149	0.81	41.2	35.8	49.6	43.1
	262.6	260.2	101.4	1.149	0.74	39.1	34.0	47.0	40.9
	265.5	253.9	100.3	1.149	0.69	40.7	35.5	50.5	43.5
	249.6	248.3	100.3	1.149	0.67	43.3	37.6	51.2	44.5
	244.1	244.1	100.4	1.149	0.66	-	-	>51.4	>44.7
12	298.4	316.2	100.5	1.149	0.85	24.4	21.2	29.4	25.6
	273.7	277.4	100.4	1.149	0.77	29.8	26.0	35.3	30.7
	269.8	272.1	100.3	1.149	0.74	31.5	27.4	38.6	33.6
	265.9	266.4	100.3	1.149	0.72	33.5	29.2	41.6	36.2
	261.5	260.7	100.3	1.149	0.71	34.0	29.6	41.6	36.2
	255.4	254.8	100.3	1.149	0.69	35.4	30.8	46.2	40.2
	249.8	251.0	100.3	1.149	0.68	38.6	33.6	45.8	39.8
	245.5	245.8	100.3	1.149	0.68	39.9	34.7	46.2	40.2
	241.3	238.9	100.3	1.149	0.67	41.6	36.2	47.7	41.5
13	304.8	320.6	101.3	1.149	0.87	26.7	23.2	42.0	36.5
	278.7	277.3	101.2	1.149	0.74	-	-	>52.5	>45.7

APPENDIX D

FUEL NOZZLE FOULING TEST DATA

Short term fuel nozzle fouling tests were conducted in a small flame tunnel rig using apparatus and procedures described in Section V.D.1. Primary results were periodic bench flow calibrations of the fuel nozzles to detect metering orifice plugging and/or flow divider valve seizure. These results were also supplemented with visual inspection of the fuel nozzle tip and flow divider valve components. Periodic flow calibration results and normalized flow calibration results are presented in Table D-1.

As described in Section V.D.2, long term fuel nozzle valve gumming tests were also conducted using JP-4 and JP-8 fuels. The flow calibration results of this testing are presented in Table D-2. Shown in Table D-2 are the measured valve flow rates, the flow ratio normalized to pretest flow rate and the ascending flow rate divided by the descending flow rate. The latter quantity is a measure of hysteresis or valve sticking tendencies.

Table D-1. Fuel Nozzle Fouling Test Results.

Fuel Nozzle Serial Number	Test Fuel Number	Fuel Temperature °C	Test Time, Minutes	Fuel Flow Rate, g/s at ΔP_f (MPa)							Fuel Flow Rate)/(Pretest Fuel Flow Rate at ΔP_f (MPa)						
				0.827	1.241	2.275	2.965	2.275	1.241	0.827	0.827	1.241	2.275	2.965	2.275	1.241	0.827
[illegible]	1	+36	0	2.13	19.5	63.0	83.3	63.0	19.2	2.14	1.000	1.000	1.000	1.000	1.000	1.000	1.000
			100	1.92	17.9	61.1	80.5	61.4	18.4	2.12	0.901	0.918	0.970	0.966	0.975	0.958	0.991
			300	1.84	17.8	61.5	82.3	61.6	17.8	2.12	0.864	0.912	0.976	0.988	0.978	0.927	0.991
01757	1	+36	0	2.23	18.6	62.9	83.3	62.7	18.8	2.32	1.000	1.000	1.000	1.000	1.000	1.000	1.000
			5	1.86	18.3	62.6	82.2	62.6	18.4	2.39	0.834	0.973	0.995	0.987	0.998	0.979	1.030
			330	1.44	17.6	61.1	81.6	61.1	18.3	1.90	0.646	0.936	0.971	0.980	0.974	0.973	0.819
[illegible]	1	+78	0	2.44	18.4	63.4	83.2	62.7	18.7	1.92	1.000	1.000	1.000	1.000	1.000	1.000	1.000
			100	1.66	18.6	62.0	82.4	62.6	18.9	1.93	0.878	1.011	0.978	0.990	0.998	1.011	1.005
			300	1.47	17.8	62.9	83.0	62.9	18.8	1.79	0.778	0.967	0.992	0.998	1.003	1.005	0.932
[illegible]	[illegible]	+78	0	2.32	18.8	63.4	83.1	61.9	18.4	2.14	1.000	1.000	1.000	1.000	1.000	1.000	1.000
			5	1.76	18.3	62.5	82.9	62.5	19.3	2.12	0.793	0.973	1.018	1.022	1.010	0.995	0.991
			300	1.76	18.4	63.5	82.4	63.4	19.3	2.14	0.973	0.979	1.018	1.016	1.024	0.995	1.000
[illegible]	3	+78	0	2.55	19.2	62.9	84.1	63.4	19.3	2.83	1.000	1.000	1.000	1.000	1.000	1.000	1.000
			100	2.33	18.3	62.2	83.2	61.5	19.3	2.66	0.903	0.979	0.989	0.986	0.970	1.000	0.965
			300	1.64	18.8	62.0	82.2	61.9	19.2	2.54	0.636	0.979	0.986	0.974	0.976	0.995	0.900
[illegible]	4	+78	0	2.41	19.0	62.2	82.4	62.2	19.0	2.46	1.000	1.000	1.000	1.000	1.000	1.000	1.000
			100	2.42	19.1	62.0	82.0	62.1	19.1	2.41	1.004	1.005	1.000	0.995	0.998	1.005	0.980
			300	2.24	19.4	62.1	81.5	62.1	19.2	2.31	0.929	1.021	0.998	0.989	0.998	1.011	0.939
[illegible]	5	+78	0	3.15	19.2	64.0	83.4	63.9	19.4	3.06	1.000	1.000	1.000	1.000	1.000	1.000	1.000
			100	2.67	19.1	63.4	83.3	63.9	19.1	2.58	0.848	0.995	0.998	0.999	1.000	0.985	0.843
			300	2.22	18.5	62.0	81.5	62.0	18.6	2.22	0.705	0.964	0.969	0.989	0.970	0.959	0.725
[illegible]	6	+78	0	2.66	19.3	62.6	82.0	62.5	19.0	2.56	1.000	1.000	1.000	1.000	1.000	1.000	1.000
			5	2.39	—	61.2	80.8	61.4	—	2.46	0.898	—	0.978	0.985	0.982	—	0.953
			300	2.27	1.93	62.0	82.4	62.1	19.3	2.24	0.853	1.000	0.990	1.005	0.994	1.016	0.868
[illegible]757	7	+78	0	2.46	19.4	61.4	80.0	61.5	19.3	2.83	1.000	1.000	1.000	1.000	1.000	1.000	1.000
			100	2.16	19.2	63.3	82.4	63.3	19.2	2.70	0.876	0.990	1.031	1.030	1.029	0.995	0.954
			300	2.09	18.9	61.6	80.6	61.6	18.9	2.66	0.827	0.974	1.003	1.008	1.002	0.974	0.990
[illegible]	8	+78	0	3.11	20.3	63.9	82.5	63.9	20.0	3.11	1.000	1.000	1.000	1.000	1.000	1.000	1.000
			100	1.76	19.7	63.0	82.1	63.3	19.8	2.46	0.566	0.985	0.986	0.994	0.991	0.990	0.791
			300	2.32	19.8	63.3	82.0	63.9	19.8	2.62	0.746	0.990	0.991	0.994	0.991	0.990	0.842
[illegible]	[illegible]	+78	0	3.05	20.1	63.2	82.8	63.2	20.1	3.13	1.000	1.000	1.000	1.000	1.000	1.000	1.000
			100	2.49	19.7	62.6	82.8	61.5	19.7	2.96	0.778	0.980	0.973	0.979	0.973	0.980	0.946
			300	2.41	19.5	62.9	82.6	61.9	19.5	2.83	0.753	0.970	0.979	0.985	0.979	0.970	0.904
[illegible]	10	+78	0	2.42	18.9	62.6	81.3	61.7	19.5	2.82	1.000	1.000	1.000	1.000	1.000	1.000	1.000
			100	3.05	19.4	62.5	83.3	61.7	19.5	3.02	1.163	1.027	0.998	1.000	1.000	1.000	0.071
			300	2.74	18.9	62.7	82.9	61.7	19.3	2.85	1.062	1.000	1.002	0.992	1.000	0.987	1.009
[illegible]787	11	+78	0	3.40	19.3	61.1	78.1	60.2	19.3	3.53	1.000	1.000	1.000	1.000	1.000	1.000	1.000
			100	3.06	19.4	63.0	77.5	59.3	19.5	3.39	0.896	1.003	0.981	0.992	0.992	1.013	1.018
			300	3.47	19.4	63.0	78.7	59.3	19.3	3.57	1.052	1.033	0.965	0.973	0.985	1.000	1.011
[illegible]	12	+78	0	3.27	19.3	62.3	80.3	61.1	19.2	2.49	1.000	1.000	1.000	1.000	1.000	1.000	1.000
			100	3.36	19.3	62.6	84.3	61.4	19.8	2.72	0.995	0.997	0.992	1.027	1.019	0.950	1.091
			300	3.27	18.9	62.7	80.6	61.7	19.3	2.72	0.961	0.977	1.010	1.032	1.025	1.007	1.091
[illegible]	13	+78	0	3.01	19.3	62.1	77.2	56.4	19.3	3.93	1.000	1.000	1.000	1.000	1.000	1.000	1.000
			100	3.05	19.5	62.8	77.2	59.0	19.4	3.70	0.811	1.010	1.049	1.000	1.045	1.007	0.948
			300	3.09	19.3	63.6	77.0	58.5	18.9	3.36	0.720	1.000	1.045	0.977	1.036	0.980	0.861

Table D-2. Fuel Nozzle Valve Gumming Test Results.

Fuel Type	Fuel Temperature, K	Run Number	Fuel Nozzle Valve S/N	Test Hours	Flow Rate, g/s at ΔP_f (MPa)							Flow Rate/Pretest Flow Rate at ΔP_f (MPa)							Ascending Flow Rate / Descending Flow Rate at ΔP_f MPa		
					0.827	1.241	2.275	2.965	2.275	1.241	0.827	0.827	1.241	2.775	2.965	2.275	1.241	0.827	0.827	1.241	2.275
JP-8	436	2	2272	0	2.05	19.6	65.1	86.7	64.5	19.7	2.37	1.000	1.000	1.000	1.000	1.000	1.000	1.000	0.865	0.995	1.009
				8	1.08	19.1	65.2	87.2	65.3	19.5	2.57	0.528	0.973	1.000	1.006	1.012	0.990	1.085	0.420	0.979	0.997
				16	1.47	19.0	65.1	87.7	65.1	19.6	2.42	0.718	0.969	1.000	1.012	1.010	0.994	1.021	0.607	0.969	1.000
				24	1.56	18.3	64.5	86.7	64.5	19.3	2.33	0.761	0.959	0.990	1.000	1.000	0.978	0.984	0.670	0.974	1.000
				32	1.01	18.9	65.1	87.4	65.3	19.2	2.20	0.491	0.965	1.000	1.009	1.010	0.971	0.931	0.468	0.984	0.997
				40	1.46	19.7	65.9	87.4	65.6	19.4	2.27	0.721	1.003	1.012	1.009	1.018	0.984	0.957	0.643	1.015	1.004
				48	1.66	18.9	65.3	86.2	64.4	19.2	2.26	0.810	0.965	1.002	0.994	0.998	0.971	0.952	0.735	0.984	1.014
				56	1.76	19.2	64.8	85.9	64.5	19.5	2.34	0.859	0.979	0.994	0.991	1.000	0.983	0.989	0.752	0.985	1.005
				64	1.75	19.5	64.5	86.1	64.5	19.5	2.27	0.853	0.994	0.990	0.993	1.000	0.987	0.957	0.770	1.000	1.000
				72	1.61	19.2	64.5	86.6	64.5	19.3	2.15	0.785	0.981	0.990	0.999	1.000	0.981	0.910	0.749	0.995	1.000
				80	1.70	19.6	65.1	86.8	65.1	19.6	2.33	0.828	1.000	1.000	1.001	1.010	0.994	0.984	0.730	1.000	1.000
				88	1.76	19.3	65.1	87.2	65.1	19.7	2.26	0.859	0.984	1.000	1.006	1.010	1.000	0.952	0.779	0.980	1.000
				96	1.22	14.1	65.1	86.6	65.1	19.4	2.26	0.595	0.720	1.000	0.999	1.010	0.984	0.957	0.540	0.726	1.000
				100	1.83	17.8	64.5	86.8	64.5	19.5	2.39	0.890	0.907	0.990	1.001	1.000	0.990	1.011	0.766	0.913	1.000
JP-8	464	4	2246	0	2.43	21.0	81.9	108.6	81.9	21.0	2.72	1.000	1.000	1.000	1.000	1.000	1.000	1.000	0.893	1.000	1.000
				6	1.17	19.4	81.9	108.6	81.9	20.5	2.10	0.482	0.925	1.000	1.000	1.000	0.976	0.773	0.557	0.946	1.000
				12	0.34	19.1	81.9	108.6	81.9	20.0	1.83	0.140	0.908	1.000	1.000	1.000	0.952	0.671	0.188	0.956	1.000
				18	0.82	18.8	81.3	108.6	81.3	20.3	1.73	0.337	0.895	0.992	1.000	0.992	0.970	0.634	0.473	0.926	1.000
				24	0	19.8	81.9	108.6	81.9	20.1	1.81	0	0.943	1.000	1.000	1.000	0.959	0.667	0	0.985	1.000
				30	0.28	16.5	79.6	107.9	80.4	20.2	1.75	0.114	0.787	0.972	0.993	0.982	0.961	0.644	0.160	0.817	0.990
				32	0	19.3	78.2	108.6	81.3	20.3	1.88	0	0.919	0.955	1.000	0.992	0.967	0.690	0	0.951	0.962
				38	0.76	14.7	81.3	108.6	81.3	20.4	1.95	0.311	0.792	0.992	1.000	0.992	0.972	0.718	0.390	0.721	1.000
				44	0	14.6	81.3	108.0	81.3	20.0	20.2	0	0.695	0.992	0.994	0.992	0.955	0.741	0	0.730	1.000
JP-8	494	3	2234	0	1.29	18.6	71.1	97.2	71.1	19.2	1.87	1.000	1.000	1.000	1.000	1.000	1.000	1.000	0.690	0.969	1.000
				6	0	10.2	70.2	95.5	70.2	19.7	1.93	0	0.546	0.861	0.983	0.987	1.024	1.030	0	0.518	1.000
				12	0	0	68.9	94.8	69.6	20.5	2.67	0	0	0.866	0.975	0.978	1.066	1.428	0	0	0.990
				18	0	0	68.3	93.5	68.3	20.7	3.81	0	0	0.838	0.962	0.960	1.079	2.034	0	0	1.000

Table D-2. Fuel Nozzle Valve Gumming Test Results (Concluded).

Fuel Type	Fuel Temperature, K	Run Number	Fuel Nozzle Valve S/N	Test Hours	Flow Rate, g/s at ΔP_f, MPa							Flow Rate/Pretest Flow Rate at ΔP_f, MPa							Ascending Flow Rate / Descending Flow Rate at ΔP_f, MPa		
					0.827	1.241	2.275	[illegible]	2.275	1.241	0.827	0.827	1.241	2.275	2.965	2.275	1.241	0.827	0.827	1.241	2.275
JP-4	436	1	2246	0	1.54	20.0	81.3	108.6	81.3	20.6	2.52	1.000	1.000	1.000	1.000	1.000	1.000	1.000	0.611	0.971	1.000
				8	2.36	19.4	80.6	108.0	81.3	19.7	2.19	0.885	0.972	0.992	0.994	1.000	0.953	0.870	0.621	0.985	0.991
				16	1.37	19.4	80.8	108.0	81.8	19.8	2.04	0.893	0.922	0.994	0.994	0.994	0.959	0.810	0.671	0.980	0.988
				24	–	17.8	80.6	109.6	81.9	19.5	2.12	–	–	0.992	1.009	1.008	0.947	0.840	–	0.913	0.984
				32	1.23	18.5	81.0	107.7	81.3	19.8	2.14	0.803	0.927	0.997	0.992	1.000	0.959	0.850	0.575	0.929	0.996
				40	1.61	19.7	81.1	107.1	81.3	20.7	2.07	1.049	0.984	0.998	0.986	1.000	1.002	0.820	0.777	0.952	0.998
				48	1.54	–	81.3	108.4	81.3	20.3	2.17	1.000	–	1.000	0.998	1.000	0.984	0.860	0.709	–	1.000
				56	1.73	19.9	80.6	107.7	82.0	20.8	2.37	1.123	0.997	0.997	0.992	1.009	1.008	0.840	0.730	0.957	0.983
				64	1.49	19.7	81.4	107.7	81.4	20.5	2.17	0.967	0.985	1.002	0.992	1.002	0.996	0.860	0.686	0.961	1.000
				72	1.39	18.9	81.1	107.7	80.9	20.3	1.97	0.902	0.946	0.998	0.992	0.995	0.984	0.780	0.706	0.931	1.002
				80	1.32	19.7	80.6	107.4	80.4	19.8	2.04	0.861	0.984	0.992	0.988	0.989	0.959	0.810	0.647	0.995	1.004
				88	1.36	20.0	81.3	108.6	81.3	20.2	2.13	0.885	1.003	1.000	1.000	1.000	0.977	0.895	0.638	0.990	1.000
				96	0.64	13.4	82.0	108.6	82.0	19.8	1.51	0.418	0.673	1.009	1.000	1.009	0.962	0.600	0.424	0.677	1.000
				100	1.13	18.5	82.5	107.4	81.9	19.8	1.97	0.738	0.927	1.016	0.988	1.008	0.959	0.780	0.574	0.954	1.007
JP-4	444	8	2252	0	16.0	158.8	567	762	567	160.8	20.5	1.000	1.000	1.000	1.000	1.000	1.000	1.000	0.780	0.988	1.000
				8	20.4	157.8	562	762	562	161.1	21.0	1.275	0.994	0.991	1.000	0.991	1.002	1.024	0.971	0.950	1.000
				16	15.0	158.8	567	767	567	160.5	21.0	.938	1.000	1.000	1.007	1.000	0.998	1.024	0.714	0.989	1.000
				21.5	11.0	86.8	561	757	561	161.3	20.8	.688	0.547	1.011	0.993	0.989	1.003	1.015	0.520	0.585	1.000
JP-4	450	6	2252	0	1.95	19.4	69.0	93.1	69.2	19.7	2.56	1.000	1.000	1.000	1.000	1.000	1.000	1.000	0.762	0.985	0.992
				4	1.30	17.5	68.0	92.0	68.0	19.2	2.49	0.665	0.898	0.985	0.987	0.989	0.974	0.975	0.522	0.912	1.000
				12	1.06	16.3	63.5	86.9	64.0	23.7	2.58	0.542	0.839	0.920	0.934	0.925	1.201	1.010	0.411	0.688	0.992
				20	0	18.3	63.0	92.6	68.0	19.7	2.49	0	0.940	0.985	0.945	0.980	0.997	0.975	0	0.929	1.000
				28	0	14.1	67.4	91.0	67.4	20.0	3.34	0	0.726	0.976	0.977	0.974	1.016	1.305	0	0.705	1.000
JP-4	455	7	2237	0	1.90	18.1	69.3	92.0	67.0	18.8	2.14	1.000	1.000	1.000	1.000	1.000	1.000	1.000	0.888	0.962	1.004
				4	0.64	16.3	69.3	92.7	69.3	18.8	1.90	0.338	0.896	1.000	1.008	1.004	1.000	0.888	0.337	0.867	1.000
				8	0.69	13.9	68.0	92.2	68.0	18.9	1.78	0.364	0.764	0.982	1.003	0.985	1.007	0.829	0.388	0.735	1.000
				12	0	15.6	66.8	91.5	66.8	18.9	1.56	0	0.861	0.964	0.995	0.967	1.007	0.729	0	0.825	1.060
				16	0	16.0	66.4	91.0	66.4	19.2	2.02	0	0.882	0.953	0.989	0.962	1.023	0.961	0	0.833	1.000
				20	0	14.3	66.7	91.1	66.8	19.8	1.55	0	0.790	0.962	0.990	0.967	1.052	0.724	0	0.722	0.998
				24	0	11.8	66.3	91.0	67.7	20.5	1.99	0	0.649	0.956	0.989	0.980	1.091	0.929	0	0.576	0.979
JP-4	464	5	2241	0	2.71	20.0	70.4	95.4	70.4	20.4	3.05	1.000	1.000	1.000	1.000	1.000	1.000	1.000	0.889	0.980	1.000
				8	0.78	17.1	70.3	95.8	70.3	19.5	2.51	0.288	0.856	0.997	1.004	0.998	0.976	0.822	0.311	0.877	1.000
				16	0	16.8	69.6	95.4	69.6	19.4	2.27	0	0.839	0.987	1.000	0.987	0.970	0.744	0	0.866	1.000
				24	0	15.1	69.3	93.2	69.9	19.8	2.65	0	0.757	0.984	0.978	0.993	0.989	0.968	0	0.762	0.991
				32	0	0	67.8	92.0	68.0	18.1	3.01	0	0	0.962	0.964	0.966	0.907	0.988	0	0	0.997

APPENDIX E

SMOKE DATA CALCULATION

In this program, combustor component rig tests were conducted in which somke emission levels were measured at the combustor exit plane by the method specified in Reference 5. The result is a Smoke Number (SN) which expresses the opacity of filter paper that has been stained by the exhaust gases. SN is, therefore, not a true thermodynamic property of the exhaust gas. A relationship between SN and carbon weight fraction (X_c), which is a thermodynamic property, is presented in Reference 12. This relationship is reproduced in Figure E-1.

When combustor exhaust gases are diluted by turbine cooling air as in the F101, by fan stream air, both SN and X_c are reduced. Smoke emission index (EI_S)g carbon/kg fuel, however. remains constant. EI_S is calculated by the relationship:

$$EI_S = \left(X_{ci}\right)\left(\frac{1000 + f_i}{f_i}\right)\left(10^{-3}\right)$$

where:

i = engine station where sample is taken

f = fuel-air weight ratio (g fuel/kg air)

Therefore, engine smoke level, which would be measured at engine Plane 8, can be calculated from combustor rig measurements, taken at simulated engine Plane 4, by the following procedure:

1. Measure (SN_4) and (f_4) at simulated engine test condition
2. $SN_4 \rightarrow X_{c4}$ (from Figure E-1)
3. $EI_S = \left(X_{c4}\right)\left(\frac{1000 + f_4}{f_4}\right)\left(10^{-3}\right)$
4. Cycle data $\rightarrow f_8$ at simulated engine test condition
5. $X_{c8} = \left(EI_S\right)\left(\frac{f_8}{1000 + f_8}\right)\left(10^{3}\right)$
6. $X_{c8} \rightarrow SN_8$ (from Figure E-1)

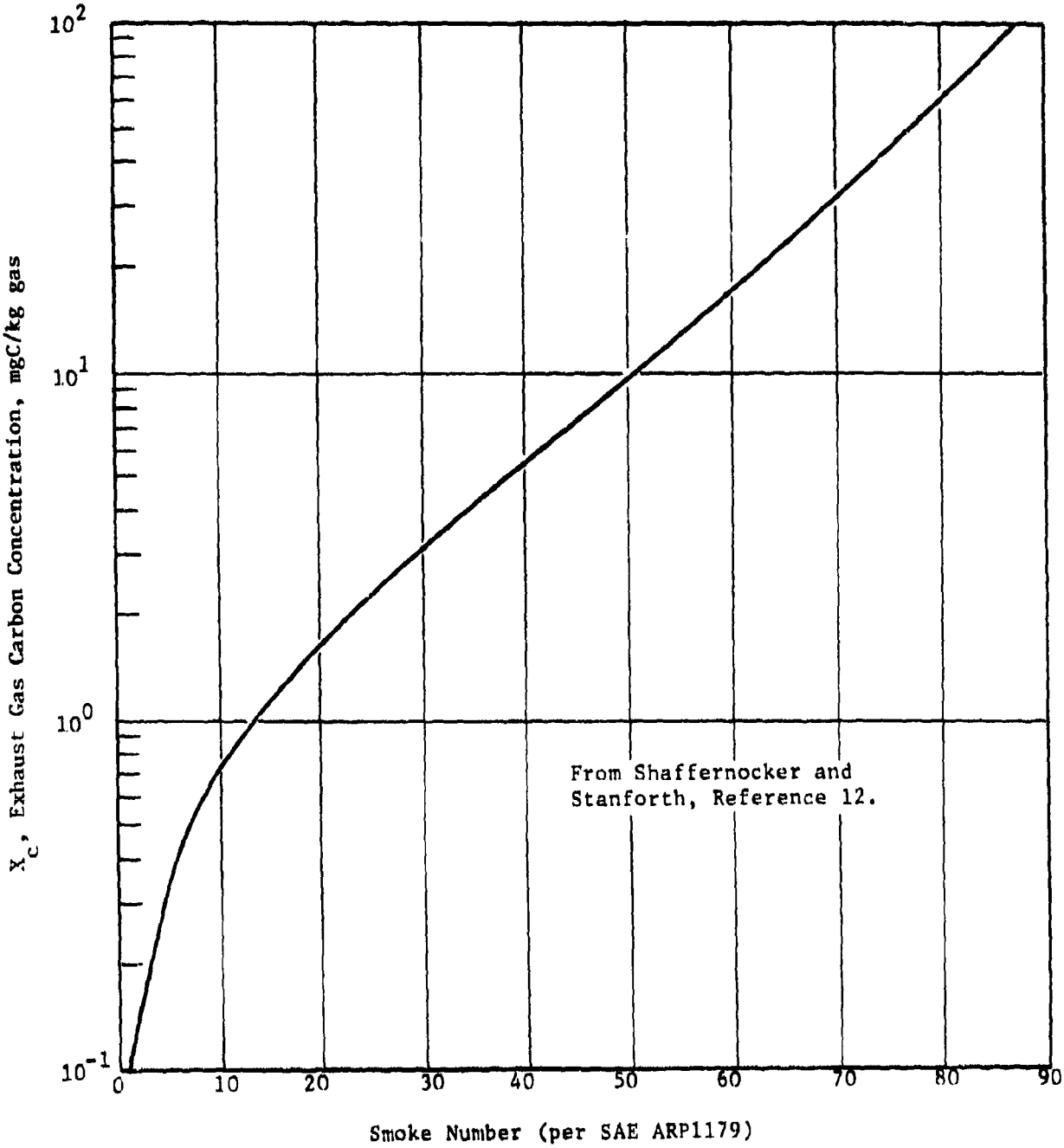

Figure E-1. Experimental Relationship Between Smoke Number and Exhaust Gas Carbon Concentration.

For the F101 engine, $f_8/f_4 = 0.130$ at idle and 0.246 at cruise, takeoff and dash operating conditions, so SN_8 is significantly less than SN_4.

SN_4 and f_4, as measured in the rig tests are tabulated in Table A-1. SN_8, calculated from the measured SN_4 and f_4 by the above procedure, is tabulated in Table A-2. Corrections to true engine density were then made by the correlation scheme illustrated in Figure 42, and these data are tabulated in Table A-6.

NOMENCLATURE

Symbol		Units
A	Area	cm^2, mm^2
CO	Carbon Monoxide	-
CO_2	Carbon Dioxide	-
CWALF	Clockwise Aft Looking Forward	-
EI	Pollutant Emission Index	g pollutant/kg fuel
FBP	Final Boiling Point	K
H	Fuel Hydrogen Content	weight percent
HC	Hydrocarbon	-
IBP	Initial Boiling Point	K
JFTOT	Jet Fuel Thermal Oxidation Tester	-
NO_x	Total Oxides of Nitrogen (= NO + NO_2)	-
Q	Heat of Combustion	MJ/kg
S	Combustor Operating Severity Parameter	-
SMD	Sauter Mean Diameter	-
SN	Smoke Number (by ARP1256)	-
T	Temperature	K
V	Velocity	m/s
W	Mass Flow Rate	g/s, kg/s
X	Exhaust Gas Pollutant Concentration	mg pollutant/kg air
b	Curve Fit Equation Intercept	-
f	Fuel-Air Ratio	g fuel/kg air
h	Absolute Humidity	g H_2O/kg air
k	Arbitrary Constant	-
m	Curve Fit Equation Slope	-

NOMENCLATURE (Continued)

Symbol		Units
n	Hydrogen-to-Carbon Atom Ratio	-
r	Curve Fit Correlation Coefficient	-
x	Independent Variable	-
y	Dependent Variable	-
ΔP	Pressure Drop	MPa
ΔT	Temperature Rise	K
η	Combustion Efficiency	Percent
ν	Viscosity	mm^2/s
ρ	Density	kg/m^3
σ	Surface Tension	mN/m
ϕ (f)	Fuel-Air Ratio Function in S_{NO_x} (Equation 8)	-
Subscripts		
3	Compressor Exit Station (Combustor Inlet)	-
4	Combustor Exit Station	
8	Engine Exit Station	
c	Combustor	
e	Effective	
f	Fuel	
m	Metered	
r	Reference	
st	Stoichiometric	
L	Liner (metal)	
gs	Gas Sample	
tc	Thermocouple	

NOMENCLATURE (Concluded)

Subscripts

s	Sample
avg	Average
max	Maximum
Imm.max	Immersion Maximum

*U.S.Government Printing Office: 1979 — 657-084/247